Chapter 5: Global Carbon and other Biogeochemical Cycles and Feedbacks

Coordinating Lead Authors:
Josep G. Canadell (Australia), Pedro M.S. Monteiro (South Africa)

Lead Authors:
Marcos Costa (Brazil), Leticia Cotrim da Cunha (Brazil), Peter Cox (UK), Alexey V. Eliseev (Russia), Stephanie Henson (UK), Masao Ishii (Japan), Samuel Jaccard (Switzerland), Charles Koven (USA), Annalea Lohila (Finland), Prabir Patra (Japan/India), Shilong Piao (China), Joeri Rogelj (Austria/Belgium), Stephen Sympungani (Zambia), Sönke Zaehle (Germany), Kirsten Zickfeld (Canada/Germany)

Contributing Authors:
Georgii Alexandrov (Russia), Lena Boysen (Germany), Long Cao (China), Naveen Chandra (Japan), Philippe Ciais (France), Piers Forster (UK), Véronique Garçon (France), Bettina Gier (Germany), Nathan Gillett (Canada), Bala Govindasamy (India), Vanessa Haverd (Australia), Jian He (USA), Forrest Hoffman (USA), Chris Jones (UK), David Keller (USA/Germany), Andrew Lenton (Australia), Laura Lorenzoni (USA), Nicole Lovenduski (USA), Andrew MacDougall (Canada), Damon Matthews (Canada), Malte Meinshausen (Germany/Australia), Igor Mokhov (Russia), Intan Nurhati (Indonesia), Julia Pongratz (Germany), Benjamin Poulter (USA), Ann Stavert (Australia), Parvadha Suntharalingham (UK), Kaoru Tachiiri (Japan), Rona Thompson (Norway), Hanqin Tian (USA), Xuhui Wang (China)

Chapter Scientist:
Alice Lebehot (South Africa/France)

Review Editors:
Victor Brovkin (Germany/Russia), Richard Feely (USA), Jose Lara Lara (Mexico)

Date of Draft: 29 April 2019

Note: TSU compiled version

Table of Content

Executive Summary

Increasing accumulation of greenhouse gases (GHGs) in the atmosphere is the dominant cause of the Earth's changing radiative properties, which are resulting in climate change. The main driver of changes in atmospheric GHGs over the past 200 years is the direct emissions from human activities, but the actual accumulation of GHGs in the atmosphere is determined by the balance between human GHG emissions and biogeochemical source-sink dynamics that exchange materials between multiple carbon reservoirs on land, oceans and atmosphere. This chapter assesses how biogeochemical processes affect the abundance of GHGs in the atmosphere and identifies biogeochemical feedbacks that have led or could lead to a future acceleration, slowdown or abrupt transition in the rate of GHG accumulation in the atmosphere, and therefore, of climate change and its impacts. The chapter also assesses the remaining carbon budget for halting global warming and large-scale consequences of carbon dioxide removal on biogeochemical cycles.

Time context of the human perturbation on biogeochemical cycles

Atmospheric concentrations of the three main GHGs reached 405 ppm for CO_2, 1850 ppb for CH_4, and 330 ppb for N_2O in 2017, and are very *likely* to be the highest in the last 800,000 years. These global mean concentrations correspond to an increase of about 46%, 156%, and 22% above pre-industrial levels, respectively. Current CO_2 concentrations are also *very likely* to be unprecedented in more than 2 million years. There have been times in Earth's history when CO_2 concentrations were much higher than at present, but multiple lines of evidence show with *medium confidence* that the rate at which CO_2 increases in the atmosphere during the Industrial Era has been by at least a factor of 10 higher than at any other time during the last 66 million years. This extraordinary speed of change characterizes the unprecedented nature of the current anthropogenic perturbation. {5.1.1, Figures 5.1, 5.2}

Paleoclimate records show abrupt changes with large pulses (>100 ppm) in atmospheric CO_2 over millennia and smaller pulses (~10 ppm) over centuries in response to climate forcing (*medium confidence*). For future warming of no more than 2ºC, paleorecords suggest, with *medium confidence*, that it is *unlikely* that a tipping point will be crossed leading to large, unpredictable changes in the state of the climate system. However, the CO_2 emissions rates from those pulses are *likely* one order of magnitude slower than the current anthropogenic emissions suggesting some limits to using the paleorecord as an analogue for contemporary and future climate change. {5.1.3.4}

Contemporary Trends of Greenhouse Gases

It is *virtually certain* that the accumulation of CO_2, CH_4, and N_2O in the atmosphere over the Industrial Era is the result of human activities. During the last decade, average annual anthropogenic emissions of CO_2, CH_4, and N_2O, reached the highest levels in the history of human civilisation (*virtually certain*) at 10.9 PgC yr^{-1}, 319 Tg CH_4 yr^{-1}, and 6.1 TgN yr^{-1}, respectively. {5.2.1.1, 5.2.2.1, 5.2.3.1}

The fate of the carbon emitted from human activities during the decade of 2008–2017 (annual average 10.9 PgC yr^{-1}) was: 44% accumulated in the atmosphere (4.7 PgC yr^{-1}), 22% was taken up by the ocean (2.4 PgC yr^{-1}) and 29% was removed by terrestrial ecosystems (3.2 PgC yr^{-1}). These quantities have an imbalance of 0.5 PgC suggesting an overestimation of the emissions, or underestimation of the sinks, or both. Of the total anthropogenic CO_2 emissions, about 87% come from the combustion of fossil fuels and the remaining from land use, land use change, and forestry. {Table 5.1, 5.2.1.2, 5.2.1.5}

The CO_2 ocean and land sinks have continued to increase at rates that remain close to the rate of increase in atmospheric CO_2 (*high confidence*), albeit with large decadal and interannual variability. However, the ocean carbonate buffering capacity is now decreasing and is *very likely* to form the basis of a long-term feedback that will reduce the effectiveness of ocean CO_2 uptake in the future. Interannual and decadal variability of the ocean and land sinks indicate that these fluxes are very sensitive to climate forcing and that this sensitivity has a strong regional character. {5.2.1.3.1, 5.2.1.4.2, Figure 5.10}.

Atmospheric CH_4 resumed its long-term growth trend in 2007 at an average rate of 7±3 ppb yr^{-1} for the last decade (2008–2017), a trend that accelerated over the last period (2014–2017). The multi-decadal growth trend in atmospheric CH_4 is *very likely* dominated by anthropogenic activities, and the resumption since 2007 is *likely* to be driven in a significant way by emissions from fossil fuels and agriculture, while the multi-year variability is predominantly driven by El Niño Southern Oscillation cycles during which biomass burning and wetland emissions play an important role. {5.2.2}

The growth rate of atmospheric N_2O has accelerated since the 1980s, and it is *virtually certain* that the growth has predominantly been driven by the global increase in emissions from the expansion and intensification of agriculture, and to lesser extent due to climate–N_2O feedbacks. Agricultural N_2O emissions have increased by about 80% since the early 1900s, and by 30% since the 1980s. Increased use of nitrogen fertiliser and manure contributed to about 70% of the increase during 1980–2016. {5.2.3.2.1}

Ocean Acidification and Ocean de-Oxygenation

It is clear with *virtual certainty* that ocean acidification is intensifying as a result of the ocean continuing to take up annually about 22% of global anthropogenic CO2 emissions. This uptake is driving changes in the ocean carbonate chemistry, which results in ocean acidification and associated carbonate undersaturation. It is *likely* that there is a threshold in the extent and persistence of undersaturation in the Southern Ocean by 2100, which increases the area affected by month-long onset of undersaturation from negligible under future low emissions scenarios (RCP2.6) to ~30% under medium emissions scenarios (RCP4.5), and to more than 95% in high emissions scenarios (RCP8.5). {Figure 5.20; 5.3.3.3}

Shelf systems, particularly upwelling systems, are *likely* susceptible to the combined and strengthening influence of ocean acidification and ocean de-oxygenation in the tropical and sub-tropical ocean interior. This effect is two-fold; the naturally low buffer factor in upwelling systems are *likely* to make them more vulnerable to the impact of anthropogenic CO_2 that results in enhanced ocean acidification and secondly, ocean-de-oxygenation in upwelled waters is *likely* to enhance N_2O, CH_4 and CO_2 emissions that are *as likely as not* to enhance greenhouse gas fluxes out of these systems (*medium confidence*). Coastal areas, especially under highly populated zones also experience acidification and deoxygenation because the inputs of effluents and its microbial degradation produce CO_2 and consume dissolved oxygen in the water column *(high confidence)* {5.3}

Future Projections of Biogeochemical Feedbacks on Climate Change

The ocean and terrestrial carbon sinks are expected to continue to grow due to increased atmospheric CO_2 but weaken with warming (*high confidence*) and stop growing or decline under high GHG emissions scenarios. All Earth System Models indicate that the global ocean sink will stop growing from around 2060 under the warmest scenarios, although at a level varying from about 4 to 6 Pg yr^{-1} Most models predict a declining land carbon sink from 2060 onwards once CO_2 emissions begins to slow down under the warmest scenarios, while some models also predict that the land becomes a carbon source by 2100 (from being sink of up to 4 PgC yr^{-1}); it is *very likely* that terrestrial nutrient shortage will limit the effect of rising atmospheric CO_2 on future land carbon sinks. It is *very likely* that the ocean sink will be limited It is *very likely* that the ocean sink will be limited by a decreasing buffer capacity. Despite the wide range of model responses, there is *high confidence* that overall uncertainty in projections of CO_2 by 2100 is dominated by uncertainties in emissions scenarios rather than uncertainties in carbon cycle feedbacks. {5.4}

It is *virtually certain* that the land and ocean sources of CH_4 and N_2O, and the atmospheric sink of methane will be affected by climate change. There is *large uncertainty* about the magnitude and timing of the responses of each individual process involved. However, there is *medium to high confidence* that at multidecadal and centennial timescales the additional radiative forcing arising from climate-CH_4 and climate–N_2O feedbacks will be small compared to the forcing from the direct anthropogenic GHG emissions in the 21st century. {5.4}

On the basis of the paleorecord, atmospheric CO_2 is sensitive to changes in the efficiency of the ocean's biological carbon pump. However, the processes that drive this sensitivity remain very uncertain. Long term projections do not provide an agreement on the magnitude and direction of climate-driven trends in ocean primary production. {5.4.4.2}

There is *high confidence* that thawing terrestrial permafrost will lead to carbon release, but *low confidence* in the timing, magnitude and the relative roles of CO_2 versus CH_4 as feedback processes. Model projections under high warming scenarios estimate carbon emissions from permafrost of between 11 and 174 PgC by 2100. Because of widespread soil saturation and anoxia in the region, part of the carbon flux from ecosystems to the atmosphere is via the production of CH_4, and the combined radiative forcing from both gases may be larger than from CO_2 emissions only. {5.4.8.2}

The response of biogeochemical cycles to human-forcing may be abrupt at regional scales, and irreversible on decadal to century timescales. The risks of crossing local thresholds (such as forest dieback) increase with climate change, but there is no consensus on a particular threshold of global warming or atmospheric CO_2 in Earth System Model projections. Models have begun to include a wider array of processes, such as permafrost and nutrient dynamics, which result in feedbacks that are substantial but do not lead to runaway feedbacks over the next 100 years (*medium confidence*). Large uncertainties remain on the possibility of additional feedbacks not represented in current models, which could lead to significant departures from the current modelled trajectories. {5.4.8}

Carbon Budgets to Climate Stabilisation

Robust physical understanding underpins the near linear relationship between cumulative CO_2 emissions and global mean temperature increase, known as the transient climate response to cumulative carbon emissions (TCRE) (*high confidence*). The TCRE implies that stabilizing global warming requires global net anthropogenic CO_2 emissions to become zero. TCRE is assessed to amount to 0.8–2.5°C per 1000 PgC (*likely* range). Additional Earth system feedbacks that operate on century timescales like permafrost thawing have the potential to break the linearity of TCRE, resulting in both higher warming or a path dependency of warming as a function of cumulative emissions of CO_2. {5.5.1}

Mitigation requirements for limiting warming to specific levels can be quantified using a carbon budget that relates cumulative CO_2 emissions to global mean temperature increase (*high confidence*). Since preindustrial times, a total of 690±90 PgC of anthropogenic CO_2 has been emitted. Besides the TCRE, estimating the remaining carbon budget is further influenced by historical warming, the warming contribution of non-CO_2 forcers, and additional Earth system feedbacks that are not typically included in coupled models informing the TCRE. The remaining carbon budget starting from the year 2019 for limiting warming to 1.5°C, 2°C, and 3°C with a probability of at least 66% is assessed to amount to X PgC, X PgC, X PgC, respectively, and Y PgC, Y PgC, and Y PgC for at least 50% probability. Following a linear trajectory from today onwards these values correspond to reaching net zero in Y, Y, and Y year, respectively. If a specific remaining carbon budget is exceeded, carbon-dioxide removal will be required to return warming to a certain temperature level. [[To be updated]] {5.5.2}

Several factors, including future emissions from permafrost thawing and wetlands, and variations in projected non-CO_2 warming, affect the precise value of carbon budgets but do not change the need for global CO_2 emissions to decline to net zero to halt global warming (*medium confidence*). Emissions of permafrost and wetlands *likely* reduces the estimated remaining carbon for 1.5°C or 2°C by about 30 PgC and continue to add to warming beyond this century. Geophysical uncertainties related to non-CO_2 response and TCRE distribution result in an uncertainty of at least ±100 PgC. Uncertainties in the level of historic warming contribute about 70 PgC. These estimates can also vary by about 70 PgC depending on projected non-CO_2 warming as found in available pathways (from 1.5°C special report. [to be updated] {5.5.2}

Biogeochemical implications of Carbon Dioxide Removal and Solar Radiation Modification

Net Carbon Dioxide Removal (CDR) from the atmosphere will be opposed by outgassing of CO_2 from land and ocean carbon reservoirs (*high confidence*). In the same way that CO_2 emissions are partitioned between atmosphere, land, and ocean carbon reservoirs, net removal of CO_2 from the atmosphere leads to repartitioning of CO_2 between reservoirs. The fraction of CO_2 removed that remains out of the atmosphere is *very likely* 50% for 100 PgC removed under current atmospheric CO_2 concentrations, but varies with the climate state from which CDR is applied and the amount of CDR implemented (*medium confidence*). {Figure 5.33, bottom panel; 5.6.2.1}

The climate-carbon cycle response to the removal of CO_2 from the atmosphere (negative emissions) is not equal and opposite to the response to positive emissions, i.e. the response is not always symmetric (*medium confidence*). Initial model runs (to be updated) show a symmetric response of the carbon cycle for pulse emissions and removals of ±100 PgC, but the response becomes increasingly asymmetric for higher pulse emissions and removals . The asymmetry originates largely from state-dependencies and nonlinearities in the ocean and will require proportionally larger removal efforts as the reliance on CDR methods increases. {Figure 5.31; 5.6.2.1}

Deployment of CDR methods can have beneficial and adverse environmental side effects (*very high confidence*). Side effects are either biogeochemical (with consequences for GHG emissions) or biophysical (changes in hydrology or reflectivity). Some side effects strengthen the climate benefits of CDR methods while others weaken them. Some CDR methods have additional non-climate benefits such as increasing soil fertility and productivity or decreasing ocean acidification. The level of confidence in positive and negative side effects of CDR methods is *low* and often very project/regionally specific. Reversing the increase in atmospheric CO_2 concentrations by CDR will reverse ocean acidification at the sea surface but will not result in rapid amelioration of ocean acidification in the deeper ocean (*medium confidence*). {5.6.2.2}

Solar Radiation Modification (SRM), with the concomitant effects of increasing anthropogenic atmospheric CO_2, will *very likely* increase global mean net primary production and carbon storage on land. This effect is the result of the CO_2 fertilisation effect on photosynthesis, which is independent from any effects from SRM, and the *highly uncertain* diffuse-radiation fertilisation effect on photosynthesis from the increase diffuse radiation fraction due to the aerosol injections in the atmosphere. Because SRM does not directly address the increase in atmospheric CO_2, it does not counteract ocean acidification. {5.6.3}

5.1 Introduction and the paleo context

Increasing the abundance of greenhouse gases (GHGs) in the atmosphere is the dominant cause of the changing Earth' radiative properties which are leading to climate change. While the main driver of changes in atmospheric GHGs over the past 200 years is the direct emissions from human activities, the actual accumulation of GHG in the atmosphere is also controlled by biogeochemical source-sink dynamics that exchange quantities between multiple carbon pools on land, oceans and atmosphere. For instance, the combustion of fossil fuels and land use change for the period 1750–2017 have released an estimated 660±90 PgC to the atmosphere (Le Quéré et al., 2018a) of which less than half remains in the atmosphere today. This underscores the large role of terrestrial and ocean carbon dioxide (CO_2) sinks in regulating the concentration of atmospheric CO_2 (Ballantyne et al., 2012; Gruber et al., 2019a; Le Quéré et al., 2018a; Li et al., 2016b).

The biogeochemical controls of GHGs is a central motivation for this chapter, which identifies biogeochemical feedbacks that have led or could lead to a future acceleration, slowdown or abrupt transitions in the rate of GHG accumulation in the atmosphere, and therefore of climate change, its impacts, and the remaining carbon budget to chosen climate stabilisation targets.

The chapter covers the three GHGs that dominate the human perturbation of the Earth's radiation budget: carbon dioxide (CO_2), methane (CH_4) and nitrous oxide (N_2O).

This section (Section 5.1) provides an overview of the place in Earth's history of the current and future scenarios of atmospheric concentrations and growth rates of the three GHGs. It also introduces the main processes involved in GHGs-climate feedbacks followed by an assessment of what can be learned from the paleo record towards a better understanding of contemporary and future GHG-climate dynamics and their response to different mitigation trajectories.

The chapter covers the historical (< 100 years) and contemporary (past decade) state of the carbon cycle and other biogeochemical cycles in Section 5.2, including the global budgets of CO_2, CH_4, and N_2O. Significant advancements have taken place since IPCC AR5, particularly in constraining the annual to decadal variability of the ocean and land carbon sinks and what that reveals about the sensitivity of carbon pools to current and future climate changes. There are also new isotopic and other data constraints on the causes of the observed CH_4 trends over the past two decades, and significantly more complete and better constrained global N_2O budget than in previous assessments.

The uptake of CO_2 by the oceans leads to ocean acidification. Section 5.3 covers the paleo, historical and future trends in ocean acidification, with consequences for biogeochemical cycles and marine life. These impacts are assessed in AR6-WG II. The section also assesses the trend in deoxygenation of the oceans due to warming, increased stratification of the surface ocean and slowing of the meridional overturning circulation, which reduce the ventilation of the ocean interior and amplify the impact of remineralisation of the biological carbon pump on DIC and pH in the ocean interior. Growing hypoxia zones in the tropical and sub-tropical oceans linked to changing ventilation are also significant sources of N_2O emissions as well as important influences on Eastern Boundary Upwelling systems where they can amplify ocean acidification and the generations of CH_4 and N_2O.

Future projections of biogeochemical cycles and their feedbacks to the climate system are in Section 5.4. Earth system models have made significant progress towards including more complex carbon cycle and associated biogeochemical processes that enable exploring a range of possible future carbon-climate feedbacks and their impacts on the climate system. Emphasis is placed in understanding processes involved in carbon-climate feedbacks and the possibility for rapid and abrupt changes brought about non-linear dynamics. Uncertainties and the limits of our models to predict future dynamics for a given GHG emissions trajectories are given.

A significant advance in the IPCC AR5 was the development of the total and remaining carbon budgets to climate stabilisation targets and the associated transient climate response to cumulative CO_2 emissions. These advances were based on the finding that the excess global warming compared to the preindustrial time

was quasi linearly related with the historical cumulative CO_2 emissions. Section 5.5 shows the progress made since the AR5 and the 1.5°C Special Report (IPCC, 2018b) particularly on key components required to estimate the remaining carbon budget. These components include transient response to cumulative emissions of CO_2, zero emission commitment, projected non-CO_2 warming, and unrepresented Earth system feedbacks.

Section 5.6 assesses the biogeochemical implications of Carbon Dioxide Removal (CDR, also known as negative emissions) and Solar Radiation Modification (SRM). CDR seeks to directly reverse the effects of greenhouse gas emissions by removing CO_2 from the atmosphere either directly or by enhancing terrestrial, marine or geological carbon sinks. SRM attempts to offset the climate effects of greenhouse gas emissions, by intentional manipulation of planetary solar absorption to counter climate change. The potential and socio-economic feasibility of such options are assessed in detail in IPCC AR6 WGIII.

Finally, Section 5.7 highlights the knowledge gaps that emerged from this assessment, which would have strengthened the assessment reported in this chapter.

5.1.1 Time context of the human perturbation of biogeochemical cycles

Measurements in air samples extracted from bubbles trapped in ice cores and collected from the ambient atmosphere show that concentrations of the three most important long-lived and well-mixed GHGs, CO_2, CH_4 and N_2O, began to rapidly increase at the onset of the Industrial era around 1750 (Figure 5.1).

Atmospheric concentrations of the three GHGs reached 405 ppm for CO_2, 1850 ppb for CH_4, and 330 ppb for N_2O in 2017, and are *very likely* to be the highest in the last 800,000 years (Figure 5.1). These concentrations correspond to about 46%, 156%, and 22% increase above pre-industrial levels, respectively (Section 5.2). For CO_2, current concentrations are also *very likely* to be unprecedented in more than 2 million years (Martínez-Botí et al., 2015b).

[START FIGURE 5.1 HERE]

Figure 5.1: Atmospheric concentrations of CO2, CH4 and N2O in air bubble trapped in ice cores, dated period from 800,000 BCE to 1990 CE (note the variable x-axis range and tick mark intervals for the 3 columns). Ice core data is over-plotted by atmospheric observations from 1958 to present for CO2, from 1984 for CH4 and from 1994 for N2O. The linear growth rates for different time periods (800K–0 BCE, 0–1900 CE and 1900–2017 CE) are given in each panel. For the BCE period, mean rise and fall rates are calculated for the individual slopes between the peaks and troughs, which are given in the panels in left column. The data for BCE period are used from the Vostok, EPICA and Dome C ice cores (Loulergue et al., 2008; Lüthi et al., 2008; Monnin, 2001; Pépin et al., 2001; Petit et al., 1999; Raynaud et al., 2005; Schilt et al., 2010a; Siegenthaler et al., 2005). The data until 0-yr CE are taken mainly from Law Dome ice core analysis (MacFarling Meure et al., 2006a). The surface observations for all species are taken from NOAA cooperative research network (Dlugokencky and Tans, 2019), where ALT, MLO and SPO stand for Alert (Canada), Mauna Loa Observatory, and South Pole Observatory, respectively.

[END FIGURE 5.1 HERE]

Further back in time, CO_2 concentrations reached much higher levels than present day. Possibly the best studied interval in the past that provides some level of comparison with the current anthropogenic increase in CO_2 emissions relates to the Palaeocene-Eocene Thermal Maximum (PETM), 55.8 Myr ago. Atmospheric CO_2 concentrations increased from ~800 to ~2200 ppm in as little as 4–20 Kyr as a result of pulsed release of geological carbon to the ocean–atmosphere system (Gutjahr et al., 2017; Turner, 2018; Zeebe et al., 2016) (Figure 5.2).

The PETM was also associated with pronounced, widespread ocean acidification, with surface ocean pH transiently decreasing by 0.15–0.30 units (Babila et al., 2018; Gutjahr et al., 2017; Penman et al., 2014) with

deleterious consequences for shelf and pelagic marine ecosystems (McInerney and Wing, 2011). These observations highlight that the rate of CO_2 emissions, and by inference the rate at which the ocean absorbs CO_2, is crucial in determining the severity of ocean acidification and other related adverse consequences, such as ocean deoxygenation (see Section 5.3).

Multiple lines of evidence show with medium confidence that the rates of CO_2 emissions to the atmosphere during the Industrial Era has been by at least a factor of 10 higher than at any other time of the last 66 million years (Zeebe et al., 2016; Zeebe and Zachos, 2013) showing the unprecedented pace of change of the current anthropogenic perturbation (Figure 5.2).

The last ~50 million years have been characterised by a gradual decline in atmospheric CO_2 levels at a rate of ~16 ppm Myr^{-1} (Anagnostou et al., 2016; Foster et al., 2017; Gutjahr et al., 2017). The most recent time interval atmospheric CO_2 concentration was as high as 1000 ppm (i.e. similar to the end-of 21st century projection for the high-end emission scenario RCP8.5) was around 33.5 million years ago, prior to the Eocene-Oligocene transition (Anagnostou et al., 2016; Zhang et al., 2013b). Atmospheric CO_2 levels then reached a critical threshold (1000–750 ppm, (DeConto et al., 2008)) enabling the development of regional ice-sheets on Antarctica.

The most recent interval characterised by atmospheric CO_2 levels similar to modern (i.e. 400–450 ppm) was the mid- to late Pliocene (3–3.3 Myr, (Martínez-Botí et al., 2015a) after which atmospheric CO_2 concentration declined gradually at a rate of 40 ppm Myr^{-1}, allowing for major advances in Northern Hemisphere ice sheets, 2.7 Myr ago (DeConto et al., 2008; Sigman et al., 2004).

During the period of 800,000–0 BCE, periodic oscillations in GHG concentrations are forced by orbital modulation as per the Milankovich theory, reinforced by feedbacks internal to the Earth climate system. Concentrations of CO_2 during that time period oscillated cyclically between 160–180 ppm and 300 ppm (Lüthi et al., 2008) (Figure 5.1). During the last deglaciation, growth rates of CO_2 concentrations peaked at 0.12 ppm yr^{-1} (Marcott et al., 2014), 6 times smaller when compared to the average growth rate of CO_2 emissions for the twentieth century (0.71 ppm yr^{-1}) (Joos and Spahni, 2008), and 20 times smaller when compared with the growth rate of 2.3 ppm yr^{-1} for the last decade (2009–2018) (Dlugokencky and Tans, 2019). The rise and decline rates for each of the glacial and interglacial peaks suggests that both the high concentrations at present and the growth rates of atmospheric accumulation of CO_2, CH_4, and N_2O in the past century are unprecedented.

For the period with the highest resolution of paleo and atmospheric records, data show growth rates of atmospheric CO_2 were about 100 times faster during the period of 1900–2017 compared to that during the period of 0–1900 (Figure 5.1).

The acceleration in the GHGs atmospheric growth over the latter period is consistent with the intensification of industrial and agricultural activities. However, beyond a causal relationship, there are multiple lines of independent evidence that make the relationship between growth of excess GHGs and human activities *virtually certain* (see Sections 5.2.1.1, 5.2.2.1, 5.2.3.1).

[START FIGURE 5.2 HERE]

Figure 5.2: CO_2 concentrations and growth rates for the past 60 million years to 2100 using RCP2.6 and RCP8.5. Concentrations data as in Figure 5.1 and data prior to 800K years from (Foster et al., 2017). BCE = Before Current Era, CE = Current Era.

[END FIGURE 5.2 HERE]

5.1.2 Biogeochemical cycling and greenhouse gases-climate feedbacks

Atmospheric concentrations of CO_2 and other GHGs are controlled by the exchange between multiple

reservoirs on land, oceans and the atmosphere involving fast and slow physical and biogeochemical processes. Carbon – Climate feedbacks link changes in the net air-sea and air-land fluxes of CO_2 driven by both anthropogenic CO_2 (carbon feedback) and warming and wind stress (climate feedback) to anomalies in the trend of the airborne fraction of anthropogenic CO_2 (the fraction of anthropogenic emissions remaining in the atmosphere), which in turn, drives climate change (Cox et al., 2000). Depending on the particular combination of driver and response dynamics, they behave as positive or negative feedbacks that amplify or dampen the magnitude and rates of climate change (Cox et al., 2000; Friedlingstein et al., 2003, 2006). Positive and negative feedbacks involve fast processes on land and oceans that expand from seconds to months such as photosynthesis, soil respiration, and net primary production, and slower processes taking decades to millennia such as ocean buffering capacity, ocean circulation, vegetation dynamics and peat formation and decomposition.

During the historical period the biogeochemical processes on land and the combined physical and biogeochemical processes in the ocean have demonstrated a remarkable capacity to keep up with the growth in anthropogenic CO_2 emissions. These processes have maintained a rather constant mean decadal (2008–2017) fraction of the total emissions going into the ocean and land, and with 50% of emissions remaining in the atmosphere (Black and magenta arrows in Figure 5.3; Section 5.2.1.5; Table 5.1). The negative feedback to CO_2 forcing is associated with its impact on the air-sea and air-land CO_2 gradient as well as the internal processes that enhance uptake: the CO_2 fertilisation effect on gross primary production and the buffering capacity of the ocean (Section 5.4.1–4). This negative feedback in the global carbon cycle has slowed the rate of global warming significantly by maintaining the Airborne Fraction of anthropogenic CO_2 at close to 45% Table 5.1. The excess heat generated by an increasing burden of GHGs in the atmosphere is itself partitioned into the ocean (93%) and the residual balance (7%) approximately equally split between atmospheric and terrestrial warming and ice melting (blue arrows: Figure 5.3 (Frölicher et al., 2015)).

The combined effect of these two large scale negative feedbacks of CO_2 and heat is reflected in the Transient Climate Response to cumulative carbon Emissions (TCRE) concept (Section 5.5), which shows that there is a linear relationship between cumulative emissions and global warming, which is used as the basis to estimate the remaining carbon budget (Section 5.5) (MacDougall and Friedlingstein, 2015). A fundamental aspect of TCRE, which makes it independent of the rate is that the ocean dominates both heat and CO_2 uptake rates and maintains the linearity. Future carbon-climate feedbacks yet unknown could break this quasi linear relationship, which relies on the dominance by the ocean CO_2 uptake in driving the airborne fraction in the historical and in the future (see Section 5.5).

[START FIGURE 5.3 HERE]

Figure 5.3: Schematic summarizing the key compartments, processes and pathways that govern historical and future carbon concentration and carbon – climate feedbacks through both terrestrial and ocean systems. Central to this is the influence of both carbon and climate feedbacks on the evolution of the GHG burden in the atmosphere and the airborne fraction of anthropogenic CO_2 (Red circle), which drives the Earth's energy imbalance that is partitioned between the ocean (93%) and the terrestrial residual (7%). The ocean dominates the heat feedback. The airborne fraction that drives this historical climate forcing (~ 44%) is largely regulated by the negative feedback of ocean (22%) and terrestrial (29%) sinks that partition anthropogenic CO_2 (black arrows) in ocean and terrestrial domains (magenta) and result in negative feedbacks (magenta)(partition excludes the estimated imbalance of 0.5PgC: see Table 5.1). Positive feedback processes (Purple arrows) although mostly weak in the historical period, are *likely* to strengthen in the coming decades and are influenced by both carbon and climate forcing simultaneously (Purple). Additional biosphere processes have been included that have an, as yet uncertain feedback bias (Brown arrows). Although this schematic is built around CO_2, the dominant GHG, some of the same processes also influence the fluxes of CH_4 and N_2O from the terrestrial and ocean systems. Those are noted as they contribute to the total radiative forcing.

[END FIGURE 5.3 HERE]

The combined effects of climate and CO_2 concentration feedbacks on the global carbon cycle are predicted by Earth System Models to modify both the processes and natural reservoirs of carbon that are *likely* to result in positive feedbacks (purple arrows in Figure 5.1.3). Examples include *inter alia* permafrost thawing on land and the combined impacts of warming on solubility and decreased buffering capacity in the ocean weakening the terrestrial and ocean carbon sinks (Section 5.4). Assessing our understanding of the mechanisms of contemporary feedbacks and their future dynamics, particularly, the potential for rapidly emerging carbon-climate feedbacks is a key focus of this Chapter.

5.1.3 Paleo trends and feedbacks

Paleoclimatic records extend beyond the noise of recent natural climate oscillations and provide an independent perspective on the links between climate and carbon cycle dynamics. These past changes tended to be slower than the current anthropogenic ones, so they do not provide a direct comparison. Nonetheless, they can help appraise sensitivities and point toward potentially dominant mechanisms of change.

Polar ice cores represent the only archives from which greenhouse concentrations can be directly reconstructed. Major GHGs, CH_4, N_2O and CO_2 generally co-vary, on both orbital and millennial timescales (Schilt et al., 2010b), with higher atmospheric concentrations during warm intervals of the past, suggesting a strong sensitivity to climate.

Major preindustrial sources of CH_4 include wetlands, biomass burning and clathrates (methane hydrates) (Bock et al., 2010, 2017). Stable isotope investigations on CH_4 extracted from Antarctic ice cores, suggest that CH4 emissions were largely controlled by tropical wetland dynamics and seasonally inundated floodplains (Bock et al., 2017). Changes in these sources are steered by variations in temperatures, precipitations and water table as modulated by insolation, local sea-level changes and monsoon intensity. Natural geological emissions, related to the destabilisation of fossil methane hydrates buried in continental margins and permafrost as a result of abrupt warming appear negligible, at least across the glacial termination and the Holocene (Bock et al., 2017; Petrenko et al., 2017).

Pre-industrial atmospheric N_2O concentrations were regulated by microbial production in marine (water column nitrification/denitrification) and terrestrial environments as well as by photochemical destruction in the stratosphere (Schilt et al., 2014). Stable isotope analysis on N_2O extracted from Antarctic and Greenland ice reveal that marine and terrestrial sources were approximately equal across the last glacial termination (Schilt et al., 2014).

Atmospheric CO_2 concentrations are regulated by rapid exchange with terrestrial and surface ocean carbon reservoirs. The dominant process controlling atmospheric CO_2 concentrations on millennial to orbital timescales involve exchange with the voluminous deep ocean reservoir (Jaccard et al., 2016; Rae et al., 2018; Schmitt et al., 2012; Sigman and Boyle, 2000). Stable carbon isotope measurement on CO_2 covering the transition from the last ice age to the Holocene highlight that the reconstructed CO_2 rise was primarily related to CO_2 outgassing from the ocean subsurface, likely due to a weakening of the biological carbon pump and rising ocean temperature and to a lesser degree by carbon sources on land (Bauska et al., 2016; Galbraith and Jaccard, 2015; Schmitt et al., 2012).

CH_4 and N_2O contribute approximately equally to the natural global radiative forcing, but their relative contribution is of secondary importance compared to the radiative forcing imposed by CO_2, which alone represents 80% of the total change in radiative forcing across the last glacial cycle (Köhler et al., 2017; Schilt et al., 2014).

5.1.3.1 High-CO_2 periods

The Pliocene Optimum (4.3-3.3 Ma) and the mid-Pliocene Warm Period (mPWP, 3.2–3.0 Myr ago) in

particular was perhaps the most recent analogue for near future climate (Burke et al., 2018) and thus offers an opportunity to investigate feedback mechanisms operating in a warmer-than-present world (Haywood et al., 2016). Many parallels can be drawn between the mPWP and modern observations as well as future climate projections, due to similar continental configuration, land elevation and ocean bathymetry. During warm intervals of the Pliocene, atmospheric CO_2 concentrations are estimated to have ranged between 350-450 ppm (Martínez-Botí et al., 2015b; Seki et al., 2010). As a result, the global average temperature was about 3-4°C warmer than pre-industrial (Haywood et al., 2016). Generally warmer temperatures were associated with reduced continental ice extent in both hemispheres, with parts of Greenland and Northern Canada being forested (Ballantyne et al., 2006). Increased SSTs combined with altered atmospheric moisture transport (Haywood et al., 2016) supported subarctic North Pacific deep convection and a Pacific meridional overturning circulation. This second Northern Hemisphere overturning cell had important consequences for heat transport and the partitioning of CO_2 between the ocean and atmosphere (Burls et al., 2017). The presence of an active, deep Pacific overturning cell would have contributed to decrease the global ocean CO_2 storage capacity (Burls et al., 2017), further weakening the global efficiency of the biological carbon pump (Sigman et al., 2004) during the mPWP.

Despite generally higher atmospheric CO_2 concentrations, the increase in radiative forcing was relatively moderate (equivalent to ≈ 2 Wm^{-2}) and thus presents a challenge to attribute mPWP warmth the CO_2 alone. Earth climate sensitivity (ECS) to CO_2 -based radiative forcing (Earth System Sensitivity, ESS) was half as strong during the Pliocene as during the colder Pleistocene epoch. The difference is attributed to the radiative impacts of continental ice-volume changes (i.e. ice-albedo feedback) during the late Pleistocene, because ESS was analogue for the two intervals (Lunt et al., 2010). Predictions of ECS for the "Pliocene-like" future are well described by the currently accepted range of an increase of 1.5–4.5 K per doubling of CO_2 (Fischer et al., 2018; Rohling et al., 2012, 2018).

5.1.3.2 Glacial-interglacial changes

The high-resolution Antarctic ice core record covering the past 800,000 years provides an important archive to explore the carbon-climate feedbacks prior to human perturbations (Brovkin et al., 2016). Paleo modelling work suggests that the carbon cycle contributes to globalise and amplify changes in orbital forcing, which are pacing glacial-interglacial climate oscillations (Ganopolski and Brovkin, 2017), with ocean biogeochemistry and physics, terrestrial vegetation, peatland and permafrost all playing a role in modulating the concentration of atmospheric GHGs prior the Industrial era.

Under the generally colder glacial climate, characterised by atmospheric CO_2 concentrations 90±10 ppm (-190±20 GtC) lower than preindustrial levels (Lüthi et al., 2008), interactions between climate and the global carbon cycle were arguably different.

During past ice ages, a generally colder climate state, associated with a weaker hydrological cycle, contributed to a substantial decline of the land biosphere carbon inventory. Early estimates assessing the glacial decrease in the terrestrial biosphere carbon stock vary widely, yet, recent, and arguably more realistic calculations cluster around 300–600 PgC (Ciais et al., 2012; Peterson et al., 2014), possibly 850 PgC when accounting for ocean-sediment interactions and burial (Jeltsch-Thömmes et al., 2018). The large uncertainty reflects a yet limited understanding on how glacially perturbed nutrient fluxes and soil dynamics as well as largely exposed shelf areas in the tropics as a result of lowered sea-level altered carbon inventories.

Vegetation regrowth and increased precipitation in wetland regions associated with the mid-deglacial Northern Hemisphere warming (referred to as the Bolling/Allerod warm interval), in particular in the (sub)tropics, accounts for large increases in both CH_4 and N_2O emissions to the atmosphere (Bock et al., 2017; Schilt et al., 2014). Rapid warming of high northern latitude has also been proposed to have destabilised permafrost, potentially liberating vast quantities of labile organic carbon to the atmosphere (Crichton et al., 2016; Köhler et al., 2014). Isotopic measurements on CO_2 extracted from Antarctic ice suggest, however, that the abrupt release of geological carbon is *unlikely* to have substantially affected the deglacial atmospheric carbon inventory (Bauska et al., 2016; Schmitt et al., 2012) and rather point to a

dominant oceanic source.

Recent estimates suggests deep-sea CO_2 storage during the last ice age exceeded modern values by as much as 750–950 PgC (Jaccard et al., 2009; Sarnthein et al., 2013; Anderson et al., 2019), sufficient to balance the removal of carbon from the atmosphere and the terrestrial biosphere reservoirs combined. A combination of increased CO_2 solubility associated with generally colder oceanic temperatures, altered oceanic alkalinity (Cartapanis et al., 2018; Hoogakker et al., 2018; Yu et al., 2010a); and a generally more efficient biological carbon pump (Galbraith and Jaccard, 2015; Hain et al., 2010; Martinez-Garcia et al., 2014; Ziegler et al., 2013); likely conspired to partition CO_2 into the ocean interior (Anderson et al., 2019). Glacial atmospheric CO_2 concentrations were kept to a temporally consistent lower level of 190±7 ppm, as a result of CO_2 limitation of photosynthesis, either directly or via CO_2-limitation on N_2 fixation (Galbraith and Eggleston, 2017).

The generally gradual increase in atmospheric CO_2 from the last ice age into the Holocene was punctuated by three sub-millennial 10–15 ppm increments (Marcott et al., 2014). These transient CO_2 outgassing events have been associated with the release of CO_2 previously sequestered in the ocean interior (Marcott et al., 2014), possibly via the Southern Ocean (Jaccard et al., 2016; Rae et al., 2018; Schmitt et al., 2012; Skinner et al., 2010). The early deglacial release of remineralised carbon from the ocean abyss coincides with the resumption of the Southern Ocean overturning circulation (Ferrari et al., 2014; Jaccard et al., 2016; Rae et al., 2018; Skinner et al., 2010). The two later pulses are associated with the rejuvenation of the Atlantic Meridional Overturning Circulation (Marcott et al., 2014). The deglacial increase in Atlantic overturning contributed to transfer the locus of remineralised carbon to intermediate depths (Schmittner et al., 2008), which contributed to reduce subsurface dissolved oxygen concentrations thereby substantially increasing marine N_2O emissions (Jaccard and Galbraith, 2012; Schilt et al., 2014).

Coupled glacial-interglacial climate and carbon cycle EMIC simulations were able to reproduce first-order changes in the atmospheric CO_2 content for the first time (Brovkin et al., 2012; Ganopolski and Brovkin, 2017). The most important processes accounting for the full deglacial CO_2 amplitude in the model include solubility changes, changes in oceanic circulation and marine inorganic carbonate chemistry. The impact of the terrestrial carbon cycle, variable volcanic outgassing, and the temperature dependence on the oceanic remineralisation length scale contribute less than 15 ppm CO_2 between the glacial and non-glacial parts of the cycles.

5.1.3.3 Holocene changes

The Holocene (11.7 ka – today) was characterised by relatively stable global climate conditions, despite large changes in insolation. This period of time is characterised by CO_2 concentration levels similar to pre-industrial times. The Early Holocene (11.7–5 ka) warmth is followed by ~0.7°C cooling through the middle to late Holocene (< 5 ka), culminating in the coolest temperatures of the Holocene during the Little Ice Age (LIA), about 200 years ago. This cooling could be associated with ~2°C change in the North Atlantic, possibly linked to a slow-down of the AMOC, although recent palaeoceanographic evidence report stable and vigorous Atlantic circulation throughout the Holocene (Hoffmann et al., 2018). Parallel increase in Southern Ocean circulation and upwelling intensity (Studer et al., 2018), possibly promoted by stronger westerly winds (Saunders et al., 2018), could account for the 20 ppm increase in atmospheric CO_2 concentrations reported for the Holocene.

Peat reservoirs have gradually increased over the Holocene, resulting in long-term sequestration of carbon (Frolking and Roulet, 2007). The Holocene Thermal Maximum rates for net carbon uptake by northern peatlands were clearly higher than those for the cooler late Holocene (Stocker et al., 2017; Yu et al., 2010b) as a result of rapid peat growth during times of ice-sheet retreat and strong seasonality, contributing to maintain Holocene atmospheric CO_2 concentrations changes within limited bounds. Stable carbon isotope values measured on CO_2 extracted from Antarctic ice are consistent with a parallel uptake of carbon by the land biosphere and carbon release from the ocean as a result of enhanced outgassing and carbonate compensation (Elsig et al., 2009; Menviel and Joos, 2012).

5.1.3.4 Past to understand the future

The geological record of past climate variability offers a unique opportunity to document how Earth system processes and feedbacks operated beyond the instrumental record and are fundamental to our ability to adequately project future climate and environmental change. These records have provided key insights in the processes involved in past dynamics of biogeochemical cycles and in the development of understanding and modelling capability.

Paleoclimatic reconstructions reveal profound ecosystem disruptions associated with pulsed CO_2 emissions to the ocean and atmosphere reservoirs in the geologic past, with multiple recent (<23,000 years) instances of rapid increases of 10 to 15 ppm of CO_2 in less than two centuries (Marcott et al., 2014). Importantly, the CO_2 emission rates from paleo records show to be likely one order of magnitude slower that the current anthropogenic change raising concerns about future ecological changes on land and related to ocean acidification (Gattuso et al., 2015) and ocean deoxygenation (Gruber, 2011).

A recent observation-based synthesis of the understanding of past intervals with temperatures within the range of projected future warming suggest that there is low risk of crossing a tipping-point in the climate system leading to large, unpredictable changes in the state of the system for warming of no more than 2°C (Fischer et al., 2018). However, the synthesis also reveals substantial regional impacts, in particular in high-latitude environments, which were more affected by warming owing to polar amplification.

5.2 Historical trends, variability and budgets of CO_2, CH_4, and N_2O

This section describes the trends and variability in atmospheric accumulation, sources and sinks, and the budgets of the three main GHGs CO_2, CH_4 and N_2O during the historical period (1750–2018). Emphasis is placed on the more recent period where understanding is tightly constrained by atmospheric, ocean and land observations. The section also shows the forcing and processes driving the trends, and how variability at the seasonal to decadal scales provide insights on the mechanism governing long term trends and emerging GHG-climate feedbacks.

5.2.1 CO_2: Trends, Variability and Budget

5.2.1.1 Atmosphere

Atmospheric CO_2 concentration measurements in remote (background) locations began in 1957 at the South Pole Observatory (SPO), and in 1958 at Mauna Loa Observatory (MLO) (Keeling et al., 1960). Since then, measurements have been extended to multiple location around the world. CO_2 concentrations grew on average 1.56±0.16 ppm yr^{-1} over the 59 years of atmospheric measurements (1959–2018), with the rate of CO_2 accumulation almost tripling from an average of 0.82±0.28 ppm yr^{-1} during the 1960s to 2.33 ppm yr^{-1} during the most recent decade of 2009–2018 (Dlugokencky and Tans, 2019).

These measurements at very high accuracy and time resolution have been critical for understanding the natural and anthropogenic processes that influence the atmospheric CO_2 trends and variability. The seasonal variation at MLO is observed due to the predominant role of northern hemispheric terrestrial biosphere uptake of CO_2 in summer and release in the winter, while a systematic increase in gradient between MLO and SPO is caused primarily by continuous increase in emissions due to fossil fuel combustion by the industrialised nations in the northern hemisphere (Figure 5.4). Further evidences for the effects of fossil fuel combustion on atmospheric CO_2 increase can be drawn from the simultaneous measurements of stable carbon isotope ($\delta^{13}C$) and O_2/N_2, which show reduction with time because both coal and oil extracted from geological storage are depleted in $\delta^{13}C$ and for every molecule of carbon compounds burned one molecule of oxygen (O_2) is consumed (Figure 5.4b, c; note inverted y-axis; (Goddard et al., 2007). An additional strong

line of evidence for fossil fuel emissions causing CO_2 increase comes from the measurements of radiocarbon (^{14}C) at Wellington, because the fossil fuels of millions of years old carbon are completely devoid of radiocarbon (Turnbull et al., 2017). The naturally occurring radiocarbon abundance (background) in the atmosphere was strongly perturbed by nuclear bomb tests in the 1940s through 1960s that increased the $\delta^{14}C$ abundance until 1965; the high levels gradually decreased back to close to background levels in 2015 due to dilution by the large amounts of ^{14}C avoided-fossil fuel emissions, and also by lost to the ocean interior and to the upper atmosphere (Levin et al., 2010; Suess, 1955).

[START FIGURE 5.4 HERE]

Figure 5.4: Time series of CO_2 concentrations and related measurements in ambient air. All the data are taken from Mauna Loa Observatory (MLO) and South Pole Observatory (SPO) operated by the Scripps Institution of Oceanography (SIO)/University of California, San Diego (Keeling et al., 2001) except for the $\delta^{14}C$-CO_2 (panel b, right y-axis). The $\delta(O_2/N2)$ are expressed in per meg units (= $(FF/M)\times10^6$, where FF = moles of O_2 consumed by fossil-fuel burning, M = 3.706×10^{19}, total number of O_2 molecules in the atmosphere) (Goddard et al., 2007). The $^{14}CO_2$ time series at Wellington, New Zealand (BHD) is provided by GNS Science and NIWA (Turnbull et al., 2017).

[END FIGURE 5.4 HERE]

The evolution of atmospheric CO_2 over the past six decades has also shown a relative unchanged airborne fraction, the fraction of anthropogenic emissions that have accumulated in the atmosphere. That suggest in part that the land and ocean CO_2 sinks have grown at a rate consistent with the growth rate of anthropogenic CO_2 emissions, albeit large inter-annual and sub-decadal variability (Ballantyne et al., 2012; Gruber et al., 2019a; P. Ciais et al., 2019).

5.2.1.2 Anthropogenic CO_2 Emissions

The two anthropogenic CO_2 sources are the combustion fossil fuels and industry, and the net flux from land use, land use change and forestry.

Fossil fuel and industry CO_2 emissions include the combustion of coal, oil and gas covering all sectors of the economy (domestic, transport and industrial use), the production of cement, and industrial processes such as the production of chemicals and fertilisers (Figure 5.5A). Emissions from these sources have grown continuously since the beginning of the Industrial era with short intermissions due to global economic crises or social instability (Peters et al., 2012). Fossil fuel and industry CO_2 emissions were responsible for 86% of all anthropogenic emissions during the most recent decade (2008–2017) and reached 9.9±0.5 PgC per year in 2017; emissions during the 1960s were 3.1±0.2 PgC per year (Le Quéré et al., 2018a).

Since AR5, fossil fuel CO_2 emissions and industry followed a period (2014–2016) with little or no growth (Jackson et al., 2016) (largely due to reductions in coal emissions), after growth rates of 3.2% per year during the 2000s and 1.5% per year for the last decade of 2008–2017. Emission growth has resumed since 2016 (Le Quéré et al., 2018a).

[START FIGURE 5.5 HERE]

Figure 5.5: Global anthropogenic CO_2 emissions: A) Historical trends of anthropogenic CO_2 emission for the period 1870 to 2016. Data sources: (Andrew, 2018; BP, 2018; IEA, 2017; Marland et al.; Quéré et al., 2018). B) The net land use change CO_2 flux (Pg yr^{-1}) from two bookkeeping and 16 dynamic global vegetation models (Le Quéré et al., 2018a). B) Bookkeeping models are BLUE (Hansis et al., 2015; Houghton and Nassikas, 2017) both updated as described in (Le Quéré et al., 2018a). All estimates are unsmoothed annual data. Note that the estimates differ in process comprehensiveness of the models and in definition

of flux components included in the net land use change flux.

[END FIGURE 5.5 HERE]

The net carbon flux from land use and land use change, including management interventions such as forestry, consists of gross sources, such as loss of biomass in deforestation, and gross sinks, such as CO_2 uptake in forest re-growing after harvesting or agricultural abandonment. The net land use change flux relates to direct human interference with the terrestrial vegetation cover, separating it conceptually from carbon fluxes occurring due to interannual variability or trends in environmental conditions (in particular climate, CO_2, nutrient deposition) (Houghton, 2013). Since AR5 progress has been made on attributing large discrepancies between estimates to divergent inclusion of synergistic effects between environmental and land use change, which led to estimates differing up to 50% (Pongratz et al., 2014; Stocker and Joos, 2015) and to large differences of scientific estimates to country's greenhouse gas inventories under the UNFCCC (Grassi et al., 2018). Also, evidence emerged that the net land use change flux might have been underestimated (which would imply an underestimation of the land sink), as DGVMs have mostly included only anthropogenic land cover change, ignoring land management (Pongratz et al., 2018a). Sensitivity studies including management practices find land use emissions increase on average 20–30% for each practice (Arneth et al., 2017), or explain about half of the cumulative loss in aboveground biomass (Erb et al., 2018a).

Industrial-era estimates have been updated routinely in the annual budgets of the Global Carbon Project, which now uses two bookkeeping models (Hansis et al., 2015; Houghton and Nassikas, 2017), with uncertainty estimates from dynamic global vegetation models (Le Quéré et al., 2018a). For the decade 2008–2017 emissions averaged to 1.5 PgC yr^{-1} with an assigned uncertainty of ±0.7 PgC $^{-1}$ (Le Quéré et al., 2018a). A general upward trend since 1850 is halted or inversed during the second part of the 20th century (Figure 5.5B), but trends differ since the 1980s related, among other, to different land use forcings used in (Hansis et al., 2015)/the DGVMs and in (Houghton and Nassikas, 2017) (FAO/FRA-based). A trend from generally lower to higher emission estimates as compared to bookkeeping estimates is expected from the DGVMs as they include the loss of additional sink capacity (Gitz and Ciais, 2003), which is growing with atmospheric CO_2 (Figure 5.5).

Cumulative (preindustrial and industrial-era) losses by land use activities have been estimated based on global compilations of carbon stocks for soils as 116 PgC (Sanderman et al., 2018), with 80 PgC [[Placeholder: confirmation of exact number by Sanderman is coming, just read from figure for now]] of this occurring prior to 1800, and for vegetation as 447 (375–525) PgC. For the latter, a share of 353 (310–395) PgC from prior to 1800 has indirectly been suggested as difference of net biosphere flux and terrestrial sink estimates (Erb et al., 2018). Earth System Models with coral reef formation and peat accumulation support the view that anthropogenic emissions are needed in the last 3 ka to explain the ice-core record (Kleinen et al., 2016), but upper-end scenarios for the extent of agricultural expansion before 1850 CE are found incompatible with the carbon budget thereafter (Stocker et al., 2017). Overall, uncertainties in attributing to processes the CO_2 increase measured from ice-cores between the early Holocene and the beginning of the industrial era are still large (Brovkin et al., 2016; Ruddiman et al., 2016).

Uncertainties related to current estimates of the net land use change flux are still large (Figure 5.5B). Carbon fluxes inferred from atmospheric inversions are used to constrain the temporal evolution of the net land use change flux (Piao et al., 2018a), but inversion products show large differences (Bastos et al., 2016) and can be used for evaluation only for regions where the fluxes due to environmental changes are known with confidence. The latter constraint applies to satellite-based biomass estimates. They have become available covering a number of regions of the globe (e.g., Baccini et al., 2017; Thurner et al., 2014) and can be used to evaluate carbon stock changes, including effects of degradation, but differ from model flux estimates because models include legacy emissions which are not included in remote sensing based estimates.

5.2.1.3 Ocean CO_2: Historical and Contemporary Variability and Trends

It is almost certain that the contemporary (past 50 years) ocean sink of CO_2 is strengthening (1.7±0.5 PgC yr^{-1} to 2.5±0.5 PgC yr^{-1} between early 1980s and the 2000s respectively; (see SROCC Chapter 5: Section 5.2.2.3) in direct response to the growing atmospheric burden of anthropogenic CO_2 corresponding to a multidecadal mean uptake of 25±5% of CO_2 emissions (Le Quéré et al., 2018b). This growing sink both mitigates global warming and drives already observable changes to ocean carbonate chemistry that drive ocean acidification and, though the effect is still small during the contemporary, drive future weakening of the ocean CO_2 sink (Bates et al., 2014; Landschützer et al., 2018; Sutton et al., 2016). Three major advances since AR5 have been the new observational constraints for decadal variability in ocean uptake and storage, and the observation product based changes in pCO_2 seasonal cycle amplitude in response to changing ocean carbonate chemistry (Landschützer et al., 2016, 2018; Rödenbeck et al., 2015; Gruber et al., 2019). These advances were made possible by the simultaneous global coordination of observations and data quality control through the Surface Ocean CO_2 Atlas (SOCAT) and LDEO) and the rapid adoption of a large variety of interpolation techniques for the surface layer and their inter-comparison to constrain uncertainties and biases (Bakker et al., 2016; Gregor et al., 2019; Landschützer et al., 2016; McKinley et al., 2017; Rödenbeck et al., 2015). Similarly, for carbon storage in the ocean interior the Global Ocean Ship-based Hydrographic Investigations Programme (GO-SHIP) coupled to the Global Ocean Data Analysis Project for Carbon (GLODAPv2) were central to supporting the advances in constraining decadal variability (Clement and Gruber, 2018; Lauvset et al., 2016; Olsen et al., 2016).

5.2.1.3.1 Ocean-Atmosphere CO_2 Exchange

Estimates of the ocean sink of CO_2 for the contemporary period have been made on the basis of surface ocean pCO_2 observations with empirical gap-filling interpolations and from Global Ocean Biogeochemistry Models (GOBMS) (Figure 5.6) (Lenton et al., 2013; McKinley et al., 2017). GOBMs simulate ocean circulation and biogeochemistry for recent decades by forcing the models with wind, heat, and freshwater fluxes derived from various atmospheric reanalysis products and at medium to high resolution grids (Aumont and Bopp, 2006; Doney et al., 2009; Hauck et al., 2018; Le Quéré et al., 2010, 2018c; Schwinger et al., 2016).

[START FIGURE 5.6 HERE]

Figure 5.6: Temporal evolution of the globally-integrated sea-air CO_2 flux as reconstructed by (grey/black) ocean physical and biogeochemical models forced with observed atmospheric history (Doney et al., 2009; Schwinger et al., 2016) (Aumont and Bopp, 2006; Hauck et al., 2018; Le Quéré et al., 2010; Paulsen et al., 2017) [[SROCC reference]], and (blue) observationally-based products that represent spatial and temporal variability in the flux from sparse observations of surface ocean pCO_2 (Denvil-Sommer et al., 2018; Gregor et al., 2019; Iida et al., 2015; Landschützer et al., 2016; Rödenbeck et al., 2013; Zeng et al., 2015). Thick lines represent the multi-model mean. Observationally-based products have been corrected for a 0.45 PgC yr^{-1} pre-industrial riverine source of carbon, as in (Le Quéré et al., 2018c). Dark blue box represents the observed range in the 1990s (using a 90% confidence interval, as in Le Quéré et al., 2018b). [[Placeholder: include ensemble from inversion models]]

[END FIGURE 5.6 HERE]

The sea-air CO_2 flux reconstructions from GOBMs span 1959–2017, and are updated every year for the Global Carbon Budget (Le Quéré et al., 2018a). GOBM reconstructions demonstrate that the global ocean carbon sink has grown over past six decades, but also reveal a slowdown in the sink in the 1990s, consistent with that found from the observationally-based products. However, variability in globally-integrated flux from the GOBMs is on average lower than that of the observationally-based and inverse modelled products and characterised by both regional differences and biases in the variability of pCO_2, which can influence the trends and the climate sensitivity in GOBM and ESMs(DeVries et al., 2019; Kessler and Tjiputra, 2016; McKinley et al., 2017; Mongwe et al., 2016, 2018) (Figure 5.6). Moreover, while it *likely* that decadal and interannual modes of variability found in ESMs are linked to natural forcing (Li and Ilyina, 2018a), the

likely link of the 1990–2000 decadal mode to climate forcing in the Southern Ocean points to a likely climate sensitivity linked to the influence of climate on winds but absent in prognostic models (Bronselaer et al., 2018; Gregor et al., 2018; Gruber et al., 2019c; Roobaert et al., 2018; Swart et al., 2014)

For data-based ocean CO_2 flux products, the sparse pCO_2 observations are interpolated in space and time and used in combination with observations of atmospheric pCO_2 and wind products to quantify the sea-air CO_2 flux (Landschützer et al., 2014; McKinley et al., 2017; Rödenbeck et al., 2014, 2015). These observationally-based estimates have provided important new insights into decadal and interannual variability in the global ocean CO_2 sink characterised especially by a slow-down in ocean carbon uptake in the 1990s and a strengthening sink thereafter, which is absent from prognostic models (Figure 5.7; (Gregor et al., 2019; Landschützer et al., 2014, 2015; Le Quéré et al., 2018b; Rödenbeck et al., 2014).

[START FIGURE 5.7 HERE]

Figure 5.7: Regional characteristics of the mean multi-decadal fluxes showing: (a) ocean CO_2 uptake is dominated by the mid-latitude oceans and (b) mid- to high latitudes contributed the most to the decadal invigoration in ocean CO_2 uptake (2000–2016). The trends plotted in the lower panels show that (1) the Southern Ocean is critical to global variability, (2) the tropics are characterised by a strengthening outgassing and 3) most of the inter-model uncertainty arises from the Southern Hemisphere where observations are sparse (Gregor et al., 2019). [[Placeholder: This figure may be changed to means of model types – empirical, inversion, ESM]]

[END FIGURE 5.7 HERE]

The variability and trend of the global ocean – atmosphere exchange of CO_2 is subject to strong regional modulation (Figure 5.7) (Gregor et al., 2019; Landschützer et al., 2014; Rödenbeck et al., 2015). Natural and climate forced modes of regional interannual and decadal variability influence global air-sea CO_2 fluxes, as has been demonstrated in the tropical Pacific and Southern Ocean. The multidecadal mean monthly CO_2 fluxes (1990–2016) highlight regional contrasts in ocean outgassing trends (Tropics) and sink (Mid to High Latitudes) of anthropogenic CO_2 (Figure 5.7). The invigoration of ocean CO_2 uptake (2000–2016) was dominated by the mid and high latitudes, particularly the Southern Ocean,which also dominates the uncertainty (Figure 5.7; The global invigoration was only offset by the tropical outgassing trend mainly in the Pacific Ocean (Franks et al., 2013; Gregor et al., 2018, 2019; Gruber et al., 2019c; Li and Ilyina, 2018b). Model ensembles are still the most widely adopted approach to overcome these biases and uncertainties ((Gregor et al., 2019; Le Quéré et al., 2018a; Li and Ilyina, 2018b).

5.2.1.3.2 Ocean storage of anthropogenic CO_2

It is virtually certain that anthropogenic CO_2 taken up from the atmosphere into the ocean surface layer is further transported at about the same rate into the ocean interior by vertical mixing and overturning circulation including the formation and advection of mode, intermediate and deep waters (DeVries et al., 2017; Gruber et al., 2019b; Nakano et al., 2015; Sallée et al., 2012; Toyama et al., 2017). The total anthropogenic CO_2 stored in the ocean in the Industrial Era has increased by 29 ±8% from 1994 to 2007 to 152±23 PgC in proportion to atmospheric CO_2 increases, showing that the effect of the decrease in the seawater CO_2 buffering capacity and changes in ocean productivity are not yet significant (Gruber et al., 2019a). The most significant advance since AR5 has been the clarification that the global decadal mean trend in storage is subject to strong regional scale variability that points to regional rather than global mean climate sensitivity in respect of carbon subduction into the ocean interior (DeVries et al., 2017; Gruber et al., 2019b; Tanhua et al., 2017). Globally, model results also showed that decadal-scale enhancement in the upper ocean overturning circulation drove a weakened sink in the 1990s, but reversed in the 2000s (DeVries et al., 2017). Based on observations, the increase in global oceanic anthropogenic CO_2 storage between 1994 and 2007 is estimated to be 34±4 PgC (Gruber et al., 2019c; Kouketsu and Murata, 2014), which is 31 ±4% of the total global anthropogenic CO_2 emissions in the same period. When corrected for the losses from the inventory of natural CO_2 due to upwelling in the Southern Ocean and ocean warming (5±3 PgC yr^{-1}) this

yields a mean annual net storage rate of 2.2 PgC yr^{-1} which corresponds closely to the global mean ocean-atmosphere flux of 2.5±0.5 PgC yr^{-1} (Gregor et al., 2019; Gruber et al., 2019b; McKinley et al., 2017; Rödenbeck et al., 2015).

[START FIGURE 5.8 HERE]

Figure 5.8: Map of column inventory change of anthropogenic CO2 between 1994 and 2007 (Gruber et al., 2019c). It shows that regional ocean inventories are dominated by the Mode and Intermediate waters of the Atlantic Ocean and to a letter extent the Indian and Pacific Ocean. Most of the net increase in storage relative to the previous decade is in the Southern Hemisphere reservoirs.

[END FIGURE 5.8 HERE]

The largest inventory increase occurred in the Southern Hemisphere mid-latitudes associated with transport by mode and intermediate waters, in the North Atlantic associated with deep-water formation, and in the shallow overturning region of the western North Pacific (Figure 5.8). In the North Atlantic and in the Indian and Pacific sectors of the Southern Ocean, however, accumulation of anthropogenic CO_2 from 1994–2007 is ~20% smaller than expected from the atmospheric CO_2 increase for the same period (Gruber et al., 2019c). This is attributable to the slow-down of the meridional overturning circulation (Pérez et al., 2013; DeVries et al., 2017; Wanninkhof et al., 2010). By contrast, an acceleration of anthropogenic CO_2 accumulation has occurred in the South Atlantic and South Pacific due to enhanced shallow overturning circulation (Carter et al., 2017; Gruber et al., 2019c). In the North Atlantic, very low anthropogenic CO_2 storage of 1.9±0.4 PgC per decade for 1989–2003 reinvigorated to 4.4 ±0.9 PgC per decade for 2003–2014. This increase in the anthropogenic CO_2 sink is attributed to the changing ventilation pattern associated with the North Atlantic Oscillation (Woosley et al., 2016). Decadal variability in downward transport of anthropogenic CO_2 in the western North Pacific is associated with changes in the formation volume of subtropical mode water linked remotely to the Pacific Decadal Oscillation (Oka et al., 2015; 2019).

5.2.1.4 Terrestrial Carbon: Historical and Contemporary Variability and Trends

5.2.1.4.1 Trend in land-atmosphere CO_2 exchange

The global net land CO_2 sink has been strengthening (*high confidence*) over the past six decades (Ballantyne et al., 2017; Ciais et al., 2018; Keenan et al., 2016; Le Quéré et al., 2018c; Sarmiento et al., 2010). Based on the residual resulting from the mass balance budget with fossil fuel emissions, atmospheric CO_2 growth rate and ocean CO_2 sink estimates, the global net land CO_2 sink increased from 0.3±0.5 PgC yr^{-1} during 1960s to 2.1±0.7 PgC yr^{-1} during 2008–2017 (Le Quéré et al., 2018c). Several lines of evidences consistently show increasing global net land CO_2 sink since 1980s (Figure 5.9), including atmospheric inversion models (e.g. Peylin et al., 2013; Rayner et al., 2015) and Dynamic Global Vegetation Models (DGVMs) (Sitch et al., 2015; Huntzinger et al., 2017).

Carbon uptake by vegetation photosynthesis exerts a first-order control over ecosystem CO_2 balance. Several lines of evidence show enhanced vegetation photosynthesis over the past decades (Figure 5.9), including increasing satellite-derived vegetation greenness (e.g. Mao et al., 2016; Zhu et al., 2016), enlarging seasonal CO_2 amplitude (Forkel et al., 2016a, 2016b; Graven et al., 2013a; Piao et al., 2018c), enhanced water use efficiency (Cheng et al., 2017) and change in atmospheric concentration of carbonyl sulphide inferring increasing photosynthesis CO_2 uptake (Campbell et al., 2017a).

It is *likely* that the increasing strength of global net land CO_2 sink is mainly driven by the fertilisation effect from rising atmospheric CO_2 concentrations (e.g. Fernández-Martínez et al., 2019; O'Sullivan et al., 2019; Schimel et al., 2015; Sitch et al., 2015). Increasing nitrogen deposition (de Vries et al., 2014; Huntzinger et al., 2017) or the synergy between increasing nitrogen deposition and atmospheric CO_2 concentration (O'Sullivan et al., 2019) could have also contributed to the increased sink. The contribution of climate

change to changes of the global net land CO_2 sink is divergent across DGVMs (Huntzinger et al., 2017; Keenan et al., 2016). Sizeable uncertainties remain in attributing change of global net land CO_2 sink due to challenges in reconciling evidences from the scale of the experiments to that of the globe (Fatichi et al., 2019) and from large spatial and inter-model differences in the dominant driving factors affecting the net land CO_2 sink (Fernández-Martínez et al., 2019; Huntzinger et al., 2017).

[START FIGURE 5.9 HERE]

Figure 5.9: Change of net land CO_2 sink, Normalised Difference Vegetation Index (NDVI) and net primary productivity during 1980–2016. Net land CO_2 sink is estimated from the global CO_2 mass balance (Le Quéré et al., 2018c). Inversion Net Biome Productivity (NBP) is the net land CO_2 flux estimated by an ensemble of atmospheric inversion models. Positive net land CO_2 sink and NBP values indicate net CO_2 uptake from the atmosphere. DGVM NBP is the ensemble net land CO_2 flux estimated by 16 Dynamic Global Vegetation Models driven by climate change, rising atmospheric CO_2, land use change and nitrogen deposition change (for carbon-nitrogen models). NDVI anomaly is the anomaly of global area-weighted NDVI observed by AVHRR and MODIS satellite sensors. AVHRR data are available during 1982–2016 and MODIS data are available during 2000–2016. Net Primary Productivity based on the two satellites data have the temporal coverage of 1982–2011 for AVHRR NPP and 2000-2012 for MODIS NPP. DGVM NPP is the ensemble global NPP estimated by the same 16 DGVMs as the DGVM NBP estimates. Shaded area for net land CO_2 sink is the uncertainty range (Le Quéré et al., 2018c). Shaded area for other panels indicates standard deviation of different atmospheric inversions or DGVMs.

[END FIGURE 5.9 HERE]

The long-term increasing trend of net land CO_2 sink has shown an acceleration since 1990s. Different mechanisms, including higher rates of photosynthesis enhancement (Keenan et al., 2016), reduced respiration (Ballantyne et al., 2017), lower land use change emissions (Piao et al., 2018a), and plant regrowth after land use change (Kondo et al., 2018) were proposed to explain the acceleration.

5.2.1.4.2 Interannual variability in land-atmosphere CO_2 exchange

AR5 concluded that Interannual variability of global land-atmosphere CO_2 exchange is dominated by tropical land ecosystems. Since AR5, studies from process and empirical carbon cycle models show that semi-arid ecosystems over the tropics, rather than moist tropical forest ecosystems, have larger contribution to interannual variability in global land-atmosphere CO_2 exchange (Korth et al., 2015; Poulter et al., 2014; Zhang et al., 2018a). The study of mechanisms driving interannual variability of the carbon cycle might help to understand whether and how much the carbon cycle might accelerate or slow down climate warming, with particular interests on the highly responsive tropical carbon cycle to interannual climate anomalies (e.g. Cox et al., 2013a; Fang et al., 2017; Humphrey et al., 2018; Jung et al., 2017a; Malhi et al., 2018; Wang et al., 2014; see Section 5.4.1).

Atmospheric inversions, satellite measurements and DGVMs consistently report that warmer and drier conditions, particularly over El Niño events, reduce the tropical land CO_2 sink (e.g. Bastos et al., 2018; Malhi et al., 2018; Rödenbeck et al., 2018; Wang et al., 2016). The interannual anomalies of atmospheric CO_2 growth rate, resulting mostly from variations in tropical land-atmosphere CO_2 exchange, are more closely correlated with temperature anomalies than with precipitation anomalies (Figure 5.10; Wang et al., 2013, 2014). However, the sensitivity of atmospheric CO_2 growth rate to temperature anomalies varies by two-folds depending on the study period and temperature data used (e.g. Cox et al., 2013a; Humphrey et al., 2018; Jung et al., 2017a; Rödenbeck et al., 2018; Wang et al., 2013, 2014). Anomalies of precipitation or moisture proxies are also significantly correlated with anomalies of land-atmosphere CO_2 exchange (Figure 5.10; Humphrey et al., 2018; Jung et al., 2017a). Distinguishing the relative contribution of moisture and temperature anomalies in carbon cycle variability, remain challenging, not only because of the covariations between anomalies of temperature and that of moisture (Humphrey et al., 2018; Jung et al., 2017a), but also because the sensitivity of land-atmosphere CO_2 exchange to temperature variations is regulated by moisture

conditions (Wang et al., 2014).

[START FIGURE 5.10 HERE]

Figure 5.10: Interannual variation in detrended anomalies of net land CO_2 sink (NLS) and temperature (T) and correlations of NLS anomalies and temperature anomalies at the globe or at the latitudinal bands during 1980–2016. NLS is estimated by atmospheric inversions and Dynamic Global Vegetation Models (DGVMs). Solid lines show model mean detrended anomalies of NLS. The ensemble mean of inversion models or TRENDY models is bounded by the 1–σ inter-model spread in each large latitude band (North 20°N–90°N, Tropics 20°S–20°N, South 90°S–20°S) and the globe. For each latitudinal band, the CO_2 flux anomalies and temperature anomalies were obtained by removing the long-term trend signal and seasonal cycle. Six-month running mean was taken to reduce high-frequency noise. Years on the horizontal axis indicate January of this year as the third month in the moving 6-month window. Correlation coefficients of NLS anomalies and temperature anomalies are shown for each region and two asterisks indicate the 99% significance and one indicates the 95% significance. Grey shaded area shows the intensity of El Niño-Southern Oscillation (ENSO) as defined by the multivariate ENSO index. Two volcanic eruptions (El Chichón eruption and Pinatubo eruption) are indicated with purple dashed lines. A positive flux anomaly means a larger than normal source of CO_2 to the atmosphere (or a smaller CO_2 sink). Net land CO_2 sink are estimated by four atmospheric inversions and thirteen DGVMs respectively (Le Quéré et al., 2018a). Temperature data are from Harris et al., (2014).

[END FIGURE 5.10 HERE]

5.2.1.4.3 Model evaluation

Since AR5, several emergent properties of the carbon cycle, such as decadal change in seasonal and interannual variability of [CO_2] has been proposed as the metrics for evaluating dynamic global vegetation models (DGVMs). The DGVM ensemble mean can generally reproduce the sensitivity of global net land CO_2 sink to interannual temperature variations (γIAV), (Huntzinger et al., 2017; Piao et al., 2013) and the significant increase of seasonal [CO_2] amplitude at boreal (north of 50°N) stations since 1980s (Piao et al., 2018b). The ensemble of 16 DGVMs (Trendy v7, (Le Quéré et al., 2018a)) can robustly reproduce the magnitude and year-to-year variations of land CO_2 sink estimated as the residual of other global carbon budget component. The large model spread, however, indicates uncertainties associated with individual model structure and parameters. The growing capacity of the DGVM ensemble has led to the decision to replace land CO_2 sink estimates from the mass balance residual to independent estimates by the DGVM ensemble ((Le Quéré et al., 2018a).

More processes are being included in DGVMs since AR5. As the major gap identified, nutrient dynamics have now been incorporated in about half of the Trendy DGVMs and growing number of earth system models. The representation of the same nitrogen processes varies greatly among models, leading to large uncertainties in the response of ecosystem carbon uptake to higher atmospheric CO_2 (Walker et al., 2015; Zaehle et al., 2014). Several DGVMs have developed more detailed representation of permafrost carbon cycle process (e.g. Guimberteau et al., 2018; Koven et al., 2015b), though the sensitivity of permafrost carbon storage to climate change remains largely uncertain (McGuire et al., 2016). Models still show biases over intensively managed ecosystems, such as croplands and managed forests (Guanter et al., 2014; Zhu et al., 2016; Thurner et al., 2017), leading to growing DGVM developments to include management practices (Pongratz et al., 2018b; Pugh et al., 2019). Growing numbers and varieties of earth observations are being used for model evaluations, which help identify key processes missing or mechanisms poorly represented in current generation of DGVMs (e.g. Collier et al., 2018).

5.2.1.5 CO_2 budget

The global carbon budget (Figure 5.11, Table 5.1) refers to the perturbation of the carbon budget since the beginning of the Industrial era, circa 1750. The human perturbation prior to the industrial era is considered to

be small based on the small changes in atmospheric CO_2 concentrations. The budget, based on the annual assessment by the Global Carbon Project (Le Quéré et al., 2018a) is constructed for the first time in the IPCC using independent estimates of all major flux components: fossil fuel and industry emissions (E_{FF}), land use change emissions (E_{LUC}), the growth rate of CO_2 in the atmosphere (G_{Atm}), and the ocean (S_{Ocean}) and land (S_{Land}) CO_2 sinks. An imbalance term (B_{Imb}) is required to ensure mass balance of the source and sinks that have been independently estimated: $E_{FF} + E_{LUC} = G_{Atm} + S_{Ocean} + S_{Land.} + B_{Imb.}$

Of the 10.9 $PgCy^{-1}$ emitted from fossil fuels and land use change during the decade of 2008–2017, about 44% remained in the atmosphere (4.7 PgC yr^{-1}), 22% were taken up by the ocean (2.4 PgC yr^{-1}) and 29% were removed by terrestrial ecosystems (3.2 PgC yr^{-1}) (Table 5.1). The budget imbalance of 0.5 $PgCy^{-1}$ suggests modest overestimation of emissions and/or underestimation of the sinks. Land and ocean sinks have increased since 1980, largely in proportion to the growth of anthropogenic emissions, albeit with significant decadal variability associated with major climate and ocean circulation modes.

Over the Industrial era (1750–2017), the cumulative CO_2 fossil fuel and industry emissions were 430±20 PgC, and 235±95 PgC from land use change. Of the total 665 PgC anthropogenic emissions about 41% (275 PgC) accumulated in the atmosphere while the rest were removed and stored, 25% in the oceans (165 PgC) and 32% on land (215 PgC) (Table 5.1).

This budget does not explicitly account for source/sink dynamics due to carbon cycling in the land–ocean aquatic continuum comprising freshwaters, estuaries, and coastal areas. While some estimates suggest that transfers from soils to freshwater systems are significant ((0.78–5.1 PgC yr^{-1}, (Drake et al., 2018; Resplandy et al., 2018) and increasing in response to human activity, an almost equivalent flux is returned to the atmosphere via outgassing in lakes, rivers and estuaries. Thus, the net export of carbon from the terrestrial domain to the open oceans is *likely* to be small (0.1 PgC yr^{-1}, (Regnier et al., 2013)) relative to either the land or ocean sinks and their uncertainty. Accounting for the land-ocean continuum carbon dynamics reduces the size of the of land sink (Regnier et al., 2013).

[START FIGURE 5.11 HERE]

Figure 5.11: The global carbon cycle. Blue arrows represent annual carbon exchange fluxes (in PgC yr^{-1}) associated with the natural carbon cycle estimated for the time prior to the Industrial Era, around 1750. Pink arrows represent anthropogenic fluxes averaged over the period 2008–2017. The rate of carbon accumulation in the atmosphere is equal to net land-use change emissions plus fossil fuel emissions, minus land and ocean sinks (plus a small budget imbalance, Table 5.1). Numbers in white circles represent pre-industrial carbon stocks in PgC. Numbers in dashed circles represent anthropogenic changes to these stocks (cumulative anthropogenic fluxes) since 1750. Anthropogenic net fluxes are reproduced from le Le Quéré et al., (2018c). The relative change of *Gross photosynthesis* since pre-industrial times is estimated as the range of observation-based of 31±3 % (Campbell et al., 2017b) and land-model of 19±12% (Sitch et al., 2015) estimates. This is used to estimate the pre-industrial *Gross photosynthesis*, assuming a present-day range of 116–175 $PgCy^{-1}$ (Joiner et al., 2018). The corresponding emissions by *Total respiration and fire* are those required to match the *Net land flux*. The cumulative change of anthropogenic carbon in the terrestrial reservoir is the sum of carbon cumulatively lost by net land use change emissions, and net carbon accumulated since 1750 in response to environmental drivers (warming, rising CO_2, nitrogen deposition) (Le Quéré et al., 2018a).The change in *Ocean-atmosphere gas exchange* (red arrows of ocean atmosphere gas exchange) is estimated from the difference in atmospheric partial pressure of CO_2 since 1750 (Sarmiento and Gruber, 2006). Individual gross fluxes and their changes since the beginning of the Industrial Era have typical uncertainties of more than 20%, while their differences (*Net ocean flux*) are determined from independent measurements with a much higher accuracy. Therefore, to achieve an overall balance, the values of the more uncertain gross fluxes have been adjusted so that their difference matches the and *Net ocean flux* estimate. The sediment storage is a sum of 150 PgC of the organic carbon in the mixed layer (Emerson and Hedges, 1988) and 1600 PgC of the deep-sea $CaCO_3$ sediments available to neutralize fossil fuel CO_2 (Archer et al., 1998). Note that the mass balance of the two ocean carbon stocks *Surface ocean* and *Intermediate and deep ocean* includes a yearly accumulation of anthropogenic carbon (not shown). Fossil fuel reserves are from (BGR, 2017). Permafrost region stores are from (Hugelius et al., 2014; Strauss et al., 2017) and soil carbon stocks outside of permafrost region from (Batjes, 2016; Jackson et al., 2017) Biomass stocks (range of seven estimates) are from (Erb et al.,

2018b). Fluxes from volcanic eruptions, rock weathering (removal of atmospheric CO_2 in weathering reactions and chemical weathering of C contained in rocks) export of carbon from soils to rivers, burial of carbon in freshwater lakes and reservoirs and transport of carbon by rivers to the ocean are all assumed to be pre-industrial fluxes and are sourced from (Regnier et al., 2013).

[END FIGURE 5.11 HERE]

[START TABLE 5.1 HERE]

Table 5.1: Global anthropogenic CO_2 budget, accumulated since the Industrial Revolution (onset in 1750) and averaged over the 1980s, 1990s, 2000s, as well as the recent decade from 2008. By convention, a negative ocean or land to atmosphere CO_2 flux is equivalent to a gain of carbon by these reservoirs. The table does not include natural exchanges (e.g., rivers, weathering) between reservoirs. Uncertainties represent the 68% confidence interval. All numbers are reproduced from (Le Quéré et al., 2018a).

	1750–2017	1980–1989	1990–1999	2000–2009	2008–2017
Atmospheric increase[a]	275 ± 5	3.4 ± 0.02	3.1 ± 0.02	4.0 ± 0.02	4.7 ± 0.02
Fossil fuel combustion and cement production[b]	430 ± 20	5.4±0.3	6.3±0.3	7.8±0.4	9.4±0.5
Ocean-to-atmosphere flux[c]	-165 ± 20	-1.7 ± 0.5	-2.0 ± 0.5	-2.1 ± 0.5	-2.4 ± 0.5
Land-to-atmosphere flux	20 ± 210	-0.6 ± 1.8	-1.0 ± 1.8	-1.4 ± 1.8	-1.7 ± 1.8
Partitioned as follows					
Net land use change[d]	235 ± 190	1.2 ± 0.7	1.4 ± 0.7	1.3 ± 0.7	1.5 ± 0.7
Terrestrial sink[e]	-215 ± 50	-1.8 ± 0.6	-2.4 ± 0.5	-2.7 ± 0.7	-3.2 ± 0.7
Budget imbalance[f]	5	-0.3	0.2	0.2	0.5

[END TABLE 5.1 HERE]

5.2.2 CH_4: Trends, Variability and Budget

The seasonal to inter–decadal variability in CH_4 in atmosphere is mainly a result of net balance between surface emissions and chemical losses. Atmospheric transport only redistributes the CH_4 variability signal to different parts of the Earth's atmosphere at monthly to annual time scales. The average atmospheric burden of CH_4 is about 5001±54 Tg, with an emission and loss of about 543±18 and 522±8 Tg yr^{-1} during 2007–2016 ($1Tg = 10^{12}g$; 1–σ standard deviation for the interannual variations is shown as the range). About 90% of CH_4 are lost in the troposphere by reaction with hydroxyl (OH) radicals and 6% by soil oxidation, and the rest is transported through the stratosphere-troposphere exchange into the stratosphere where CH_4 is lost by chemical reactions with OH, excited state oxygen (O^1D), atomic chlorine (Cl) (Patra et al., 2016; Saunois et al., 2016). Methane has significant emissions from both natural and anthropogenic origins, but a clear demarcation of their nature is difficult because of the use and conversions of natural ecosystem for human purposes. Methane sources, however, can also be divided into thermogenic, biogenic or pyrogenic processes. The greatest natural sources are wetlands, freshwaters and coastal oceans, while the largest anthropogenic emissions are due to ruminant farming and manure treatment, waste treatment (including landfills), rice cultivation and fossil fuels (Saunois et al., 2016; details in Section 5.2.2.5, Table 5.2). In the past two centuries, CH_4 emissions have significantly exceeded the losses (*virtually certain*), thereby increasing the atmospheric abundance (Dalsøren et al., 2016; Ferretti et al., 2005; Ghosh et al., 2015).

5.2.2.1 Atmosphere

During the period with direct measurements of CH_4 in the atmosphere beginning in the 1970s (Figure 5.12), the increase rate was most rapid at the rate of 18±4 ppb yr^{-1} during 1977–1986 (Rice et al., 2016). The rapid growth was due to the green revolution and fast global industrialisation causing rapid increases in emissions

from ruminant animals, landfills, coal mining, oil and gas exploration, and rice cultivation (Ferretti et al., 2005; Ghosh et al., 2015; Janssens–Maenhout et al., 2017). Due to increases in oil prices in the early 1980s, emissions from gas flaring declined significantly (Stern and Kaufmann, 1996). This is *likely* to explain the first reduction in CH_4 growth rates during 1985–1990. The causes of progress toward a temporary pause in CH_4 increase after 1990 and persistence through 2006 are debated (Dlugokencky, 2003; Steele et al., 1992). CH_4 growth rates were about 6±4 and 0.5±3 ppb yr^{-1} during the 1990s and 2000–2006, respectively. Recent studies suggest a decrease in wetland emissions due to cooler surface temperature under the Mt Pinatubo aerosols in 1991 triggered further reduction in CH_4 growth rate (Bândă et al., 2016; Chandra et al., 2019). The cause of the renewed high CH_4 growth rate since 2007 is highly debated even today (Nisbet et al., 2019), with studies conflicting on the relative contribution of pyrogenic and biogenic emissions (see Cross-Chapter Box 5.1).

[START FIGURE 5.12 HERE]

Figure 5.12: Time series of CH_4 mole fraction (in ppb), growth rate (ppb yr^{-1}) and $\delta^{13}C$ from selected sites from NOAA, AGAGE and PDX surface networks (data sources: Portland State University - PDX; www.esrl.noaa.gov/gmd/ccgg/trends_ch4/; https://agage.mit.edu/data/agage-data). To maintain clarity, data from many other measurement networks are not included here. Global mean values of XCH_4 (total-column) from Greenhouse gases Observation SATellite (GOSAT; www.gosat.nies.go.jp/en/recent-global-ch4.html) are shown. Cape Grim Observatory (CGO) and Trinidad Head (THD) data are taken from the AGAGE network, NOAA global (GL) and northern hemispheric (NH) means for $\delta^{13}C$ are calculated from 10 and 6 sites, respectively. The PDX data adjusted to NH (period: 1977–1996) are merged with THD (period: 1997–2018) for CH_4 concentration and growth rate analysis, and PDX and NOAA NH means of $\delta^{13}C$ data are used for joint interpretation of long-term trends analysis.

[END FIGURE 5.12 HERE]

5.2.2.2 Anthropogenic CH_4 emissions

CH_4 emissions from fossil fuels are mainly attributed to coal, gas, and oil emissions during their excavation, pumping, transport and use (Table 5.2.). Coal mining contributes to about 35% of the total CH_4 emissions from fossil fuels. Top-down estimates of fossil fuel emissions (101 Tg yr^{-1}) are slightly smaller than bottom-up estimates (113 Tg yr^{-1}) during 2010–2017. Both top–down and bottom–up methods suggest that emissions in 2008–2012 have increased from 2002–2006, with the BU method showing a larger increase (17 Tg yr^{-1}) than top–down (7 Tg yr^{-1}) (Patra et al., 2016; Saunois et al., 2016), which can be largely explained by the uncertainties in fugitive emissions from Chinese coal mines (Peng et al., 2016). The latest edition of the Emissions Database for Global Atmospheric Research (EDGAR, v4.3.2; Janssens-Maenhout et al., 2019) is in better agreement with the top-down estimates for the period 2007–2012 but a faster emission increase still persists between 2003–2007. Schwietzke et al. (2016) have suggested, by applying a box model on atmospheric CH_4 and $\delta^{13}C$ data, that methane emissions from natural gas, oil and coal production and their usage are 20 to 60% greater than shown by the inventories and a gradual decrease in fossil fuel emission by about 25 Tg yr^{-1} during 2001–2014.

Enteric fermentation is the greatest source among agricultural CH_4 producing categories, and the largest single greenhouse gases source in the livestock sector (Herrero et al., 2016). Anthropogenic ruminant emissions are driven by anaerobic CH_4 production in livestock rumen (dairy, beef, goats, sheep, etc.). The highest emissions are attributed to cattle, whereas pigs and poultry together contribute to about 20% of the livestock emissions. Ruminant emissions are affected by the type, amount and quality of feeds, energy consumption, animal size and growth rate, production rate, and temperature (Broucek, 2014). CH_4 emissions from ruminants (enteric fermentation and manure) in 2010–2017 equalled to 102 Tg yr^{-1}. The estimate has not changed significantly from that of Saunois et al. (2016), although EDGARv4.3.2 and Food and Agriculture Organisation (Statistics division. Food and Agriculture Organisation of the United Nations, 2018) time series data all show slight but continuous increases since ~2000. AR5 showed that there was a clear increase from 89 Tg yr^{-1} in 2000–2009 period, which is in line with Wolf et al. (2017) who suggested

an increase from 100 to ~120 Tg yr^{-1} in 2000–2011 in total global livestock CH_4 emission. Manure emissions are only about 10% of the enteric fermentation but have been continuously increasing since 2000, with a total of 12 Tg yr^{-1} in 2011 (~11% of the emissions from enteric fermentation). Methane is mainly emitted during the storage of manure, when anoxic conditions are developed (Hristov et al., 2013).

[START TABLE 5.2 HERE]

Table 5.2: Sources and sinks of CH_4 for the 4 recent decades from bottom–up (e.g., inventories, terrestrial models) and top-down estimations (atmospheric inversions) (updated from Saunois et al., 2016; (Etiope et al., 2019; FAOSTAT, 2018; Herrero et al., 2016; Hristov, et al., 2013; Janssens-Maenhout et al., 2019; Poulter et al., 2017; Van Der Werf et al., 2017; Wik et al., 2016; Wolf et al., 2017)). Note that the most top-down estimations cannot distinguish between various source sectors due to limited observations of molecular CH_4 and measurements of carbon and hydrogen isotopes.

	1980-1989		1990-1999		2000-2009		2010-2017	
Tg CH4/yr	Top-Down	Bottom-Up	Top-Down	Bottom-Up	Top-Down	Bottom-Up	Top-Down	Bottom-Up
Natural sources	203 (150-267)	355 (244-466)	182 (230-465)	336 (230-456)	234 (194-292)	382 (255-519)	234 (194-292)	382 (255-519)
Wetlands	167 (115-231)	225 (183-266)	150 (144-160)	206 (169-265)	166 (125-204)	183 (151-222)	166 (125-204)	183 (151-222)
Other Sources	35 (35-36)	130 (61-200)	32 (23-37)	130 (61-200)	68 (21-130)	199 (104-297)	68 (21-130)	199 (104-297)
Freshwater (lakes and rivers)		40 (8-73)		40 (8-73)		122 (60-180)		122 (60-180)
Wild animals		15 (15-15)		15 (15-15)		10 (5-15)		10 (5-15)
Wildfires		3 (1-3)		3 (1-5)		3 (1-5)		3 (1-5)
Termites		11 (2-11)		11 (2-22)		9 (3-15)		9 (3-15)
Geological (inc. Oceans)		54 (33-75)		54 (33-75)		52 (35-76)		52 (35-76)
Hydrates		6 (2-9)		6 (2-9)		2 (0-5)		2 (0-5)
Permafrost (excl. lakes and wetlands)		1 (0-1)		1 (0-1)		1 (0-1)		1 (0-1)
Anthropogenic sources	348 (305-383)	308 (292-323)	372 (290-453)	313 (281-347)	319 (255-357)	338 (329-342)	319 (255-357)	330
Agriculture & Waste	208 (187-220)	185 (172-197)	239 (180-30)	188 (177-196)	183 (112-241)	190 (174-201)	183 (112-241)	193 (163-224)
Enteric fermentation & Manure		85 (81-90)		87 (82-91)		103 (95-109)		102 (87-117)
Landfills & waste		55 (50-60)		65 (63-68)		57 (51-61)		61 (55-70)
Rice		45 (41-47)		35 (32-27)		29 (23-35)		30 (55-70)
Biomass burning & biofuels	46 (43-55)	34 (31-37)	38 (26-45)	42 (38-45)	35 (16-53)	30 (26-34)	35 (16-53)	24
Biomass burning						18 (15-20)		14
Biofuels						12 (9-14)		10 (7-14)
Fossil fuels	94 (75-108)	89 (89-89)	95 (84-107)	84 (66-96)	101 (77-126)	112 (107-126)	101 (77-126)	113 (93-141)
Coal		27 (27-27)		24 (19-28)		36 (24-43)		33 (24-43)
Oil and gas		61 (61-61)		58 (46-67)		74 (62-83)		74 (68-86)
Transport		1 (1-1)		1 (1-1)		1 (1-1)		5 (1-10)
Industry		1 (1-1)		1 (1-1)		1 (1-1)		1 (0-2)
Sinks	511 (460-559)	567 (420-718)	552 (518-581)	599 (530-668)	550 (514-560)	632 (492-785)	550 (514-560)	632 (492-785)
Total chemical loss	490 (450-533)	539 (411-671)	525 (491-554)	571 (521-621)	518 (510-538)	604 (483-738)	518 (510-538)	604 (483-738)
Tropospheric OH		468 (382-567)		479 (457-501)		528 (454-617)		528 (454-617)
Stratospheric loss		46 (16-67)		67 (51-83)		51 (16-84)		51 (16-84)
Tropospheric Cl		25 (13-37)		25 (13-37)		25 (13-37)		25 (13-37)
Soil uptake	21 (10-27)	28 (9-47)	27 (27-27)	28 (9-47)	32 (26-42)	28 (9-47)	32 (26-42)	28 (9-47)
Sum of sources	551 (500-592)	663 (536+789)	554 (529-596)	649 (511-569)	553 (526-569)	719 (583-861)	553 (526-569)	712
Sum of sinks	511 (460-559)	567 (420-718)	552 (518-581)	599 (530-668)	550 (514-560)	632 (492-785)	550 (514-560)	632 (492-785)
Imbalance	30 (16-40)		12 (7-17)		3 (-3-19)		3 (-3-19)	
Atmospheric growth rate	34		17		6			

[END TABLE 5.2 HERE]

5.2.2.3 Land biospheric emissions and sinks

Freshwater wetlands are the single largest global source of CH_4 into the atmosphere, accounting for about 30% of the total CH_4 source (*medium agreement, robust evidence*). Bottom-up and top-down estimates for 2010–2017 are 183 and 166 Tg CH_4 yr^{-1}, respectively, with a top-down uncertainty range of 125–204 Tg CH_4 yr^{-1} (updated from (Saunois et al., 2016)). The large uncertainties stem from challenges in mapping wetland area and temporal dynamics, and in scaling methane production, transport, and consumption processes, that are measured with small chambers or flux towers, to landscape estimates (Pham-Duc et al., 2017). Both the top-down and bottom-up estimates presented in Saunois et al. (2017) indicate little increase in wetland CH_4 emissions during the last three decades but are slightly smaller than in AR5. It is *likely* that the bulk of the post–2006 increase in atmospheric CH_4 concentration should be attributed to sources other than wetlands, but their role cannot be totally ruled out. The evidence from land-surface models (Poulter et al., 2017), isotopic $^{13}CH_4$ data (Schaefer et al., 2016) and inverse modelling (Patra et al., 2016) together suggest that sources other than wetlands are mainly responsible for the increase from 2002–2006 to 2008–2012. The biogenic methane fluxes due to enteric fermentation, waste and manure management are also

depleted in ^{13}C.

Although significant direct production of CH_4 by vegetation is considered *uncertain* and *unlikely*, there is emerging evidence of the role of trees in transporting and conducting CH_4 from soils into the atmosphere, which is potentially relevant considering global budget, particularly in tropics and in forested wetlands of temperate region (Pangala et al., 2017).

Rice is typically cultivated in flooded soils which makes rice fields significant CH_4 sources. Emissions from rice cultivation tended to decrease from about 42 Tg yr^{-1} in the 1980s to about 33 Tg yr^{-1} in 2003 but have increased gradually by about 20% between 2003 and 2012 as per EDGARv4.3.2 (*low agreement, limited evidence*). Emissions are partly affected by climate, elevated CO_2 in atmosphere and site-specific soil C content, but can, to a large extent, be controlled by modifying management-related factors such as organic amendments, water management (from intermittent irrigation to continuous flooding), use of inorganic and organic fertilizers, and rice cultivars (Feng et al., 2013; Jiang et al., 2017; Liu et al., 2017; Oo et al., 2018; Yang et al., 2018).

Biomass burning and biofuel consumption, causing an emission of at least 24 Tg CH_4 yr^{-1} constitute a large fraction, up to about 8%, of global anthropogenic CH_4 emissions (*likely*). Wildfires comprise a small CH_4 source globally, with 3 Tg yr^{-1} being liberated into the atmosphere. The satellite observed burned area anomaly provided critical information for estimation of open biomass burning, which showed tight link with the natural climate variability, e.g, ENSO and explained a large part of the interannual variability in atmospheric CH_4 (Patra et al., 2016; Saunois et al., 2017; van der Werf et al., 2017). CH_4 emissions from biomass burning show a decreasing trend during past two decades (van der Werf et al., 2017; Worden et al., 2017). There is recent evidence from the tropics that fire occurrence is non-linearly related to the precipitation, implying that severe droughts will increase CH_4 emissions from fires, particularly from the degraded peatlands (Field et al., 2016).

Microbial methane uptake by soil comprises about 5% of the total chemical CH_4 sink (Table 5.2). In AR5, the methane uptake by microbial oxidation in upland soils during three decades was reported to increase and stay unchanged according to top-down and bottom-up estimates, respectively. Saunois et al. (2016) report similar increase but suggest revised, higher uptake rates. Recently a decreased sink in forest soils, explained by higher precipitation, has been observed using direct observations (Ni and Groffman, 2018).

5.2.2.4 Ocean and freshwater emissions and sinks

Coastal oceans, fjords and mud volcanos are the major source of CH_4 in marine environment and measurement of CH_4 fluxes are sparse. However, there are increasing amount of evidence of CH_4 seepage from the Arctic shelf, possibly triggered by the melting of geological storage in the sediments, permafrost and hydrates (Shakhova et al., 2010, 2017). These emissions are estimated to be 2–9 Tg yr^{-1}, and although they are *likely* to increase in a warmer world, the current flux is l*ikely* to be a mix of pre-industrial and climate change-driven fluxes. All geological sources, including the coastal oceans and fjords around the world are estimated to emit CH_4 in the range of 35–76 Tg yr^{-1} (Etiope et al., 2019). There are evidence that the ventilation of geological CH4 is *likely* to be smaller than about 15 Tg yr^{-1} (Petrenko et al., 2017). A lower geological CH_4 ventilation will reduce the gap between top-down and bottom-up estimations.

Freshwater (lakes, rivers, streams, ponds, estuaries) emissions are proportionally the largest source of uncertainty in the CH_4 budget. Since AR5, the estimate of freshwater CH_4 source has been revised from 40 to ~122 Tg yr^{-1} with the availability of more observational data and improved areal estimates (Saunois et al., 2016). The freshwater CH_4 emission remains unaccounted in the top-down models, leading to the largest gap in bottom-up and top-down budgets of global CH_4 (Table 5.2). The very large uncertainty in the global CH_4 emission from freshwaters is attributed to the large spatial and temporal variation in lake and river CH_4 fluxes (Natchimuthu et al., 2017; Wik et al., 2016) and uncertainties in global area of them (Allen and Pavelsky, 2018). It is *very likely* that the estimates of the emissions from freshwaters and wetlands are partially overlapping (Thornton et al., 2016), explaining some part of the gap in bottom-up and top-down

budgets.

5.2.2.5 CH_4 budget

A summary of top-down and bottom-up estimations of CH_4 emissions and sinks for the period 2010–2017 are depicted in Figure 5.13 (details in Table 5.2). Since AR5, the uncertainty in sectorial emissions have reduced significantly, except for the emissions from freshwaters (60–180 Tg yr^{-1}). Presently freshwater emissions are not considered in the top-down model simulations. The decadal mean CH_4 burden increase has been about 42, 17, 6 and 20 Tg yr^{-1} in the 1980s, 1990s, 2000s and 2010s, respectively as can be estimated from observed atmospheric increase (*virtually certain*). It is *very likely* that the inter-decadal differences in CH_4 growth rate is driven by changes in emissions rather than the OH variability. Variability in OH is very uncertain and is *likely* to be of some importance at interannual or shorter time scales (Chapter 6 and Cross-Chapter Box 5.1).

[START FIGURE 5.13 HERE]

Figure 5.13: Schematic diagram of major sources and sinks of CH_4 for the decade 2010–2017. Values and data sources as in Table 5.2.

[END FIGURE 5.13 HERE]

[START CROSS-CHAPTER BOX 5.1 HERE]

Cross-Chapter Box 5.1: Drivers of methane changes during 1980–2017

Atmospheric methane (CH_4) growth rate varied widely over the past three decades. The mean growth rate decreased from 15±5 ppb yr^{-1} in the 1980s to 0.5±3 ppb yr^{-1} during 2000–2006 (the so-called quasi-equilibrium phase) and returned to a rate of 7±3 ppb yr^{-1} in the past decade (2008–2017) (based on data in Figure 5.12). Over the last four years (2014–2017), atmospheric CH_4 grew sharply at rates not observed since the 1980s (Nisbet et al., 2019), a period that included a prolonged El Niño condition covering 2014–2015. CH_4 growth rates are observed to be high during El Niño. Because of large uncertainties in both the emissions and sinks of CH_4, it has been challenging to quantify accurately the methane budget and ascribe reasons for the growth over the past decade. To address greenhouse gas mitigation, it is critical to know if changes are related to emissions from human activities, which once identified could be reduced, or from natural processes responding to changing climate. Due to these uncertainties, projections of atmospheric methane considered in AR5 and the IPCC 1.5ºC Special Report (IPCC, 2018a) did not anticipate this renewed growth after a period of stabilisation (Ciais et al., 2013; Rogelj et al., 2018). A sustained growth of CH_4 at rates similar to those observed over the past decade might lead to higher temperatures (Saunois et al., 2016) and challenges countries ability to meet the Paris agreement goal of keeping global average temperature well below 2°C (Nisbet et al., 2019).

Cross-Chapter Box 5.1 Figure 1 shows the decadal CH_4 budget derived from the Global Carbon Project (GCP)-CH_4 synthesis for 1980s, 1990s and 2000s (Kirschke et al., 2013), and for 2010-2017 (update from Saunois et al., 2016). The natural sources include emissions from natural wetlands, lakes and rivers, geological (on shore), wild animals, termites, wildfires, permafrost soils, and oceans (offshore and hydrates). Anthropogenic sources include emissions from enteric fermentation and manure, landfills and waste, rice cultivation, coal mining, oil and gas industry, biomass and biofuel burning. The top-down total sink determined from global mass balance, includes loss due to hydroxyl (OH), atomic Cl, O^1D, and soil oxidation.

[START CROSS-CHAPTER BOX 5.1, FIGURE 1 HERE]

Cross-Chapter Box 5.1, Figure 1: Methane budget estimates for four decades from top-down (light colour, left) and bottom-up (dark colour, right) analyses (plotted on the left y axis). Sources are positive and sinks are negative. The black dots represent observed global monthly mean atmospheric CH_4 dry-air mole fractions for 1983–2017 (Dlugokencky et al.) (www.esrl.noaa.gov/gmd/ccgg/trends_ch4) and the solid black line represents the smoothed global monthly means (plotted on the right y axis). The bottom-up total sinks are inferred from the global mass balance (i.e., source minus growth) and not directly computed. [[Placeholder: To be updated]].

[END CROSS-CHAPTER BOX 5.1, FIGURE 1 HERE]

Since AR5, a large number of studies have discussed the role of emissions in explaining the recent increase in CH_4 growth rate since 2007 and a fairly coincident decrease of $\delta^{13}C$-CH_4 and δD-CH_4 isotopes (Figure 1). Both C and H isotopes in CH_4 emissions are enriched in thermogenic (e.g., coal, oil and gas) and pyrogenic (biomass burning), and depleted in biogenic (e.g., wetlands, rice paddies, enteric fermentation, landfill and waste) sources. Proposed hypotheses for CH_4 growth (2007–2017) vary from a decrease in thermogenic and increase in biogenic emissions (Schwietzke et al., 2016), an increase in wetland and other biogenic emissions (Nisbet et al., 2016), emissions increase from agriculture in tropics (Schaefer et al., 2016), a reduction in pyrogenic and increase in thermogenic emissions (Worden et al., 2017) or emission increase from biogenic sources and a slower increase in emissions from thermogenic sources compared to inventory emissions (Patra et al., 2016; Saunois et al., 2017). Ethane (C_2H_6), the 2nd most abundant hydrocarbon after CH_4 in the remote atmosphere, also help understanding the decrease in CH_4 growth rate during the 1980s and 1990s due to decreasing fugitive emissions from venting and flaring of natural gas in oil fields (Simpson et al., 2012).

A few studies have emphasised the role of OH, the primary sink of methane, in driving changes in the growth of atmospheric methane abundance, in particular after 2006. Atmospheric box-model studies using measurements of methyl chloroform (CH_3CCl_3), methane and $\delta^{13}C_{CH4}$ infer larger variability in OH – increasing by ~7%–10% in the 1990s and early 2000s and then a decline of ~7%–11% up to 2014 (Rigby et al., 2017; Turner et al., 2017). However, [OH] trends in both studies have large uncertainties arising from uncertainty in CH_3CCl_3 emissions, e.g., the full range of OH trends and variability is within their estimated uncertainty range (Rigby et al., 2017), and possibly likely from the inherent configuration of their box modelling framework (Naus et al., 2019). Another study applying 3-dimensional inverse modelling with observations of methane and $\delta^{13}C_{CH4}$ finds a smaller decline (~2%) in OH post-2007 and a consequent smaller role of OH in the post-2006 methane growth (McNorton et al., 2018). Similarly, studies applying simple multi-species inversion (Thompson et al., 2018) as well as empirical method using a variety of observational constraints based on OH chemistry (Nicely et al., 2018) did not find any trends in OH significant enough to play role in methane changes over the last three decades. On the contrary, global chemistry-climate models based on fundamental principles of atmospheric chemistry simulate an increasing trend in OH (more than 8%) over the past three decades with small interannual variability (Dalsøren et al., 2016). Due to uncertainties and contradictions in the temporal evolution of OH derived from inverse box models as well as from global chemistry-climate models (Section 6.2.3) there is *low confidence* in the role of OH changes in driving the observed methane changes.

Methane emissions corresponding to their best OH estimates (Rigby et al., 2017; Turner et al., 2017), require increase sharply by up to about 40 Tg yr^{-1} in the mid-2000s and stay stable or decrease slightly afterwards. The sharp increase is inconsistent with anthropogenic inventory emissions estimated for farmed animals, fossil fuel industry and waste management (e.g., Janssens-Maenhout et al., 2019). However, a more consistent picture emerges for the regional trends of emission rates from high-resolution inverse modelling, where observations from individual sites are utilised to optimise subcontinental scale CH_4 emissions (Cross-Chapter Box 5.1 Figure 2). Because the emissions are optimised at monthly or shorter time scales, the effect of OH inter-annual variability does not strongly influence the determination of regional emission trends. CH_4 lifetime in any latitude band is one year or longer, and its global mean lifetime is about 9 years; both much longer than the mixing timescales of regional emissions hemispherically (~weeks). Cross-Chapter Box 5.1 Figure 2 suggests that progress toward atmospheric CH_4 quasi-equilibrium was primarily driven by

reductions in emissions in Europe, Boreal Asia and Temperate North America over 1988-2000. In the global totals, emissions equalled loss in the early 2000s. The recent growth since 2006 is driven by emissions from East Asia (1997–2016), West Asia (2005–2016), Brazil (1988–2016), temperate North America (2010–2016), Northern Africa (2015–2016). A recent study using a variety of sensitivity simulations by changing OH, provides further evidence for strong link between the emissions and CH_4 growth rate at inter-decadal time periods, and only minor role of OH on the interannual CH_4 variability (Chandra et al., in prep).

[START CROSS-CHAPTER BOX 5.1 FIGURE 2 HERE]

Cross-Chapter Box 5.1, Figure 2: Anomalies in regional CH4 emissions during 1988-2016. Results for 2000-2016 are shown for 8 inversion models that participated in GCP-CH4 budget assessment (update from Saunois et al., 2017), and results for 1988-1999 are available from only one inversion (Chandra, in prep). A long-term mean is subtracted from the annual-mean time series for the calculation of anomalies for each region.

[END CROSS-CHAPTER BOX 5.1, FIGURE 2 HERE]

Although a consensus on the inter-decadal variability of OH could not be achieved using box modelling of CH_3CCl_3 and chemistry-climate model simulations, there is strong evidence from inventory emissions at country level and regional inverse modelling that CH_4 growth rate variability during the 1980s through the 2010s is closely linked with anthropogenic activities (*likely, medium agreement*). Isotopes and inventory data suggest that both fossil fuels and agriculture are *likely* playing a role in the resumed CH_4 growth and trends since 2007. Shorter-term variability is predominantly driven by the El Niño Southern Oscillation cycles, and *very likely* associated with emissions from wetland and biomass burning, and loss due to OH. By synthesising all available information regionally from a priori emissions and inverse modelling (top-down observation constraints), the capacity to track "changes" in natural and anthropogenic emissions is developed. For example, emissions inventory data suggest increase in emissions from East Asia and Temperate North America are primarily of industrial origin, while the emission increase from West Asia, Southeast Asia and Brazil are driven by agricultural sectors.

[END CROSS-CHAPTER BOX 5.1 HERE]

5.2.3 N_2O: Trends, Variability and Budget

5.2.3.1 Atmosphere

The present-day level of atmospheric abundance N_2O, of 329.7 ppb (parts per billion) for 2017, is 22% higher than preindustrial levels (Figure 5.14), (Elkins et al., 2018; MacFarling Meure et al., 2006b; Prinn et al., 2016)). Direct atmospheric measurements of N_2O are available from the late 1970s, and are currently recorded at more than 140 surface sites, ship tracks, and aircraft profiles (Thompson et al., 2014). Prior to this, atmospheric N_2O has been indirectly observed by firn air samples and ice cores (MacFarling Meure et al., 2006). Combined firn ice air and atmospheric measurements show that the 15N/14N isotope ratio, as well as the 15N site preference, in N_2O has changed since 1940 (Figure 5.14b, c) (Ishijima et al., 2007; Park et al., 2012; Prokopiou et al., 2017). This change indicates that the N-substrate available for nitrification and denitrification, and the relative contribution of nitrification to the global N_2O source have *very likely* increased. Both of these phenomena are *very likely* associated with increased fertiliser use in agriculture (Park et al., 2012).

Since the late 1990s, atmospheric measurements with high accuracy and density show an average

atmospheric growth rate of 0.83±0.01 ppbv yr^{-1} (1998 to 2017, Figure 5.14a). The growth rate exhibits large interannual variations and shows an increase of nearly 20% between the decade 1998 to 2007 and the most recent decade (2008 to 2017; 0.94±0.01 ppbv yr^{-1}) (Elkins et al., 2018)). This growth rate is higher than during 1970–2000 of 0.6–0.8 ppbv yr^{-1} (Ishijima et al., 2007) and for the thirty-year period prior to 2011 (0.73±0.03 ppb yr^{-1}), as reported by AR5. In the tropics and sub-tropics, inter-annual variations in the growth rate are negatively correlated with the multivariate ENSO index (MEI) (Ishijima et al., 2009; Thompson et al., 2013) (Figure 5.14). This is *likely* associated with reduced tropical N_2O emissions from land related to a reduction in precipitation in the tropics and sub-tropics (Werner et al., 2007), and ocean, due to reduced upwelling in the eastern tropical Pacific (Nevison et al., 2007) during El Niño conditions. In the mid to high latitudes of both hemispheres, inter-annual variations in the seasonal minima of N_2O abundance are correlated with anomalies in the winter-spring temperature of the lower stratosphere (Nevison et al., 2011). This suggests that inter-annual variations in the stratosphere to troposphere air mass transport, coupled with the stratospheric depletion of N_2O, contribute to the inter-annual variability of atmospheric N_2O in the mid to high latitudes. However, the quantitative understanding of the processes influencing the inter-annual variations of natural N_2O emissions and tropospheric abundance is poor.

[START FIGURE 5.14 HERE]

Figure 5.14: (a) Atmospheric N_2O abundance (parts per billion, ppb) and growth rate (ppb yr^{-1}), (b) δ15N of atmospheric N_2O, and (c) alpha-site 15N–N_2O, based on direct atmospheric measurements in the AGAGE and NOAA (Elkins et al., 2018; Hall et al., 2007; Prinn et al., 2000, 2016) networks, archived air samples from Cape Grim, Australia (Park et al., 2012), and firn air from NGRIP Greenland and H72 Antarctica (Ishijima et al., 2007), and Law Dome Antarctica (Park et al., 2012). Grey shading in (a) are times of positive values of the multivariate ENSO index, indicating El Nino conditions (Wolter and Timlin, 1998).

[END FIGURE 5.14 HERE]

5.2.3.2 Anthropogenic N_2O emissions

5.2.3.2.1 Agricultural sources

Agriculture is the largest anthropogenic source of N_2O emissions and emits 3.8 (3.0–5.2) TgN yr^{-1} (average 2007–2016), owing to the widespread use of nitrogen fertiliser and manure on cropland and pasture, manure management, and aquaculture (see Table 5.3 (Bouwman et al., 2013; Dangal et al., 2019; Janssens-Maenhout et al., 2017; Tian et al., 2019; Winiwarter et al., 2010). The global total emission from aquaculture due to nitrogen enrichment in inland and coastal waters (Williams and Crutzen, 2010) is estimated to be 0.05 (0.02–0.23) TgN yr^{-1} for 2010 (Bouwman et al., 2013). Estimates of agricultural emissions are either based on empirical emission factors (De Klein et al., 2006; Smith et al., 2012) or process-based modelling (Tian et al., 2016). Research since AR5 has demonstrated that both approaches are subject to large uncertainties regarding the extrapolation of data in space and time and the ability to adequately account for the heterogeneity in environmental factors affecting emissions (Gerber et al., 2016; Shcherbak et al., 2014; Wagner-Riddle et al., 2017; Zhou et al., 2015). Agricultural N_2O emissions have increased by approximately 80% since the early 1900s, and by 30% since the 1980s. Increased use of nitrogen fertiliser and manure contributed to about 70% of the increase, followed by manure application in pasture/range/paddock (20%) and manure management (10%) during 1980–2016

[START FIGURE 5.15 HERE]

Figure 5.15: Trends in the N_2O emissions from terrestrial soils (natural and agriculture) simulated from the NMIP ensemble of terrestrial biosphere models (Tian et al., 2019). The effect of anthropogenic nitrogen additions (atmospheric deposition, manure addition, fertiliser use) is evaluated against the background flux driven by changes in atmospheric CO_2 concentration, climate change, and land cover change. The map in the centre shows the ensemble average of the decadal mean N_2O emissions for 2007–2016 including all forcings.

[END FIGURE 5.15 HERE]

5.2.3.2.2 Non-agricultural sources

The principal non-agricultural anthropogenic sources of N_2O are industry, specifically chemical processing, combustion of fossil fuels and biomass, and wastewater. Industrial emissions of N_2O are mainly due to nitric and adipic acid production, in which N_2O is a by-product (Bouwman et al., 2013). Since the wide-spread installation of abatement technologies in the 1990s, the emissions from industrial sources have decreased by 24% to approximately 0.22 TgN yr^{-1} in 2007 (Janssens-Maenhout et al., 2017; Lee et al., 2011; Pérez-Ramírez et al., 2003). Fossil fuel combustion emissions from stationary sources, such as power plants, amount to 0.48 (0.32–0.80) TgN y-1, with smaller contributions from mobile sources such as road transport 0.095 ± 0.042 TgN y-1 (Bouwman et al., 2013) and aviation 0.020 ± 0.005 TgN yr^{-1} (Graham et al., 2009; Heland and Schäfer, 1998; Wiesen et al., 1994, 1996).

Wastewater sources of N_2O result from chemical and biological transformations in the water, which can occur at the time of its treatment or when it is discharged to inland or coastal waters (Law et al., 2012). Wastewater N_2O emissions, including those from domestic and industrial sources are estimated to be 0.16 (0.02–0.77) TgN yr^{-1} for the year 2010 (Bouwman et al., 2013). Biomass burning releases N_2O during the combustion of organic matter. Biomass burning emissions include those from crop residue burning, grassland, savannah and forest fires, as well as biomass burnt in household stoves, and have contributed around 0.7 (0.5–1.7) TgN yr^{-1} (Bouwman et al., 2013) .

5.2.3.3 Ocean and freshwater emissions

N_2O is produced in the sub-surface ocean during remineralisation of organic matter via the primary pathways of nitrification and denitrification. Net N_2O production from these processes is sensitive to local oxygen concentration. In the oxic ocean (> 97% of ocean volume), nitrification is believed to be the primary N_2O source (Freing et al., 2012). In sub-oxic ocean zones where denitrification prevails, higher N_2O yields and turnover rates make these regions potentially significant sources of N_2O (Arévalo-Martínez et al., 2015; Babbin et al., 2015; Ji et al., 2015). Recent estimates of the global ocean N_2O source derived from ocean biogeochemistry models are 3.8±1.6 TgN yr^{-1}, and slightly lower than some of the earlier empirically based-methods (Battaglia and Joos, 2018; Bianchi et al., 2012; Buitenhuis et al., 2018; Landolfi et al., 2017; Manizza et al., 2012; Martinez-Rey et al., 2015; Suntharalingam et al., 2012). N_2O processes in coastal upwelling zones are only poorly represented in these global estimates (Kock et al., 2016), but may account for 0.2 to 0.6 TgN yr^{-1} of the global ocean source (Nevison et al., 2004; Seitzinger et al., 2000).

The relative proportion of ocean N_2O from oxygen-minimum zones is *highly uncertain* (Zamora et al., 2012). Estimates derived from in-situ sampling, particularly in the eastern tropical Pacific, suggest significant fluxes from these regions, and potentially up to 50% of the global ocean source (Arévalo-Martínez et al., 2015; Babbin et al., 2015; Codispoti, 2010). However, recent global-scale analyses estimate lower contributions (4 to 7%, Battaglia and Joos, 2018; Buitenhuis et al., 2018). Further investigation is required to reconcile these estimates and provide improved constraints on the N_2O source from low-oxygen zones.

Anthropogenic N-deposition on oceans can stimulate marine productivity and influence ocean emissions of N_2O. Recent ocean model analyses suggest a relatively modest global potential impact of 0.01–0.32 TgN yr^{-1} (pre-industrial to present-day) equivalent to 0.5% – 3.3% of the global ocean N_2O source (Jickells et al., 2017; Landolfi et al., 2017; Suntharalingam et al., 2012). However, larger proportionate impacts are predicted in nitrogen-limited coastal and inland waters down-wind of continental pollution outflow (Jickells et al., 2017; Suntharalingam et al., 2012).

5.2.3.4 Land emissions and sinks

5.2.3.4.1 Soils under non-agricultural vegetation and surface sinks

Soils are the largest natural source of N_2O, arising from nitrogen processing associated with nitrification and denitrification (Butterbach-Bahl et al., 2013). Ensemble simulations with process-models suggest a present-day source of 6.7±1.4 TgN yr^{-1} from non-agricultural soils during the period 2007–2016, with a large range between models due to alternative process formulations and lacking data to constrain the model ranges (Tian et al., 2019). This estimate is in broad agreement with the previous assessment based on empirical upscaling in AR5 but allows separating the natural N_2O source from the anthropogenic increase in N_2O emissions due to nitrogen enrichment following chronic nitrogen deposition (Figure 5.16 and Table 5.3). The largest source of natural terrestrial N_2O emissions is in the tropics, 4.3 TgN yr^{-1} for 23.5°N-23.5°S during the period 1980–2016. Model simulations do not suggest a trend over this time, but do not account for increased N_2O emissions from tropical peatland due to land-use change (Hadi et al., 2000). Simulated N_2O emissions from the mid latitudes (23.5°–55°) show a gradual increase from 1.7 TgN yr^{-1} in the 1980s to 2.1 TgN yr^{-1} during 2007–2016 due to a combination of climatic variability and change, and Nr deposition (Tian et al., 2019; Zaehle et al., 2011). Boreal and arctic regions (>55°) contribute little to the overall natural N_2O flux (0.3 TgN yr^{-1} during 1980–2016). New field instruments with high sensitivity and precision confirmed that under some conditions soils can act as small sinks of N_2O (Davidson, 2015). However, global soil N_2O uptake is not *likely* to exceed 0.3 TgN yr^{-1} (Schlesinger, 2013).

5.2.3.4.2 Inland water bodies and Estuaries

Inland waters are generally sources of N_2O as a result of nitrification and denitrification of dissolved inorganic nitrogen (DIN). Based on improved emission factors, their spatio-temporal scaling, and consideration of transport within the aquatic system, recent studies, point to lower range of emissions than AR5 of 0.3 TgN yr^{-1} (range: 0.1–1 TgN yr^{-1}) resulting from for inland waters, including 0.01–0.07 TgN yr^{-1} for rivers (Hu et al., 2016; Maavara et al., 2019), 0.02–0.07 TgN yr^{-1} for reservoirs (Deemer et al., 2016; Maavara et al., 2019), and 0.06–0.9 TgN yr^{-1} for estuaries (Maavara et al., 2019; Murray et al., 2015).

5.2.3.5 N_2O budget

[START FIGURE 5.16 HERE]

Figure 5.16: Global nitrous oxide (N_2O) budget for the period 2007–2016. Annual nitrous oxide fluxes (TgN_2O–N yr^{-1}) and nitrous oxide pools (TgN_2O–N), as described in Table 5.3.

[END FIGURE 5.16 HERE]

The N_2O budget derived from the synthesis of empirical and process-based bottom-up sources in Section 5.2.3.2 yield a global N_2O source of 17.2 (10.8–27.2) TgN yr^{-1} for the years 2007–2016 (Figure 5.16, Table 5.3). This estimate is comparable to AR5, but the range has been reduced primarily due to improved estimates of the ocean and anthropogenic N_2O sources. Anthropogenic emissions from agricultural nitrogen use and indirect effects for instance due to nitrogen deposition have increased by approximately 1.3 TgN yr^{-1} (Tian et al., 2019) from the 1980s to 2007–2016, and in total accounted for 6.1 (4.6–9.9) TgN yr^{-1}, compared to natural emission of 11.1 (6.1–17.3) TgN yr^{-1} during 2007–2016.

A number of studies have estimates the global N_2O budget by inversion of atmospheric N_2O measurements using atmospheric transport models(Saikawa et al., 2014; Thompson et al.). The inversion-based estimate a global mean N_2O source for 1998–2014 averages 16.6±0.6 TgN yr^{-1} (Thompson et al.). The split between land and ocean sources based on atmospheric inversions is less well constrained, yielding 10.6±1.4 TgN yr^{-1} and 6.0±1.5 TgN yr^{-1} for land and ocean, respectively. Based on the observed growth rate of atmospheric N_2O and simulations of the atmospheric loss of N_2O, the inversions suggest an increase in global emissions from 2000–2005 to 2010–2015 of 1.6 (1.4–1.7) TgN yr^{-1}, primarily caused by land-based changes in Central

and South America (27%), China (26%) and Africa (20%), as well as 10% to increased ocean emissions (Thompson et al.).

N_2O loss in the stratosphere by photolysis and oxidation by O(1D) radicals amounts to approximately 13.2±1.0 TgN yr^{-1} (Minschwaner et al., 1993; Prather et al., 2015). The imbalance between the sum of N_2O sources and atmospheric loss results in an increase in atmospheric N_2O abundance 4.0±0.1 TgN yr^{-1} as determined from the atmospheric growth rate for 2000–2016. The atmospheric loss estimates combined with satellite-based estimates of N_2O atmospheric abundance (1539 TgN in the year 2010) results in a mean atmospheric lifetime of ~116±9 years (Prather et al., 2015). The long atmospheric lifetime of N_2O implies that it will take more than a century before atmospheric abundances stabilise after the stabilisation of global emissions. This is of concern not only because of its contribution to the radiative forcing, but also because of the importance of N_2O in stratospheric ozone loss (Fleming et al., 2011; Ravishankara et al., 2009).

[START TABLE 5.3 HERE]

Table 5.3: Global N_2O budget (units TgN yr^{-1}). References: [a] (Bouwman et al., 2013; Graham et al., 2009; Heland and Schäfer, 1998; Janssens-Maenhout et al., 2017; Lee et al., 2011; Wiesen et al., 1994, 1996), [b] (Bouwman et al., 2013; Dangal et al., 2019; Janssens-Maenhout et al., 2017; Tian et al., 2019; Winiwarter et al., 2010), [c] (Bouwman et al., 2013; Davidson and Kanter, 2014), [d](Bouwman et al., 2013), [e] (Tian et al., 2019), [f] (Jickells et al., 2017; Landolfi et al., 2017; Suntharalingam et al., 2012), [g] (Deemer et al., 2016; Hu et al., 2016; Maavara et al., 2019; Murray et al., 2015; Nevison et al., 2004; Seitzinger et al., 2000), [h] (Battaglia and Joos, 2018; Bianchi et al., 2012; Buitenhuis et al., 2018; Landolfi et al., 2017; Manizza et al., 2012; Martinez-Rey et al., 2015; Suntharalingam et al., 2012), [i] AR5, [k] (Schlesinger, 2013), [l] (Elkins et al., 2018; Prather et al., 2015), [m] (Prather et al., 2015), [n] (Thompson et al.)

	AR6 (2007–2016)	AR5 (2006)
Bottom-up budget		
Antropogenic Sources		
Fossil Fuel combustion and Industry[a]	0.8 (0.7–1.2)	0.7 (0.2–1.8)
Agriculture (incl. Aquaculture)[b]	3.8 (3.0–5.2)	4.1 (1.7–4.8)
Biomass and biofuel burning[c]	0.7 (0.5–1.7)	0.7 (0.2–1.0)
Wastewater[d]	0.2 (0.02–0.7)	0.2 (0.1–0.3)
Atmospheric N deposition on land[e]	0.5 (0.4–0.8)	0.4 (0.3–0.9)
Atmospheric N deposition on ocean[f]	0.2 (0.01–0.3)	0.2 (0.1–0.4)
Total Anthropogenic	**6.1 (4.6–9.9)**	**6.3 (2.6–9.2)**
Natural Sources and Sinks		
Soils under natural vegetation[e]	6.2 (3.6–8.8)	6.6 (3.3–9.0)
Rivers, estuaries, and coastal zones[g]	0.5 (0.2–1.4)	0.6 (0.1–2.9)
Oceans[h]	3.8 (2.1–6.0)	3.8 (1.8–9.4)
Atmospheric chemistry[i]	0.6 (0.3–1.2)	0.6 (0.3–1.2)
Surface sink[k]	-0.01 (-0.3–0)	-0.01 (-1–0)
Total natural	**11.1 (6.1–17.3)**	**11.6 (5.5–23.5)**
Total bottom-up source	**17.2 (10.8–27.2)**	**17.9 (8.1–30.7)**
Observed growth rate[l]	**4.0 (3.9–4.2)**	**3.6 (3.5–3.8)**
Inferred stratospheric sink	13.2 (6.9–23.0)	14.3 (4.3–28.7)
Top-down budget[m]		
Atmospheric loss	13.2±1.0	11.9±0.9
Anthropogenic source	10.5±1.0	9.1±1.0
Natural source	6.6±1.3	6.7±1.3
Imbalance	3.9±0.5	4.0±0.5
Atmospheric inversion[n]		
Atmospheric loss	12.0	
Total source	16.6±0.6	
Imbalance	4.6	

[END TABLE 5.3 HERE]

5.2.4 The relative importance of CO_2, CH_4, and N_2O

The total influence of anthropogenic GHGs on the Earth's radiative balance needs to be understood as the combined effect of those gases, which the three most important were discussed separately in the previous sections. GHGs include short-lived gases such as ozone and black carbon, and long-lived gases with both anthropogenic sources and sinks (e.g. CO_2, CH_4, N_2O), and sources for GHGs produced by industrial processes, also called synthetic GHGs (e.g., perfluoro-compounds, chlorofluorocarbons, HCFCs, HFCs). Figure 5.17 shows that CO_2 is by far the single most important GHG, with greater increase of its radiative forcing since the 1960s. For the period 2007–2016, the relative contribution to the total radiative forcing was 65% for CO_2, 17% for CH_4, 6% for N_2O, and 11% synthetic gases.

[START FIGURE 5.17 HERE]

Figure 5.17: Change in radiative forcing by long-lived GHGs since 1900 (values relative to 1750, as a reference of the preindustrial era). The concentration time series of CO_2, CH_4 and N_2O are taken from Figure 5.1 for the calculation of radiative forcings using the simplified expressions given in (Etminan et al., 2016); the calculation includes shortwave forcing and the overlap between CO_2 and N_2O. The radiative forcing of synthetic gases (others) for the period 1979–2017 is taken from (Hofmann et al., 2006), with an extrapolation to 0 at 1940 when the CFCs were first introduced for industrial use.

[END FIGURE 5.17 HERE]

To compare the relative importance of the three GHGs (Figure 5.18), two approaches are used: The Global Temperature Potential (GTP), which measures the temperature at the end of a chosen period; and the Global Warming Potential (GWP), which measures the heat absorbed over a given period of time (Chapter 7). Thus, while GTP provides information to reach an end goal temperature (e.g., the climate targets of the Paris Agreement), GWP at various time scales provides relevant information on the warming path (and therefore impacts) along the way to an end temperature target.

For most developed nations in North America, Europe and Asia, net CO_2 flux overwhelms the emissions for CH_4 and N_2O when the GTP metric used for comparing emissions. Interestingly, the significance of CH_4 to the global climate is dwarfed when GTP is chosen over GWP over a 100-year time horizon (*virtually certain*), especially for the West Asia region. Both the boreal regions in America and Asia are net sink of CO_2, while close to flux neutrality is observed for Temperate South America, Southern Africa, and Australia and New Zealand. Only weak but persistent emission of CO_2 is observed for Tropical North America, Brazil and Southeast Asia. The 100-year time horizon is most relevant for the success of limiting global warming below 2^{o}C under the Paris Agreement. However, the pathways to reaching the goal depend on the management of non-CO_2 greenhouse gases. For instance, the GTP of CH_4 at 20-year time horizon is as high as 67 (AR5), having an overwhelming effect on global climate stabilisation in short-medium time periods.

[START FIGURE 5.18 HERE]

Figure 5.18: Regional attribution of global fluxes of CO_2, CH_4 and N_2O derived from concentrations as in Figure 5.1. The fluxes include anthropogenic sources and sinks, and natural fluxes that result from responses to anthropogenic GHGs and climate forcing (feedbacks) as in the three budgets shown in Sections 5.2.1.5, 5.2.2.5, and 5.2.3.5. The CH_4 and N_2O emissions are weighted by their global warming potential (GWP) and global temperature-change potential (GTP) over 100-year time horizon (GTP and GWP values from Chapter 7). Fluxes are from MIROC4-ACTM inverse modelling (updated from (Patra et al., 2016; Saeki and Patra, 2017; Thompson et al.)) and will be replaced by multi-model results from GCP budgets-2019 and AR6.

[END FIGURE 5.18 HERE]

5.3 Ocean acidification and de-oxygenation

The surface ocean absorbs up to a quarter of all anthropogenic CO_2 emissions mainly through physical-chemical processes. Once dissolved in seawater, CO_2 reacts with water and forms carbonic acid, that in turns dissociates, leading to changes in the concentrations of carbonate (CO_3^{-2}) and bicarbonate (HCO_3^-), and increasing the concentration of H^+ ions which turns the water more acidic (Doney et al., 2009). Although the societal concern for this problem is relatively recent (~ last 20 years), the physical-chemical basis for the ocean absorption (sink) of atmospheric CO_2 have been discussed much earlier by Revelle and Suess (1957). The effects of increased H^+ ions (reduced water pH) on marine biota are known with ~~r~~obust confidence, and changes in the trophic chain are ~~e~~xpected to happen (*medium confidence*, Hofmann et al., 2011).

The observed and modelled increase in ocean heat content from increasing GHG concentrations in the atmosphere warms the oceans and strengthens water column stratification. The former decreases the solubility of dissolved oxygen in seawater, and the latter reduces the ventilation flux into the ocean interior, leading to the ocean deoxygenation process. Deoxygenation may enhance the emissions of nitrous oxide, especially from oxygen minimum zones or hypoxic coastal areas (Breitburg et al., 2018; Oschlies et al., 2018). The coupled effects of acidification on deoxygenation also occur at the level of marine organisms metabolism, as the excess CO_2 dissolved in the oceans lead to a respiratory stress and reduction of thermal tolerance by organisms (Gruber, 2011) [[Placeholder: +SROCC citation]]. Since AR5 in 2013 and SROCC [[update SROCC reference]], other ocean modelling and observation-based studies have projected a general decline in the total dissolved oxygen content in the ocean, such as 2%-loss since 1960 to present (Schmidtko et al., 2017).

5.3.1 Paleo context

5.3.1.1 Paleaocene-Eocene Thermal Maximum (PETM)

The Palaeocene-Eocene Thermal Maximum (PETM) was an episode of transient global warming likely exceeding 5–8°C (Dunkley Jones et al., 2013) that occurred 55.8 Myr ago. The PETM involved a large pulse of volcanic CO_2 released into the ocean-atmosphere system within 5–20 kyrs (Turner, 2018) and was associated with profound perturbations of the global carbon cycle. Estimates of the total amount of carbon released during the PETM vary from around 3000 Pg C to more than 10,000 Pg C (Cui et al., 2011; Gutjahr et al., 2017; Zeebe et al., 2009). The estimated carbon input is similar to the RCP8.5 scenario, although CO2 release rates during the PETM were about an order of magnitude slower than today (i.e. 0.5–1.1 PgC yr^{-1}; (Panchuk et al., 2008; Zeebe et al., 2016)). Methane emission related to hydrate and terrestrial permafrost destabilisation may have acted as positive feedbacks (DeConto et al., 2012), as the inferred increase in atmospheric CO_2 can only account for approximately half of the reported temperature increase (Zeebe et al., 2009). The PETM thus provides a test for our understanding of the ocean's response to the rapid invasion of carbon (and heat).

In response to carbon emissions during the PETM, observation-constrained model simulations report a CO_2 increase ranging from about 800 ppm to a peak value of > 2000 ppm (Gutjahr et al., 2017). As a result, the PETM was associated with a transient and negative surface ocean pH excursion likely ranging from 0.15 to 0.30 units (Babila et al., 2018; Gutjahr et al., 2017; Penman et al., 2014). It was also accompanied by a rapid (< 10 kyrs) shoaling of the carbonate compensation depth of more than 2000 m, followed by a gradual (100 kyrs) recovery (Bralower et al., 2018; Zachos, 2005). The remarkable similarity among sedimentary records spanning a wide range of ecosystems suggests that the perturbation in the ocean carbonate saturation was *likely* globally uniform (Babila et al., 2018) and directly resulted from elevated atmospheric CO_2 levels. The degree of acidification is similar to the 0.4 pH unit decrease predicted for the end of the twenty-first century (RCP8.5) due to anthropogenic carbon emissions (Gattuso et al., 2015) and *likely* occurred at one order of magnitude slower than the current rate of ocean acidification (Zeebe et al., 2016).

This event was characterised by widespread ecological disruptions (Honisch et al., 2012; McInerney and

Wing, 2011). Continental shelf ecosystems (Bralower et al., 2018) and planktonic communities (including both phyto- and zooplankton) show reductions in diversity (Robinson, 2011). For calcifiers residing deeper in the ocean, the impact of the PETM was much more deleterious, with a major extinction affecting 30–50% of the benthic foraminifera species, globally (Thomas, 2007). It is not yet established, however, whether the mass mortality affecting benthic organisms was related to a decrease in oxygenation (see below), bottom ocean warming and/or carbonate undersaturation (Ridgwell and Schmidt, 2010; Thomas, 2007).

Recent model outputs as well as geochemical data reveal widespread ocean deoxygenation during the PETM (Dickson et al., 2012; Winguth et al., 2012), with parts of the ocean potentially becoming drastically oxygen-depleted (anoxia) (Yao et al., 2018). Deoxygenation affected the surface ocean globally (including the Arctic Ocean (Sluijs et al., 2006), due to vertical and lateral expansion of oxygen minimum zones (OMZs) (Zhou et al., 2014) that resulted from warming and related changes in ocean stratification as well as the oxidation of methane hydrates (Pälike et al., 2014). Expansion of OMZs may have stimulated N_2O production through water-column denitrification (Junium et al., 2018). The degree to which N_2O production impacted PETM warming has not yet been established.

The feedbacks associated with recovery from the PETM are uncertain, with hypotheses that include drawdown associated with silicate weathering (Zachos, 2005), rapid regrowth of organic carbon stocks (Bowen and Zachos, 2010; Gutjahr et al., 2017), and global increase in marine export production (Bains et al., 2000).

5.3.1.2 Last deglaciation (18-11 kyr ago)

The last deglaciation is the best documented climatic transition in the past associated with a substantial atmospheric CO_2 rise ranging from 190 to 265 ppm (equivalent to 160 PgC) between 17.8 and 11.6 kyr ago (Marcott et al., 2014). The amplitude of the deglacial CO_2 rise is thus on the order of magnitude of the increase undergone since the Industrial Revolution. The increase in atmospheric CO_2 was punctuated by three abrupt 10–15 ppm increments spanning a few hundred years, associated with the rapid transfer of CO_2 previously sequestered in the ocean interior and permafrost (Bauska et al., 2016; Köhler et al., 2014). Emission rates during these transient events remained lower than 0.5 PgC yr^{-1} (Marcott et al., 2014).

Geochemical proxy data show a 0.15–0.05 unit decrease in sea-surface pH (Hönisch and Hemming, 2005; Martínez-Botí et al., 2015c) across the deglacial transition – an average rate of decline of ~0.002 units per 100 years compared with the current rate of more than 0.1 units per 100 years. Planktonic foraminiferal shell weights decreased by 40 to 50% (Barker, 2002), and coccolith mass decreased by ~25% (Beaufort et al., 2011) across the last glacial termination.

Geochemical and micropaleontological evidence suggest that intermediate-depth OMZs almost totally vanished during the LGM (Jaccard et al., 2014). On the other hand, the deep (> 1,500 m) ocean became depleted in O_2 (concentrations were *likely* lower than 50 μmol kg^{-1}) globally (Anderson et al., 2019; Gottschalk et al., 2016; Hoogakker et al., 2015; Hoogakker et al., 2018; Jaccard and Galbraith, 2012) related to sluggish ventilation of the ocean subsurface (e.g. Gottschalk et al., 2016; Skinner et al., 2017) and increased (T-dependent) remineralisation length scale (Matsumoto, 2007). As a result, the ocean interior is thought to have stored an additional 750–950 Gt C compared to today (Anderson et al., 2019; Jaccard et al., 2009; Sarnthein et al., 2013; Skinner et al., 2015). This highlights the contribution of apparent oxygen utilisation (AOU), which overcompensated changes in T-dependent O_2 saturation (Bopp et al., 2017; Jaccard et al., 2014).

During the deglaciation, deep ocean ventilation increased as Antarctic Bottom Water (Gottschalk et al., 2016; Jaccard et al., 2016; Skinner et al., 2010) and subsequently North Atlantic Deep Water (Lippold et al., 2016; McManus et al., 2004) circulation resumed, transferring previously sequestered remineralised carbon from the ocean interior to the upper ocean and eventually the atmosphere (Galbraith and Jaccard, 2015), contributing to the CO_2 rise. Intermediate depths lost oxygen as a result of sluggish ventilation and increasing temperatures (decreasing saturation) as the world emerged from the last ice age. OMZs underwent

a large volumetric increase at the beginning of the Bølling-Allerød a northern-hemisphere wide abrupt warming event, 14.5 kyr ago (Jaccard and Galbraith, 2012; Praetorius et al., 2015) with deleterious consequences for benthic ecosystems (e.g. Moffitt et al., 2015).

The expansion of OMZs contributed to a widespread increase in water column denitrification (Galbraith and Kienast, 2013), which contributed to substantially enhance atmospheric N_2O concentrations (Schilt et al., 2014; Suthhof et al., 2001). Stable isotope measurements on N_2O extracted from ice cores suggest that approximately half (on the order of 1–1.25 TgN yr^{-1}) of the deglacial increase in N_2O emissions relates to oceanic sources, while the other half results from tropical vegetation regrowth (Schilt et al., 2014).

5.3.2 Historical trends and spatial characteristics in the "upper ocean"

5.3.2.1 Observations of ocean acidification over the past decades

Acidification of seawater is continuing to occur from tropical through to polar oceans because of growing anthropogenic CO_2 uptake (*virtually certain*). Decreasing pH trends and declining calcium carbonate saturation level as well as the increasing trends of surface ocean CO_2 have currently been observed at several ocean time-series stations and in several regions where underway surface ocean pCO_2 observations have been made repeatedly providing temporally resolved datasets over the past decades (Figure 5.19).

In the subtropical zones of the open ocean, pH is decreasing at a rate about -0.018 pH unit per decade (Bates et al., 2014; González-Dávila et al., 2010; Ishii et al., 2011; Midorikawa et al., 2010), i.e., about 4% increase in hydrogen ion concentration ($[H^+]$) per decade, and the saturation level of calcium carbonate mineral aragonite is declining at about -0.10 per decade. This is consistent with the rates expected from the transient equilibration with the increasing atmospheric CO_2 concentrations (Bates et al., 2014). In the western tropical Pacific, the rate of $[H^+]$ increase is about 20% lower than in the subtropics (Midorikawa et al., 2010), which is attributable to the shallow overturning circulation that brings anthropogenic CO_2 from the extra-tropics into the tropics at time scales of a decade, and thus delays the $[H^+]$ increase. In subpolar oceans and in coastal regions, uncertainty in the rate of pH change is larger, reflecting the complex interplay between physical forcing and biological activities, which can be further mixed by local processes (Bates et al., 2014; Merlivat et al., 2018; Wakita et al., 2017). Nevertheless, the trend of acidification is significant at most sites. In the Southern Ocean, the rate of pH decrease has been determined from the integrated data of surface ocean pCO_2 and total alkalinity measurements (Lauvset et al., 2015; Midorikawa et al., 2012; Takahashi et al., 2014). Its rate, ranging between -0.002±0.004 and -0.023±0.004 pH unit per decade, depends on the region of observation, periods and methods used (Fay et al., 2014). In the Arctic Ocean, there is no ocean CO_2 time-series data long enough to make a robust analysis of the ocean acidification. However, calcium carbonate saturation level is generally low, and the undersaturation of aragonite has been observed in response to large freshwater inputs due to the recent extensive melting of sea ice and river discharge (Azetsu-Scott et al., 2010; Bates et al., 2009; Chierici and Fransson, 2009; Yamamoto-Kawai et al., 2009).

[START FIGURE 5.19 HERE]

Figure 5.19: Time-series of pH (red) and seasonally-detrended pH (blue) in surface layer at various sites of the oceans. [[Placeholder: to be updated]]

[END FIGURE 5.19 HERE]

5.3.2.2 Reconstructed centennial ocean acidification trends

Ocean pH time series reconstructed from coral boron isotopic ($\delta^{11}B$) records evident a prominent ocean acidification trend since mid-20th century (*high confidence*) underlying strong imprints of internal climate variability (*high confidence*). A majority of coral $\delta^{11}B$ data have been generated from the western Pacific

regions with a few from the Atlantic Ocean. Biweekly resolution paleo-pH records show monsoonal variation of ~0.5 in the South China Sea (Liu et al., 2015). Interannual ocean pH variability in the range of 0.07–0.16 characterize SW Pacific corals that are attributed to ENSO (Wu et al., 2018) and river runoff (D'Olivo et al., 2015). Decadal (10, 22 and 48-year) ocean pH variations in the SW Pacific have been linked to the Interdecadal Pacific Oscillation, causing up to 0.30 in ocean pH changes in the Great Barrier Reef (Pelejero, 2005; Wei et al., 2009) but weaker (~0.08) in the open ocean setting (Wu et al., 2018). Decadal variation in the South China Sea of 0.10–0.20 ocean pH changes also have been associated with ocean advection (Liu et al., 2015; Wei et al., 2015). Since the beginning of the Industrial Period in the mid-19th century, coral δ^{11}B-derived ocean pH has decreased by 0.06–0.24 in the South China Sea (Liu et al., 2015; Wei et al., 2015) and 0.12 in the SW Pacific (Wu et al., 2018). A distinct feature of coral δ^{11}B records is ocean acidification trends since the mid-20th century albeit having wide-range values. The trends are 0.12–0.40 in the Great Barrier Reef (D'Olivo et al., 2015; Wei et al., 2009), 0.05–0.08 in the NW Pacific (Shinjo et al., 2013), 0.9–1.16 in the subtropical western Pacific (Kubota et al., 2017), and 0.04–0.09 in the Atlantic Ocean (Fowell et al., 2018; Goodkin et al., 2015). Concurrent coral carbon isotopic (δ^{13}C) measurements infer the ocean uptake of anthropogenic CO_2 from the combustion of fossil fuel characterised based on the isotopically depleted δ^{13}C of fossil fuels or the Suess effect. Western Pacific coral records show depleted δ^{13}C trends since the late 19th century that are more prominent since the mid-20th century (*high confidence*) (Kubota et al., 2017; Liu et al., 2015; Pelejero, 2005; Shinjo et al., 2013; Wei et al., 2009; Wu et al., 2018) where coral δ^{13}C leads δ^{11}B in these anthropogenic trends by about 2 years (Shinjo et al., 2013). Overall, there is a consistent depleted coral δ^{11}B trends particularly in recent decades with further works needed for assessing *in situ* and inter-colony calibration.

5.3.3 Ocean interior change

5.3.3.1 Ocean memory – acidification in the ocean interior

Anthropogenic CO_2 taken up into the ocean surface layer is further spreading downward through the vertical mixing and advection (see Section 5.2.2.3.2), thereby causing acidification in the ocean interior (*virtually certain*). Its trend is modulated by the changes in ocean circulation through those in the net anthropogenic CO_2 transport (Gruber et al., 2019b) and in the cumulative impact of CO_2 released from the metabolic process of organisms (remineralisation of organic matter) that accompanies the changes in the dissolved oxygen (Breitburg et al., 2018; Chen et al., 2017; Gattuso et al., 2015; Gruber, 2011; Levin, 2018; Mora et al., 2013; Robinson, 2019) (see Section 5.3.3.2).

The signal of acidification tends to diminish with depth while it has been amplified over time (*virtually certain*). The depth at which its signal has been found so far varies largely connecting with the structure of the ocean circulation. It is deeper in the subpolar North Atlantic (Perez et al., 2018) and mid-latitudinal zones in both hemispheres, and is shallower in the tropics (Carter et al., 2017; Murata and Saito, 2012; Ríos et al., 2015) and in the Southern Ocean with a significant pH decrease on the Antarctic continental slope (Hauck et al., 2010; Williams et al., 2015). In the subpolar North Atlantic, the trend of acidification has been observed during 1991–2016 even at the depth of 3000m with the shoaling of aragonite saturation horizon below which aragonite is undersaturated ($\Omega_{arag} < 1$) at a rate of 10–15 m per year to 2250m. At 30°S-40°S in the South Atlantic, a distinct pH decrease that reached -0.029 ±0.014 pH unit has been observed at 1000m in two decades during 1993–2013 (Ríos et al., 2015). It is attributable to the increased impacts of the remineralisation as well as the anthropogenic CO2 invasion into the Antarctic Intermediate Water.
A significant reinforcement of acidification by the increased remineralisation is also evident in the broad range of the intermediate water in the North Pacific (Byrne et al., 2010; Carter et al., 2017; Chu et al., 2016; Dore et al., 2009). Taken the long-term trend of decline in the dissolved oxygen (-4.0 μmol kg^{-1} per decade) in the intermediate water of the North Pacific as revealed by time-series measurements (Sasano et al., 2015, 2018; Takatani et al., 2012), this is thought to have been occurring persistently in the past several decades (*medium confidence*). By contrast, in the North Pacific Subtropical Mode Water (~200–300 m), large decadal variability in pH and aragonite saturation level with their amplitudes of ~0.02 and ~0.1 have been observed on their secular trend of decrease due to anthropogenic CO_2 invasion (Oka et al., 2019). This is associated with the variability in the impact of remineralisation driven by the ~50% variation in the formation volume

of the mode water that is forced remotely by the Pacific Decadal Oscillation (Oka et al., 2015). The trend and variability of the modulation of ocean interior acidification in space and time in the coming decades is also thought to be linked with those of deoxygenation due to changes in ventilation (Section 5.3.3.2).

5.3.3.2 Deoxygenation and its implications for GHGs and pH decline

The rate of oxygen decrease in the ocean interior exhibits large variability in space, depth and time, but in total more than 2% (4.8±2.1 Petamoles) of the global ocean oxygen content has been lost since 1960 (Helm et al., 2011; Ito et al., 2017; Schmidtko et al., 2017). Substantial changes in thermocline oxygen concentrations have been observed (i.e. (Deutsch et al., 2014; Hahn et al., 2017)) but attribution to different forcing agents such as anthropogenic warming, internal climate variability or a combination of both (i.e., changing internal variability in a warming world) is challenging (Oschlies et al., 2018).Climate models confirm this decline and predict continuing and accelerating ocean deoxygenation (Bopp et al., 2013). However current models for instance do not reproduce observed patterns for oxygen changes in the ocean's tropical thermocline and generally simulate only about half the oceanic oxygen loss inferred from observations (Oschlies et al., 2018).

The areas with relatively rapid oxygen decrease and with its large impact include the OMZs found in the tropical oceans, where oxygen content is decreasing at a rate of 0.9 to 3.4 µmol kg^{-1} per decade in the thermocline for the past five decades (Stramma et al., 2008). Low oxygen, low pH and shallow aragonite saturation horizons in the OMZ in the eastern boundary upwelling regions co-occur within them, affecting ecosystem structure (Chavez et al., 2008) and function in the water column, including the present unbalanced nitrogen cycle (Paulmier and Ruiz-Pino, 2009). The coupling between upwelling, productivity, and oxygen depletion feeds back to biological productivity and their role as sinks or sources of climate active gases. When OMZ waters upwell and impinge on the euphotic zone, they release significant quantities of greenhouse gases, including CO_2, N_2O and CH_4, to the atmosphere (*i.e.* (Arévalo-Martínez et al., 2015; Babbin et al., 2015; Farías et al., 2015; Kock et al., 2012; Naqvi et al., 2010) exacerbating global warming with feedbacks to stratification, biological productivity and the oxygen inventory. According to modelling projections of oceanic N_2O emissions in 2100 under RCP8.5 emission scenario, the expansion of OMZs could thus increase N_2O production and net CO_2 emissions, associated primarily to denitrification (Martinez-Rey et al., 2015). Denitrification depletes nitrate and thus, when upwelled waters reach the photic zone, primary production is N-limited and CO_2 is emitted to the atmosphere (Tyrrell and Lucas, 2002). However, in other oceanic regions, further stratification of the ocean due to warming may reduce the amount of N_2O reaching the surface inducing a decreased N_2O flux to the atmosphere. Landolfi et al., (2017) suggest that by 2100, under the same RCP8.5 scenario, total N_2O production may have declined by 5% and N_2O emissions be reduced by 24% due to decrease in organic matter export and anthropogenic driven changes in ocean circulation and atmospheric N_2O concentrations. It is yet unclear whether N_2O production from bacterial nitrification increases exponentially or linearly with decreasing oxygen and whether a threshold oxygen value exists below which net N_2O production switches to N_2O consumption. Furthermore, the correlation between N_2O and oxygen varies with microorganisms present, nutrient concentrations, and other environmental variables.

5.3.4 Future projections

Ocean acidification is projected to continue as atmospheric CO_2 levels continue to rise, with Earth system models showing similar net change in the surface ocean in the period to 2100, primarily determined by atmospheric CO_2 concentration and the existing regional carbonate chemistry (Hurd et al., 2018). The Arctic Ocean is an exception due to freshwater input from rivers and sea-ice melt, as well as circulation changes, which leads to a faster rate of change than waters in other regions (Qi et al., 2017), that continues through to 2100 (Hurd et al., 2018).

Earth system models project significant and irreversible changes that start to occur in polar regions within the next 15 years, as surface waters begin to become seasonally undersaturated with respect to aragonite,

which is predicted to occur in Southern Ocean surface waters by 2030 under all emissions pathways except very low RCP2.6 (Hauri et al., 2016; Negrete-García et al., 2019; Sasse et al., 2015). It is *likely* that the extent and persistence of ocean acidification in the high latitude oceans is very sensitive to the emissions scenarios. For the Southern Ocean, the extent of seasonal month-long undersaturation for aragonite by 2100 were calculated to vary from negligible (less than 2%) under RCP2.6 to ~30% for RCP4.5 and more than 95% for RCP8.5 (Sasse et al., 2015). These long term projections are modulated at interannual timescales by large-scale climate modes (Ríos et al., 2015), such as the representation of the El-Niño/Southern Oscillation and the Southern Annular Mode in models (Conrad and Lovenduski, 2015).

As atmospheric CO_2 levels continue to rise, the seasonal cycle of ocean acidification will continue to be modulated, with each part of the carbonate system responding differently. Overall a decrease in pH seasonality is anticipated globally, but in contrast, hydrogen ion seasonality concentration increases. However, the aragonite saturation state shows a reduction in all basins except for the subtropical gyres, which show an amplification of the seasonal cycle due to warming under high emissions scenarios (Kwiatkowski and Orr, 2018). The magnitude of these changes, however, will be sensitive to the future emissions pathway followed and highlights the interplay between warming and ocean chemistry in future projections.

[START FIGURE 5.20 HERE]

Figure 5.20: Upper the observed aragonite saturation state in the present day (Hurd et al., 2018), and lower year that surface waters will become undersaturated and its extent with respect to aragonite at the monthly scale for high and low emissions pathways (RCP2.6 and RCP8.5) from Sasse et al., (2015).

[END FIGURE 5.20 HERE]

At regional scale, these changes are modulated by local variability due to a range of processes that includes circulation, temperature changes, carbon cycling, carbonate chemistry and the structure of the marine ecosystem. As current model projections don't resolve these fine-scale temporal and spatial variability and processes, this suggests that current projections are *unlikely* to fully capture the chemical changes that the marine environment will experience in the future (Takeshita et al., 2015; Turi et al., 2016).

As atmospheric CO_2 concentrations rather than emissions often drive models used to project future changes, important carbon-climate feedbacks (more positive than negative) have been overlooked, which will directly impact the rates of ocean acidification suggesting changes possibly occurring more quickly than currently modelled (Matear and Lenton, 2018; Zhang et al., 2018a). Equally, feedbacks of the marine ecosystem on ocean chemistry have also been overlooked, and while the magnitude and sign of many of these feedbacks are still poorly known, nevertheless studies that explore these feedbacks suggest a potentially very significant and long-lasting impact (Matear and Lenton, 2014).

5.3.5 Coastal ocean acidification and deoxygenation

5.3.5.1 Drivers

High spatial and temporal variability characterise the coastal ocean marine carbonate system, thus surface pCO_2, pH, and sea-air CO_2 fluxes. Typically, inner seas, bays and estuaries are saturated with CO_2, despite the latitude region (i.e. tropical, temperate, polar) because heterotrophic respiration of organic matter from basin drainage prevails over photosynthesis. Additionally, highly populated coastal areas receive large amounts of organic matter from domestic and industrial sewage (Chen and Borges, 2009). On the contrary, continental shelves, excluding estuaries and near-shore areas, act as CO_2 sinks at a rate of ~0.2 PgC yr^{-1} (Laruelle et al., 2014) or a sink yield of 0.7 molC m^{-2} yr^{-1}, considering ice-free areas. Under scenarios of concomitant increasing atmospheric CO_2 and eutrophication, such ecosystems would be more vulnerable to

ecological and biogeochemical changes, impacting local economical activities. Nevertheless, coastal and shelf seas acidification, whether induced by the increasing atmospheric CO_2 or by enhancement of eutrophication, is *very likely* to have negative effects on groups of marine organisms (Dupont et al., 2010), especially when combined to other stressors such as temperature and metallic ions (Boyd et al., 2015; Breitburg et al., 2018).

5.3.5.2 Spatial characteristics

Reported long-term decline in seawater pH for coastal areas in the north-western USA (Pacific coast) are related to local metabolism, and relates more significantly to the dissolved oxygen saturation state than the increasing trends in atmospheric CO_2 (Lowe et al., 2019). Non-upwelling coastal areas, such as in the north-eastern USA also present a significant positive correlation between pH and dissolved oxygen, where more acidic waters (i.e. pH ≈ 7.00) are found in hypoxic areas (Wallace et al., 2014). Model results predict a concomitant increase in bottom waters acidification and deoxygenation in the northern shelf of the Gulf of Mexico with increasing eutrophication, implying that this situation could be managed with regulation of the riverine input of nutrients (Laurent et al., 2017). Similarly to the former examples, although in a smaller spatial scale, (Cotovicz et al., 2018; Cotovicz Jr. et al., 2015) observations show that eutrophication induces net atmospheric CO_2 absorption in tropical, shallow and vertically stratified ecosystems in spite of the presence of bottom water acidification and hypoxia, driven by autochthonous primary production. In addition to that, more acidic coastal sub-surface waters are also found close to wastewater effluents, where microbial respiration lowers water pH (Cotovicz Jr. et al., 2015; Fennel and Testa, 2019; Lowe et al., 2019; Wallace et al., 2014). Cai et al., (2011) showed through observations, that the CO_2 production from the decomposition of organic matter in eutrophic coastal areas (off the Mississippi and Chanjiang rivers) has already increased acidification levels in adjacent subsurface waters.

Spatial distribution of hypoxic coastal areas is highly heterogeneous, but more severe hypoxia or anoxia is *likely* to occur in highly populated coastal areas, or in regions where local water circulation, water column stratification and wind patterns lead to an accumulation of organic matter (Breitburg et al., 2018; Ciais et al., 2013; Rabalais et al., 2014). The signal for deoxygenation trends is thus heterogeneous and can be only assessed by making available coastal water quality surveys, many times not obtainable in the peer-reviewed literature.

The Baltic Sea is the largest regional sea where hypoxia is reported to happen before the 1950s (Carstensen et al., 2014; Łukawska-Matuszewska et al., 2019; Rabalais et al., 2014). The frequency and volume of North Seawater inflows to the Baltic Sea decreased after 1950, leading to an expansion of hypoxic areas from 40,000 to 60,000 km² in combination with increasing eutrophication (Carstensen et al., 2014) [reference missing]. Chesapeake Bay, a densely populated coastal ecosystem on the North American east coast, displays summer hypoxia with large interannual variation (Li et al., 2016a). Wang et al. (2017)*[reference missing]* showed, using sedimentary record, that since about 1850 the oxygen minimum zone off southern California in the Pacific Ocean has become more intense since the 1990s, with high interannual variability due to the Southern Oscillation. The East China Sea is one of the largest coastal oxygen-depleted areas in the world, where observed summer hypoxia has been related to increasing inputs of riverine nutrients (Chen et al., 2007). Recently, Qian et al., (2017) have shown that regional seawater circulation processes (i.e. non local) also play a role in the intensity of East China Sea summer hypoxia. On the north-western Atlantic shelf, (Claret et al., 2018) in a combined observation and model approach show that the observed shelf deoxygenation trends are related to changes (retreat) in the Labrador Current circulation patterns.

Shelf waters in the Arabian Sea display seasonal hypoxia driven by the summer monsoon upwelling (Madhupratap et al., 1996). A comparison of observational data from the late 1950's with a modern time-series does not show an increase in hypoxia in this area (Gupta et al., 2016). Djakovac et al., (2015) have analysed a 40-year time-series and concluded that changes in regional circulation in the Adriatic Sea alleviated the local strong summer/autumn bottom hypoxia events in its eastern portion while on the north-western Adriatic Sea, the decrease in nutrient and freshwater inputs lead to present less severe hypoxic conditions when compared to the 1970s and 1980s decades.

5.4 Biogeochemical Feedbacks on Climate Change

This section is covers biogeochemical feedbacks on climate change, which represent one of the largest sources of uncertainty in projections of climate change. The relevant processes are discussed, prior to discussing the simulation and projection of the carbon cycle in Earth System Models, emergent constraints on future projections, non-CO_2 feedbacks, and possible biogeochemical tipping points.

5.4.1 Direct CO_2 effects on land carbon uptake

As detailed in AR5, the CO_2 fertilisation effect, the leaf-level increase of photosynthesis and an associated decline in stomatal conductance as a consequence of elevated CO_2, is the dominant cause for the projected increase in global land productivity and land carbon uptake between 1850 and 2099 in Earth System Models (ESMs) in the Coupled Model Intercomparison Project Phase 5 (CMIP5) ensemble (Arora et al., 2013; Wenzel et al., 2016). Increased productivity is one key driver of increases in vegetation carbon storage, but processes affecting vegetation turnover such as allocation changes, mortality, and vegetation structural changes also play an important role (Friend et al., 2014; Walker et al., 2019). Changes in plant carbon inputs to soils are the major cause for changing soil carbon stocks, which represent a significant contribution to the carbon-concentration feedback (Todd-Brown et al., 2013).

AR5 concluded that the CO_2 fertilisation effect included in ESMs has been corroborated by many experimental studies (e.g. Ainsworth and Long, 2005). Interactions of leaf-level CO_2 fertilisation with light availability, growth temperature, and seasonal drought at ecosystem level contribute to the spread in model projections of productivity increase as they are as yet insufficiently constrained by observations (Baig et al., 2015; Kelly et al., 2016; Zaehle et al., 2014). New syntheses since AR5 corroborate the earlier assessment that the effect of elevated CO_2 on ecosystem-scale productivity and carbon storage is much less clear (Walker et al., 2019). Field studies with elevated CO_2 have demonstrated that the initial stimulation of above-ground growth may decline, if insufficient amounts of nitrogen are available to support the increased growth (Finzi et al., 2007; Norby et al., 2010; Reich and Hobbie, 2013; Terrer et al., 2018).

Model-data intercomparisons using CO_2 manipulation experiments have demonstrated that the long-term model projections depend on their ability to predict soil-vegetation interactions (Medlyn et al., 2015; Zaehle et al., 2014). Meta-analyses of CO_2 manipulation experiments point to accelerated turnover of soil organic matter (van Groenigen et al., 2017) as a result of increased plant below ground carbon allocation, increased root exudation or mycorrhizal activity (Drake et al., 2011; Meier et al., 2017), which may depend on the dominant type of mycorrhizal associated (Terrer et al., 2016, 2017). Such effects are not considered in the ESMs included in CMIP5 or CMIP6 (CMIP Phase 6). Representation of soil microbial dynamics in ecosystem models leads to a reduced effect of increased C inputs on soil carbon storage, because elevated CO_2 stimulates the decomposer community (e.g., Guenet et al., 2018; Sulman et al., 2014; Wieder et al., 2013, 2017). It is unclear whether this effect reduces the carbon-concentration interaction because of the increase in soil C losses, or increases the carbon-concentration interaction because increased N availability and subsequent stimulation of plant growth and carbon storage.

The two ESMs in CMIP5 with N dynamics reported in AR5, which relied on the same land model, showed a very strong reduction in the land carbon sensitivity to atmospheric CO_2 (Arora et al., 2013). Since AR5, an increasing number of land surface models have incorporated a representation of the nitrogen cycle to account for potential progressive nitrogen limitation of the CO_2 fertilisation effect (Goll et al., 2017; Wania et al., 2012; Wårlind et al., 2014). Improvements in process representation and the larger ensemble size allow now for a better quantification of this effect (Figure 5.29; Table 5.5). Based on independent assessments by stand-alone land model simulations (Wårlind et al., 2014; Zaehle et al., 2010; Zhang et al., 2014), and analyses of CMIP5 simulations (Wieder et al., 2015; Zaehle et al., 2015), the land nitrogen cycle *very likely* reduces the sensitivity of the land carbon cycle to CO_2, however, the magnitude is *likely* less than in the CMIP5 ensemble.

Understanding of the effect of phosphorus limitation in large parts of the tropical zone and Australia (Grandy et al., 2013; Vitousek et al., 2010) on CO_2 fertilisation is less well developed. Since AR5, the first free-air CO_2 enrichment experiment in a phosphorus-limited mature forest ecosystem did not find an increase in biomass growth despite increases in photosynthesis after three years of CO_2 exposure (Drake et al., 2018; Ellsworth et al., 2017). Models accounting for the effects of P availability in addition to N generally show a stronger reduction of the response of the ecosystem carbon storage to elevated CO_2 (Goll et al., 2012; Medlyn et al., 2016; Zhang et al., 2014). This suggests that the carbon-concentration interactions in CMIP5 ESMs maybe overestimated for predominantly P limited regions. Land P cycling will be represented in at least two of the ESMs participating in C^4MIP of CMIP6, providing an opportunity to assess the strength of the P–effect in the second-order draft.

Independent indirect evidence based on the interpretation of the ^{13}C–isotopic signature in tree rings support the observations from CO_2 enrichment experiments that water-use efficiency respond positively to changes in CO_2 (but see Brienen et al., 2017; Frank et al., 2015; van der Sleen et al., 2015). Idealised simulations from seven ESMs suggest that increased water-use efficiency reduces future water loss from vegetation, thereby also contributing to surface warming, because the effect of decreased leaf-level conductance outweighs the projected increases in leaf area index (Swann et al., 2016).

5.4.2 Direct CO_2 effects on ocean carbon uptake

A persistent increase in the atmospheric CO_2 concentration will drive further net CO_2 uptake into the ocean. During 2008–2017 the ocean has taken up around 30% of anthropogenic CO_2 emissions (Section 5.2.2.3). However, there is broad agreement among Earth system models that the anthropogenic CO_2 uptake by the ocean as a fraction of anthropogenic emissions will decrease with the increase in the ocean CO_2 inventory (Arora et al., 2013a; Wang et al, 2016) (*very likely*). For the RCP8.5 scenario, it is projected that the oceanic CO_2 uptake fraction of fossil fuel CO_2 emissions will decrease from 32% in the 1990s to 23% on average over the twenty-first century (Jones et al., 2013b; Wang et al., 2016). This decrease is a result of the impact of CO_2 uptake on the carbonate chemistry of seawater that lowers the capacity of absorbing CO_2 from the atmosphere (buffering capacity) (Katavouta et al., 2018). It will have a positive feedback on the sensitivity of global warming to the cumulative anthropogenic CO_2 emission through the elevation of the airborne fraction.

Due to the lowering of the CO_2 buffering capacity of seawater, biological CO_2 assimilation increases its importance for CO_2 uptake in the Southern Ocean, even if biological productivity remains unchanged. This is because the decreasing buffering capacity results in a larger draw-down of pCO_2 in sea-water, and hence a larger CO_2 gradient between ocean and atmosphere (Hauck and Völker, 2015). Changes in seawater carbonate chemistry due to cumulative CO_2 uptake is also *likely* to amplify the seasonal cycle of hydrogen ion concentration (+81±16%) during the twenty-first century (Ishii et al., 2011; Kwiatkowski et al., 2018; see also Chapter 5.3.2). Depending on the seasons and regions, it may exacerbate or ameliorate the impacts of ocean acidification on marine organisms (see Section 5.3).

Ocean acidification is *very likely* to reduce the calcification rate of marine organisms (e.g. Kroeker et al., 2013) and so may form a negative feedback on atmospheric CO_2 levels. However, the predicted sensitivity of atmospheric CO_2 is fairly small; under RCP8.5, the decrease in $CaCO_3$ production and dissolution due to increasing ocean acidification are predicted to result in a small negative feedback on atmospheric CO_2 of -2 to -11 ppm by 2100 (Gangstø et al., 2011). However, different model parameterisations for the CO_2–calcification feedback result in widely diverging estimates of the feedback magnitude, which range from -1 ppm to -125 ppm (part of this spread is also due to use of different forcing scenarios) (Heinze, 2004; Hofmann and Schellnhuber, 2009; Ridgwell et al., 2007; Zhang and Cao, 2016). The magnitude of the feedback effect will also depend on the parameterisation of the ballast effect on export fluxes of organic carbon, which acts to counteract the negative calcification response to increased CO_2 (Barker et al., 2003).

5.4.3 Climate effects on land carbon uptake

CMIP5 ESMs project that a warming climate will lead to losses of carbon from vegetation and soils, due to a variety of factors, which include: reduced photosynthetic uptake, particularly in tropical ecosystems, due to temperature and water stresses; elevated rates of plant (autotrophic) respiration with warmer temperatures; changes to plant mortality and disturbance rates; and increases to heterotrophic respiration rates with warmer temperatures. ESMs also indicate areas of carbon gain that offset some of these losses due to processes that include: longer growing seasons in colder climates and increased nutrient availability from mineralisation of organic matter that accompanies elevated decomposition rates. Uncertainty on the magnitude and geographic pattern of these feedbacks remain high, but it is *likely* that ecosystem responses to climate change will act as a positive feedback that will enhance global warming.

Plant productivity is highly dependent on local climate. In cold environments, warming has generally led to an earlier onset of the growing season, and with it vegetation productivity (e.g. Forkel et al., 2016). However, this trend is affected by adverse effects of climate variability and other emerging limitations of vegetation production by water, energy or nutrients, which may gradually reduce the effects of warming (Buermann et al., 2018; Piao et al., 2017).

In warmer environments, high temperatures are observed to correlate with reduced photosynthetic rates (e.g. Pau et al., 2018), suggesting that further warming may reduce vegetation productivity. A key question is whether the observed relationships are due to the exceedance of temperature thresholds in photosynthetic biochemistry itself, with higher vapour pressure deficit accompanying high temperatures; observations and models suggest that the vapour pressure deficit effects are strongest, and that acclimation of photosynthetic optimal temperature may mitigate productivity losses of tropical forests under climate change (Lloyd and Farquhar, 2008; Tan et al., 2017). Since AR5, some ESMs have begun to include these acclimation responses, both in photosynthesis (Lombardozzi et al., 2015; Mercado et al., 2018) as well as in autotrophic respiration (Huntingford et al., 2017). However, these acclimation effects remain a large uncertainty in estimates of carbon-climate feedbacks.

Since AR5, research has been conducted to better understand the effect of variability in water availability on plant production and net land carbon uptake. Much of the local scale year-to-year variability in global vegetation production and net carbon uptake is associated with interannual variability in total and seasonal precipitation and therefore the extend of drought. In particular, semi-arid regions with substantial variability in the interannual rainfall appear to an important driver of the global interannual variability of productivity (Jung et al., 2017; Korth et al., 2015). ENSO-related occurrence of drought in the Amazon basin is a further large contributor to interannual variability in carbon exchange (Bastos et al., 2018; Humphrey et al., 2018; Lee et al., 2013), and may also play a role in carbon storage through changing mortality rates (Brienen et al., 2015). Analyses of offline land models show that they underestimate the correlation between terrestrial water storage and carbon fluxes (Humphrey et al., 2018), thus suggesting a similar pattern in fully-coupled ESMs. All CMIP5 ESMs predict that changes to productivity will outweigh changes to mortality in governing biomass changes (Koven et al., 2015a). However, an ensemble of land models that include additional ecological processes suggest that changes to mortality may be a more important driver of carbon dynamics in the real world (Friend et al., 2014). The role of longer-term changes in water availability in governing carbon fluxes remains an important uncertainty in carbon feedback estimates.

The majority of terrestrial ecosystem carbon resides in soils, where it is cycled back to the atmosphere by decomposers. Changes to soil carbon stocks in response to global change have long been considered a likely and potentially strong positive? feedback (Cox et al., 2000). Since the AR5, there have been important changes to our understanding of soil carbon dynamics, and thus the likely strength of feedbacks from soils. These include: (1) an increased recognition of the role of high latitude soils in storing large amounts of potentially decomposable soil carbon, and an increased focus on modelling these dynamics in ESMs; (2) a shift in the understanding of the causes responsible for soil carbon persistence on long timescales, away from earlier theories governed mainly by the intrinsic chemical recalcitrance of soil organic matter to a view of soil organic matter persistence as governed by complex ecological dynamics of the decomposer community interacting with soil organic matter and mineral assemblages (Luo et al., 2016; Schmidt et al., 2011).

In the CMIP5 ESMs, soils represented a significant contributor to both the carbon-concentration and carbon-climate feedbacks. The *uncertainty* on this feedback is *large*, as demonstrated by both the large model ensemble spread for carbon stock changes, as well as the large spread in current soil carbon stocks predicted by the models (Todd-Brown et al., 2013). Soil contributions to both feedbacks can often be traced to changes in plant carbon inputs to soils, which then result in changing soil carbon stocks. Changes to the lifetime of carbon in the soil, in response to elevated decomposition rates under global warming, were relatively weak in the CMIP5 ESMs (Koven et al., 2015a). This may be an artefact of the lack of permafrost carbon representation in any of the models. Changes to soil decomposition rates due to interactions between elevated productivity under elevated CO_2 and changing decomposer dynamics were also not included in any of the models.

For CMIP6, at least one ESM includes permafrost carbon cycle dynamics, which changes the sign of the carbon-climate feedback from the high latitudes from a weak sink with warming to a strong source of carbon with warming (Burke et al., 2018; Koven et al., 2011; McGuire et al., 2016; Schaefer et al., 2011). This response arises from the enormous stocks of carbon stored in high latitude soils (Hugelius et al., 2014), which are highly decomposable upon thaw (Schädel et al., 2014). Experimental warming treatments that thaw permafrost demonstrate a high potential for ecosystem carbon losses with warming (Schuur et al., 2009). Interactions between permafrost C and N cycles under warming weakens but does not offset feedback (Koven et al., 2015b). The uncertainty in this process remains large (McGuire et al., 2016), and the degree to which ESMs represent the feedback varies greatly.

Representation of soil microbial dynamics modify the response to temperature, as the longer-term microbial community responses are more complex than short-term temperature sensitivity. Such responses are observed in response to long-term warming experiments (Melillo et al., 2017). Complex responses show no clear pattern in meta-analyses of soil responses to warming, partially due to inability to separate decomposition from productivity changes (van Gestel et al., 2018). Using natural gradients of soil carbon turnover as a constraint on long-term responses to warming suggests that the CMIP5 ESMs may systematically underestimate the temperature sensitivity at high latitudes, and may overestimate the temperature sensitivity in the tropics (Koven et al., 2017; Wieder et al., 2018).

In nutrient limited ecosystems, prolonged soil warming can induce a fertilisation effect through increased decomposition, which increases nutrient availability and thereby vegetation productivity (Melillo et al., 2011). Models that include this process tend to have weaker carbon-climate feedbacks than those that do not (Thornton et al., 2009; Wårlind et al., 2014; Zaehle et al., 2010). In CMIP5, only one land model included nutrient dynamics, and it was an outlier in its feedback strength as compared to models that did not include nutrients. Several ESMs include nutrients in CMIP6 but only partly account for the interactions of nutrient effects with other processes such as shift of vegetation zones under climate changes (Sakaguchi et al., 2016) leading to either changes in species composition or changes in plant stoichiometry (Achat et al., 2016; Du et al., 2019; Thomas et al., 2015). Early analyses suggest that these models tend to have a less negative climate-carbon feedback than models not including nitrogen dynamics. However, the overall effect of nutrients is weaker than was inferred in AR5 [[Placeholder: needs update]].

5.4.4 Climate effects on ocean carbon uptake

5.4.4.1 Physical drivers of ocean carbon uptake

It is *likely* that the heat and anthropogenic CO_2 storage in the ocean show a common broad-scale pattern of change (Frölicher et al., 2015) and the ocean warming tends to reduce the CO_2 uptake from the atmosphere, resulting in a positive climate-carbon cycle feedback (Randerson et al., 2015). The cumulative ocean CO_2 uptake has been projected to reduce by 20 PgC by 2100 due to climate-driven perturbations to the natural carbon cycle (Bernardello et al., 2014). Changing buoyancy fluxes (heat, freshwater) result in circulation-driven changes in carbon storage, which decrease CO_2 uptake (Bernardello et al., 2014; Ito et al., 2015). Ocean carbon is also redistributed, with higher concentration at high latitudes and increased vertical

gradients in low latitude regions (Khatiwala et al., 2018). Ocean warming reduces the solubility of CO_2, increases stratification, which limits air-sea CO_2 exchange, and may contribute to slower meridional overturning circulation (Section 5.2.2.3.2; Chapter 9) (Matsumoto et al., 2010). With deep ocean circulation weakening, the downward transport of CO_2 from the surface to the deep ocean results in decreased CO_2 uptake in high latitudes, although at the same time weaker equatorial upwelling reduces upward transport of CO_2 therefore enhancing CO_2 uptake in low latitudes (Yamamoto et al., 2018). The warming of the ocean and its circulation changes in a high-CO_2 world also explains in part the lowering of the oceanic CO_2 uptake fraction. Sensitivity tests with an Earth system model driven by the RCP8.5 scenario suggests that these changes will reduce oceanic CO_2 uptake by 20% by the end of the twenty-first century compared to the case when these changes will not occur. Nearly half this decrease is attributed to warming surface waters in the shallow meridional overturning region (45°S–45°N) at high surface ocean pCO_2 conditions, with the remainder being due to circulation changes in the Southern Ocean and the northern North Atlantic (Rodgers and others No title).

Sea-ice processes may also affect the air-sea CO_2 exchange. During sea-ice growth, seawater total alkalinity (TA) and dissolved organic carbon (DIC) are concentrated in the brine and hence brine rejection during sea-ice melt increases the underlying DIC and TA (Søren et al., 2011). In regions of net export of sea ice, the polar mixed layer may become enriched in brine-associated TA and DIC, driving a sea-ice induced flux of CO_2 to the atmosphere (Rysgaard et al., 2013). This sea-ice induced CO_2 uptake is however a small fraction of net regional oceanic CO_2 uptake: ~1% in the Arctic and 5% in the Antarctic under the RCP4.5 warming scenario (Grimm et al., 2016).

5.4.4.2 Biological drivers of ocean carbon uptake

Currently, even the sign of the response of primary production (PP) to increased atmospheric CO_2 concentration and climate warming remains unclear, as it did at the time of AR5 (Taucher and Oschlies, 2011). Several interacting processes drive the response of PP to a changing climate and the choice of model parameterisation can result in different projections. Warmer temperatures increase metabolic rates, including PP, but also increase respiration rate (Boscolo-Galazzo et al., 2018). Warming also acts to increase stratification which reduces nutrient supply to the upper ocean (Chapter 9) and would thus result in decreased PP. However, experimental studies have shown that nutrient limitation reduces the temperature dependence of metabolic rates (Marañón et al., 2018), implying that the dominant effect of warming may be through indirect (nutrient supply) rather than direct (metabolic rates). Enhanced dust input into the ocean from desertification could alleviate iron limitation and result in increased PP. Alternatively, changes in ocean circulation and increased stratification could result in reduced iron supply to iron-limited regions, decreasing PP. Tagliabue et al., (2014) show that atmospheric CO_2 increases by only 2 ppmv if dust deposition is completely shut off, but incorporating light-iron colimitation leads to an increase of 9.6 μatm at low dust deposition (Nickelsen and Oschlies, 2015). An additional effect of increased warming is predicted to be changes in phytoplankton community structure towards smaller functional types that are adapted to low nutrient conditions, and also as a result of ocean acidification reducing the viability of calcareous organisms (Fu et al., 2016); both are expected to reduce PP. These stressors will not change in isolation in the future ocean, and the potential for synergistic, or antagonistic, effects of multiple stressors is unclear (Brennan and Collins, 2015; Boyd et al., 2015).

As a result of this complexity, CMIP5 model-simulated PP responses to the RCP8.5 scenario have a wide spread (Laufkötter et al., 2015), from -4.3 to +10 GtC yr^{-1} (median -0.2 GtC yr^{-1}), with 5 out of 9 models analysed showing a decrease in global PP to 2100. The reduction in PP at low latitudes in 3 of the models is driven by nutrient limitation due to increased stratification, whereas in the other models temperature-driven increases in loss processes (grazing, sinking, mortality) outweigh the higher phytoplankton growth rates (Laufkötter et al., 2015). Observations provide little constraint on the modelled responses of PP to climate change, partly due to insufficiently long records (Henson et al., 2016).

As climate change exposes phytoplankton to lower nutrient supply and potentially increased light levels, phytoplankton community structure changes may affect the nutrient stoichiometry of organic matter.

Biogeochemical models which incorporate variable stoichiometry predict that the C:N ratio will increase by 0.4% and the C:P ratio by 4.3% under RCP8.5 (Kwiatkowski et al., 2018), i.e. the amount of carbon stored via the soft tissue pump increases relative to the amount of PP. In a 5 box ocean model with variable stoichiometry, declines in subtropical phosphate supply driven by an increase in ocean temperature of 5 °C resulted in a decrease in atmospheric CO_2 concentrations of 60 ppm (Moreno et al., 2018). By overlooking variable organic matter stoichiometry, the fixed stoichiometry models (as used in CMIP5) may underestimate cumulative ocean carbon uptake to 2100 by 0.5–3.5% (2–15 PgC) (Kwiatkowski et al., 2018).

The mechanisms underlying the remineralisation of particulate organic carbon (POC) in the water column are myriad, interlinked and difficult to quantify observationally. Alterations to the efficiency and functioning of the soft tissue pump may arise due to changing circulation, altered phyto- and zooplankton community structure (altering both the magnitude of POC export and the type of sinking material produced), warming affecting metabolic rates, changing stoichiometry of organic matter, etc. In addition, a reduction in the viability of calcifying organisms due to ocean acidification may affect the soft tissue pump by reducing the amount of material available to 'ballast' POC. Other climate effects such as deoxygenation and warming could also result in alterations to the magnitude and efficiency of the carbonate pump via changes in phytoplankton community composition (Fu et al., 2016). POC export flux is expected to decline by 1-12% by 2100 with CMIP5 models run under RCP8.5 (Laufkötter et al., 2016), with the mechanisms driving these changes varying widely between models due to differences in parameterisation of particle formation, remineralisation and phytoplankton community structure. The model simulation by Matear and Lenton (2014) suggested that if POC export increases under RCP8.5, atmospheric CO_2 drops by ~43ppm by 2100, while enhanced remineralisation of POC and dissolution of particulate organic carbon (PIC) could increase atmospheric CO_2 by ~18 ppm by 2100. The combination of the above processes reduced atmospheric CO_2 by 38ppm by 2100. However, the complexity of the mechanisms involved in the remineralisation of POC represent a significant uncertainty in the magnitude and sign of ocean carbon cycle feedback to changes in atmospheric CO_2 and climate (Hülse et al., 2017). Improved model representation (which will require better observational constraints) of the soft tissue pump is required, as the contribution of biological processes to CO_2 uptake is expected to become more significant with continued climate change, due to a combination of decreasing buffer capacity and strong seasonality in the pump (at high latitudes) resulting in strengthening seasonality in anthropogenic carbon uptake (Hauck et al., 2015).

5.4.5 Carbon Cycle Projections in Earth System Models

This section analyses the future projections of land and ocean carbon sinks, and of atmospheric CO_2, from the latest Earth System Models (ESMs). ESMs are the basis for century timescale projections, and for detection and attribution studies (Chapter 3). These models aim to simulate the evolution of the carbon sources and sinks on land and in the ocean, in addition to the physical components of the climate system.

Land-atmosphere and ocean-atmosphere carbon fluxes are sensitive to changes in climate and atmospheric CO_2, for the many reasons outlined in Sections 5.4.2 and 5.4.3. Early attempts to include the carbon cycle as an interactive element within GCM climate models showed the potential for the carbon cycle to accelerate the rate of global warming (Cox et al., 2000; Friedlingstein et al., 2001). The subsequent C^4MIP project compared coupled climate-carbon cycle simulations from six models, highlighting the uncertainties associated with carbon cycle feedbacks (Friedlingstein et al., 2006). By the time of the IPCC AR5 most climate modelling groups had included an interactive carbon cycle, leading to the evolution of climate models into ESMs.

The CMIP5 ESMs discussed in the AR5 produced a wide range of projections of future CO_2 (Friedlingstein et al., 2014) primarily associated with different magnitudes of carbon-climate and carbon-concentration feedbacks (Arora et al., 2013), but also exacerbated by differences in the simulation of the net carbon release from land-use change (Brovkin et al., 2013). A key difference among the CMIP5 models was the extent to which nutrient availability limited the CO_2-fertilisation of plant photosynthesis, with most models assuming no nutrient limitations (Zaehle et al., 2015). The CMIP6 models considered in this report now include nutrient limitations on vegetation growth, along with many other improvements (see Table 5.4).

[START TABLE 5.4 HERE]

Table 5.4: CMIP6 Earth System Models considered in this subsection [[Placeholder: needs to be updated for CMIP6 rather than CMIP5 models]].

Model name	Model name expanded	Land carbon component	Ocean carbon component	Land use emissions	Terrestrial nitrogen cycle	Reference
CanESM2	Second Generation Canadian Earth System Model	Canadian Terrestrial Ecosystem Model (CTEM)	Canadian Model of Ocean Carbon (CMOC)	Computed	No	Arora et al. (2011)
GFDL-ESM2G	Geophysical Fluid Dynamics Laboratory Earth System Model with Generalized Ocean Layer Dynamics (GOLD) component (ESM2G)	Land Model LM3V	Tracers of Ocean Phytoplankton with Allometric Zooplankton (TOPAZ)	Computed	No	Dunne et al. (2013)
HadGEM2-ES	Hadley Centre Global Environment Model, version 2 - Earth System	Met Office Surface Exchange Scheme–Top-down Representation of Interactive Foliage and Flora Including Dynamics (MOSES-TRIFFID)	Diatom version of the Hadley Centre Ocean Carbon Cycle model (Diat-HadOCC)	Computed and prescribed	No	Collins et al. (2011)
IPSL-CM5A-LR	L'Institut Pierre-Simon Laplace Coupled Model, version 5, coupled with NEMO, low resolution	Organizing Carbon and Hydrology in Dynamic Ecosystems (ORCHIDEE)	Pelagic Interactive Scheme for Carbon and Ecosystem Studies (PISCES)	Computed	No	Dufresne et al. (2103)
MIROC-ESM	Model for Interdisciplinary Research on Climate, Earth System Model	Spatially Explicit Individual-Based Dynamic Global Vegetation Model (SEIB-DGVM)	Nutrients–phytoplankton–zooplankton-detritus (NPZD)	Computed	No	Watanabe et al. (2011)
MPI-ESM-LR	Max Planck Institute Earth System Model, low resolution	Jena Scheme for Biosphere–Atmosphere Coupling in Hamburg (JSBACH)	Hamburg Model of the Ocean Carbon Cycle (HAMOCC)	Computed	No	Ilyina et al. (2013)
CESM1-BGC	Community Earth System Model, version 1–Biogeochemistry	Community Land Model (CLM)	Biogeochemical Elemental Recycling (BEC)	Computed	Yes	Long et al. (2013)
NorESM1-ME	Norwegian Earth System Model, version 1 (carbon cycle)	Community Land Model (CLM)	Miami Isopycnic Coordinate Ocean Model (MICOM)	Computed	Yes	Tjiputra et al. (2012)
BCC-CSM-1	Beijing Climate Center, Climate System Model, version 1	BCC Atmosphere–Vegetation-Interaction Model (BCC-AVIM1)	Ocean Carbon-Cycle Model Intercomparison Project Phase 2 (OCMIP-2)	Prescribed	No	Wu et al. (2010), Xin et al. (2013a,b)
INM-CM4.0	Institute of Numerical Mathematics Coupled Model, version 4.0	—	—	Prescribed	No	Volodin et al. (2010)
MRI-ESM1	Meteorological Research Institute Earth System Model, version 1	—	—	Prescribed	No	Adachi et al. (2013)

[END TABLE 5.4 HERE]

5.4.5.1 Evaluation of carbon cycle simulations against observations

To have confidence in their projections the models must be compared to as wide an array of observational benchmarks as possible. This is particularly the case for highly-uncertain land carbon cycle feedbacks (Friedlingstein et al., 2003, 2006, 2014b). Land models within ESMs should be compared to multiple different datasets of processes such as gross carbon uptake, physical predictions such as leaf are and carbon stocks which influence carbon fluxes and are diagnostic of carbon turnover times, as well as linkages between carbon and water cycles and other aspects of the terrestrial carbon cycle. To address this, a model benchmarking system, ILAMB has been developed (Collier et al., 2018) to provide these multiple orthogonal

constraints. Figure 5.21 shows an overview of an initial set of terrestrial benchmarks applied to both the CMIP5 and CMIP6 models. [[Placeholder: On the whole, and provisional statement based on incomplete data thus far available from CMIP6. Based on preliminary data from CMIP6 models, it appears that model benchmarking scores have generally improved from the CMIP5 to the CMIP6 generation of models, which is consistent with the models providing a more useful estimate of feedback parameters than the CMIP5 generation of ESMs.]]

[START FIGURE 5.21 HERE]

Figure 5.21: Overview scores of CMIP5 (left hand side of table) and CMIP6 (right hand side of table) models, for multiple land-surface benchmarks against different datasets. Scores are relative to other models within each benchmark row, with positive scores indicating a better agreement with observations. [[Placeholder: Figure to be updated in SOD to include all and only the models used for carbon cycle feedback parameter assessments in AR5 and AR6, as well as to sort out some artefacts in current figure associated with unit conversions that are resulting in missing values (grey squares), etc.]]

[END FIGURE 5.21 HERE]

When used within fully coupled ESM historical simulations (with prescribed emissions) ocean carbon cycle models reproduce historical carbon uptake well, with a current day sink of 2.0–2.7 PgC yr^{-1}. Simulated changes in ocean carbon storage (1860–2005) range from 75 to 160 PgC, but most models are within 25 PgC of the observational estimate of 125 PgC (Figure 5.22).

[START FIGURE 5.22 HERE]

Figure 5.22: Modelled ocean carbon sink for 1850 to 2005 in historical ESM simulations, compared to observation-based estimates (from GCP); panel (a): uptake rate (PgC yr^{-1}), panel (b): change in carbon store (PgC).

[END FIGURE 5.22 HERE]

The land carbon cycle components of historical ESM simulations show a much larger range, with simulated historical changes in land carbon storage (1850–2005) spanning the range from -130 to +80 PgC (Figure 5.23). This range is due in part to the complications of simulating the difference between carbon uptake by intact ecosystems (e.g. due to CO_2 fertilisation of photosynthesis) and the direct release of carbon due to land-use change (e.g. tropical deforestation). It also reflects the much higher-interannual variability of net land carbon uptake compared to ocean carbon uptake. However, the tendency for the land carbon cycle to be a dominant source of uncertainty in the climate-carbon cycle projections of C^4MIP and CMIP5 models, is also clear in CMIP6.

[START FIGURE 5.23 HERE]

Figure 5.23: Modelled net land carbon sink for 1850 to 2005 in historical ESM simulations, compared to observation-based estimates (from GCP); panel (a): net uptake rate (PgC yr^{-1}), panel (b): change in carbon store (PgC).

[END FIGURE 5.23 HERE]

This distinction between the relatively high-fidelity with which the ocean carbon sink is simulated, and the much wider range of simulations of the land carbon sink, is also evident in the zonal distribution of the sinks (Figure 5.24a). When compared to estimates from a state-of-the-art atmospheric inversion, the ocean carbon cycle components of ESMs are able to simulate the tropical CO_2 source and mid-latitude CO_2, and with

relatively small model spread. The ensemble mean simulates a larger ocean carbon sink at 50°N and a weaker sink in the Southern Ocean, than the inversion estimate.

By contrast, the land carbon components of ESMs produce a wide range in the latitudinal distribution of net land carbon uptake (Figure 5.24b). Most ESMs tend to overestimate net land carbon uptake in the tropics, and underestimate the northern hemisphere land carbon sink. [[Placeholder: this error in the geographical location of the land carbon sink is however less obvious than it was in the previous generation CMIP5 models (Anav et al., 2013), perhaps because the CMIP6 models now include the impacts of nitrogen deposition.]]

[START FIGURE 5.24 HERE]

Figure 5.24: Evaluation of the modelled zonal distribution of carbon sinks against atmospheric inversion estimates for 2000–2009, (a) ocean carbon uptake; (b) net land uptake. The model results are shown as the mean plus and minus one standard deviation of the annual values across the model ensemble.

[END FIGURE 5.24 HERE]

5.4.5.2 Coupled Climate-Carbon Cycle Projections

Here we briefly describe results from the emissions-driven projections carried out with the ESMs (only RCP8.5 from CMIP5 available to date), and also from the RCP2.6 and RCP8.5 concentration-driven runs, which enable a cleaner comparison of the differences across the carbon cycle components of the ESMs.

The carbon cycle feeds back to climate change by affecting the evolution of atmospheric CO_2, so firstly, we look at the projections of atmospheric carbon dioxide concentrations from the emission-driven ESM projections. For each model, common future scenarios of anthropogenic fossil fuel CO_2 emissions and land-use change were prescribed [[Placeholder: consistent with the RCP8.5 and RCP2.6 scenarios]] (Jones et al., 2016a). As for the CMIP5 models (Friedlingstein et al., 2014b), the CMIP6 ESMs project a range of CO_2 concentrations under each scenario, with a spread of almost 250 ppmv by 2100 for RCP8.5 [[Placeholder: needs checking]] (Figure 5.25a).

[START FIGURE 5.25 HERE]

Figure 5.25: Modelled global mean, annual mean, carbon dioxide concentration compared to observations. (a) CO_2 concentration for 1860 to 2100 from emissions-driven RCP8.5 runs, compared to observed global mean CO_2 concentration (as used in prescribed concentration runs) for 1860–2018; (b) Relationship between CO_2 concentration simulated for 2014 and CO_2 concentration projected for 2060 under RCP8.5 emissions (after Hoffman et al., 2014).

[END FIGURE 5.25 HERE]

Models that tend to have higher-CO_2 by 2100 also tend to overestimate CO_2 by the current day in historical simulations (1860–2005 in Figure 5.25a). This implies an emergent relationship between current and future CO_2 in each model (Figure 5.25b), and therefore the possibility of constraining future CO_2 levels using that relationship plus the observed value of current CO_2. This is an example of an *emergent constraint* on projections (see Section 5.4.6).

The differences in projected CO_2 concentrations arise primarily because the models simulate different futures for the ocean and land carbon sinks. Figure 5.26 shows the projected evolution of the global ocean carbon sink (left panel) and accumulated change in ocean carbon storage from the current day (right panel), from RCP2.6 and RCP8.5 concentration-driven ESM runs. The colour wedges represent the ensemble mean plus

and minus one standard deviation of the individual ESM values across the ensemble.

[START FIGURE 5.26 HERE]

Figure 5.26: Projected evolution of the ocean carbon sink for 2005 to 2090 in concentration-driven RCP2.6 (blue) and RCP8.5 (red) scenarios. Panel (a): net uptake rate (PgC yr^{-1}); panel (b): change in carbon store (PgC). Thick lines represent the ensemble mean of the available ESM runs, and the shaded area represents ± one standard deviation about that mean.

[END FIGURE 5.26 HERE]

All ESMs predict a declining global ocean carbon sink once the CO_2 concentration starts to decline from the mid–2020s onwards under RCP2.6, such that the projected ocean sink is around 1±0.3 PgC yr^{-1} by 2090 [[Placeholder: Numbers to be updated]]. Stabilisation of CO_2 from 2070 onwards under RCP8.5 leads to a saturation of the ocean carbon sink by 2090 at 5.5±0.7 PgC yr^{-1}. The change in ocean carbon storage from the present day until 2090 is very different between RCP8.5 (350±40 PgC) and RCP2.6 (160±30 PgC), with different consequences for ocean acidification (see Section 5.3).

[START FIGURE 5.27 HERE]

Figure 5.27: Projected evolution of the net land carbon sink for 2005 to 2090 in concentration-driven RCP2.6 (blue) and RCP8.5 (red) scenarios. Panel (a): net uptake rate (PgC yr^{-1}); panel (b): change in carbon store (PgC). Thick lines represent the ensemble mean of the available ESM runs, and the shaded area represents ± one standard deviation about that mean.

[END FIGURE 5.27 HERE]

One again, we see a much larger range in future projections of the land carbon sink (Figure 5.27). The model ensemble projects a change in land carbon storage from 2005 to 2090 of 70±80 PgC under RCP2.6 and 90±200 PgC under RCP8.5. Even the sign of the change in land carbon storage, which depends on the difference between the net carbon uptake by existing vegetation and net carbon release from land-use change, is therefore disputed.

5.4.5.3 Linear Feedback Analysis

In order to diagnose the causes of the varying time-evolution of carbon sinks, the traditional linear feedback approach is adopted (Friedlingstein et al., 2003), as used previously to analyse C^4MIP (Friedlingstein et al., 2006) and CMIP5 models (Arora et al., 2013). Changes in land carbon storage (ΔC_L) and changes in ocean carbon storage (ΔC_o) are decomposed into contributions arising from warming (ΔT) and increases in CO_2 (ΔCO_2):

$$\Delta C_L = \beta_L \, \Delta CO_2 + \gamma_L \, \Delta T$$

where β_L and γ_L the coefficients that represent the sensitivity of land carbon storage to changes in CO_2 and climate respectively.

Although this quasi-equilibrium framework is known to be dependent on scenario because of the timescales associated with land and ocean carbon uptake, we retain it here for consistency with the AR5, and because it has been used to define a number of emergent constraints on carbon cycle feedbacks (see below). In order to minimise the confounding effect of the scenario dependence, β and γ values are diagnosed from idealised runs in which a 1% per year increase in atmospheric CO_2 concentration is prescribed, as for AR5 (Arora et

al., 2013). Values of β are calculated from 'biogeochemical' runs in which the prescribed CO_2 increases do not affect climate, and these are then used to isolate γ values in fully-coupled runs in which both climate and CO_2 change (Friedlingstein et al., 2003).

Table 5.5 shows the global and tropical (30°N–30°S) values of β and γ for each of the CMIP6 ESMs. As for AR5, the largest uncertainties are in the sensitivity of land carbon storage to CO_2 (β_L) and the sensitivity of tropical carbon storage to climate change (γ_{LT}). Emergent constraints have been suggested for both of these sensitivities.

[START TABLE 5.5 HERE]

Table 5.5: Diagnosed feedback parameters for ESMs. [[Placeholder from (Arora et al., 2013), needs to be updated to latest CMIP6 models, and with columns consistent with the emergent constraints to be presented in the next section, e.g. global, tropical land (30°N–30°S), mid & high latitudes land (30°N–90°N), tropical ocean, Southern Ocean. We do not need beta and gamma for the atmosphere.]]

	Carbon–concentration feedback parameter β (Pg C ppm^{-1})			Carbon–climate feedback parameter γ (Pg C °C^{-1})		
Model	β_A Atmosphere	β_L Land	β_O Ocean	γ_A Atmosphere	γ_L Land	γ_O Ocean
MPI-ESM-LR	−2.29	1.46	0.83	92.2	−83.2	−9.0
IPSL-CM5A-LR	−2.04	1.14	0.91	64.8	−58.6	−6.2
BCC-CSM1	−2.19	1.36	0.83	87.6	−77.8	−9.8
HadGEM2	−1.95	1.16	0.79	40.1	−30.1	−10.0
UVic ESCM 2.9	−1.75	0.96	0.78	85.8	−78.5	−7.3
CanESM2	−1.65	0.97	0.69	79.7	−71.9	−7.8
NorESM-ME	−1.07	0.22	0.85	21.4	−15.6	−5.7
CESM1-BGC	−0.96	0.24	0.72	23.8	−21.3	−2.4
MIROC ESM	−1.56	0.74	0.82	100.7	−88.6	−12.1
Model mean (std dev)	−1.72 (0.47)	0.92 (0.44)	0.80 (0.07)	66.2 (30.4)	−58.4 (28.5)	−7.8 (2.9)
C^{4}MIP mean (std dev) (FEA)	−2.48 (0.59)	1.35 (0.61)	1.13 (0.26)	109.6 (50.6)	−78.6 (45.8)	−30.9 (16.3)

[END TABLE 5.5 HERE]

5.4.6 Emergent constraints to reduce uncertainties in projections

Emergent constraints are based-on relationships between observable aspects of the current or past climate (such as trends or variability), and uncertain aspects of future climate change (such as the strength of particular feedbacks) – relationships which are evident across an ensemble of models. When combined with an observational estimate of the trend or variability in the real climate, such emergent relationships can yield 'emergent constraints' on the future climate change. The term was coined in 2002 (Allen and Ingram, 2002), but the archetypal example is an emergent constraint on snow-albedo feedback (Hall and Qu, 2006). At the time of the AR5, there had been relatively few applications of the technique to constrain carbon cycle sensitivities (Cox et al., 2013), but there have been many relevant studies published since. The concept of emergent constraints is explained in more depth in Chapter 1 Section 1.?? [[Update]].

The simplest type of emergent constraint is a relationship between a past-to-present change and a present-to-future change. For example, a relationship was noted in ESM runs between the simulated CO_2 concentration by 2010, and the projected CO_2 concentration in the future under the RCP8.5 scenario (Friedlingstein et al., 2014b). As the CO_2 concentration in 2010 is known from observations, there is a potential emergent constraint on the future CO_2 concentration under this common scenario (Hoffman et al., 2014), as shown in Figure 5.28a. Such trend-on-trend relationships depend on models being similarly forced (in this case by CO_2 emissions consistent with RCP8.5).

Other emergent constraints assume relationships between short-term variability and long-term sensitivity to forcing, and are often motivated by ideas related to the fluctuation-dissipation theorem (Leith, 1975). These constraints can also be understood as utilizing relationships between the sensitivity of fluxes and the

sensitivity of stores. For example, the observed interannual variability in the growth-rate of atmospheric CO_2 is known to be due to variability in land uptake of CO_2 which is itself driven by ENSO climate variability. Interannual variations in CO_2 in response to ENSO therefore reveal the sensitivity of the net atmosphere-land CO_2 flux to temperature. In ESMs this flux sensitivity has been shown to be approximately proportional to the sensitivity of the tropical land carbon store to future warming (γ_{LT}). Since CO_2 and climate records allow the observed flux sensitivity to be estimated, this implies an emergent constraint on γ_{LT}, which was originally reported for C^{4}MIP models (Cox et al., 2013) and confirmed for CMIP5 models (Wenzel et al., 2014) – see Figure 5.28b. In a similar way, satellite estimates of the variability in ocean productivity constrain projected changes in tropical marine productivity under long-term warming (Kwiatkowski et al., 2017).

Other constraints relate the seasonal cycle (Hall and Qu, 2006), or changes in the seasonal cycle (Wenzel et al., 2016), to the strength of particular feedbacks. A recent carbon cycle example uses the well-documented increase in the amplitude of the seasonal cycle of atmospheric CO_2 as measured at Mauna Loa and Point Barrow (Graven et al., 2013) to constrain CO_2–fertilisation of photosynthesis on mid and high-latitude (Wenzel et al., 2016), as shown in Figure 5.28c.

[START FIGURE 5.28 HERE]

Figure 5.28: Examples of emergent constraints on the carbon cycle in ESMs. (a) projected global mean atmospheric CO_2 concentration by 2100 under the RCP8.5 emissions scenario against the error in simulation of global mean atmospheric CO_2 by 2010 in historical simulations (Friedlingstein et al., 2014b; Hoffman et al., 2014); (b) γ-factor for tropical land (γ_{LT}) against the sensitivity of the atmospheric CO_2 growth-rate to tropical temperature variability (Cox et al., 2013b; Wenzel et al., 2014); (c) β-factor for mid and high-latitude land (β_{LM}) against the sensitivity of the amplitude of the CO_2 seasonal cycle at Kumukahi, Hawaii to atmospheric CO_2 concentration (Wenzel et al., 2016).

[END FIGURE 5.28 HERE]

5.4.7 Non-CO_2 feedbacks

Sources and sinks of non-CO_2 greenhouse gases such as methane (CH_4) and nitrous oxide (N_2O) respond to atmospheric CO_2 concentration and climate change, and therefore give rise to CO_2-concentration and climate feedbacks. These feedbacks are not yet routinely included in ESMs. Nevertheless, the likely strength of these feedbacks can be approximated in a similar, linear framework as for CO_2 based on simulations with standalone models or ESMs of intermediate complexity (Figure 5.29).

[START FIGURE 5.29 HERE]

Figure 5.29: A synthesis of the magnitude of biogeochemical feedbacks on climate expressing non-climate feedbacks in common units (W m^{-2} K^{-1}) with physical feedbacks, following (Arneth et al., 2010; Gregory et al., 2009) and revised radiative forcing calculations (Etminan et al., 2016). Black dots represent single estimates, and coloured bars denote the simple mean of the dots with no weighting or assessment being made to likelihood of any single estimate. These feedback metrics have, where possible, been assessed for the RCP8.5 scenario in year 2100. They may be state or scenario dependent and therefore cannot always be compared like-for-like. Note the different x-axis scale for the lower portion of the Figure. There is low confidence in the magnitude of the feedbacks in the lower panel of the figure. The role of nitrogen limitation on terrestrial carbon sinks is also shown this is not a separate feedback, but rather a modulation to the climate-carbon and concentration-carbon feedbacks. Results have been compiled from (a) C-cycle ESMs of C^{4}MIP (Arora et al., 2013); (b) CN-cycle ESMs of C^{4}MIP (Arora et al., 2013) and (Sokolov et al., 2008; Thornton et al., 2009; Zaehle et al., 2010; Zhang et al., 2013a); (c) (Arneth et al., 2010; Eliseev et al., 2014; Harrison et al., 2018); (d) (Burke et al., 2013; Gasser et al., 2018; Koven et al., 2015b; Schneider von Deimling et al., 2012), (e) (Schneider von Deimling et al., 2012, 2015; Turetsky et al.); (f) (Denisov et al., 2013; Stocker et al., 2013a; Zhang et al., 2017); (g) (Voulgarakis et al., 2013); (h)

(Stocker et al., 2013a; Tian et al., 2019; Xu-Ri et al., 2012; Zaehle, 2013); (i) (Battaglia and Joos, 2018; Landolfi et al., 2017; Martinez-Rey et al., 2015).

[END FIGURE 5.29 HERE]

CH_4 feedbacks may arise from changing wetland and permafrost CH_4 emissions and the response of atmospheric chemistry to climate change. CH_4 emissions from wetlands generally respond positive to warming due to enhanced decomposition with higher temperatures, thereby potentially providing a positive CH_4 feedback on climate (Dean et al., 2018; van Groenigen et al., 2011). The contribution of wetlands to interannual variability of atmospheric CH_4 is shaped by the diverging impacts of temperature and precipitation anomalies on wetland emissions and therefore the relationship between climate anomalies and the wetland contribution to the CH_4 growth rate is less clear (Pison et al., 2013; Zhang et al., 2018b). In model simulations, the climate-CH_4 cycle feedback enhances the CH_4 build up in the atmosphere under RCP emission scenarios at decadal to multidecadal timescales, but the effect on the methane radiative forcing is low (Denisov et al., 2013; Gedney, 2004; Ringeval et al., 2011; Volodin, 2008). Model simulations further suggest that the climate-CH_4 feedback from wetlands is weaker than the effect of rising atmospheric CO_2 on CH_4 emissions feedback due to the effect of increased plant productivity on methane production (Melton et al., 2013; Ringeval et al., 2011). However, insufficient studies are available to assess the effect of the CO_2-wetland CH_4 on radiative forcing. Permafrost thaw and methane emissions from thermokarst may further contribute to a positive land-CH_4-climate feedback, but the quantitative understanding of the magnitude and timing of CH_4 release is low (Schneider von Deimling et al., 2012, see Section 5.4.8; 2015; Turetsky et al.). Higher temperatures affect atmospheric chemistry and thereby reduce the lifetime of methane in the atmosphere, providing a negative feedback (Stevenson et al., 2006; Voulgarakis et al., 2013).

Both land and ocean N_2O emissions respond to climate change. At the interannual time-scale, land N_2O emissions respond to anomalies in temperature and precipitation, likely leading to lower emissions in warmer, but dryer El Nino years (Thompson et al., 2014). Land biosphere models suggest that longer-term global warming is accompanied by enhanced N_2O release from terrestrial ecosystems (Stocker et al., 2013a; Tian et al., 2019; Xu-Ri et al., 2012; Zaehle, 2013). The response of terrestrial N_2O emissions to CO_2 is dependent on nitrogen availability, where generally nitrogen rich ecosystems, such as highly fertilised fields show a positive interaction, whereas nitrogen poor ecosystems may show also declines in N_2O emissions (Butterbach-Bahl et al., 2013; Tian et al., 2019; van Groenigen et al., 2011). Climate change will also affect N_2O production in the ocean through changes in productivity, stronger vertical stratification and ocean de-oxygenation (Bopp et al., 2013; Codispoti, 2010; Freing et al., 2012). Model projections under the RCP8.5 scenario suggest ocean N_2O emissions may decrease by 4–12% over the 21st century due to a combination of factors including increased ocean stratification, decreases in ocean productivity, and the impact of increasing atmospheric N_2O abundance on the air-sea flux (Battaglia and Joos, 2018; Landolfi et al., 2017; Martinez-Rey et al., 2015). Ocean N_2O emissions may recover on longer timescales owing to ocean de-oxygenation and long-term increases in remineralisation, leading to a positive correlation of N_2O emission and climate at the timescale of millennia (Battaglia and Joos, 2018). The magnitude of the terrestrial and oceanic N_2O feedbacks combined with the long atmospheric lifetime of N_2O imply that their effect on radiative forcing in the next century will be low, but may become important if the terrestrial emission changes are sustained beyond that time scale (Xu-Ri et al., 2012).

Despite these uncertainties, there is *medium to high confidence* that at multidecadal and centennial timescales the additional radiative forcing arising from climate-CH_4 and climate-N_2O feedbacks will be small compared to anthropogenic forcing in the 21st century.

5.4.8 Abrupt changes and tipping points

The utility of the linear feedback framework (Section 5.4.4.1) and the existence of emergent constraints (Section 5.4.4.2) suggest that large-scale biogeochemical feedbacks are approximately linear in the forcing from changes in CO_2 and climate. Nevertheless, regionally the biosphere is known to be capable of

producing abrupt changes or 'tipping points' (see Chapter 1, Section/Box 1.?.? [[Update]]). The catalogue of possible Earth System tipping points identified to date includes a number related to ecosystems and biogeochemistry (Lenton et al., 2008) – including tropical and boreal forest dieback, greening of sub-Sahara Africa, and release of carbon from permafrost. Some of the proposed tipping points are essentially bifurcations of a system with multiple steady-states. These cases are described as 'irreversible' when crossing the bifurcation point leads to a new steady-state that is not destabilised by merely passing back through the bifurcation point. This section focuses on non-linear changes that could have a significant impact on greenhouse gases concentrations to 2100, relative to changes caused directly by anthropogenic emissions (see Section 5.4.9 for longer time scales).

5.4.8.1 Forest dieback

Known examples of tipping points with apparent changes in biogeochemical cycles functioning are tropical rain forests dieback (Cox et al., 2004; Le Page et al., 2017; Zemp et al., 2017) and temperate and boreal forests dieback (Joos et al., 2001; Lasslop et al., 2016; Lucht et al., 2006; Scheffer et al., 2012) diebacks. Such tipping point may be related to (i) large-scale change in climate conditions (Cox et al., 2004; Hirota et al., 2011; Joos et al., 2001; Le Page et al., 2017; Lucht et al., 2006; Scheffer et al., 2012; Zemp et al., 2017) and may be traced to crossing of particular climatic thresholds,(ii) to temperature and precipitation extremes (Higgins and Scheiter, 2012; Pavlov, 2015; Staver et al., 2011), or (iii) to possible intermittency in fire activity (Higgins and Scheiter, 2012; Lasslop et al., 2016; Staver et al., 2011) occurring either due to climate feedbacks or due to human (ignition) forcing. For large-scale change of climate conditions and associated crossing of climatic threshold the confidence is low because there is a disagreement between different simulations: some of them do not exhibit tropical forests dieback partly due to climate changes, which are insufficient for crossing climatic thresholds (Boulton et al., 2017; Huntingford et al., 2013), a greater degree of ecosystem stability due to environmental heterogeneity and plant trait diversity (Levine et al., 2016; Sakschewski et al., 2016), or possible acclimation of terrestrial vegetation to imposed climate changes (Lloret et al., 2012). In the latter case, acclimation is more likely to occur for relatively slow climate changes. In general, forest dieback is more probable under higher-emission scenarios of anthropogenic forcing leading to more prominent climate changes (Lyra et al., 2017) as well as under more intensive land use (Le Page et al., 2017). For the RCP8.5 scenario (Anadón et al., 2014) estimate that 24% (range 9–39%) of the contemporary American tropical rainforests may be converted to savanna until the late 21st century. Extrapolating this estimate for whole tropical forests, and using the estimate of the tropical forest carbon stock (Saatchi et al., 2011), an upper bound for the respective carbon release into the atmosphere is ~100 PgC, which translates to dCO_2/dt O(0.1 ppmv yr^{-1}). Boreal forest dieback is *unlikely* to change the atmospheric perturbation substantially. Tropical and boreal dieback tipping trajectories are slow, associated with a multi-decadal development timescale.

There is a *high confidence* that forest dieback will not release more than 100 Pg of carbon over the 21st century.

5.4.8.2 Biogenic emissions from permafrost

The permafrost region has acted as either a weak carbon sink or source historically (Belshe et al., 2013; McGuire et al., 2012), but the source strength could strengthen considerably under warming. Model projections of CO_2 emissions by 2100 under a high warming scenario have been estimated at 37–174 Pg (Schuur et al., 2015); 28–113 Pg (Koven et al., 2015c); 11–143 Pg (Gasser et al., 2018), and strengthen even further by 2300. Of the CMIP6 ESMs that include permafrost, they estimate gains/losses of XX Pg [[Placeholder: needs update]]. Because of widespread soil saturation and anoxia in the region, part of the carbon flux from ecosystems to the atmosphere is via production of CH_4, and the respective radiative forcing may be larger. Methane release from thermokarst lakes under warming has been estimated at 663-2440 Tg CH_4 over the 21st century (Schneider von Deimling et al., 2015), and from all abrupt thaw processes as 9000 Tg CH_4 over the 21st century (Turetsky and others). Internal heat production in organic permafrost soils is able to amplify permafrost thawing and accelerate organic matter decomposition, thus, increasing carbon loss (Hollesen et al., 2015). In the case of carbon in deep peat and carbon-rich permafrost sediments, warming accompanied by drying may also induce internal heat production leading to the compost-bomb

instability (Koven et al., 2011; Luke and Cox, 2011), though the uncertainty on this process is particularly high. Coupled CH_4-climate models show that possible increases in CH_4 lead to similar patterns in the global pattern of radiative forcing of CH_4, irrespective of where the CH_4 sources are located (Volodin, 2015). Another possible source of CH_4 from the terrestrial cryosphere are relict gas hydrates in deeper permafrost, which may have caused recent craters in the Russian North (Arzhanov et al., 2016; Kizyakov et al., 2017, 2018), and which might indicate that the contemporary warming already exceeded the mid-Holocene climate in these regions (Arzhanov and Mokhov, 2017).

There is *high confidence* that thawing terrestrial permafrost will lead to carbon releases, but *low confidence* in the timing, magnitude and the relative roles of CO_2 versus CH_4 as feedback processes.

5.4.8.3 Clathrate release

Methane release from shelf clathrates is <10 $TgCH_4$ yr^{-1} (Saunois et al., 2016b). Abrupt change is *very unlikely* for the permafrost-embedded subsea clathrates owing to a long response time, which makes the 'clathrate gun' hypothesis *extremely unlikely* at the centennial and millennium timescales. Early estimates had suggested that the ocean may release 600 $PgCH_4$ in response to 1000 PgC of cumulative emissions from fossil fuels (Archer et al., 2009), indicating that this hypothesis would be plausible at multi-millennium and longer time scales (Majorowicz et al., 2014; Zeebe, 2013). This tipping point is also associated with a slow, from multi-decadal to centennial timescale. More recent estimates of the amount of carbon stored in methane clathrates are much smaller, at around 2000 PgC total (Ruppel and Kessler, 2017). Because the amount of clathrate that might be destabilised due to warming is a small fraction of this, the long timescales associated with clathrate destabilisation, and because much of that CH_4 would likely be oxidised in the process, leading to estimated fluxes of less than 5 $TgCH_4$ yr^{-1} over the next century (Kretschmer et al., 2015). Thus there is *medium confidence* that this tipping point is *unlikely* to substantially warm the climate system.

5.4.8.4 Weakening of the Southern Ocean carbon sink

In the ocean, a tipping point is possible due to suppression of the carbon uptake in the Southern Ocean, which was already observed during 1990s and 2000s with a rebound in 2010s (Gruber et al., 2019b; Landschützer et al., 2016). The former suppression is attributed to the southward shift of westerlies (Lenton and Matear, 2007; Lovenduski et al., 2015), and the latter rebound is linked to the diminishing of the Southern Ocean upwelling because of overall reduction of the global oceanic circulation (DeVries et al., 2017). Both southward shift of westerlies and the reduction of global oceanic circulation are expected under anthropogenic greenhouse-gases increase with an unknown compensation between these two processes. Given the Southern Ocean is currently responsible for ~50% of the total oceanic CO_2 uptake (Section 5.2.2.3.1), this tipping-point could be amplified by the decreasing buffer capacity of within this century and beyond. There is only a limited evidence for development and direction of this tipping point during next several centuries though.

5.4.8.5 Abrupt changes detected in ESM projections

Predicting abrupt changes is intrinsically difficulty because by definition they occur in a small region of the parameter and/or forcing space. Fortunately though, many bifurcation-like tipping points exhibit time-series precursors that may be used to detect them (Scheffer et al., 2009). The most commonly used tipping point precursors relate to 'critical slowing down' (Lenton, 2011). These detect the reducing resilience of the current state through fluctuations about that state. Essentially, less resilient systems exhibit longer and larger oscillations about their steady-state, as revealed by the variance and autocorrelation of the key state variables (such as temperature of CO_2). Through detecting changes in these metrics, it has been possible to identify tipping points in many past climate records (Dakos et al., 2008). At the time of the AR5, there was however no available systematic study of tipping points in ESMs.

An analysis of ESMs since the AR5 has however identified a number of tipping points in the CMIP5 ensemble (Drijfhout et al., 2015) (Figure 5.30). The most commonly detected abrupt changes in the CMIP5

archive relate to sea-ice changes, but there also a number of detected changes in the land biosphere especially in that subset of models which included dynamic vegetation. These include abrupt changes in tropical forests and high-latitude greening, permafrost thaw, and vegetation composition change. Projected dynamics of some of these tipping elements under an RCP8.5 scenario from CMIP5 ESMs is shown in Figure 5.30 [[Placeholder: current figure based on CMIP5 results, to be updated with CMIP6 and possibly expanded to include other tipping elements for FOD]]. There is a medium confidence that abrupt changes may occur during next several centuries but with only a limited evidence for their impact on atmospheric GHG concentrations.

[START FIGURE 5.30 HERE]

Figure 5.30: Projections of some tipping points in the Earth system: physical permafrost extent, boreal forest area, and tropical forest area. Each curve is from a different CMIP5 model, for the historical and RCP8.5 scenarios. For forest area projections, only models with active dynamic vegetation models were used. [[Placeholder: To be updated and expanded for CMIP6 models when available]].

[END FIGURE 5.30 HERE]

5.4.9 Long term response past 2100

The strength of carbon cycle feedbacks is dependent on the state of the system, the specific scenarios followed, and the timescale of interest. Feedback strengths estimates from an idealised and rapid 1% yr^{-1} experiment for the period to CO_2 quadrupling may be different from those on longer timescales beyond 2100. Few of the CMIP5-era ESMs have explored these longer timescales. However, experiments with the CESM1 for the period 1850-2300 suggest that both land and ocean carbon-climate feedbacks strengthen in time, while both land and ocean carbon-concentration feedbacks weaken, and the relative role of ocean versus the land increasing in time. The projected overall strengthening of carbon feedbacks beyond 2100 offsets the declining climate sensitivity to incremental increases of CO_2, leading to an overall strengthening of the carbon cycle gain from one century to the next (Randerson et al., 2015). Experiments with permafrost-enabled models suggest that the magnitude of the permafrost C feedback strengthens considerably over the period 2100-2300 under a high-emissions scenario (McGuire et al., 2018). It has been estimated that thawing permafrost could release 115–172 PgC of CO_2 and 2.8–7.4 $PgCH_4$ in the period from 2100 to 2300 under the RCP8.5 scenario' leading to a 0.23K increase in global temperature. Under RCP2.6, permafrost has been projected to release less than 40 PgC over the same period. (Schneider von Deimling et al., 2015) .

[[Placeholder: CMIP6 experiments for the SSP5-8.5 scenario extension out to 2300 feedback parameters]]

5.5 Remaining Carbon Budgets

Science at the time of the IPCC AR5 established a near-linear relationship between cumulative emissions of CO_2 and global average temperature increase (Allen et al., 2009; Collins et al., 2013; Matthews et al., 2009; Meinshausen et al., 2009; Stocker et al., 2013b; Zickfeld et al., 2009), called the transient climate response to cumulative emissions of carbon dioxide or TCRE. This relationship is now used to estimate the amount of CO_2 emissions that would be consistent with limiting global average temperature increase to specific levels (Allen et al., 2009; Collins et al., 2013; Knutti and Rogelj, 2015; Matthews et al., 2009, 2012; Meinshausen et al., 2009; Rogelj et al., 2016; Stocker et al., 2013b; Zickfeld et al., 2009) noting that this relies on more than CO_2 emissions only (Meinshausen et al., 2009; Mengis et al., 2018; Rogelj et al., 2015a, 2015b, 2016; Simmons and Matthews, 2016; Tokarska et al., 2018). Acknowledging that warming to date has been largely driven by cumulative emissions of CO_2 (Chapter 3 and Section 5.2) the remainder of CO_2 emissions that would be in line with limiting warming to a specific temperature threshold is referred to as the remaining

carbon budget. This section first assesses the TCRE as one of the core concepts underlying the notion of a remaining carbon budget (Section 5.5.1) and then integrates this with the assessment of other contributing factors to provide a consolidated assessment of remaining carbon budgets (Section 5.5.2).

5.5.1 Transient climate response to cumulative emissions of carbon (TCRE)

5.5.1.1 Contributing physical processes and theoretical frameworks

The processes that translate emissions of CO_2 into a change in global temperature (terrestrial and oceanic carbon uptake, radiative forcing from CO_2, and ocean heat uptake) are governed by complex mechanisms that all evolve in time (Gregory et al., 2009). Finding a simple proportional relationship between cumulative emissions of CO_2 and change in global temperature was thus initially met with surprise (Allen et al., 2009; Matthews et al., 2009). Since AR5 (Collins et al., 2013; Stocker et al., 2013b) a body of literature has proposed physical mechanisms from which the TCRE relationship arises.

Studies have focused on two key features of the TCRE relationship: i) why the relationship is nearly constant in time (Ehlert et al., 2017; Goodwin et al., 2015; Katavouta et al., 2018; MacDougall and Friedlingstein, 2015; Williams et al., 2016); and ii) why the relationship is independent of the pathway of CO_2 emissions (MacDougall, 2017; Seshadri, 2017).

Studies have used a variety of methods to examine the near-constancy of TCRE including: sensitivity studies with Earth-system Models of Intermediate Complexity (EMICs) (Ehlert et al., 2017); analytical methods to decompose and examine Earth System Model (ESM) and EMIC output (Goodwin et al., 2015; Williams et al., 2016); and simple analytical models that capture aspects of the relationship (MacDougall and Friedlingstein, 2015). These methods vary in the specific approach and processes considered, however all studies agree that the near-constancy of the TCRE arises from compensation between the diminishing sensitivity of radiative forcing to CO_2 at higher atmospheric concentration (Matthews et al., 2009), and the diminishing ability of the ocean to take up heat and carbon at higher cumulative emissions (Ehlert et al., 2017; Goodwin et al., 2015; MacDougall, 2016; MacDougall and Friedlingstein, 2015). The approach of Williams et al. (2016) decomposes TCRE into terms of TCR and the airborne fraction of anthropogenic CO_2 emissions over time. These two terms, which can be assessed individually (see Section 5.4 and Chapter 7, respectively), allow to verify internal consistency between the TCRE assessment and assessment of other factors in this report (Section 5.5.1.3).

The pathway independence of TCRE has been examined by using simple mathematically-tractable models that capture pathway independence (MacDougall, 2017; Seshadri, 2017). Both studies conducted to date agree that pathway independence is sensitive to the rate of CO_2 emissions, such that pathway independence is expected to breakdown at both very high and very low CO_2 emission rates (MacDougall, 2017; Seshadri, 2017). The studies also agree that no similar relationship analogous to TCRE can be expected for non-CO_2 greenhouse gases. (MacDougall, 2017) suggests that two additional constraints are required to create pathway independence. First, the transport of heat and carbon into the deep ocean should be governed by the same physical process; and second, the ratio of the net change in the atmospheric carbon pool to the net change in the ocean carbon pool should be close to the ratio of the radiative response of the surface to ocean heat uptake. If these ratios are identical then TCRE would be completely path independent. If the ratios are close but not identical, TCRE would be only approximately path independent over a wide range of cumulative emissions (MacDougall, 2017).

The land carbon cycle does not appear to play a fundamental role in the physical origin of TCRE (Ehlert et al., 2017; Goodwin et al., 2015; MacDougall and Friedlingstein, 2015). However, carbon cycle feedbacks have the potential to break both the constancy and pathway independence of TCRE, if such feedbacks significantly contribute carbon to the atmosphere (MacDougall and Friedlingstein, 2015) (Section 5.5.1.2.3).

5.5.1.2 Assessment of TCRE limits

[[Placeholder: Potentially an illustration of the influence of feedbacks on linearity of TCRE relationship.]]

5.5.1.2.1 Sensitivity to quantify of cumulative CO_2 emissions

AR5 assessed that the TCRE remains approximately constant for scenarios with increasing CO_2 emissions, and for cumulative emissions up to 2000 PgC (Collins et al., 2013). More recent modelling studies support this finding up to a similar limit (Herrington and Zickfeld, 2014; Steinacher and Joos, 2016) or extend this limit up to at least 3000 PgC (Leduc et al., 2015; Tokarska et al., 2016). Going beyond these upper limits, these studies suggest that TCRE will decrease. Using an analytical approach, MacDougall and Friedlingstein (2015) quantified a window of constant TCRE – defined as the range in cumulative emissions over which the TCRE remains within 95 % of its peak value – as between 360 to 1560 PgC, while models with a more sophisticated ocean representation support expanding the high-end of this window further (Franks et al., 2013; Tokarska et al., 2016).

As cumulative emissions increase, weakening land and ocean carbon sinks tend to increase the airborne fraction of CO_2 emissions, but each unit increase in atmospheric CO_2 has a smaller effect on global temperature owing to the saturation of CO_2 radiative forcing (Matthews et al., 2009). At high values of cumulative emissions, some models simulate less warming per unit CO_2 emitted, suggesting that the saturation of CO_2 radiative forcing becomes more important than the effect of weakened carbon sinks (Herrington and Zickfeld, 2014; Leduc et al., 2015). Most of the models used to assess the limits of the TCRE, however, do not include the effect of permafrost carbon feedbacks (Section 5.5.1.2.3), which would tend to further increase the airborne fraction of emissions at high emissions levels, and could therefore extend the window of linearity to higher total amounts of emissions (MacDougall et al., 2015). Leduc et al. (2016) suggested further that a declining strength of snow and sea-ice feedbacks in a warmer world would also contribute to a smaller TCRE at high amounts of cumulative emissions. On the other hand, Tokarska et al. (2016) suggested that a large decrease in TCRE for high cumulative emissions is only associated with some EMICs, although in four ESMs analysed in their study TCRE remains approximately constant up to 5000 PgC.

5.5.1.2.2 Sensitivity to the rate of CO_2 emissions

There is about a 10-year response timescale to a 100 PgC pulse of CO_2 emissions (Joos et al., 2013; Ricke and Caldeira, 2014), with a longer timescale associated with larger emission pulses and vice versa for shorter timescales and smaller pulses (Joos et al., 2013; Matthews and Solomon, 2013; Zickfeld and Herrington, 2015). Studies that have calculated the temperature response to CO_2 emission pulses (or instantaneous doubling/quadrupling of atmospheric CO_2) have shown an initial deviation from a linear temperature response to cumulative emissions that is consistent with this decadal response timescale to large emission pulses (Gillett et al., 2013; Herrington and Zickfeld, 2014; Leduc et al., 2015; Matthews et al., 2009). This suggests that the TCRE would also be sensitive to the rate of emissions, though this sensitivity is expected to be relatively small for small changes in emission rates. Studies that have assessed the sensitivity of the TCRE to emission rates have found varying results. Herrington and Zickfeld (2014) and Leduc et al. (2015) found a decrease in TCRE with increasing emission rates in their EMIC experiment, which is consistent with the finding of a longer temperature response timescale for larger CO_2 emission pulses. However, Krasting et al. (2014) found in their ESM experiment that TCRE is highest for low and high emission rates (2 and 25 PgC yr^{-1}) but is lower for current emission rates (between 5–10 PgC yr^{-1}). This finding is supported by another ESM study (Hajima et al., 2012) of which results might, however, be affected by model drift. Ultimately, Tachiiri et al. (2015) found that the uncertainty in TCRE increased in cases in which CO_2 concentrations were stabilised (and implied annual CO_2 emissions hence gradually decline). A robust finding of these studies is that the TCRE would in most cases be expected to increase in ambitious climate mitigation scenarios with decreasing annual emissions rates (see also Section 5.5.2.2.4 and the zero emissions commitment).

5.5.1.2.3 Reversibility and Earth system feedbacks

There are relatively few studies that have assessed how the TCRE is expected to change in scenarios of declining followed by net negative annual CO_2 emissions. Conceptually, the literature assessed here suggests that the small lag between CO_2 emissions and temperature change would result in more warming at a given amount of cumulative emissions in a scenario where that emission level is reached via overshoot followed by negative emissions. Zickfeld et al. (2016) showed this to hold across a range of scenarios with positive emissions followed by negative emissions, whereby the TCRE increased by about 10% across the transition from positive to negative emissions as a result of the thermal and carbon inertia of the deep ocean.

The AR5 assessed range of the TCRE was based on the ESMs available at the time, which did not include some potentially important Earth system feedbacks. Since then, a number of studies have assessed the importance of permafrost carbon feedbacks in particular on remaining carbon budgets (Burke et al., 2017; Gasser et al., 2018; Lowe and Bernie, 2018; MacDougall et al., 2015; MacDougall and Friedlingstein, 2015), a development highlighted and assessed in the IPCC Special Report on Global Warming of 1.5°C (Rogelj et al., 2018). MacDougall and Friedlingstein (2015) showed that the TCRE increased by about 15% in a model version that included permafrost carbon feedbacks; while the overall linearity of the TCRE during the 21st century was not affected, they did find that permafrost carbon feedbacks also caused a larger increase in the TCRE on multi-century timescales in response to declining CO_2 emission rates. In addition, other processes that are currently not explicitly considered in ESMs could cause a further increase of TCRE. These are discussed in detail in Section 5.4, but their quantitative effects on TCRE have not been explored by the literature.

5.5.1.3 Literature estimates of TCRE

IPCC AR5 (Collins et al., 2013) assessed TCRE to *likely* fall in the range of 0.8–2.5°C per 1000 PgC for cumulative emissions up to 2000 PgC, based on multiple lines of evidence. These include estimates based on carbon-cycle models (Matthews et al., 2009), EMICs (Zickfeld et al., 2013), ESMs (Gillett et al., 2013), simple carbon-cycle and climate models reflecting uncertainties in forcing, climate sensitivity and observational constraints (Rogelj et al., 2012), or other approaches that use either simple climate modelling approaches (Allen et al., 2009) or observational constraints and attributable warming (Gillett et al., 2013).

Since IPCC AR5, new studies have further expanded the evidence base for estimating the value of TCRE (Ehlert et al., 2017; Goodwin et al., 2015; MacDougall et al., 2017; Millar and Friedlingstein, 2018; Steinacher and Joos, 2016; Tachiiri et al., 2015) (Table 5.6). These studies rely on (i) EMICs (combined with observational constraints) (Ehlert et al., 2017; MacDougall et al., 2017; Steinacher and Joos, 2016; Tachiiri et al., 2015), (ii) concepts of attributable warming from observations (Millar and Friedlingstein, 2018), or (iii) theoretically derived equations (Goodwin et al., 2015).

[START TABLE 5.6 HERE]

Table 5.6: Overview of literature TCRE estimates. GSAT = Global average surface air temperature increase

Study	TCRE Range [K EgC^{-1}]	Notes
Studies available at the time of IPCC AR5		
(Matthews et al., 2009)	1–2.1	5 to 95% range GSAT C^4MIP model range
(Allen et al., 2009)	1.4–2.5	5 to 95% range Blended global mean surface air and sea-surface temperatures (no infilling of coverage gaps) Simple model
(Zickfeld et al., 2009)	1.5	Best estimate GSAT, EMIC
(Rogelj et al., 2012)	About 1–2	5 to 95% range

		Mixed definition of global average temperature increase MAGICC model calibrated to C^{4}MIP model range and 2°C to 4.5°C *likely* equilibrium climate sensitivity
(Zickfeld et al., 2013)	1.4–2.5 mean: 1.9	Model range GSAT
(Gillett et al., 2013)	0.8–2.4	Model range GSAT, CMIP5 ESMs
(Gillett et al., 2013)	0.7–2.0	5 to 95% range Blended global mean surface air and sea-surface temperatures Observationally constrained estimates of historical warming and emissions
IPCC AR5 (Collins et al., 2013)	0.8–2.5	Assessed *likely* range Multiple lines of evidence. Mixed definition of global average temperature increase
Studies published after IPCC AR5		
(Tachiiri et al., 2015)	0.3–2.4	5 to 95% range Blended global mean surface air and sea-surface temperatures JUMP-LCM model perturbed physics ensemble (EMIC)
(Tachiiri et al., 2015)	1.1–1.7	5 to 95% range Blended global mean surface air and sea-surface temperatures Observationally constrained JUMP-LCM perturbed physics ensemble
(Steinacher and Joos, 2016)	1.0–2.7 median: 1.7	5 to 95% range GSAT, observationally constrained BERN3D-LPJ EMIC
(MacDougall et al., 2017)	0.9–2.5 mean: 1.7	5 to 95% range GSAT, emulation of 23 CMIP5 ESMs
(Millar and Friedlingstein, 2018)	0.9–2.6 best estimate: 1.3	5 to 95% range Blended global mean surface air and sea-surface temperatures (HadCRUT4) (Cowtan and Way, 2014) Detection attribution with observational constraints
(Millar and Friedlingstein, 2018)	best estimate: 1.5	Blended global mean surface air and sea-surface temperatures (Berkeley Earth) Detection attribution with observational constraints
(Millar and Friedlingstein, 2018)	best estimate: 1.2	Blended global mean surface air and sea-surface temperatures (HadCRUT4) (Cowtan and Way, 2014) Detection attribution with observational constraints, with updated historical CO_2 emissions (Le Quéré et al., 2018b)
(Ehlert et al., 2017)	1.2– 2.1	Model range GSAT, UVIC EMIC with varying ocean mixing parameters
Overall assessment	**TBD**	**TBD**

[END TABLE 5.6 HERE]

5.5.1.4 Combined assessment of TCRE

All available evidence currently continues to support an assessed *likely* TCRE range of 0.8–2.5 K EgC^{-1}, with *medium confidence*. Warming here reflects the globally averaged surface air temperature increase. Forthcoming literature based on simulations from and understanding of the latest version of ESMs as part of the Sixth Phase of the Coupled Model Intercomparison Project (CMIP6) might further inform the robustness of this range. Taking into account the evidence discussing the impact of permafrost and potentially other feedbacks suggests that values at the lower end of the above-mentioned range have become *less likely*. However, given the large uncertainties in projections of these Earth-system feedback processes and the limited amount of studies, there is *low confidence* in their precise quantitative impact on TCRE. Further integration of assessments of the transient climate response (TCR) and the projected airborne fraction could allow to further limit the TCRE range in the future. These potential additional lines of evidence might also provide additional information that can inform the shape of the uncertainty distribution surrounding TCRE.

5.5.2 Remaining carbon budget assessment

Estimates of remaining carbon budgets consistent with holding global warming below a specific temperature threshold depend on a range of factors which are increasingly being studied and quantified. These factors include (1) well-understood methodological and definitional choices (Friedlingstein et al., 2014a; Rogelj et al., 2016, 2018) (Section 5.5.2.1), and (2) a set of contributing factors like historical warming, the TCRE and its limitations, as well as contributions of non-CO_2 climate forcers (Section 5.5.2.2) (Ehlert et al., 2017; Goodwin et al., 2018; MacDougall, 2016; MacDougall and Friedlingstein, 2015; Matthews et al., 2017; Mengis et al., 2018; Millar et al., 2017; Pfleiderer et al., 2018; Rogelj et al., 2015a, 2015b; Simmons and Matthews, 2016; Tokarska et al., 2018). These contributing factors are integrated in an overarching assessment of remaining carbon budgets for limiting global average warming to levels ranging from 1.5°C to 3°C relative to preindustrial levels provided in Section 5.5.2.3.

5.5.2.1 Framework and earlier approaches

Remaining carbon budgets can be defined in a variety of ways. For example, remaining carbon budgets can be defined as the cumulative emissions at the time when global-mean temperature increase would reach, exceed, avoid, or peak at a given warming level with a given probability (Rogelj et al., 2016). These definitional choices affect the approach by which remaining carbon budgets are estimated as well as assumptions about the contributions of the various factors listed above (see also Section 5.5.2.2). The choice of remaining carbon budget definition and associate methods for their estimation thus determines the domain in which these estimates can be appropriately used and the questions they can inform. Here, the remaining carbon budget is defined as the amount of cumulative CO_2 emissions starting today (or at a point in the recent past) that could be emitted while still holding global warming below a specific temperature threshold, consistent with its use in the IPCC Special Report on Global Warming of 1.5°C (Rogelj et al., 2018). Following the near-linear TCRE relationship, this definition implies that global CO_2 emissions decline to net zero levels in order to hold warming below a specific threshold.

Two approaches were used in AR5 to determine carbon budgets (Clarke et al., 2014; Collins et al., 2013; IPCC, 2014; Rogelj et al., 2016; Stocker et al., 2013b). Working Group I (WGI) reported Threshold Exceedance Budgets (TEB) that correspond to the amount of cumulative CO_2 emissions at the time a specific temperature threshold is exceeded with a given probability in a particular multi-gas and aerosol emission scenario (Collins et al., 2013; IPCC, 2013; Stocker et al., 2013b). WGI also reported TEBs for the hypothetical case that only CO_2 would be emitted by human activities (Collins et al., 2013; IPCC, 2013; Stocker et al., 2013b). Working Group III (WGIII) used Threshold Avoidance Budgets (TAB) that correspond to the cumulative CO_2 emissions over a given time period of a subset of multi-gas and aerosol emission scenarios in which global-mean temperature stays below a specific temperature threshold with a given probability (Clarke et al., 2014). The AR5 Synthesis Report used TABs defined until the time of peak warming over the 21st century (IPCC, 2014). Drawbacks have been identified for both TEBs and TABs (Rogelj et al., 2016). TABs provide an estimate of the cumulative CO_2 emissions under pathways that have as a common characteristic that they do not exceed a specific global warming threshold. The actual level of maximum warming can however vary between pathways, leading to an unnecessary and poorly constrained spread in TAB estimates (Rogelj et al., 2016). Drawbacks of TEBs are that they provide an estimate of the cumulative CO_2 emissions at the time global warming crosses a given threshold of interest in a specific emissions scenario. Because of potential variations in the non-CO_2 warming contribution at that point or lags of about a decade in warming (Joos et al., 2013; Ricke and Caldeira, 2014; Rogelj et al., 2015a, 2016, 2018; Zickfeld and Herrington, 2015), TEBs are thus not necessarily providing a precise estimate of the remaining carbon budget for limiting warming to a specific level.

Since the publication of AR5, several new approaches have been proposed to estimate carbon budgets compatible with limiting warming to specific temperature levels. Most of these approaches indirectly rely on the TCRE (Section 5.5.1), for example (Friedlingstein et al., 2014a; Matthews et al., 2017; Millar et al., 2017; Tokarska et al., 2018). Here we use the assessment framework as applied in the IPCC Special Report on Global Warming of 1.5°C to estimate remaining carbon budgets compatible with a range of maximum global warming levels (Rogelj et al., 2018). This framework builds on the advances in estimating remaining carbon budgets or related quantities that have been published since AR5 (Gasser et al., 2018; Haustein et al.,

2017; Lowe and Bernie, 2018; Matthews et al., 2017; Millar et al., 2017; Rogelj et al., 2015a; Tokarska et al., 2018) and combines the assessment of four contributing factors (historical warming, TCRE, non-CO_2 warming contribution, and adjustments due to additional Earth system feedbacks, see Section 5.5.2.2) to estimate remaining carbon budgets from 2018 onwards[1]. Together with estimates of historical CO_2 emissions to date (Section 5.2.2), these remaining carbon budgets provide the overall amount of cumulative CO_2 emissions consistent with limiting global warming to specific levels, although no formal method is available to combine the uncertainty estimates surrounding these values. A comparison with the approach applied in AR5 (Clarke et al., 2014; Collins et al., 2013) is available in the IPCC Special Report on Global Warming of 1.5°C Section 2.2.2 (Rogelj et al., 2018).

5.5.2.2 Assessment of individual components

Remaining carbon budgets are estimated through the combination of four components that are estimated separately (Forster et al., 2018; Rogelj et al., 2018). Each component is discussed separately in the sections below.

5.5.2.2.1 TCRE

The first and central component for estimating remaining carbon budgets is the TCRE. Based on the assessment in Section 5.5.1.4, an assessed *likely* range for TCRE of 0.8–2.5°C/1000 PgC is used. The value and uncertainty surrounding TCRE directly affects estimates of the remaining carbon budget (Matthews et al., 2017; Millar and Friedlingstein, 2018; Rogelj et al., 2018). As in IPCC AR5 (Collins et al., 2013), a normal uncertainty distribution with a one-sigma range corresponding to the *likely* range is applied.

5.5.2.2.2 Historical warming

Advances in methods to estimate remaining carbon budgets have shown the importance of applying an as precise as possible estimate of historical warming to date (Millar et al., 2017; Tokarska et al., 2018). This becomes particularly important when assessing remaining carbon budgets for global warming thresholds that are relatively close to present-day warming, like a 1.5°C or 2°C threshold (Rogelj et al., 2018). Also the definition of global average temperature by which historical warming is estimated is shown to be important (Allen et al., 2018; Cowtan and Way, 2014; Pfleiderer et al., 2018; Richardson et al., 2018) as is the correct isolation of human-induced global warming (Allen et al., 2018; Haustein et al., 2017). We here apply a historical warming expressed in global average surface air temperatures (SAT) of 0.97°C between the 1850–1900 and 2006–2015 periods, based on the assessment of human-induced global warming by the IPCC Special Report on Global Warming of 1.5°C, which will be updated to the most up to date assessment reported in Chapter 3.

[[Placeholder : Confidence statement in line with Chapter 3 assessment: to be added with cross-reference to Chapter 3.]]

5.5.2.2.3 Non-CO_2 warming contribution

Projected global average warming of non-CO_2 emissions affects estimates of remaining carbon budgets consistent with limiting warming to specific temperature thresholds by reducing the amount of warming that could still result from CO_2 emissions (Collins et al., 2018; Friedlingstein et al., 2014a; Knutti and Rogelj, 2015; Matthews et al., 2017; Meinshausen et al., 2009; Mengis et al., 2018; Rogelj et al., 2015a, 2016; Tokarska et al., 2018). The size of this contribution has been estimated by both implicitly (Friedlingstein et al., 2014a; Matthews et al., 2017; Meinshausen et al., 2009; Mengis et al., 2018; Rogelj et al., 2016; Tokarska et al., 2018) and explicitly (Collins et al., 2018; Rogelj et al., 2015a, 2018) varying the assumptions of non-CO_2 emissions and associated warming. Internally consistent evolutions of future CO_2 and non-CO_2 emissions allow to derive non-CO_2 warming contributions that reflect societal developments by which global

[1] This start year will be updated depending on latest year available from the historical carbon budget assessment.

CO_2 emissions are held to within a finite remaining carbon budget (Clarke et al., 2014; Rogelj et al., 2018; Smith and Mizrahi, 2013) – that is, developments in which global CO_2 emissions decline to net zero levels. Integrated pathways (Clarke et al., 2014; Huppmann et al., 2018) allow the assessment of non-CO_2 emission contributions at the time global CO_2 emissions reach net zero levels (Rogelj et al., 2018). These emission contributions can subsequently be assessed in terms of their estimated global average temperature outcome with simple climate model and emulator approaches which incorporate synthesised knowledge of climate and carbon-cycle response and uncertainty (Gasser et al., 2018; Goodwin et al., 2018; Meinshausen et al., 2009; Millar et al., 2017; Rogelj et al., 2018; Smith et al., 2018a). Section [[Placeholder reference cross-box Chapter 1 on emulators]] and Section 7.6 provide an assessment of these tools and of how they are used to reflect the assessment and uncertainty in climate (Chapter 7) and carbon-cycle (Section 5.4) response in line with historical observations (Chapters 1–4).

[[Placeholder: Pending updated assessments of Chapters 1–4 and 7, this estimate is still based on IPCC SR15.]]
[[Placeholder: Confidence statement based on integrated assessment of Chapters 1–4 and 7 confidence statements.]]

5.5.2.2.4 Adjustments due to other not represented feedbacks and potential limitations of TCRE

Recent literature has led to an improved understanding of the limitations and applicability of TCRE (Section 5.5.1.2), which is here reflected in the assessment of remaining carbon budgets. A first aspect affecting the use of TCRE for estimating remaining carbon budgets is whether there is any expected additional warming after a complete cessation of net CO_2 emissions, also referred to as zero emissions commitment (ZEC) of CO_2 emissions. Estimates of the ZEC are assessed in Chapter 4. At present no conclusive evidence is available about the sign of the ZEC and estimates range from slightly negative (i.e. global average temperatures decline slightly after a complete cessation of CO_2 emissions) to slightly positive (Collins et al., 2013; Frölicher and Joos, 2010; Gillett et al., 2011; Lowe et al., 2009; Matthews and Caldeira, 2008; Matthews and Zickfeld, 2012), but in most cases showing that once CO_2 emissions decline to net zero levels, they do not contribute to substantial further warming (Allen et al., 2018; Matthews and Solomon, 2013; Smith et al., 2019; Solomon et al., 2010). Studies that do suggest a higher ZEC identify this only for cumulative CO_2 emissions that lay beyond the range cumulative CO_2 emissions consistent with keeping warming to 1.5°C–3°C relative to preindustrial levels and add to future warming over century to millennial timescales (Ehlert and Zickfeld, 2017; Frölicher et al., 2014). Based on this assessment, the ZEC of CO_2 is considered zero for this estimation of the remaining carbon budget, although because of the diverging evidence on this matter there is overall *low confidence* in it being precisely zero.

As highlighted in Section 5.5.1.2, recent literature has described potential impacts of Earth system feedbacks that have typically not been included in standard ESMs (Burke et al., 2017; Comyn-Platt et al., 2018; Gasser et al., 2018; Lowe and Bernie, 2018; MacDougall and Friedlingstein, 2015; Mahowald et al., 2017; Schädel et al., 2016; Schneider von Deimling et al., 2015), the most important of which is carbon release from thawing permafrost. Due to the long-term and potentially non-linear reinforcing feedbacks (see Section 5.4) this process is anticipated to both increase the value of TCRE and add additional carbon emissions to the atmosphere over timescales of centuries to millennia. The IPCC Special Report on Global Warming of 1.5°C (Rogelj et al., 2018) estimated unrepresented Earth system processes to result in a reduction of remaining carbon budgets of about 100 $GtCO_2$ over the course of this century, and more thereafter. There is robust agreement across all available studies that unrepresented Earth system feedbacks related to permafrost thawing will result in more carbon being released into the atmosphere and hence a reduction in the size of remaining carbon budgets over century timescales; this results in *high confidence* about the direction of the overall effect of these additional processes on estimates of the remaining carbon budget. However, the large range in potential magnitude of permafrost thawing effects in the available literature and the absence of dedicated multi-model intercomparison exercises leads to overall *low confidence* in the quantified magnitude of this effect. For other not represented Earth system feedbacks very few to no studies are available and both the sign and magnitude of their effect on the remaining carbon budget is hence uncertain.

[[Placeholder: Statement about high-risk events identified in Section 5.4.]]

5.5.2.3 Remaining budget overview

The combination of the four contributions assessed in Sections 5.5.2.2.1–4 allows for an overall assessment of the remaining carbon budget in line with different levels of global average warming, as documented in the IPCC Special Report on Global Warming of 1.5°C (Rogelj et al., 2018). The overall assessment of remaining carbon budgets (Table 5.7) reflects the uncertainty in TCRE quantification and provides estimates of the uncertainties surrounding the contributions of each of the respective further components. A formal combination of these uncertainties is not possible because they are not independent and no estimates of the correlation between them are available in the literature. There is robust evidence supporting the concept of TCRE as well as the *high confidence* in the range of historical human-induced warming. Combined with the assessed uncertainties in the Earth system's response to non-CO_2 emissions and less well-established quantification of some of the effect of non-linear Earth system feedbacks, this leads to *medium confidence* being assigned to the assessed remaining carbon budget estimates.

[[Placeholder: A discussion of how uncertainties of various components affect the assessment of remaining carbon budgets – yet only once other chapters have finalised their respective assessments of ZEC, historical warming, forcing and transient climate sensitivity.]]

[START TABLE 5.7 HERE]

Table 5.7: The assessed remaining carbon budget and corresponding uncertainties. Assessed estimates are provided for additional human-induced warming expressed as global average surface air temperature since the recent past [[Placeholder: insert range provided by Chapter 3]], which amounted to X.X°C +- Y.Y°C relative to the 1850–1900 period [[Placeholder: use values from Chapter 3]]. [[Draft Table design only. To be updated once assessment of other chapters is available (current values from IPCC SR15 Table 2.2).]]

Additional warming since 2006-2015 [°C]*(1)	Appr. warming since 1850-1900 [°C]*(1)	Remaining carbon budget (excluding additional Earth-system feedbacks*(5))			Key uncertainties and variations*(4)					
		Percentiles of TCRE*(3)			Earth-system feedbacks*(5)	Non-CO2 scenario variation*(6)	Non-CO2 forcing and response uncertainty	TCRE distribution uncertainty*(7)	Historical temperature uncertainty*(1)	Recent emissions uncertainty*(8)
		33rd	*50th*	*67th*	*[GtCO2]*	*[GtCO2]*	*[GtCO2]*	*[GtCO2]*	*[GtCO2]*	*[GtCO2]*
0.3		290	160	80	Budgets on the left are reduced by about -100 on centennial time scales	+-250	-400 to +200	+100 to +200	+-250	+-20
0.4		530	350	230						
0.5		770	530	380						
0.53	**~1.5°C**	**840**	**580**	**420**						
0.6		1010	710	530						
0.63		1080	770	570						
0.7		1240	900	680						
0.78		1440	1040	800						
0.8		1480	1080	830						
0.9		1720	1260	980						
1		1960	1450	1130						
1.03	**~2.°C**	2030	1500	1170						
1.1		2200	1630	1280						
1.13		2270	1690	1320						
1.2		2440	1820	1430						

*(1) Chapter 1 has assessed historical warming between the 1850-1900 and 2006-2015 periods to be 0.87°C with a +/- 0.12°C *likely* (1-standard deviation) range, and global near-surface air temperature to be 0.97°C. The temperature changes from the 2006-2015 period are expressed in changes of global near-surface air temperature.
*(2) Historical CO2 emissions since the middle of the 1850-1900 historical base period (mid-1875) are estimated at 1940 GtCO2 (1640-2240 GtCO2, one standard deviation range) until end 2010. Since 1 January 2011, an additional 290 GtCO2 (270-310 GtCO2, one sigma range) has been emitted until the end of 2017 (Le Quéré et al., 2018).
*(3) TCRE: transient climate response to cumulative emissions of carbon, assessed by AR5 to fall *likely* between 0.8-2.5 °C / 1000 PgC (Collins et al., 2013), considering a normal distribution consistent with AR5 (Stocker et al., 2013). Values are rounded to the nearest 10 GtCO2.
*(4) Focussing on the impact of various key uncertainties on median budgets for 0.53°C of additional warming.
*(5) Earth system feedbacks include CO2 released by permafrost thawing or methane released by wetlands, see main text.
*(6) Variations due to different scenario assumptions related to the future evolution of non-CO2 emissions.
*(7) The distribution of TCRE is not precisely defined. Here the influence of assuming a lognormal instead of a normal distribution shown.
*(8) Historical emissions uncertainty reflects the uncertainty in historical emissions since 1 January 2011.

[END TABLE 5.7 HERE]

5.6 Biogeochemical implications of Carbon Dioxide Removal and Solar Radiation Modification

5.6.1 Introduction

Carbon Dioxide Removal (CDR) and Solar Radiation Modification (SRM) refer to deliberate actions taken to either reverse or offset the effects of greenhouse gas emissions on the atmospheric CO_2 concentration and climate. They contrast with climate mitigation, which aims to reduce greenhouse gas emissions to the atmosphere.

CDR, also referred to as "negative CO_2 emissions", seeks to directly reverse greenhouse gas emissions by removing CO_2 from the atmosphere and durably storing it in geological, terrestrial or ocean reservoirs. CO_2 is removed from the atmosphere either directly or by enhancing biological or geochemical carbon sinks. SRM, on the other hand, SRM attempts to offset the climate effects of greenhouse gas emissions, by intentional modification of the Earth's shortwave radiative budget.

This section assesses the biogeochemical implications of CDR and SRM. Specifically for CDR, there has been growing interest in light of the finding that it is *very likely* that removal of CO_2 from the atmosphere will be required to meet the Paris climate targets (AR5; SR1.5). The climate effects of CDR and SRM are assessed in Chapter 4, and a detailed assessment of the socio-economic dimensions of these options is done in AR6 WGIII.

5.6.2 Biogeochemical responses to Carbon Dioxide Removal (CDR)

CDR methods seek to remove CO_2 from the atmosphere either directly or by enhancing terrestrial, marine or geological carbon sinks to accelerate removal of CO_2 from the atmosphere. Several CDR methods have been proposed, with distinct effects on carbon and other biogeochemical cycles. Commonly discussed CDR methods are summarised in Table 5.8.

The scope of this section is to assess the general and methods-specific effects of CDR on the global carbon cycle and other biogeochemical cycles. Global carbon sequestration potentials of CDR methods are briefly discussed, but a comprehensive assessment is left to the AR6 Working Group III report, as these potentials depend on socio-economic factors (e.g. availability of land, carbon pricing). Instead the focus is on sequestration biophysical potentials per unit deployment (e.g. per hectare for land-based methods) and on biogeochemical feedbacks that either amplify or reduce carbon sequestration of specific CDR methods, determining their *effectiveness* in reducing atmospheric CO_2. Side effects on other biogeochemical cycles, climate and ecosystems are also assessed. The assessment emphasizes literature published since AR5; the IPCC Special Reports on the global warming of 1.5 degrees (SR1.5) and on climate change and land (SRCCL) assessed CDR potentials and side effects but did not address the effects of CDR on carbon and other biogeochemical cycles in detail.

CDR methods may be divided in four major categories, according to the carbon cycle processes that result in CO_2 removal: (1) enhanced net biological uptake and storage by land ecosystems, (2) enhanced net biological uptake and storage in the ocean, (3) enhanced geochemical processes on land and in the ocean, (4) direct air capture by chemical processes with carbon storage. The main methods suggested are summarised in Table 5.8.

[START TABLE 5.8 HERE]

Table 5.8: Carbon Dioxide Removal methods

Category	Methods	Nature of CO_2 Removal Process / Storage Form	Description

Enhanced biological production and storage on land	Afforestation, reforestation and forest management	Biological / Organic	Store carbon in trees and soils by planting, restoring or managing forests
	Agricultural soil management	Biological / Organic	Use agricultural management practices to improve soil carbon storage
	Biochar	Biological / Organic	Pyrolyze terrestrial biomass to form biochar and add to soils
	Bioenergy with carbon capture and storage (BECCS)	Biological / Organic	Capture and storage of CO_2 produced by burning of bioenergy crops
	Wetland restoration	Biological / Organic	Store C in soil by creating or restoring wetlands and restoring peatlands
Enhanced biological production and storage in ocean	Ocean fertilisation	Biological / organic	Fertilize upper ocean with micro (Fe) and macronutrients (N, P) to increase phytoplankton photosynthesis and biomass and deep ocean carbon storage through the biological pump
	Artificial ocean upwelling	Biological / organic	Pump nutrient rich deep ocean water to the surface
	Blue carbon management	Biological / organic	Manage coastal ecosystems to increase Net Primary Production and store C in sediments
Geochemical	Enhanced weathering	Geochemical / inorganic	Spread alkaline minerals on land to chemically remove atmospheric CO_2 in reactions that form solid minerals (carbonates and silicates) that are stored in soils or in the ocean
	Ocean alkalinisation	Geochemical / inorganic	Deposit alkaline minerals (e.g. olivine) on the ocean surface to increase CO_2 uptake by increasing ocean alkalinity
Chemical	Direct air capture with carbon storage (DACCS)	Chemical / inorganic	Direct removal of CO_2 from air and storage underground or in long-lasting usable materials

[END TABLE 5.8 HERE]

Many other CDR options have been suggested, but there is insufficient literature for an assessment. These include biomass burial, ocean downwelling, removal of CO_2 from seawater with storage, and cloud alkalinisation (Keller et al., 2018b). The use of harvested wood products as a carbon storage option (e.g., houses) has no other biogeochemical implications and is therefore not covered here to discuss its potential.

5.6.2.1 Global carbon cycle responses to CDR

This section assesses evidence about the response of the global carbon cycle to CDR from idealised model simulations which assume that CO_2 is removed from the atmosphere directly and stored permanently in the geologic reservoir, which is analogous to direct air capture with carbon storage (DACCS; Table 5.8). The carbon cycle response to specific CDR methods will be discussed in Section 5.6.2.2.2.

Although our understanding of the climate-carbon cycle response to CDR has evolved since AR5, a limited numbers of modelling studies exists (Cao and Caldeira, 2010; Jones et al., 2016b; Tokarska and Zickfeld, 2015; Vichi et al., 2013). We assess results from two types of model simulations: idealised "pulse removal" simulations, whereby a specified amount of CO_2 is removed instantly from the atmosphere, and scenario simulations, whereby CO_2 emissions and CDR follow a plausible trajectory. The assessment is based on a review of the literature since AR5 and results from the Carbon Dioxide Removal Model Intercomparison Project (CDR-MIP) (Keller et al., 2018b) and the Scenario Model Intercomparison Project (ScenarioMIP) (O'Neill et al., 2018), which include pulse removal simulations as well as scenario simulations. This section

will focus on three aspects of the climate-carbon cycle response to CDR: the symmetry of the response to positive and negative CO_2 emissions, the time-dependent behaviour of CO_2 fluxes in scenarios with CDR, and the effectiveness of CDR in drawing down atmospheric CO_2.

[START BOX 5.1 HERE]

BOX 5.1: Carbon cycle response to CO_2 removal from the atmosphere

During the industrial era, CO_2 emitted by human activities such as fossil-fuel combustion and land-use change, has been redistributed between atmosphere, land, ocean and geologic carbon reservoirs (Figure 1b of Box 5.1). Over the past decade (2007–2016) 47% of the emitted CO_2 remained in the atmosphere, 23% was stored in the ocean and 30% in the terrestrial biosphere (Le Quéré et al., 2018b) (see Section 5.6.2.1). When CDR is applied during periods of positive CO_2 emissions and is smaller in magnitude than these emissions (*net positive* emissions), it acts to counteract these emissions, reducing their magnitude (Figure 1c of Box 5.1). The excess CO_2 in the atmosphere is partly taken up by the land and the ocean, as in the case of industrial era emissions without CDR. When CDR exceeds CO_2 emissions (net removal of CO_2 from the atmosphere or *net negative* emissions) and atmospheric CO_2 declines, CO_2 is also redistributed between reservoirs, but in the opposite direction as under positive emissions: CO_2 removal from the atmosphere is opposed by outgassing from the land and ocean carbon reservoirs (Figure 1d of Box 5.1).

[START BOX 5.1, FIGURE 1 HERE]

Box 5.1, Figure 1: Schematic representation of carbon fluxes between atmosphere, land, ocean and geologic reservoirs for (a) an unperturbed Earth System, (b) an Earth system perturbed by fossil fuel CO_2 emissions, (c) an Earth system with fossil fuel CO_2 emissions are partially offset by CDR, (d) an Earth system in which CDR exceeds CO_2 emissions from fossil fuels ("net negative emissions"). Carbon fluxes depicted in (a) (solid and dashed black lines) also occur in (b)-(d). From (Keller et al., 2018b).

[END BOX 5.1, FIGURE 1 HERE]

[END BOX 5.1 HERE]

5.6.2.1.1 Symmetry of carbon cycle response to positive and negative CO_2 emissions

Since the first coupled-climate carbon cycle models were developed in the late 1990s, enormous progress has been made in understanding and quantifying the carbon cycle response to increasing atmospheric CO_2 concentrations and the associated climate changes (Section 5.4). To quantify the effectiveness of CDR in reducing atmospheric CO_2, it is important to establish whether the insights gained about carbon cycle responses and feedbacks under positive CO_2 emissions can be applied to responses under negative emissions. This would be the case if the climate-carbon cycle response to negative emissions were equal and opposite to the response to positive emissions, i.e. if the response were *symmetric*. This section assesses the symmetry in the coupled climate-carbon cycle response to positive and negative emission pulses of the same magnitude released from different climate states. Simulations with the UVic ESCM, an Earth system model of intermediate complexity, suggests that the response is approximately symmetric for pulse emissions/removals of ±100 PgC, but becomes increasingly asymmetric for higher pulse emissions/removals (Zickfeld et al., 2019) (Figure 5.31). This asymmetry originates largely from state-dependencies and nonlinearities in the ocean response.

[[Placeholder for assessment based on results of CDR-MIP simulations with positive and negative 100 PgC emission pulses released from a climate state in equilibrium with the pre-industrial atmospheric CO_2 concentration (Keller et al., 2018b).]]

[START FIGURE 5.31 HERE]

Figure 5.31: Changes in carbon stores (atmosphere, ocean, land) as a fraction of cumulative CO_2 emissions (equivalent to CO_2 pulse size) 1000 years after the pulse emission/removal (±100 PgC, ±500 PgC, ±1000 PgC) for simulations initialised from different equilibrium states (1 to 4 times the pre-industrial atmospheric CO_2 concentration). Changes in carbon stores are positive (i.e. uptake) for positive CO_2 pulses and negative (i.e. outgassing) for negative CO_2 pulses. (Top) Atmospheric carbon burden change fraction, (Middle) ocean carbon store change fraction, (Bottom) land carbon store change fraction. In each panel the parts of the graph on the left and right hand-side of the zero line (black dashed line) are not mirror images of each other, indicating that the response is asymmetric, particularly for higher pulse emissions/removals. From (Zickfeld et al., 2019). [[Placeholder: Will be updated based on results from CDR-MIP simulations.]]

[END FIGURE 5.31 HERE]

5.6.2.1.2 Carbon cycle response over time in scenarios with CDR

Since AR5 studies with Earth System Models have explored the land and ocean carbon sink response to scenarios with CO_2 emissions gradually declining during the 21st century, as CDR and other mitigation activities are ramped up, until they become net zero and, as removals exceed emissions, net negative (such as in RCP2.6). These studies suggest that when net CO_2 emissions are positive, but start to decline, the land and ocean carbon sinks begin to weaken and take up less CO_2 (Figure 5.32a, b) (Jones et al., 2016b; Tokarska and Zickfeld, 2015). Decades to centuries after CO_2 emissions become net negative, the terrestrial biosphere becomes a net emitter of CO_2 to the atmosphere (Figure 5.32d). This source-to-sink transition lags the time CO_2 emissions become net negative, as carbon sinks respond to the history of atmospheric CO_2 (not the instantaneous emissions rate) and continue to take up CO_2 for decades to centuries after emissions become net negative (Jones et al., 2016b; Tokarska and Zickfeld, 2015; Zickfeld et al., 2016). While the general response is robust across models, the magnitude of the CO_2 fluxes and the timing of the source-to-sink transition are uncertain, particularly for the land sink (Jones et al., 2016b). These uncertainties mirror the large spread in simulated terrestrial carbon cycle responses under positive CO_2 emissions associated with differences in model representations of system processes (Section 5.4).

[[Placeholder: This section will be expanded based on analysis of CMIP6 simulations. It is planned to repeat the analysis of Jones et al. (2016) for SSP1-2.6 and SSP5-3.4OS scenarios and their long-term extensions. Such an analysis will allow to investigate the time and scenario dependence of the carbon cycle response to CDR. It is expected that the source-to-sink transition will occur with a longer lag relative to the time emissions become net negative in SSP5-3.4OS than in SSP1-2.6.]]

[START FIGURE 5.32 HERE]

Figure 5.32: Carbon flux components during different stages of ESM simulations driven by RCP2.6. (a) Large positive CO_2 emissions, (b) Small net positive CO_2 emissions, (c) Net negative CO_2 emissions (short-term response), (d) Net negative CO_2 emissions (long-term response). From (Jones et al., 2016a). [[Placeholder. Will be replotted based on CMIP6 simulations (scenarios SSP1-2.6 and SSP5-3.4OS)]].

[END FIGURE 5.32 HERE]

5.6.2.1.3 Effectiveness of CDR

It is well known that the response of land and ocean carbon sinks is sensitive to the level of atmospheric CO_2 and climate change and differs under different future scenarios (Section 5.4). It is therefore important to establish to what extent the effectiveness of CDR – i.e. the reduction in atmospheric CO_2 per unit CDR – is dependent on the climate scenario from which it is applied. Different metrics have been used to quantify the effectiveness of CDR (Jones et al., 2016b; Tokarska and Zickfeld, 2015; Zickfeld et al., 2016). One is the airborne fraction of cumulative CO_2 emissions (AF), defined in the same way as for positive emissions (i.e. as the ratio of change in atmospheric CO_2 at a given point in time to the cumulative emissions up to that time), with its use extended to periods of declining and net negative CO_2 emissions. This metric, however,

has not proven to be useful to quantify the effectiveness of CDR in simulations where CDR is applied from a transient state, as it measures the carbon cycle response to CDR as well as to the prior history of increasing atmospheric CO_2 concentration (Jones et al., 2016b; Tokarska and Zickfeld, 2015). Therefore, an alternative metric has been proposed: the airborne fraction of the perturbation relative to a reference scenario (Jones et al., 2016b; Tokarska and Zickfeld, 2015), dubbed the "perturbation airborne fraction" (PAF) (Jones et al., 2016b). The advantage of this metric is that it separates the response to a positive or negative emission perturbation from the response to the history of CO_2 prior to the point in time the perturbation is applied. A disadvantage is that the PAF cannot be calculated from a single model simulation but requires a reference simulation relative to which the effect of the perturbation can be evaluated.

Based on scenario simulations and idealised model simulations with pulse removals applied from an equilibrium state, the effectiveness of CDR is found to be rather insensitive to the rate and amount of CDR (Jones et al., 2016b; Tokarska and Zickfeld, 2015), but to be strongly dependent on the emission scenario from which CDR is applied (Jones et al., 2016b) (Figure 5.33). The effectiveness of CDR is larger in scenarios with higher background atmospheric CO_2 concentration, due state dependencies and climate-carbon cycle feedbacks that lead to a weaker overall response to CO_2 removal (Zickfeld et al., 2019). [[Placeholder: Will be expanded based on new studies and analysis of CDR-MIP simulations]].

[START FIGURE 5.33 HERE]

Figure 5.33: Effectiveness of CDR. (Top) Perturbation airborne fraction (PAF) for model simulations where CDR is applied from four different RCPs (shown on the horizontal axis in terms of their cumulative CO_2 emissions over the 2020–2099 period). Symbols indicate results for four CDR scenarios, which differ in terms of the magnitude and rate of CDR (see Jones et al., (2016b) for details). Results are based on simulations with the Hadley Centre Simple Climate-Carbon Model. From Jones et al., (2016b). (Bottom) Airborne fraction of cumulative emissions (AF) for idealised model simulations with CDR applied instantly (pulse removals) from climate states in equilibrium with different atmospheric CO_2 concentration levels (shown on the horizontal axis). Symbols indicate results for different magnitudes of CDR. Based on simulations with the UVic ESCM model of intermediate complexity. From (Zickfeld et al., 2019). [[Placeholder: Will be supplemented with results from new studies and CDR-MIP simulations]].

[END FIGURE 5.33 HERE]

5.6.2.2 Effects of specific CDR methods on biogeochemical cycles and climate

5.6.2.2.1 Land-based biological CDR methods

Land biological processes are the main drivers of CO_2 exchange between the land and the atmosphere. CO_2 is removed by GPP and returned to the atmosphere mainly by autotrophic and heterotrophic respiration, but also by deforestation and disturbances. As long as GPP is greater than these three sources, global land will act as a net sink, as is the case today (Section 5.3.2.2). Biological CDR methods seek to take deliberate measures to increase the difference between GPP and the CO_2 sources leading to increased carbon storage on land.

CO_2 sequestration rates via reforestation and afforestation depend on forest age and are highest for young, productive trees, but decrease as forest matures, usually after several decades to a few centuries. Forest management (e.g. fire suppression, wood harvest) is *likely* to be needed to maintain carbon stocks from depletion and sustaining CO_2 sequestration rates (Griscom et al., 2017; Kurz et al., 2016; Naudts et al., 2016; Yousefpour et al., 2018). Global sequestration potential varies substantially with the amount of marginal land available to forestation, and the age of forest (Fuss et al., 2018). Dynamic global vegetation models (DGVMs) further incorporate carbon-climate-vegetation feedbacks such as the CO_2 fertilisation effect on forest productivity, soil carbon enrichment due to enhanced litter input or the northward shift of the tree-line in future climate projection favouring higher CO_2 sequestration potentials (Bathiany et al., 2010; Boysen et al., 2017; Harper et al., 2018; Sonntag et al., 2015). The cooling effectiveness of carbon (C) sequestration

can be offset by the temperature increase arising from biophysical effects (Table 5.9).

Methods to increase soil carbon content include the restoration of marginal or degraded land (Paustian et al., 2016; Smith, 2016) and improved management practices of cultivated land. The latter include selection of appropriate varieties or species with greater root mass, selection of crop rotation cycles which improve C sequestration, increasing the amount of crop residues, using cover crops which prevent periods of bare soil (Paustian et al., 2016), applying optimised grazing (Henderson et al., 2015), planting cover crops in fallow periods (Griscom et al., 2017; Poeplau and Don, 2015), selecting cultivars with deeper roots (Kell, 2011) or higher yields (Burney et al., 2010), optimizing residue management (Wilhelm et al., 2004) and employing low-tillage. The carbon sequestration potential of re-/afforestation and soil carbon sequestration methods is substantial (*medium confidence*) but they both have several beneficial (*low confidence*) and adverse (*low confidence*) side-effects. With *high confidence*, deployment of both methods will decrease biodiversity unless wisely adopted (Table 5.9).

Biochar is produced by burning biomass at high temperatures under anoxic conditions (pyrolysis) and can, when added to soils, increase soil carbon stocks and fertility for decades to centuries (Lehmann et al., 2015; Woolf et al., 2010). Sequestration potentials depend on the biomass feedstock source and the residence time, in turn determined by the feedstock type and the applied pyrolysis temperature.

Sequestration potentials from bioenergy combined with carbon capture and storage (BECCS) depend strongly on the feedstock, climate and management practices (Beringer et al., 2011; Heck et al., 2016; Kato & Yamagata, 2014; Andreas Krause et al., 2017; Smith et al., 2016). DGVMs simulate increases in net carbon uptake if marginal land is replaced by woody bioenergy plants enriching soil carbon (Boysen et al., 2017; Don et al., 2012; Heck et al., 2016; Kraxner et al., 2013; Smith et al., 2012b) while replacing carbon-rich ecosystems with herbaceous bioenergy plants could deplete soil-carbon stocks and reduce the additional sink capacity of standing forests (Boysen et al., 2017b, 2017a; Elshout et al., 2015; Harper et al., 2018; Heck et al., 2018; Vaughan et al., 2018). Further, carbon losses along the biomass transport, conversion and capture chain could reduce the overall CDR potential of BECCS to 50 to >90% of the initially sequestered carbon (Creutzig et al., 2015; Fuss et al., 2018; Harper et al., 2018; Heck et al., 2018; Humpenöder et al., 2014; Andreas Krause et al., 2017; Vaughan & Gough, 2016). Leakage and uncertain permanence of carbon capture and storage could substantially diminish the anticipated CDR goal (Scott et al., 2015; Vaughan et al., 2018). BECCS has moderate potential to sequester C (*medium confidence)* but has several adverse side effects (*low confidence*) and will decrease biodiversity (*medium confidence*).

Wetlands are less extensive than forests, croplands and grazing lands, yet per unit area they hold a high carbon stock. This option relies on restoration or build of high-carbon-density soils, essentially through flooding.

[START TABLE 5.9 HERE]

Table 5.9: Characteristics of specific CDR methods: time scale of carbon storage, global CDR potential, CDR potential per unit deployment, CDR reversibility by natural and anthropogenic processes, feedbacks on CO_2 sequestration potential, side-effects on other BGC cycles and climate. In 'Impacts on other BGC cycles', asterisks indicate the confidence for each BGC impact (*low, **medium, *** high confidence).

Methods	Time Scale of C Storage	CDR Potential Range (median) PgC yr^{-1}	CDR Potential Per Unit Deployment	CDR Reversibility	Feedbacks on CO_2 Sequestration Potential	Impacts on Other BGC Cycles, Climate and Biodiversity (BD)

Afforestation, reforestation and forest management	Decades to centuries	0.14–3.3 (1.3) (Fuss et al., 2018a)	Global: 1.0–4.1 MgC ha^{-1} yr^{-1} (Griscom et al., 2017a; Lenton, 2014) China : 1.6 MgC ha^{-1} yr^{-1} (Lenton, 2014), Tropics: 2 MgC ha^{-1} yr^{-1} (Houghton et al., 2015) Europe : 2 MgC ha^{-1} yr^{-1} (Naudts et al., 2016)	Easily reversible	Warming to increase soil respiration; reduced soil moisture to cause drought stress and increased fire risk; warming to increase the occurrence of pests, diseases and extreme weather	Increased transpiration and decreased soil moisture to suppress runoff and threaten water supply (Farley et al., 2005), N_2O emissions if fertilised, VOC emissions (Krause et al., 2017), decreased and increased surface temperature, in tropics and boreal region, respectively, due to changes in reflectivity, evapotranspiration and surface roughness (Fuss et al., 2018; Griscom et al., 2017; Pongratz et al., 2010; Jackson et al., 2008; Bright et al., 2015), decreased BD if not adopted wisely (Smith et al., 2018b; Williamson, P., & Bodle, 2016)
Soil carbon sequestration	Decades to centuries	0.11–3.3 (1.0) (Fuss et al., 2018a)	0.1–1.0 MgC ha^{-1} yr^{-1} (Paustian et al., 2016a; Smith, 2016)	Easily reversible	Warming to increase soil respiration; reduced soil moisture to cause drought stress and increased fire risk	N_2O emissions if fertilised (Gu et al., 2017), reduction of N_2O emissions, reduced nutrient losses, increased biological activity (Fornara et al., 2011; Paustian et al., 2016; Tonitto et al., 2006), increased BD (Paustian et al., 2016)
Biochar	Decades to centuries	0.08–9.5 (1.2) (Fuss et al., 2018a)	30–60 MgC ha^{-1} yr^{-1}	Reversible by fire	Reduced soil moisture to cause increased fire risk	Improved soil fertility and productivity, reduced nutrient losses, enhanced fertilizer N use efficiency (Clough et al., 2013; Liu et al., 2017; Shen et al., 2016, Woolf et al., 2010), reduced N_2O emissions (Cayuela et al., 2014; Kammann, C., 2017), local warming related to darkened surface (Smith et al., 2016),

						decreased BD (Smith et al., 2018b)
BECCS	Potentially permanent	0.14–1.4 (Fuss et al., 2018a)	1.5–8.7 MgC ha^{-1} yr^{-1} (Lenton, 2014; Smith et al., 2016)	Partially reversible by leakage		Land-use change related emissions of CO_2 and N_2O (Creutzig et al., 2015), changes in reflectivity and water use similar to those in re/afforestation; VOC emissions (Krause et al., 2017b); decreased BD (Smith et al., 2018b); see DACCS for storage-related side effects
Wetland restoration	Decades to centuries	0.19–0.67 (0.22) (Griscom et al., 2017b)	1.5–7.9 MgCe ha^{-1} yr^{-1} (Griscom et al., 2017b)	Easily reversible	Higher temperature to increase CH_4 emission; drought to increase risk of fire	Enhanced CH_4 emission; increased nutrient infiltration and retention to increase water quality (Daneshvar et al., 2017; Kluber et al., 2014); protection from fire, increased BD (Smith et al., 2018b)
Ocean fertilisation	Centuries to millennia	0.32–12 (1.0) (Fuss et al., 2018a)	46–125 kgC per ton of iron deposited (Aumont and Bopp, 2006b; Zahariev et al., 2008)	Cannot be easily reversed.	Decreased productivity in unfertilised regions (Oschlies, 2010); carbonate counter pump could decrease C sequestration (Salter et al., 2014)	Perturbation to marine ecosystems (Oschlies et al., 2010a); Enhanced ocean acidification; Increased suboxic zone extent in fertilised areas; Shrinkage of suboxic zones outside fertilised areas (Keller et al., 2014)
Artificial ocean upwelling	Centuries to millennia	0.9–4.3 (Keller et al., 2014b; Oschlies, 2010)	1.2 x 10^5 kgC yr^{-1} removed from atmosphere per upwelling pipe, assuming deployment of 7 million pipes to 1000 m depth for 100 years.	Cannot be easily reversed or safely stopped. Causes subsequent warming beyond temperatures experienced	Cooling effect & increased terrestrial C storage.	Perturbation to marine ecosystems* (Oschlies et al., 2010a, 2010b) Enhanced ocean acidification Increased suboxic zone extent in fertilised areas

			(Oschlies et al., 2010c)	if AOUp not started.		Alters ocean temperature, salinity, circulation Alters Earth's heat and water budget (Keller et al., 2014)
Blue carbon management	Decades to centuries	0.17–0.29 (0.23) (Griscom et al., 2017b)	1.9–18.4 MgC ha^{-1} yr^{-1} (Griscom et al., 2017b)	Easily reversed, if C is stored on land (similar to wetland restoration)		Provision of ecosystem services (recreation and tourism, key fishery habitats, improved water quality, and flood and erosion mitigation); CH4 emissions (Rosentreter et al., 2018)
Enhanced weathering - terrestrial	Centuries to millennia for carbonates, permanent for silicates	0.05–26 (1.3) (Fuss et al., 2018a)				Soil fertilisation and stimulated biological production (Hartmann et al., 2013) ; can liberate toxic trace metals into soil or water bodies (Keller et al., 2018a); can decrease drinking water quality by causing freshwater salinisation (Kaushal et al., 2018); increases alkalinity and pH of natural waters, helps dampen ocean acidification, increases ocean carbon uptake (Beerling et al., 2018). Decreased BD (Smith et al., 2018b)
Ocean alkalinisation	10,000 to 100,000 years	<27 (González, 2016; Sonntag et al., 2018)	220 kgC per ton of olivine/lime (González, 2016; Sonntag et al., 2018)	Not easily reversible	Enhanced primary production through addition of iron and silicic acid (Köhler et al., 2013a) (Hauck et al., 2016)	Decreased ocean acidification (surface waters only)*** Decreased deoxygenation (González, 2016) Release of toxic trace metals* (Hartmann et al., 2013)

Direct air carbon capture and storage (DACCS)	Potentially permanent	0.14–1.4 (Fuss et al., 2018a)		Can be partially reversed by leakage		Pollution of drinking water; seismic activity (Fuss et al., 2018); Perturbation of marine ecosystems through leakage of CO_2 from submarine storage (Molari et al., 2018)

[END TABLE 5.9 HERE]

5.6.2.2.2 Ocean-based biological CDR methods

Both ocean biological and physical processes drive the CO_2 exchange between the ocean and atmosphere. However, the ocean physical processes that remove CO_2 from the atmosphere, such as large-scale circulation and mixing, cannot be feasibly altered, so ocean CDR methods focus on increasing the productivity of ocean ecosystems, and subsequent sequestration of carbon.

Artificial ocean upwelling (AOUpw) brings nutrient-rich water to the ocean surface to alleviate nutrient limitation of (near-)surface phytoplankton growth and thus boost primary production and subsequent ocean CO_2 uptake. For AOUpw to be effective at increasing ocean carbon storage, the increased primary production has to result in increased export of organic carbon out of the upper ocean and no change (or a deepening) in its remineralisation depth. In model simulations (Keller et al., 2014; Oschlies, 2010) where AOUpw is applied continuously and at the largest feasible scales, cumulative atmospheric carbon dioxide removal is up to 4.3 PgC yr^{-1} during the first decade, and decreases afterwards to 0.9 to 1.5 PgC yr^{-1} (average), with 50-80% of this removal results from cooling-induced enhancement of the terrestrial carbon sink (Keller et al., 2014). AOUpw is expected to have widespread side effects (Table 5.9).

Ocean fertilisation (OF) aims to boost primary production and subsequently organic carbon export by seeding the ocean surface with nutrients, typically in iron-limited areas such as the Southern Ocean or North Pacific. Iron fertilisation experiments have been inconclusive on deep-sea carbon sequestration enhancement (Boyd et al., 2007; Yoon et al., 2018), with only one observing an increase in the biological pump below 1000 m (Smetacek et al., 2012). Model simulations (Keller et al., 2014; Oschlies et al., 2010) suggest that if OF is applied continuously under a high CO_2 emission scenarios, CO_2 sequestration rates are initially between 2 and 4 PgC yr^{-1}, but then decrease to 0.4 to 1 PgC yr^{-1} (average) after the initial decade. Increased productivity in the fertilised areas is *likely* to result in decreased productivity in unfertilised regions (Oschlies, 2010). The carbonate counter pump could also potentially reduce iron fertilisation-induced C sequestration by 6–32% (Salter et al., 2014). Upon fertilisation termination, up to a third of the sequestered carbon may be returned to the atmosphere within a century (Robinson et al., 2014). The carbon sequestration potential of AOUpw and OF is moderate (*high confidence*), but both have a multitude of negative side effects (*high confidence)* (Table 5.9).

Blue carbon refers to carbon sequestration by plant growth and burial of plant organic carbon in the soil of coastal wetlands (including salt marshes and mangroves) and seagrass ecosystems. Coastal wetlands and seagrass meadows are among the most productive ecosystems per unit area, with a global annual sequestration rate of 0.084–0.233 PgC yr^{-1} (Mcleod et al., 2011). Current sequestration rates are *unlikely* to be maintained into the future due to changing environmental conditions, including sea level rise, changes in the availability of sediments, temperature, salinity and light availability, and coastal development (National Academies of Sciences and Medicine, 2019). Although increase sea level rise might lead to long term carbon sequestration in coastal wetlands and seagrass meadows (Rogers et al., 2019), more immediate increase in frequency and intensity of marine heatwaves poses a threat to the long term conservation, let alone expansion of existing carbon stocks (Smale et al., 2019). Blue carbon approaches seek to maintain or increase the rate of carbon sequestration against this baseline through management and restoration of coastal wetlands and seagrass meadows. Globally it is estimated that these measures combined have a potential to

maintain and accelerate the rate of CO_2 sequestration at a scale of 0.17–0.29 $PgCO_2$ yr^{-1} (Griscom et al., 2017). Part of the climate benefits of blue carbon might be offset by increased CH_4 production (Rosentreter et al., 2018). The carbon sequestration potential of blue carbon approaches is moderate (*low confidence*), but these approaches have several positive side-effects through the provision of valuable ecosystem services (*medium confidence*) (Table 5.9).

5.6.2.2.3 Geochemical and chemical CDR methods

Enhanced weathering (EW) is based on naturally occurring weathering process in which rock minerals are decomposed and at the same time dissolved CO_2 is converted to bicarbonate which is then leached to surface waters and ultimately to the ocean. Weathering is accelerated by spreading grinded rocks on e.g. managed croplands which will increase the reactive surface area and accelerate the rate of weathering (Taylor et al., 2015). For enhanced weathering the carbon sequestration potential is higher and the time scale of C storage is longer than those of most land-based methods (*high confidence*). Enhanced weathering has several potential side-effects which can be both beneficial and adverse (*low confidence*).

Ocean alkalinisation, via the deposition of alkaline minerals (e.g. olivine) or their dissociation products (e.g. quicklime) at the ocean surface, can increase surface total alkalinity and thus increase CO_2 uptake and storage. Modelling studies suggest that massive additions of alkalinity (e.g., 114 Pmol by the end of the century) during high CO_2 emission scenarios could increase ocean uptake by up to 27 Pg C yr^{-1} by the end of the century, and permanently keep it there (100 ka residence time; Renforth & Henderson, 2017) even if additions were stopped (Feng et al., 2017; González et al., 2016; Sonntag et al., 2018). Enhanced ocean carbon uptake rapidly stops upon termination of ocean alkalinisation (González et al., 2018). Modelling studies suggest that the carbon sequestration potential is higher under high emissions scenarios (Hauck et al., 2016), although the potential for climate change mitigation is higher under low emission scenarios. If olivine is deposited, the associated addition of iron and silicic acid is predicted to enhance primary production (Köhler et al., 2013; Hauck et al., 2016). The carbon sequestration potential of ocean alkalinisation is high (*high confidence*). Ocean alkalinisation has positive side effects on the marine ecosystem (*medium confidence*), but also adverse ones (*low confidence*), most of which are poorly understood or quantified.

Direct air capture with carbon storage is a combination of two techniques, direct air capture of CO_2 (DAC) and carbon storage. DAC entails the flow of large amounts of air through a filter that separates carbon dioxide from air, producing a concentrated CO_2 gas stream. The CO_2 stream then may be either stored geologically as a high-pressure gas or sequestered by a mineral carbonation process. DACCS has significant requirements of water and energy, and carbon storage has additional energy requirements. Storage is potentially permanent in both pressurised gas form and mineral form. The main risks and side effects of DACCS are largely related to the high pressure at which CO_2 is stored in geologic formations (Table 5.9). The conversion of CO_2 captured by BECCS/DACCS to ocean alkalinity and subsequent storage in the ocean has been proposed (Rau, 2014) and carries with it the same potential feedbacks and side effects as ocean alkalinisation.

[START FIGURE 5.34 HERE]

Figure 5.34: Relative sequestration potentials of CDR methods plotted against the time scale of C storage. Colour of the full circle indicate whether side effects act to weaken or enhance the carbon sequestration potential, surrounding dashed lines denote the sign of other environmental impacts. Vertical bars indicate the uncertainty ranges in potentials, horizontal bars the uncertainty ranges in the time scale of C storage. [[Placeholder: To be completed and underlying numbers to be checked and updated]].

[END FIGURE 5.34 HERE]

5.6.2.3 Reversal of ocean acidification by CDR

Reversing the increase in atmospheric CO_2 concentrations will reverse ocean acidification at the sea surface but will not result in rapid amelioration of ocean acidification in the deeper ocean, which is already occurring (see Section 5.3.3.1). The ocean's uptake of atmospheric CO_2 will start to decrease if atmospheric CO_2 decreases, and the ocean will gradually become a source, rather than sink, of CO_2 (Mathesius et al., 2015; Tokarska and Zickfeld, 2015). However, because of the long timescales of the ocean turnover that transfers CO_2 from the upper to the deep ocean, excess carbon will continue to accumulate in the deep ocean even after a decrease in atmospheric CO_2 (Cao et al., 2014; Mathesius et al., 2015; Tokarska and Zickfeld, 2015). In model simulations with a strong increase in atmospheric CO_2 and a subsequent decrease to pre-industrial levels, *surface* pH returns to its pre-industrial value in ~100 years after atmospheric CO_2 returns to pre-industrial levels (Cao et al., 2014). The ocean mean-pH, however, does not return to its pre-industrial starting point when atmospheric CO_2 returns to pre-industrial levels. The global mean ocean pH remains ~0.1 units lower than its pre-industrial value, even 200 years after atmospheric CO_2 returns to pre-industrial levels (Mathesius et al., 2015; Section 5.3.3.1). Even with a probably unfeasible CO_2 extraction rate of 25 PgC yr^{-1}, global ocean pH does not return to pre-industrial levels by 2700 (Mathesius et al., 2015).

The slow timescales of ocean circulation result in an inability to restore the mean ocean pH to pre-industrial levels even with an aggressive atmospheric CO_2 removal rate. Even with reversal of the atmospheric CO_2 increase, CO_2 emissions leave a long-term legacy in ocean acidification, and are therefore irreversible at multi-human generational scales.

[[Placeholder: Update with CDR-MIP results, when available]]

5.6.3 Biogeochemical responses to Solar Radiation Modification (SRM)

Solar Radiation Modification (SRM) approaches are deliberate attempts to reduce the amount of sunlight absorbed by the planet in order to counteract global warming due to greenhouse gases (Shepherd, 2012). SRM proposals (Section 4.6.3) include those that increase surface albedo (e.g. by painting the buildings bright white, or by engineering crops to be brighter in near-infrared wavelengths), brighten clouds (e.g. by increasing the amount of sea-salt cloud condensation nuclei), or even reduce the amount of sunlight incident at the top of the Earth's atmosphere (e.g. using hypothetical space mirrors). However, the most commonly-studied approaches attempt to mimic the cooling effects of volcanoes by injecting bright aerosols, or aerosol precursors such sulphur dioxide, into the stratosphere (Crutzen, 2006). SRM is not part of the standard RCP and SSP scenarios considered throughout this report, but it continues to be discussed because the direct costs of large-scale SRM implementation have been estimated as small compared to the cost of rapid decarbonisation of the global economy (Smith and Wagner, 2018). The risks of unintended consequences due to SRM may however be significant, such as regional climate changes, and rapid changes on termination (Jones et al., 2013a). In this section we assess the possible impacts of SRM on the biosphere and on global biogeochemical cycles, calling on published model sensitivity studies that focus on stratospheric aerosol injection, such as GEOMIP (Kravitz et al., 2015). The climate response to SRM is assessed in detail in Chapter 4 (Section 4.6.3)

5.6.3.1 Impacts of elevated CO_2 relatives to pre-industrial conditions

As atmospheric CO_2 continues to increase under SRM, current Earth System Models typically simulate a sizeable CO_2-fertilisation effect on the photosynthesis of land plants. Therefore, Gross Primary Production (GPP) on land is modelled to be higher under high-CO_2 SRM conditions, leading to both higher net primary production and higher land carbon storage. CO_2-fertilisation is smaller in ESMs that include strong nitrogen limitations on plant growth, which implies a smaller increase in land carbon storage in a high-CO_2 SRM world relative to pre-industrial. Plant stomata also open less widely under elevated CO_2, leading to reduced plant transpiration and reduced evaporative cooling of the land. Because SRM does not directly address the increase in atmospheric CO_2, it does not counteract ocean acidification. In the ocean, acidification caused by elevated CO_2 would be detrimental to many shell-forming marine organisms (see Section 5.3). SRM may even accelerate acidification in the deep ocean as a result of SRM-induced ocean circulation change (Tjiputra et al., 2016).

5.6.3.2 Impacts of changes in incident solar radiation

Stratospheric aerosol injection acts to reduce the sunlight reaching the Earth's surface, but also increases the fraction of that light that is diffuse. These changes in the quantity and quality of the sunlight have opposing effects on the photosynthesis of land plants. On their own, reductions in Photosynthetic Active Radiation (PAR) will reduce photosynthesis. However, diffuse light is more effective than direct light in accessing the light-limited leaves within plant canopies, leading to the so-called 'diffuse-radiation' fertilisation effect (Mercado et al., 2009). The balance between the negative impacts of reducing PAR and the positive impacts of increasing diffuse fraction differ between models (Kalidindi et al., 2015; Mercado et al., 2009) and across different ecosystems. For the moderately small changes in surface PAR implied by SRM, diffuse-radiation fertilisation seems *likely* to overcome the reduction in total PAR, at least for dense canopies with high leaf area index (Ito, 2017). However, based-on the response of crop yields to the eruption of the Mount Pinatubo volcano (as a surrogate of SRM), there is a risk that the decrease in incident solar radiation could reduce the yields of maize, soy, rice and wheat (Proctor et al., 2018). The SRM-induced cooling could also cause a reduction in nitrogen mineralisation and limit nutrient availability (Dagon and Schrag, 2019).

5.6.3.3 Net impacts of SRM compared to pre-industrial

Compared to pre-industrial conditions, a high-CO_2 SRM climate scenario produced by uniform stratospheric aerosol injection, would be cooler in the tropics, warmer in the high-latitudes, and have reductions in global mean precipitation (reference). The higher CO_2 relative to pre-industrial would increase land and ocean carbon storage but increase ocean acidification. The photosynthesis of land plants would *likely* be larger in the high-CO_2 SRM climate, but by an uncertain amount that depends on the extent to which CO_2 fertilisation of land plants is limited by other constraints, such as nutrient and water availability. Modelling studies suggest that sunlight reduction will tend to limit changes in vegetation distribution caused by radiatively-induced climate warming but would not prevent increase in terrestrial plant productivity and carbon stocks due to CO_2-fertilisation (Glienke et al., 2015; Govindasamy et al., 2002) – see Figure 5.35.

5.6.3.4 Net impacts of SRM compared to unmitigated climate change

Compared to unmitigated climate change under a given scenario of anthropogenic emissions, SRM is *likely* to reduce the burden of atmospheric CO_2 by enhancing global land and ocean sinks. SRM acts to cool the planet relative to unmitigated climate change, which reduces plant and soil respiration, and also reduces the negative impacts of warming on ocean carbon uptake. Cao and Jiang (2017) reported that SRM would reduce atmospheric burden of CO_2 by about by 47 PgC in 2100, under RCP8.5. Keith et al. (2017) reported that if SRM was used to hold radiative forcing at current level under RCP8.5, SRM may reduce atmospheric CO_2 by about 100 PgC. However, Tjiputra et al. (2016) reported a much smaller reduction of atmospheric CO_2 in response to SRM probably because of the inclusion of the nitrogen cycle that leads to a weaker terrestrial carbon sink. In the case of a halt or termination of an SRM scheme, a sudden warming would cause the additional carbon stored in the land and ocean reservoir to be released into the atmosphere, triggering a further warming that is much faster than in the absence of SRM (Jones et al., 2013a), with potentially dangerous consequences for biodiversity (Trisos et al., 2018).

Based-on current knowledge, SRM with elevated CO_2 would *very likely* increase global mean net primary production and carbon storage on land, relative to both the pre-industrial climate (because of CO_2 fertilisation of photosynthesis), and also relative to an elevated CO_2 world without SRM (because of reduced plant and soil respiration at the lower temperatures). However, SRM plus elevated CO_2 is *very likely* to have negative impacts on ocean ecosystems relative to the pre-industrial due to ocean acidification, with poorly-known consequences for the biological carbon pump and the ocean carbon sink.

[START FIGURE 5.35 HERE]

Figure 5.35: [[Placeholder: From (Glienke et al., 2015). abrupt4×CO_2 is an experiment with an abrupt quadrupling of atmospheric CO_2 and G1 is a GEOMIP experiment in which a decrease in the solar constant offsets the global radiative forcing of 4×CO_2.]]

[END FIGURE 5.35 HERE]

5.7 Knowledge gaps

Contemporary GHG Trends and Attribution

Two key developments require further development on terrestrial models assessing the magnitude and trends of the land CO_2 sink. First, to further constrain the flux from the land use, land use change and forestry. Models have inadequate resolution or lack of representation of land management, such forestry, grazing and cropland management, which covers three quarters of the ice-free land surface. Second, the movement of carbon through the land to ocean continuum has implications for the strength of the land CO_2 sink. Land surface modelling is only at the beginning of representing lateral flows of carbon resulting in carbon accumulation (sinks) in freshwater reservoirs and carbon releases to the atmosphere through the whole continuum of freshwater bodies, rivers to coastal zones.

Improved constraints for air-sea fluxes: Data gaps in space and time for surface ocean CO_2 observations are one of the main obstacles to reducing the biases and uncertainties and provide improved global constraints to the variability and trends of air-sea CO_2 fluxes, particularly to resolve the seasonal cycle bias in sampling. This applies particularly for the Southern Ocean and the Southern Hemisphere oceans in general, which account for most of the uncertainty in global estimates of the air-sea fluxes.

Full attribution of observed CH_4 trends in atmosphere to the underlying drivers has not been fully resolved, yet it is a fundamental to design mitigation activities and incorporate potential future CH_4-climate feedback mechanisms into scenario projections. Difficulties remain to partition the contributions from human activity sources, natural sources, and fluxes associated with emerging CH_4-climate feedbacks under a warmer and higher atmospheric CO environment. Particularly, wetlands are the single largest source term in the global CH_4 budget, proportionally with the largest source of uncertainty, and have the highest potential for producing CH_4-climate feedbacks.

Despite important progress, large uncertainties remain in the contemporary N_2O budget, specifically the magnitude and underlying process-contribution of land and ocean N_2O sources. There is only weak quantitative understanding of the processes leading to inter annual variations of N_2O emissions. This hampers the attribution of the recent increase in the growth rate to underlying causes, including the increased anthropogenic N_2O emissions.

As the budgets of all three major greenhouse gases (CO_2, CH_4, N_2O) remain uncertain from process level understanding, atmospheric and oceanic inverse models have the potential to provide key information on regional sources and sinks from atmospheric observations using chemistry-transport models. Presently inverse models are limited by long-term observational data coverage. The space-borne remote sensing retrievals may relax this limitation if biases can be identified and properly corrected. The chemistry-transport models are often biased for parameterisations of photo-chemical sinks and strength of tracer transport. When improved, inverse models can provide an independent assessment of the emission estimates and track emissions mitigation progress towards defined targets.

Ocean Acidification and Deoxygenation

The rate of ocean acidification and its changes are largely uncertain particularly in subpolar and coastal regions. This is because of the undersampling and strong interplay between carbonate chemistry and a

variety of biogeochemical and physical processes including river water inflow. Current model projections potentially overlook the important future changes in the marine biogeochemistry such as the acidification, as they do not resolve fine-scale temporal and spatial variability and processes, the magnitude and sign of many feedbacks of marine ecosystem are poorly quantified, and atmospheric CO_2 concentrations rather than emissions often drive models.

Trends in ocean acidification and deoxygenation in the ocean interior are linked to changes in water mass ventilation, the evolution of which is poorly constrained. Many Earth System Models project a global decline in the oxygen content of the ocean in the future, but uncertainties remain for the subtropical oceans where the major oxygen-depleted environments reside. The primary uncertainty on future ocean deoxygenation in the subsurface tropical ocean relates to a consistent compensation between oxygen saturation due to warming and decreasing apparent oxygen utilisation as a result of increased ventilation.
Nitrous oxide (N_2O) is produced hypoxic areas, mediated by bacteria. It is still unclear at which threshold of oxygen concentration does N_2O production turn into consumption, and how it would affect ocean emissions.

Future ocean model projections use atmospheric CO_2 concentrations instead of emissions, which might underestimate ocean acidification rates.

Biogeochemical Feedbacks on Climate Change

Changes in land carbon storage remain the key uncertainty in carbon cycle projections. Models differ in the treatment of CO_2-fertilisation, nutrient-limitations, and the net effect of land-use change. The challenge is to better constrain the land carbon components of ESMs with observations, including using the findings of emergent constraint and process-based studies to focus model evaluation and development.

Development and evaluation of coupled carbon-nitrogen-phosphorus land cycle models remains a challenge at any scale, but in particular with respect to understanding and projecting regional patterns of nutrient limitation. New experimental studies highlight the important role of soil processes, which may alter the projections of the current generation of global carbon-nitrogen cycle models. However, the available experimental evidence insufficiently constrains new modelling approaches and therefore hampers their inclusion into large-scale assessments.

Several key processes are missing from the majority of terrestrial carbon cycle models, each of which may systematically bias the ensemble of ESM results. In order to more confidently project carbon cycle feedbacks, models may also need to include soil microbial and mineral stabilization processes, large-scale and fine-scale permafrost processes, the growth and mortality dynamics of individual trees rather than ecosystem canopies as a whole, competition between plants with differing traits across multiple axes of plant functional diversity, and more explicit representation of disturbance processes. For each of these, better global-scale observational constraints are needed to test emerging model approaches that include each of these processes. Further, the high degree of complexity in current ESMs requires numerous parameters, which project on carbon cycle feedbacks in poorly understood ways. Understanding and reducing this parametric and structural uncertainty remains a major problem for projecting feedbacks.

Although model projections of changes in carbon storage agree much better for the ocean than for land, projections of future global ocean primary production do not even agree on the direction of change to 2100. Improved understanding of the processes affecting the efficiency and climate sensitivity of the biological carbon pump, and additional data to constrain large-scales models, are required to improve confidence in projections of ocean primary production.

The estimated risks associated with tipping points in the Earth System are based largely on palaeoclimate data, for which the rates of change are much lower than expected in the next 100 years. New conceptual models, analyses, and ESM runs, are needed to understand how tipping point risks vary with the rate of change of climate and CO_2.

Biases in the physics and biogeochemical drivers of the seasonal cycle of air-sea CO_2 fluxes in ESMs may be

one of the main sources of uncertainties for future projections of air-sea fluxes. Of particular importance are the drivers of the seasonal cycle of sea surface temperature and DIC which control the variability of ocean CO_2. These two drivers determine the climate sensitivity of CO_2 in any particular model. Improved constraints from observational products will provide greater confidence to the model outputs.

Remaining Carbon Budget to Climate Stabilization

Important areas for advancing the more precise estimation of carbon budgets remain. These include a better understanding in both the sign and magnitude of a possible Zero Emissions Commitment (ZEC) and its impact on the Transient Climate Response to cumulative carbon dioxide Emissions (TCRE). ZEC is particularly relevant for cumulative emissions and emissions rates that are consistent with limiting warming to policy-relevant levels.

A better and more broadly supported understanding of the potential magnitude of permafrost thawing feedbacks and their effect on TCRE, as well as the effect on TCRE of other currently not represented Earth system feedbacks can also contribute to a further improved understanding of the remaining carbon budget until peak warming and beyond.

The development of translation tools that allow the easy and internally consistent integration of radiative forcing and other assessments in the estimation of non-CO_2 warming for remaining carbon budgets remains an important avenue for further interdisciplinary advancement.

Carbon Dioxide Removal and Solar Radiation Modification

Assessment of the global carbon cycle response to Carbon Dioxide Removal (CDR) is based on a limited number of modelling studies. Simulations with Earth System Models and the exploration of a broader range of scenarios would increase confidence in the assessment, particularly with regard to the effectiveness of CDR in reducing atmospheric CO_2 and the symmetry in the climate-carbon cycle response to CO_2 emissions and removals. A common limitation of existing studies is the assumption of idealized CDR deployment, without specification of the CDR method. Explicit representation of CDR methods in Earth System models would advance our understanding of the carbon cycle response and Earth System feedbacks associated with these methods.

Large uncertainties exist regarding global CO_2 sequestration potentials of specific land- and ocean-based CDR methods. Most studies of the sequestration potential of land-based CDR methods are at the plot scale, and scaled up globally with models, with no independent verification to evaluate the results. Large-scale and long-term field-based experiments or assessments that involve independent verification are still needed to demonstrate that these methods are not only feasible regionally, but also present an actual and verifiable negative regional carbon balance, with no negative unintended consequences. Potential carbon sequestration for blue carbon ecosystems needs to be better assessed.

Estimation of global CDR potentials of other ocean-based methods (ocean alkalinisation, artificial ocean upwelling) relies exclusively on model simulations, often with experiments that assume unrealistic deployment scenarios. Research is required to understand the potential for scalability of CO_2 sequestration potentials for ocean-based methods for which field-based experiments exist (iron fertilization, blue carbon), and their potential unintended negative consequences.

Key uncertainties in the assessment of the effects of Solar Radiation Modification (SRM) on the carbon cycle are related to the response of terrestrial and marine ecosystems and associated carbon storage. Several of these uncertainties are in common with the assessment of the land and ocean carbon cycle response to CO_2 increase and warming, such as the impact of ocean acidification on the biological carbon pump and the impact of nutrient limitation on soil respiration and land carbon storage.

Frequently Asked Questions

FAQ 5.1: Are the ways nature removes carbon from the atmosphere slowing down?

For decades, nature has removed about half of the carbon dioxide (CO_2) that human activities have emitted to the atmosphere by increasing the amount of carbon stored in vegetation, soils and oceans. These processes have thus roughly halved the rate at which atmospheric CO_2 concentrations have increased, and therefore slowdown global warming. There is as yet no observable evidence that this natural removal is slowing down or that the processes underlying this removal are changing.

Since scientists began measuring CO_2 concentrations in the atmosphere in 1959, only about half of all emissions from the combustion of fossil fuels and land-use change (e.g. deforestation) has remained in the atmosphere, the so-called air-borne fraction. Natural carbon sinks, processes on land and oceans that remove CO_2 from the atmosphere, have removed the other half of the emissions.

The key land process that removes CO_2 from the atmosphere is plant photosynthesis, which for most plants increases as the concentration of atmospheric CO_2 rises, due to what is known as the CO_2 fertilisation effect. Longer growing seasons in cold places due to global warming might also contribute to increased land CO_2 uptake. A large part of the CO_2 captured is lost back to the atmosphere through respiration, fires, other disturbances, and the net balance among all these processes constitutes the net land carbon sink.

The processes involved in the land CO_2 uptake are affected by many factors, and as climate and other biophysical properties changes, the land CO_2 uptake will change too. For instance, higher temperatures and droughts reduce the land sink, a process that is, often observed during El Nino years, a frequent climate event when the Earth surface has well above average temperatures. Other natural factors and human activities also influence the net removal of carbon by the land biosphere, either causing an increase in carbon storage (e.g. reforestation, nitrogen deposition) or a decrease (e.g. deforestation and land degradation, disturbances such as fire or windthrow, air pollution). The natural land sink varies strongly from year to year, making it challenging to detect long-term trends.

In the ocean, the CO_2 uptake is primarily driven by three physical and chemical factors: the difference in CO_2 concentration between the atmosphere and the surface ocean (approximately the upper 50m, but with important variations across seasons), the chemical capacity of seawater to take up CO_2 (or buffering capacity), and wind speeds at the ocean surface. Surface ocean water with elevated CO_2 is transported to the deep ocean in specific deep-water formation zones around the globe (like the Northern Atlantic and the Southern Ocean), effectively storing it away from the surface ocean and atmosphere for many decades to centuries.

Remarkably, both the land and ocean sinks have been growing largely proportional to the increase in CO_2 emissions. This has made the airborne fraction, the fraction of CO_2 emissions staying in the atmosphere, to remain on average unchanged over the last five decades despite continuously increasing CO_2 emissions from human activities. There is currently no evidence that the land or ocean sinks are slowing down, and also no evidence that the way these sinks respond to the excess of anthropogenic CO_2 in the atmosphere is fundamentally changing (see Figure).

The fact that both the land and ocean sink respond to excess anthropogenic CO_2 in the atmosphere, suggests that the absolute sink strength of land and ocean will vary in proportion to future anthropogenic emissions. Hence this implies that if countries manage to strongly reduce global CO_2 emissions or even reach net zero or negative emission levels, these sinks will in all likelihood also again become smaller. Also, if emissions are not reduced that strongly, the ocean sink is expected to become smaller. For the land sink, model simulations suggest that if emissions are not reduced sufficiently strongly so as to cap warming at 2°C the combined effect of increasing atmospheric CO_2 and climate change may weaken the land sink in the second half of this century. In summary, CO_2 sinks will change in the future and understanding the directions of change will be fundamental to design mitigation pathways.

[START FAQ 5.1, FIGURE 1 HERE]

FAQ 5.1, Figure 1: Growth rate of the CO_2 inventory in the atmosphere, ocean and land, as well as the air-borne fraction of anthropogenic CO_2 emissions, and the efficiency of the ocean and land carbon sinks (defined as the size of the sink divided by the excess of anthropogenic CO_2 in the atmosphere). Estimates are derived from atmospheric observations, process-based models, data-driven ocean flux products, and atmospheric inversions (Le Quéré et al., 2018a). Dots and arrow bars denote the year-to-year variability as ±1 standard deviation. Uncertainties in the estimates will be added for the SOD.

[END FAQ 5.1, FIGURE 1 HERE]

FAQ 5.2: Can thawing permafrost or ocean warming substantially increase global temperatures?

Carbon released as carbon dioxide (CO_2) or methane (CH_4) as a result of increased rates of decomposition in thawing permafrost soils may add an additional amount of warming, that is significant enough that it should be considered in carbon estimates, but does not appear to be a process that will lead to runaway warming. Warming of frozen sediments beneath the ocean and deeper on land appears to be a weaker potential source of greenhouse gases.

Across arctic ecosystems, where deep soils remain frozen throughout the year, there are enormous amount of carbon in accumulated soil organic matter: more than twice the amount of CO_2 that is currently in the atmosphere. This carbon has built up over thousands of years, through the growth of plants that become thick organic litter layers when they die, which then can be buried into deeper, permanently-frozen soil layers, where the cold conditions slow the rate of their decomposition for as long as the soils remain frozen. These processes have led permafrost soils to act as carbon sinks historically, but experiments have shown that, by warming these ecosystems, the carbon in these soils will begin to decompose rapidly and return to the atmosphere as either CO_2 or CH_4, which are both important greenhouse gases. Climate models project that much of the near-surface permafrost throughout the arctic would thaw under moderate to high amounts of global warming, and thus the carbon stored in this ecosystem is at risk.

Thawing of permafrost carbon has already began due to the rapid warming experienced in the Arctic, twice as fast as the global average. With this thawing there are measurements showing very old carbon frozen for thousands of years being emitted to the atmosphere and transported into waterways. There are many processes that can speed up the loss of carbon from these northern ecosystems. Melting of massive blocks of ice in the soils can cause the landscape to sink and erode. Ponds and lakes that are common in some arctic ecosystems can expand and move across the landscape. Thick surface organic layers can dry out in warmer summers and catch fire. The same warming also releases nutrients from the decomposing soils, and warmer and longer growing seasons favours plants to grow and store carbon as it is being observed in some regions of tundra.

While these processes are complex, they are beginning to be included in models that represent the climate and the carbon cycle in an interactive manner. The projections from these models show a wide range in the estimated strength of a carbon-climate self-reinforcing loop, but the general results are: (a) that this extra warming is strong enough that it must be included to estimate the total amount of emissions permitted to stabilise the climate at a given level, but (b) not so strong that they would lead to warming that is greater than the warming from fossil fuel burning itself at any level of warming, and (c) that emissions of greenhouse gases from permafrost are projected to be higher under high emissions scenarios.

In addition to carbon within permafrost soils, concern has been raised about carbon frozen in sediments deep below the soils of permafrost ecosystems or frozen in ocean sediments, known as methane hydrates or clathrates, which are methane molecules locked within a cage of ice molecules. Hydrates are stable at low temperatures and high pressures, conditions that are found below permafrost and in ocean sediments. As global warming affects both the permafrost and the oceans, there are concerns this warming could destabilise hydrates, releasing methane into the atmosphere and significantly exacerbating climate change.

Current understanding shows that the global marine hydrate reserve is probably smaller than initially thought, now at 2000 PgC. Global warming also takes millennia to penetrate into the deep ocean and reach these hydrates, so the hydrate that could be destabilised during a century timescale is a small fraction of the total estimated marine hydrate reserve. Finally, even when methane is released from hydrates, most of it is expected to be either consumed or oxidised to carbon dioxide in the ocean before reaching the atmosphere. The most complete modelling of these processes to date suggests a release of less than 5 $TgCH_4\ yr^{-1}$ over the next century, which is less than 2% of current anthropogenic methane emissions.

[[Figure Placeholder: Schematic of the processes that effect permafrost thawing (what speeds up or slows down the release of GHG emissions.)]]

FAQ 5.3: Can negative emissions reverse climate change?

Negative emissions refer to removal of carbon dioxide (CO_2) from the atmosphere by deliberate human activities; that means, in addition to the removal that would occur naturally. If CO_2 removal from the atmosphere is greater than CO_2 release, emissions are said to be net negative. The effect of negative emissions on atmospheric CO_2 depends on the balance between CO_2 releases, deliberate removals and removals by natural carbon sinks. Generally, net negative emissions results in a decline in atmospheric CO_2. However, because of the delayed reaction of many climate system components such as vegetation, soils, the deep ocean, ice sheets, a decline in atmospheric CO_2 will not result in immediate reversal of climate changes. While some parts of the Earth's climate system such as surface air temperature will follow a decline in atmospheric CO_2 quite rapidly, others will take decades to millennia to reverse.

[Concept of negative and net negative emissions] Negative emissions refer to removal of carbon dioxide (CO_2) from the atmosphere by deliberate human activities; that means, in addition to the removal that would occur naturally. The term negative emissions is often used as synonymous with carbon dioxide removal (CDR). Negative emission can compensate release of CO_2 into the atmosphere. If CO_2 removal from the atmosphere is greater than CO_2 release, emissions are said to be *net* negative.

[Carbon bathtub] In the absence of negative emissions, the CO_2 concentration in the atmosphere (a measure of the amount of CO_2 in the atmosphere) results from a balance between CO_2 release and removal by natural processes on land and in the ocean (natural "carbon sinks"). If CO_2 release exceeds removal by carbon sinks, the CO_2 concentration in the atmosphere will increase; if CO_2 release equals removal the, atmospheric CO_2 concentration will stabilise; and if CO_2 removal exceeds release, the CO_2 concentration will decline. In the same way, if <u>*net*</u> emissions (i.e. the sum of releases and deliberate removals) exceed removals by natural carbon sinks, atmospheric CO_2 will go up; if net emissions equal removals by sinks, atmospheric CO_2 will not change; and if removals exceed net emissions, or emissions are net negative, atmospheric CO_2 will go down.

[Climate system inertia, reversibility] If the CO_2 concentration in the atmosphere starts to go down, the Earth's climate will respond to this change. Some parts of the climate system have a delayed reaction to a change in CO_2 in the atmosphere and a decline in atmospheric CO_2 through net negative emissions would therefore not imply a simultaneous reversal of climate change. Recent studies have shown that surface air temperature starts to decline within a few years following a decline in atmospheric CO_2. Other components of the climate system, however, such as vegetation, soils, the deep ocean, ice sheets, take decades to millennia to react to the decline in atmospheric CO_2. For these components, net negative emissions would not result in an immediate reversal of changes caused by CO_2. For instance, warming, acidification and oxygen loss of the deep ocean would take centuries to reverse following a decline in the atmospheric CO_2 concentration. Sea level rise due to warming and expansion of seawater would continue for centuries even if large amounts of negative emissions would be implemented.

[Overshoot scenarios] A class of future scenarios that is receiving increasing attention, particularly in the context of ambitious climate targets, such as the 1.5°C and 2°C targets included in the Paris Agreement, are so-called "overshoot" scenarios. In these scenarios slow emission reductions in the near term are compensated by net negative CO_2 emissions in the later part of this century, which results in a temporary breach or "overshoot" of a specific temperature level. Due to the delayed reaction of several climate system components it follows that the temporary breach of a temperature target level will result in additional climate changes (compared to a scenario that reaches the target level without overshoot) that will take decades to many centuries to reverse.

In conclusion, negative emissions can only reverse climate change to a limited degree. Some parts of the Earth's climate system such as surface air temperature will follow a decline in atmospheric CO_2 quite rapidly, while others such as sea level rise will take multiple centuries to reverse.

[[Figure suggestion – Time series of responses of climate system components with short to long response time scales (short term would include things like surface air temperature, long term would be warming,

acidification and oxygen loss of the deep ocean, sea level etc.).]]

FAQ 5.4: What is a carbon budget?

The term carbon budget refers to two major concepts depending on how it is used. It can refer to how emissions of carbon dioxide from human activities get redistributed in the Earth system: how much of those emissions accumulate in the atmosphere and how much are taken up by the ocean or the land biosphere. It is then referred to as the "human perturbation carbon budget" or the 'historical/contemporary carbon budget'. However, carbon budget can also refer to the total net amount of carbon dioxide emission that can still be emitted by human activities, while managing to keep global warming below a specific maximum temperature threshold. It is then called the 'remaining carbon budget'.

The term carbon budget is a widely used term but refers to different concepts depending on its context. First, the term is used when describing the historical carbon budget. The historical carbon budget describes all past and present sources and sinks of carbon dioxide. It thus describes how the carbon dioxide emissions that were emitted by human activities have redistributed across the various reservoirs of the Earth system. These are the ocean, the land biosphere, and the atmosphere, into which carbon dioxide emissions were emitted to start with. Whatever amount of carbon dioxide emissions that is not taken up by the ocean or the land biosphere results in an increase of atmospheric carbon dioxide concentrations, and therewith further drives global warming. Carbon dioxide taken up by the ocean is not harmless, because it results in changing the chemistry of the ocean water, reducing its alkalinity. This process is known as ocean acidification. The study of the historical carbon budget teaches us that of the about 2440 billion tonnes of carbon dioxide that were released into the atmosphere by human activities between 1750 and 2017, about a quarter was absorbed by the ocean, and about a third by the land biosphere. About 40% of these emissions remains currently in the atmosphere.

The term carbon budget is also used when describing the total net amount of carbon dioxide that human activities would still be allowed to release into the atmosphere while keeping global warming to a specific temperature threshold, like 1.5°C or 2°C relative to preindustrial levels. In this context it is referred to as the 'remaining carbon budget'. Underlying the concept of a remaining carbon budget is our understanding that global warming is roughly linearly proportional to the total net amount of carbon dioxide emissions – also referred to as cumulative carbon dioxide emissions – that are released into the atmosphere by human activities. This characteristic only holds true for carbon dioxide, because of the specific way carbon dioxide behaves in the Earth system. The concept of a remaining carbon budgets comes with some direct implications. It means that to stay to halt global warming, global emissions of carbon dioxide need to be reduced to net zero levels. It also means that if emissions are not reduced in the next decade, deeper and faster reductions in carbon dioxide emissions are required thereafter. The exact size of the remaining carbon budget depends on the global warming level that we set as a limit, the probability with which we want to ensure that warming is held below that limit, and how successful we are in limiting emissions of other emissions that affect the climate, like methane or nitrous oxide. [[Sentence on the AR6 WG1 remaining carbon budget assessment.]]

[[Figure idea: visual combining the historical carbon budget, with straight lines going down from today's emissions to zero, and in line with the remaining carbon budget for 1.5°C or 2°C – coloured and labelled differently to make the difference clear.]]

References

Achat, D. L., Augusto, L., Gallet-Budynek, A., and Loustau, D. (2016). Future challenges in coupled C–N–P cycle models for terrestrial ecosystems under global change: a review. *Biogeochemistry* 131, 173–202. doi:10.1007/s10533-016-0274-9.

Ainsworth, E. A., and Long, S. P. (2005). What have we learned from 15 years of free-air CO2 enrichment (FACE)? A meta-analytic review of the responses of photosynthesis, canopy properties and plant production to rising CO2. *New Phytol.* 165, 351–372. doi:10.1111/j.1469-8137.2004.01224.x.

Allen, G. H., and Pavelsky, T. M. (2018). Global extent of rivers and streams. *Science (80-.).* 361, 585–588. doi:10.1126/science.aat0636.

Allen, M. R., Dube, O. P., Solecki, W., Aragón-Durand, F., Cramer, W., Humphreys, S., et al. (2018). "Framing and Context," in *Global Warming of 1.5°C. An IPCC Special Report on the impacts of global warming of 1.5°C above pre-industrial levels and related global greenhouse gas emission pathways, in the context of strengthening the global response to the threat of climate change,* eds. V. Masson-Delmotte, P. Zhai, H.-O. Pörtner, D. Roberts, J. Skea, P. R. Shukla, et al. (In Press).

Allen, M. R., Frame, D. J., Huntingford, C., Jones, C. D., Lowe, J. A., Meinshausen, M., et al. (2009). Warming caused by cumulative carbon emissions towards the trillionth tonne. *Nature* 458, 1163–1166. doi:10.1038/nature08019.

Allen, M. R., and Ingram, W. J. (2002). Constraints on future changes in climate and the hydrologic cycle. *Nature* 419, 228–232. doi:10.1038/nature01092.

Anadón, J. D., Sala, O. E., and Maestre, F. T. (2014). Climate change will increase savannas at the expense of forests and treeless vegetation in tropical and subtropical Americas. *J. Ecol.* 102, 1363–1373. doi:10.1111/1365-2745.12325.

Anagnostou, E., John, E. H., Edgar, K. M., Foster, G. L., Ridgwell, A., Inglis, G. N., et al. (2016). Changing atmospheric CO2 concentration was the primary driver of early Cenozoic climate. *Nature* 533, 380–384. doi:10.1038/nature17423.

Anav, A., Friedlingstein, P., Kidston, M., Bopp, L., Ciais, P., Cox, P., et al. (2013). Evaluating the Land and Ocean Components of the Global Carbon Cycle in the CMIP5 Earth System Models. *J. Clim.* 26, 6801–6843. doi:10.1175/JCLI-D-12-00417.1.

Anderson, R. F., Sachs, J. P., Fleisher, M. Q., Allen, K. A., Yu, J., Koutavas, A., et al. (2019). Deep-Sea Oxygen Depletion and Ocean Carbon Sequestration During the Last Ice Age. *Global Biogeochem. Cycles* (in press). doi:10.1029/2018GB006049.

Andrew, R. M. (2018). Global CO2 emissions from cement production. *Earth Syst. Sci. Data* 10, 195–217. doi:10.5194/essd-10-195-2018.

Archer, D., Buffett, B., and Brovkin, V. (2009). Ocean methane hydrates as a slow tipping point in the global carbon cycle. *Proc. Natl. Acad. Sci.* 106, 20596–20601. doi:10.1073/pnas.0800885105.

Archer, D., Kheshgi, H., and Maier-Reimer, E. (1998). Dynamics of fossil fuel CO2 neutralization by marine CaCO3. *Global Biogeochem. Cycles* 12, 259–276. doi:10.1029/98GB00744.

Arévalo-Martínez, D. L., Kock, A., Löscher, C. R., Schmitz, R. A., and Bange, H. W. (2015). Massive nitrous oxide emissions from the tropical South Pacific Ocean. *Nat. Geosci.* 8, 530–533. doi:10.1038/ngeo2469.

Arneth, A., Harrison, S. P., Zaehle, S., Tsigaridis, K., Menon, S., Bartlein, P. J., et al. (2010). Terrestrial biogeochemical feedbacks in the climate system. *Nat. Geosci.* 3, 525–532. doi:10.1038/ngeo905.

Arneth, A., Sitch, S., Pongratz, J., Stocker, B. D., Ciais, P., Poulter, B., et al. (2017). Historical carbon dioxide emissions caused by land-use changes are possibly larger than assumed. *Nat. Geosci.* 10, 79–84. doi:10.1038/ngeo2882.

Arora, V. K., Boer, G. J., Friedlingstein, P., Eby, M., Jones, C. D., Christian, J. R., et al. (2013). Carbon–Concentration and Carbon–Climate Feedbacks in CMIP5 Earth System Models. *J. Clim.* 26, 5289–5314. doi:10.1175/JCLI-D-12-00494.1.

Arzhanov, M. M., and Mokhov, I. I. (2017). Stability of continental relic methane hydrates for the holocene climatic optimum and for contemporary conditions. *Dokl. Earth Sci.* 476, 1163–1167. doi:10.1134/S1028334X17100026.

Arzhanov, M. M., Mokhov, I. I., and Denisov, S. N. (2016). Impact of regional climatic change on the stability of relic gas hydrates. *Dokl. Earth Sci.* 468, 616–618. doi:10.1134/S1028334X1606009X.

Aumont, O., and Bopp, L. (2006). Globalizing results from ocean in situ iron fertilization studies. *Global Biogeochem. Cycles* 20, GB2017. doi:10.1029/2005GB002591.

Azetsu-Scott, K., Clarke, A., Falkner, K., Hamilton, J., Jones, E. P., Lee, C., et al. (2010). Calcium carbonate saturation states in the waters of the Canadian Arctic Archipelago and the Labrador Sea. *J. Geophys. Res.* 115, C11021. doi:10.1029/2009JC005917.

Babbin, A. R., Bianchi, D., Jayakumar, A., and Ward, B. B. (2015). Rapid nitrous oxide cycling in the suboxic ocean. *Science (80-.).* 348, 1127–1129. doi:10.1126/science.aaa8380.

Babila, T. L., Penman, D. E., Hönisch, B., Kelly, D. C., Bralower, T. J., Rosenthal, Y., et al. (2018). Capturing the global signature of surface ocean acidification during the Palaeocene–Eocene Thermal Maximum. *Philos. Trans. R. Soc. A Math. Phys. Eng. Sci.* 376, 20170072. doi:10.1098/rsta.2017.0072.

Baccini, A., Walker, W., Carvalho, L., Farina, M., Sulla-Menashe, D., and Houghton, R. A. (2017). Tropical forests are a net carbon source based on aboveground measurements of gain and loss. *Science (80-.).* 358, 230–234. doi:10.1126/science.aam5962.

Baig, S., Medlyn, B. E., Mercado, L. M., and Zaehle, S. (2015). Does the growth response of woody plants to elevated CO2increase with temperature? A model-oriented meta-analysis. *Glob. Chang. Biol.* 21, 4303–4319. doi:10.1111/gcb.12962.

Bains, S., Norris, R. D., Corfield, R. M., and Faul, K. L. (2000). Termination of global warmth at the Palaeocene/Eocene boundary through productivity feedback. *Nature* 407, 171–174. doi:10.1038/35025035.

Bakker, D. C. E., Pfeil, B., Landa, C. S., Metzl, N., O'Brien, K. M., Olsen, A., et al. (2016). A multi-decade record of high-quality fCO2 data in version 3 of the Surface Ocean CO2 Atlas (SOCAT). *Earth Syst. Sci. Data* 8, 383–413. doi:10.5194/essd-8-383-2016.

Ballantyne, A. P., Alden, C. B., Miller, J. B., Tans, P. P., and White, J. W. C. (2012). Increase in observed net carbon dioxide uptake by land and oceans during the past 50 years. *Nature* 488, 70–72. doi:10.1038/nature11299.

Ballantyne, A. P., Rybczynski, N., Baker, P. A., Harington, C. R., and White, D. (2006). Pliocene Arctic temperature constraints from the growth rings and isotopic composition of fossil larch. *Palaeogeogr. Palaeoclimatol. Palaeoecol.* 242, 188–200. doi:10.1016/j.palaeo.2006.05.016.

Ballantyne, A., Smith, W., Anderegg, W., Kauppi, P., Sarmiento, J., Tans, P., et al. (2017). Accelerating net terrestrial carbon uptake during the warming hiatus due to reduced respiration. *Nat. Clim. Chang.* 7, 148–152. doi:10.1038/nclimate3204.

Bândă, N., Krol, M., van Weele, M., van Noije, T., Le Sager, P., and Röckmann, T. (2016). Can we explain the observed methane variability after the Mount Pinatubo eruption? *Atmos. Chem. Phys.* 16, 195–214. doi:10.5194/acp-16-195-2016.

Barker, S. (2002). Foraminiferal Calcification Response to Glacial-Interglacial Changes in Atmospheric CO2. *Science (80-.).* 297, 833–836. doi:10.1126/science.1072815.

Barker, S., Higgins, J. A., and Elderfield, H. (2003). The future of the carbon cycle: review, calcification response, ballast and feedback on atmospheric CO2. *Philos. Trans. R. Soc. London. Ser. A Math. Phys. Eng. Sci.* 361, 1977–1999. doi:10.1098/rsta.2003.1238.

Bastos, A., Friedlingstein, P., Sitch, S., Chen, C., Mialon, A., Wigneron, J.-P., et al. (2018). Impact of the 2015/2016 El Niño terrestrial carbon cycle constrained by bottom-up and top-down approaches. *Philos. Trans. R. Soc. B Biol. Sci.* 373, 1–11. doi:10.1098/rstb.2017.0304.

Bastos, A., Janssens, I. A., Gouveia, C. M., Trigo, R. M., Ciais, P., Chevallier, F., et al. (2016). European land CO2 sink influenced by NAO and East-Atlantic Pattern coupling. *Nat. Commun.* 7, 10315. doi:10.1038/ncomms10315.

Bates, N., Astor, Y., Church, M., Currie, K., Dore, J., Gonaález-Dávila, M., et al. (2014). A Time-Series View of Changing Ocean Chemistry Due to Ocean Uptake of Anthropogenic CO2 and Ocean Acidification. *Oceanography* 27, 126–141. doi:10.5670/oceanog.2014.16.

Bates, N. R., Mathis, J. T., and Cooper, L. W. (2009). Ocean acidification and biologically induced seasonality of carbonate mineral saturation states in the western Arctic Ocean. *J. Geophys. Res.* 114, C11007. doi:10.1029/2008JC004862.

Bathiany, S., Claussen, M., Brovkin, V., Raddatz, T., and Gayler, V. (2010). Combined biogeophysical and biogeochemical effects of large-scale forest cover changes in the MPI earth system model. *Biogeosciences* 7, 1383–1399. doi:10.5194/bg-7-1383-2010.

Batjes, N. H. (2016). Harmonized soil property values for broad-scale modelling (WISE30sec) with estimates of global soil carbon stocks. *Geoderma* 269, 61–68. doi:10.1016/j.geoderma.2016.01.034.

Battaglia, G., and Joos, F. (2018). Marine N2O Emissions From Nitrification and Denitrification Constrained by Modern Observations and Projected in Multimillennial Global Warming Simulations. *Global Biogeochem. Cycles* 32, 92–121. doi:10.1002/2017GB005671.

Bauska, T. K., Baggenstos, D., Brook, E. J., Mix, A. C., Marcott, S. A., Petrenko, V. V., et al. (2016). Carbon isotopes characterize rapid changes in atmospheric carbon dioxide during the last deglaciation. *Proc. Natl. Acad. Sci.* 113, 3465–3470. doi:10.1073/pnas.1513868113.

Beaufort, L., Probert, I., de Garidel-Thoron, T., Bendif, E. M., Ruiz-Pino, D., Metzl, N., et al. (2011). Sensitivity of coccolithophores to carbonate chemistry and ocean acidification. *Nature* 476, 80–83. doi:10.1038/nature10295.

Beerling, D. J., Leake, J. R., Long, S. P., Scholes, J. D., Ton, J., Nelson, P. N., et al. (2018). Farming with crops and rocks to address global climate, food and soil security. *Nat. Plants* 4, 138–147. doi:10.1038/s41477-018-0108-y.

Belshe, E. F., Schuur, E. A. G., and Bolker, B. M. (2013). Tundra ecosystems observed to be CO 2 sources due to differential amplification of the carbon cycle. *Ecol. Lett.* 16, 1307–1315. doi:10.1111/ele.12164.

BERINGER, T., LUCHT, W., and SCHAPHOFF, S. (2011). Bioenergy production potential of global biomass plantations under environmental and agricultural constraints. *GCB Bioenergy* 3, 299–312. doi:10.1111/j.1757-1707.2010.01088.x.

Bernardello, R., Marinov, I., Palter, J. B., Sarmiento, J. L., Galbraith, E. D., and Slater, R. D. (2014). Response of the Ocean Natural Carbon Storage to Projected Twenty-First-Century Climate Change. *J. Clim.* 27, 2033–2053. doi:10.1175/JCLI-D-13-00343.1.

BGR (2017). BGR Energy Study 2017 - Data and Developments Concerning German and Global Energy Supplies. Hannover.

Bianchi, D., Dunne, J. P., Sarmiento, J. L., and Galbraith, E. D. (2012). Data-based estimates of suboxia, denitrification, and N 2 O production in the ocean and their sensitivities to dissolved O 2. *Global Biogeochem. Cycles* 26, GB2009. doi:10.1029/2011GB004209.

Bock, M., Schmitt, J., Beck, J., Seth, B., Chappellaz, J., and Fischer, H. (2017). Glacial/interglacial wetland, biomass burning, and geologic methane emissions constrained by dual stable isotopic CH 4 ice core records. *Proc. Natl. Acad. Sci.* 114, E5778–E5786. doi:10.1073/pnas.1613883114.

Bock, M., Schmitt, J., Möller, L., Spahni, R., Blunier, T., and Fischer, H. (2010). Hydrogen isotopes preclude marine hydrate CH4 emissions at the onset of Dansgaard-Oeschger events. *Science (80-.).* 328, 1686–9. doi:10.1126/science.1187651.

Bopp, L., Resplandy, L., Orr, J. C., Doney, S. C., Dunne, J. P., Gehlen, M., et al. (2013). Multiple stressors of ocean ecosystems in the 21st century: projections with CMIP5 models. *Biogeosciences* 10, 6225–6245. doi:10.5194/bg-10-6225-2013.

Bopp, L., Resplandy, L., Untersee, A., Le Mezo, P., and Kageyama, M. (2017). Ocean (de)oxygenation from the Last Glacial Maximum to the twenty-first century: insights from Earth System models. *Philos. Trans. R. Soc. A Math. Phys. Eng. Sci.* 375, 20160323. doi:10.1098/rsta.2016.0323.

Boscolo-Galazzo, F., Crichton, K. A., Barker, S., and Pearson, P. N. (2018). Temperature dependency of metabolic rates in the upper ocean: A positive feedback to global climate change? *Glob. Planet. Change* 170, 201–212. doi:10.1016/j.gloplacha.2018.08.017.

Boulton, C. A., Booth, B. B. B., and Good, P. (2017). Exploring uncertainty of Amazon dieback in a perturbed parameter Earth system ensemble. *Glob. Chang. Biol.* 23, 5032–5044. doi:10.1111/gcb.13733.

Bouwman, L., Daniel, J. S., Davidson, E. A., de Klein, C., Holland, E., Ju, X., et al. (2013). *Drawing down N2O to protect climate and the ozone layer. A UNEP Synthesis report*. United Nations Environment Programme (UNEP).

Bowen, G. J., and Zachos, J. C. (2010). Rapid carbon sequestration at the termination of the Palaeocene–Eocene Thermal Maximum. *Nat. Geosci.* 3, 866–869. doi:10.1038/ngeo1014.

Boyd, P. W., Jickells, T., Law, C. S., Blain, S., Boyle, E. A., Buesseler, K. O., et al. (2007). Mesoscale Iron Enrichment Experiments 1993-2005: Synthesis and Future Directions. *Science (80-.).* 315, 612–617. doi:10.1126/science.1131669.

Boyd, P. W., Lennartz, S. T., Glover, D. M., and Doney, S. C. (2015). Biological ramifications of climate-change-mediated oceanic multi-stressors. *Nat. Clim. Chang.* 5, 71–79. doi:10.1038/nclimate2441.

Boysen, L. R., Lucht, W., and Gerten, D. (2017a). Trade-offs for food production, nature conservation and climate limit the terrestrial carbon dioxide removal potential. *Glob. Chang. Biol.* 23, 4303–4317. doi:10.1111/gcb.13745.

Boysen, L. R., Lucht, W., Gerten, D., Heck, V., Lenton, T. M., and Schellnhuber, H. J. (2017b). The limits to global-warming mitigation by terrestrial carbon removal. *Earth's Futur.* 5, 463–474. doi:10.1002/2016EF000469.

BP (2018). BP Statistical Review of World Energy June 2018. Available at: https://www.bp.com/content/dam/bp/%0Aen/corporate/pdf/energy-economics/statistical-review/%0Abp-stats-review-2018-full-report.pdf.

Bralower, T. J., Kump, L. R., Self-Trail, J. M., Robinson, M. M., Lyons, S., Babila, T., et al. (2018). Evidence for Shelf Acidification During the Onset of the Paleocene-Eocene Thermal Maximum. *Paleoceanogr. Paleoclimatology* 33, 1408–1426. doi:10.1029/2018PA003382.

Breitburg, D., Levin, L. A., Oschlies, A., Grégoire, M., Chavez, F. P., Conley, D. J., et al. (2018). Declining oxygen in the global ocean and coastal waters. *Science (80-.).* 359, eaam7240. doi:10.1126/science.aam7240.

Brennan, G., and Collins, S. (2015). Growth responses of a green alga to multiple environmental drivers. *Nat. Clim. Chang.* 5, 892–897. doi:10.1038/nclimate2682.

Brienen, R. J. W., Gloor, E., Clerici, S., Newton, R., Arppe, L., Boom, A., et al. (2017). Tree height strongly affects estimates of water-use efficiency responses to climate and CO2 using isotopes. *Nat. Commun.* 8, 288. doi:10.1038/s41467-017-00225-z.

Brienen, R. J. W., Phillips, O. L., Feldpausch, T. R., Gloor, E., Baker, T. R., Lloyd, J., et al. (2015). Long-term decline of the Amazon carbon sink. *Nature* 519, 344–348. doi:10.1038/nature14283.

Bronselaer, B., Zanna, L., Munday, D. R., and Lowe, J. (2018). Southern Ocean carbon-wind stress feedback. *Clim. Dyn.* 51, 2743–2757. doi:10.1007/s00382-017-4041-y.

Broucek, J. (2014). Production of Methane Emissions from Ruminant Husbandry: A Review. *J. Environ. Prot. (Irvine,. Calif).* 05, 1482–1493. doi:10.4236/jep.2014.515141.

Brovkin, V., Boysen, L., Arora, V. K., Boisier, J. P., Cadule, P., Chini, L., et al. (2013). Effect of Anthropogenic Land-Use and Land-Cover Changes on Climate and Land Carbon Storage in CMIP5 Projections for the Twenty-First Century. *J. Clim.* 26, 6859–6881. doi:10.1175/JCLI-D-12-00623.1.

Brovkin, V., Brücher, T., Kleinen, T., Zaehle, S., Joos, F., Roth, R., et al. (2016). Comparative carbon cycle dynamics of the present and last interglacial. *Quat. Sci. Rev.* 137, 15–32. doi:10.1016/j.quascirev.2016.01.028.

Brovkin, V., Ganopolski, A., Archer, D., and Munhoven, G. (2012). Glacial CO₂ cycle as a succession of key physical and biogeochemical processes. *Clim. Past* 8, 251–264. doi:10.5194/cp-8-251-2012.

Buermann, W., Forkel, M., O'Sullivan, M., Sitch, S., Friedlingstein, P., Haverd, V., et al. (2018). Widespread seasonal compensation effects of spring warming on northern plant productivity. *Nature* 562, 110–114. doi:10.1038/s41586-018-0555-7.

Buitenhuis, E. T., Suntharalingam, P., and Le Quéré, C. (2018). Constraints on global oceanic emissions of N2O from observations and models. *Biogeosciences* 15, 2161–2175. doi:10.5194/bg-15-2161-2018.

Burke, E. J., Chadburn, S. E., Huntingford, C., and Jones, C. D. (2018). CO2 loss by permafrost thawing implies additional emissions reductions to limit warming to 1.5 or 2°C. *Environ. Res. Lett.* 13, 024024. doi:10.1088/1748-9326/aaa138.

Burke, E. J., Ekici, A., Huang, Y., Chadburn, S. E., Huntingford, C., Ciais, P., et al. (2017). Quantifying uncertainties of permafrost carbon–climate feedbacks. *Biogeosciences* 14, 3051–3066. doi:10.5194/bg-14-3051-2017.

Burke, E. J., Jones, C. D., and Koven, C. D. (2013). Estimating the Permafrost-Carbon Climate Response in the CMIP5 Climate Models Using a Simplified Approach. *J. Clim.* 26, 4897–4909. doi:10.1175/JCLI-D-12-00550.1.

Burls, N. J., Fedorov, A. V., Sigman, D. M., Jaccard, S. L., Tiedemann, R., and Haug, G. H. (2017). Active Pacific meridional overturning circulation (PMOC) during the warm Pliocene. *Sci. Adv.* 3, e1700156. doi:10.1126/sciadv.1700156.

Burney, J. A., Davis, S. J., and Lobell, D. B. (2010). Greenhouse gas mitigation by agricultural intensification. *Proc. Natl. Acad. Sci.* 107, 12052–12057. doi:10.1073/pnas.0914216107.

Butterbach-Bahl, K., Baggs, E. M., Dannenmann, M., Kiese, R., and Zechmeister-Boltenstern, S. (2013). Nitrous oxide emissions from soils: how well do we understand the processes and their controls? *Philos. Trans. R. Soc. B Biol. Sci.* 368, 20130122–20130122. doi:10.1098/rstb.2013.0122.

Byrne, R. H., Mecking, S., Feely, R. A., and Liu, X. (2010). Direct observations of basin-wide acidification of the North Pacific Ocean. *Geophys. Res. Lett.* 37, L02601. doi:10.1029/2009GL040999.

C, De Klein, A, R. S., Novoa, S, Ogle, et al. (2006). "Agriculture, Forestry and Other Land Use," in *2006 IPCC Guidelines for National Greenhouse Gas Inventories*, 11.1-11.54.

Cai, W.-J., Hu, X., Huang, W.-J., Murrell, M. C., Lehrter, J. C., Lohrenz, S. E., et al. (2011). Acidification of subsurface coastal waters enhanced by eutrophication. *Nat. Geosci.* 4, 766–770. doi:10.1038/ngeo1297.

Campbell, J. E., Berry, J. A., Seibt, U., Smith, S. J., Montzka, S. A., Launois, T., et al. (2017a). Large historical growth in global terrestrial gross primary production. *Nature* 544, 84–87. doi:10.1038/nature22030.

Campbell, J. E., Berry, J. A., Seibt, U., Smith, S. J., Montzka, S. A., Launois, T., et al. (2017b). Large historical growth in global terrestrial gross primary production. *Nature* 544, 84–87. doi:10.1038/nature22030.

Cao, L., and Caldeira, K. (2010). Atmospheric carbon dioxide removal: long-term consequences and commitment. *Environ. Res. Lett.* 5, 024011. doi:10.1088/1748-9326/5/2/024011.

Cao, L., and Jiang, J. (2017). Simulated Effect of Carbon Cycle Feedback on Climate Response to Solar Geoengineering. *Geophys. Res. Lett.* 44, 12,484-12,491. doi:10.1002/2017GL076546.

Cao, L., Zhang, H., Zheng, M., and Wang, S. (2014). Response of ocean acidification to a gradual increase and decrease of atmospheric CO 2. *Environ. Res. Lett.* 9, 024012. doi:10.1088/1748-9326/9/2/024012.

Carstensen, J., Andersen, J. H., Gustafsson, B. G., and Conley, D. J. (2014). Deoxygenation of the Baltic Sea during the last century. *Proc. Natl. Acad. Sci.* 111, 5628–5633. doi:10.1073/pnas.1323156111.

Cartapanis, O., Galbraith, E. D., Bianchi, D., and Jaccard, S. L. (2018). Carbon burial in deep-sea sediment and implications for oceanic inventories of carbon and alkalinity over the last glacial cycle. *Clim. Past* 14, 1819–1850. doi:10.5194/cp-14-1819-2018.

Carter, B. R., Feely, R. A., Mecking, S., Cross, J. N., Macdonald, A. M., Siedlecki, S. A., et al. (2017). Two decades of Pacific anthropogenic carbon storage and ocean acidification along Global Ocean Ship-based Hydrographic Investigations Program sections P16 and P02. *Global Biogeochem. Cycles* 31, 306–327. doi:10.1002/2016GB005485.

Cayuela, M. L., van Zwieten, L., Singh, B. P., Jeffery, S., Roig, A., and Sánchez-Monedero, M. A. (2014). Biochar's role in mitigating soil nitrous oxide emissions: A review and meta-analysis. *Agric. Ecosyst. Environ.* 191, 5–16. doi:10.1016/j.agee.2013.10.009.

Chandra, N. (2019). Global inversion of regional methane emissions over past 4 decades (1988-2016). (in prep).

Chandra, N., Patra, P. K., Bisht, J. S. H., Ito, A., Morimoto, S., Janssens-Maenhout, G., et al. (2019a). Dominance of anthropogenic emissions on the global methane growth rate during 1988-2016. Yokohama.

Chavez, F. P., Bertrand, A., Guevara-Carrasco, R., Soler, P., and Csirke, J. (2008). The northern Humboldt Current System: Brief history, present status and a view towards the future. *Prog. Oceanogr.* 79, 95–105. doi:10.1016/j.pocean.2008.10.012.

Chen, C.-C., Gong, G.-C., and Shiah, F.-K. (2007). Hypoxia in the East China Sea: One of the largest coastal low-oxygen areas in the world. *Mar. Environ. Res.* 64, 399–408. doi:10.1016/j.marenvres.2007.01.007.

Chen, C.-T. A., and Borges, A. V. (2009). Reconciling opposing views on carbon cycling in the coastal ocean: Continental shelves as sinks and near-shore ecosystems as sources of atmospheric CO2. *Deep Sea Res. Part II Top. Stud. Oceanogr.* 56, 578–590. doi:10.1016/j.dsr2.2009.01.001.

Chen, C.-T. A., Lui, H.-K., Hsieh, C.-H., Yanagi, T., Kosugi, N., Ishii, M., et al. (2017). Deep oceans may acidify faster than anticipated due to global warming. *Nat. Clim. Chang.* 7, 890–894. doi:10.1038/s41558-017-0003-y.

Cheng, L., Zhang, L., Wang, Y.-P., Canadell, J. G., Chiew, F. H. S., Beringer, J., et al. (2017). Recent increases in terrestrial carbon uptake at little cost to the water cycle. *Nat. Commun.* 8, 110. doi:10.1038/s41467-017-00114-5.

Chierici, M., and Fransson, A. (2009). Calcium carbonate saturation in the surface water of the Arctic Ocean: undersaturation in freshwater influenced shelves. *Biogeosciences* 6, 2421–2431. doi:10.5194/bg-6-2421-2009.

Chu, S. N., Wang, Z. A., Doney, S. C., Lawson, G. L., and Hoering, K. A. (2016). Changes in anthropogenic carbon storage in the Northeast Pacific in the last decade. *J. Geophys. Res. Ocean.* 121, 4618–4632. doi:10.1002/2016JC011775.

Ciais, P., Sabine, C., Bala, G., Bopp, L., Brovkin, V., Canadell, J., et al. (2013). "Carbon and Other Biogeochemical Cycles," in *Climate Change 2013: The Physical Science Basis. Contribution of Working Group I to the Fifth Assessment Report of the Intergovernmental Panel on Climate Change*, eds. T. F. Stocker, D. Qin, G.-K. Plattner, M. Tignor, S. K. Allen, J. Boschung, et al. (Cambridge, United Kingdom and New York, NY, USA: Cambridge University Press). Available at: http://www.ipcc.ch/report/ar5/wg1/.

Ciais, P., Tagliabue, A., Cuntz, M., Bopp, L., Scholze, M., Hoffmann, G., et al. (2012). Large inert carbon pool in the terrestrial biosphere during the Last Glacial Maximum. *Nat. Geosci.* 5, 74–79. doi:10.1038/ngeo1324.

Ciais, P., Tan, J., Wang, X., Rödenbeck, C., Chevallier, F., Piao, S.-L., et al. (2018). Five decades of carbon uptake by northern lands revealed by the north-south gradient of atmospheric CO2. *Nat. Geosci.* (in press).

Claret, M., Galbraith, E. D., Palter, J. B., Bianchi, D., Fennel, K., Gilbert, D., et al. (2018). Rapid coastal deoxygenation due to ocean circulation shift in the northwest Atlantic. *Nat. Clim. Chang.* 8, 868–872. doi:10.1038/s41558-018-0263-1.

Clarke, L., Jiang, K., Akimoto, K., Babiker, M., Blanford, G., Fisher-Vanden, K., et al. (2014). "Assessing transformation pathways," in *Climate Change 2014: Mitigation of Climate Change. Contribution of Working Group III to the Fifth Assessment Report of the Intergovernmental Panel on Climate Change*, eds. O. Edenhofer, R. Pichs-Madruga, Y. Sokona,

Clement, D., and Gruber, N. (2018). The eMLR(C*) Method to Determine Decadal Changes in the Global Ocean Storage of Anthropogenic CO 2. *Global Biogeochem. Cycles* 32, 654–679. doi:10.1002/2017GB005819.

Clough, T., Condron, L., Kammann, C., and Müller, C. (2013). A Review of Biochar and Soil Nitrogen Dynamics. *Agronomy* 3, 275–293. doi:10.3390/agronomy3020275.

Codispoti, L. A. (2010). Interesting Times for Marine N2O. *Science (80-.).* 327, 1339–1340. doi:10.1126/science.1184945.

Collier, N., Hoffman, F. M., Lawrence, D. M., Keppel-Aleks, G., Koven, C. D., Riley, W. J., et al. (2018). The International Land Model Benchmarking (ILAMB) System: Design, Theory, and Implementation. *J. Adv. Model. Earth Syst.* 10, 2731–2754. doi:10.1029/2018MS001354.

Collins, M., Knutti, R., Arblaster, J., Dufresne, J.-L., Fichefet, T., Friedlingstein, P., et al. (2013). "Long-term Climate Change: Projections, Commitments and Irreversibility Pages 1029 to 1076," in *Climate Change 2013 - The Physical Science Basis*, ed. Intergovernmental Panel on Climate Change (Cambridge: Cambridge University Press), 1029–1136. doi:10.1017/CBO9781107415324.024.

Collins, W. J., Webber, C. P., Cox, P. M., Huntingford, C., Lowe, J., Sitch, S., et al. (2018). Increased importance of methane reduction for a 1.5 degree target. *Environ. Res. Lett.* 13, 054003. doi:10.1088/1748-9326/aab89c.

Comyn-Platt, E., Hayman, G., Huntingford, C., Chadburn, S. E., Burke, E. J., Harper, A. B., et al. (2018). Carbon budgets for 1.5 and 2°C targets lowered by natural wetland and permafrost feedbacks. *Nat. Geosci.* 11, 568–573. doi:10.1038/s41561-018-0174-9.

Conrad, C. J., and Lovenduski, N. S. (2015). Climate-Driven Variability in the Southern Ocean Carbonate System. *J. Clim.* 28, 5335–5350. doi:10.1175/JCLI-D-14-00481.1.

Cotovicz Jr., L. C., Knoppers, B. A., Brandini, N., Costa Santos, S. J., and Abril, G. (2015). A strong CO2 sink enhanced by eutrophication in a tropical coastal embayment (Guanabara Bay, Rio de Janeiro, Brazil). *Biogeosciences* 12, 6125–6146. doi:10.5194/bg-12-6125-2015.

Cotovicz, L. C., Knoppers, B. A., Brandini, N., Poirier, D., Costa Santos, S. J., Cordeiro, R. C., et al. (2018). Predominance of phytoplankton-derived dissolved and particulate organic carbon in a highly eutrophic tropical coastal embayment (Guanabara Bay, Rio de Janeiro, Brazil). *Biogeochemistry* 137, 1–14. doi:10.1007/s10533-017-0405-y.

Cowtan, K., and Way, R. G. (2014). Coverage bias in the HadCRUT4 temperature series and its impact on recent temperature trends. *Q. J. R. Meteorol. Soc.* 140, 1935–1944. doi:10.1002/qj.2297.

Cox, P. M., Betts, R. A., Collins, M., Harris, P. P., Huntingford, C., and Jones, C. D. (2004). Amazonian forest dieback under climate-carbon cycle projections for the 21st century. *Theor. Appl. Climatol.* 78, 137–156. doi:10.1007/s00704-004-0049-4.

Cox, P. M., Betts, R. A., Jones, C. D., Spall, S. A., and Totterdell, I. J. (2000). Acceleration of global warming due to carbon-cycle feedbacks in a coupled climate model. *Nature* 408, 184–187. doi:10.1038/35041539.

Cox, P. M., Pearson, D., Booth, B. B., Friedlingstein, P., Huntingford, C., Jones, C. D., et al. (2013). Sensitivity of tropical carbon to climate change constrained by carbon dioxide variability. *Nature* 494, 341–344. doi:10.1038/nature11882.

Creutzig, F., Ravindranath, N. H., Berndes, G., Bolwig, S., Bright, R., Cherubini, F., et al. (2015). Bioenergy and climate change mitigation: an assessment. *GCB Bioenergy* 7, 916–944. doi:10.1111/gcbb.12205.

Crichton, K. A., Bouttes, N., Roche, D. M., Chappellaz, J., and Krinner, G. (2016). Permafrost carbon as a missing link to explain CO2 changes during the last deglaciation. *Nat. Geosci.* 9, 683–686. doi:10.1038/ngeo2793.

Crutzen, P. J. (2006). Albedo Enhancement by Stratospheric Sulfur Injections: A Contribution to Resolve a Policy Dilemma? *Clim. Change* 77, 211–220. doi:10.1007/s10584-006-9101-y.

Cui, Y., Kump, L. R., Ridgwell, A. J., Charles, A. J., Junium, C. K., Diefendorf, A. F., et al. (2011). Slow release of fossil carbon during the Palaeocene–Eocene Thermal Maximum. *Nat. Geosci.* 4, 481–485. doi:10.1038/ngeo1179.

D'Olivo, J. P., McCulloch, M. T., Eggins, S. M., and Trotter, J. (2015). Coral records of reef-water pH across the central Great Barrier Reef, Australia: assessing the influence of river runoff on inshore reefs. *Biogeosciences* 12, 1223–1236. doi:10.5194/bg-12-1223-2015.

Dagon, K., and Schrag, D. P. (2019). Quantifying the effects of solar geoengineering on vegetation. *Clim. Change*. doi:10.1007/s10584-019-02387-9.

Dakos, V., Scheffer, M., van Nes, E. H., Brovkin, V., Petoukhov, V., and Held, H. (2008). Slowing down as an early warning signal for abrupt climate change. *Proc. Natl. Acad. Sci.* 105, 14308–14312. doi:10.1073/pnas.0802430105.

Dalsøren, S. B., Myhre, C. L., Myhre, G., Gomez-Pelaez, A. J., Søvde, O. A., Isaksen, I. S. A., et al. (2016). Atmospheric methane evolution the last 40 years. *Atmos. Chem. Phys.* 16, 3099–3126. doi:10.5194/acp-16-3099-2016.

Daneshvar, F., Nejadhashemi, A. P., Adhikari, U., Elahi, B., Abouali, M., Herman, M. R., et al. (2017). Evaluating the significance of wetland restoration scenarios on phosphorus removal. *J. Environ. Manage.* 192, 184–196. doi:10.1016/j.jenvman.2017.01.059.

Dangal, S. R. S., Tian, H., Xu, R., Chang, J., Canadell, J. G., Ciais, P., et al. (2019). Global Nitrous Oxide Emissions From Pasturelands and Rangelands: Magnitude, Spatiotemporal Patterns, and Attribution. *Global Biogeochem. Cycles* 33, 200–222. doi:10.1029/2018GB006091.

Davidson, E. A. (2015). Soil carbon in a beer can. *Nat. Geosci.* 8, 748–749. doi:10.1038/ngeo2522.

Davidson, E. A., and Kanter, D. (2014). Inventories and scenarios of nitrous oxide emissions. *Environ. Res. Lett.* 9, 105012. doi:10.1088/1748-9326/9/10/105012.

de Vries, W., Du, E., and Butterbach-Bahl, K. (2014). Short and long-term impacts of nitrogen deposition on carbon sequestration by forest ecosystems. *Curr. Opin. Environ. Sustain.* 9–10, 90–104. doi:10.1016/j.cosust.2014.09.001.

Dean, J. F., Middelburg, J. J., Röckmann, T., Aerts, R., Blauw, L. G., Egger, M., et al. (2018). Methane Feedbacks to the Global Climate System in a Warmer World. *Rev. Geophys.* 56, 207–250. doi:10.1002/2017RG000559.

DeConto, R. M., Galeotti, S., Pagani, M., Tracy, D., Schaefer, K., Zhang, T., et al. (2012). Past extreme warming events linked to massive carbon release from thawing permafrost. *Nature* 484, 87–91. doi:10.1038/nature10929.

DeConto, R. M., Pollard, D., Wilson, P. A., Pälike, H., Lear, C. H., and Pagani, M. (2008). Thresholds for Cenozoic bipolar glaciation. *Nature* 455, 652–656. doi:10.1038/nature07337.

Deemer, B. R., Harrison, J. A., Li, S., Beaulieu, J. J., DelSontro, T., Barros, N., et al. (2016). Greenhouse Gas Emissions from Reservoir Water Surfaces: A New Global Synthesis. *Bioscience* 66, 949–964. doi:10.1093/biosci/biw117.

Denisov, S. N., Eliseev, A. V., and Mokhov, I. I. (2013). Climate change in IAP RAS global model taking account of interaction with methane cycle under anthropogenic scenarios of RCP family. *Russ. Meteorol. Hydrol.* 38, 741–749. doi:10.3103/S1068373913110034.

Denvil-Sommer, A., Gehlen, M., Vrac, M., and Mejia, C. (2018). FFNN-LSCE: A two-step neural network model for the reconstruction of surface ocean pCO2 over the Global Ocean. *Geosci. Model Dev. Discuss.*, 1–27. doi:10.5194/gmd-2018-247.

Deutsch, C., Berelson, W., Thunell, R., Weber, T., Tems, C., McManus, J., et al. (2014). Centennial changes in North Pacific anoxia linked to tropical trade winds. *Science (80-.).* 345, 665–668. doi:10.1126/science.1252332.

DeVries, T., Holzer, M., and Primeau, F. (2017). Recent increase in oceanic carbon uptake driven by weaker upper-ocean overturning. *Nature* 542, 215–218. doi:10.1038/nature21068.

DeVries, T., Quéré, C. Le, Andrews, O. D., Berthet, S., Hauck, J., Ilyina, T., et al. (2019). Decadal Trends in the Ocean CO2 Sink. *Proc. Natl. Acad. Sci.* doi:doi/10.1073/pnas.

Dickson, A. J., Cohen, A. S., and Coe, A. L. (2012). Seawater oxygenation during the Paleocene-Eocene Thermal Maximum. *Geology* 40, 639–642. doi:10.1130/G32977.1.

Djakovac, T., Supić, N., Bernardi Aubry, F., Degobbis, D., and Giani, M. (2015). Mechanisms of hypoxia frequency changes in the northern Adriatic Sea during the period 1972–2012. *J. Mar. Syst.* 141, 179–189. doi:10.1016/j.jmarsys.2014.08.001.

Dlugokencky, E. J. (2003). Atmospheric methane levels off: Temporary pause or a new steady-state? *Geophys. Res. Lett.* 30, 1992. doi:10.1029/2003GL018126.

Dlugokencky, E. J., Lang, P. M., Crotwell, A. M., Mund, J. W., Crotwell, M. J., and Thoning, K. W. Atmospheric Methane Dry Air Mole Fractions. *NOAA ERSL Carbon Cycle Coorperative Glob. Air Sampl. Netw.* Available at: ftp://aftp.cmdl.noaa.gov/data/trace_gases/ch4/flask/surface/ [Accessed August 1, 2018].

Dlugokencky, E., and Tans, P. (2019). Trends in atmospheric carbon dioxide. *Natl. Ocean. Atmos. Adm. Earth Syst. Res. Lab.*

Don, A., Osborne, B., Hastings, A., Skiba, U., Carter, M. S., Drewer, J., et al. (2012). Land-use change to bioenergy production in Europe: implications for the greenhouse gas balance and soil carbon. *GCB Bioenergy* 4, 372–391. doi:10.1111/j.1757-1707.2011.01116.x.

Doney, S. C., Lima, I., Feely, R. A., Glover, D. M., Lindsay, K., Mahowald, N., et al. (2009). Mechanisms governing interannual variability in upper-ocean inorganic carbon system and air–sea CO2 fluxes: Physical climate and atmospheric dust. *Deep Sea Res. Part II Top. Stud. Oceanogr.* 56, 640–655. doi:10.1016/j.dsr2.2008.12.006.

Dore, J. E., Lukas, R., Sadler, D. W., Church, M. J., and Karl, D. M. (2009). Physical and biogeochemical modulation of ocean acidification in the central North Pacific. *Proc. Natl. Acad. Sci.* 106, 12235–12240. doi:10.1073/pnas.0906044106.

Drake, J. E., Gallet-Budynek, A., Hofmockel, K. S., Bernhardt, E. S., Billings, S. A., Jackson, R. B., et al. (2011). Increases in the flux of carbon belowground stimulate nitrogen uptake and sustain the long-term enhancement of forest productivity under elevated CO2. *Ecol. Lett.* 14, 349–357. doi:10.1111/j.1461-0248.2011.01593.x.

Drake, J. E., Macdonald, C. A., Tjoelker, M. G., Reich, P. B., Singh, B. K., Anderson, I. C., et al. (2018). Three years of soil respiration in a mature eucalypt woodland exposed to atmospheric CO2 enrichment. *Biogeochemistry* 139, 85–101. doi:10.1007/s10533-018-0457-7.

Drijfhout, S., Bathiany, S., Beaulieu, C., Brovkin, V., Claussen, M., Huntingford, C., et al. (2015). Catalogue of abrupt shifts in Intergovernmental Panel on Climate Change climate models. *Proc. Natl. Acad. Sci.* 112, E5777–E5786. doi:10.1073/pnas.1511451112.

Du, C., Wang, X., Zhang, M., Jing, J., and Gao, Y. (2019). Effects of elevated CO2 on plant C-N-P stoichiometry in terrestrial ecosystems: A meta-analysis. *Sci. Total Environ.* 650, 697–708. doi:10.1016/j.scitotenv.2018.09.051.

Dunkley Jones, T., Lunt, D. J., Schmidt, D. N., Ridgwell, A., Sluijs, A., Valdes, P. J., et al. (2013). Climate model and proxy data constraints on ocean warming across the Paleocene–Eocene Thermal Maximum. *Earth-Science Rev.* 125, 123–145. doi:10.1016/j.earscirev.2013.07.004.

Dupont, S., Dorey, N., and Thorndyke, M. (2010). What meta-analysis can tell us about vulnerability of marine biodiversity to ocean acidification? *Estuar. Coast. Shelf Sci.* 89, 182–185. doi:10.1016/j.ecss.2010.06.013.

Ehlert, D., and Zickfeld, K. (2017). What determines the warming commitment after cessation of CO2 emissions? *Environ. Res. Lett.* 12, 015002. doi:10.1088/1748-9326/aa564a.

Ehlert, D., Zickfeld, K., Eby, M., and Gillett, N. (2017). The Sensitivity of the Proportionality between Temperature Change and Cumulative CO 2 Emissions to Ocean Mixing. *J. Clim.* 30, 2921–2935. doi:10.1175/JCLI-D-16-0247.1.

Eliseev, A. V., Mokhov, I. I., and Chernokulsky, A. V. (2014). Influence of ground and peat fires on CO2 emissions into the atmosphere. *Dokl. Earth Sci.* 459, 1565–1569. doi:10.1134/S1028334X14120034.

Elkins, J. W., Dlugokencky, E., Hall, B., Dutton, G., Nance, D., and Mondeel, D. J. (2018). Combined Nitrous Oxide data from the NOAA/ESRL Global Monitoring Division. *Earth Syst. Res. Lab. (ESRL), Natl. Ocean. Atmos. Adm.* Available at: https://www.esrl.noaa.gov/gmd/hats/combined/N2O.html [Accessed January 24, 2019].

Ellsworth, D. S., Anderson, I. C., Crous, K. Y., Cooke, J., Drake, J. E., Gherlenda, A. N., et al. (2017). Elevated CO2 does not increase eucalypt forest productivity on a low-phosphorus soil. *Nat. Clim. Chang.* 7, 279–282. doi:10.1038/nclimate3235.

Elshout, P. M. F., van Zelm, R., Balkovic, J., Obersteiner, M., Schmid, E., Skalsky, R., et al. (2015). Greenhouse-gas payback times for crop-based biofuels. *Nat. Clim. Chang.* 5, 604–610. doi:10.1038/nclimate2642.

Elsig, J., Schmitt, J., Leuenberger, D., Schneider, R., Eyer, M., Leuenberger, M., et al. (2009). Stable isotope constraints on Holocene carbon cycle changes from an Antarctic ice core. *Nature* 461, 507–510. doi:10.1038/nature08393.

Emerson, S., and Hedges, J. I. (1988). Processes controlling the organic carbon content of open ocean sediments. *Paleoceanography* 3, 621–634. doi:10.1029/PA003i005p00621.

Erb, K.-H., Kastner, T., Plutzar, C., Bais, A. L. S., Carvalhais, N., Fetzel, T., et al. (2018a). Unexpectedly large impact of forest management and grazing on global vegetation biomass. *Nature* 553, 73–76. doi:10.1038/nature25138.

Erb, K.-H., Kastner, T., Plutzar, C., Bais, A. L. S., Carvalhais, N., Fetzel, T., et al. (2018b). Unexpectedly large impact of forest management and grazing on global vegetation biomass. *Nature* 553, 73–76. doi:10.1038/nature25138.

Etiope, G., Ciotoli, G., Schwietzke, S., and Schoell, M. (2019). Gridded maps of geological methane emissions and their isotopic signature. *Earth Syst. Sci. Data* 11, 1–22. doi:10.5194/essd-11-1-2019.

Etminan, M., Myhre, G., Highwood, E. J., and Shine, K. P. (2016). Radiative forcing of carbon dioxide, methane, and nitrous oxide: A significant revision of the methane radiative forcing. *Geophys. Res. Lett.* 43, 12,614-12,623. doi:10.1002/2016GL071930.

Fang, Y., Michalak, A. M., Schwalm, C. R., Huntzinger, D. N., Berry, J. A., Ciais, P., et al. (2017). Global land carbon sink response to temperature and precipitation varies with ENSO phase. *Environ. Res. Lett.* 12, 064007. doi:10.1088/1748-9326/aa6e8e.

Farías, L., Besoain, V., and García-Loyola, S. (2015). Presence of nitrous oxide hotspots in the coastal upwelling area off central Chile: an analysis of temporal variability based on ten years of a biogeochemical time series. *Environ. Res. Lett.* 10, 044017. doi:10.1088/1748-9326/10/4/044017.

Farley, K. A., Jobbagy, E. G., and Jackson, R. B. (2005). Effects of afforestation on water yield: a global synthesis with implications for policy. *Glob. Chang. Biol.* 11, 1565–1576. doi:10.1111/j.1365-2486.2005.01011.x.

Fatichi, S., Pappas, C., Zscheischler, J., and Leuzinger, S. (2019). Modelling carbon sources and sinks in terrestrial vegetation. *New Phytol.* 221, 652–668. doi:10.1111/nph.15451.

Fay, A. R., McKinley, G. A., and Lovenduski, N. S. (2014). Southern Ocean carbon trends: Sensitivity to methods. *Geophys. Res. Lett.* 41, 6833–6840. doi:10.1002/2014GL061324.

Feng, E. Y., Koeve, W., Keller, D. P., and Oschlies, A. (2017). Model-Based Assessment of the CO2 Sequestration Potential of Coastal Ocean Alkalinization. *Earth's Futur.* 5, 1252–1266. doi:10.1002/2017EF000659.

Feng, J., Chen, C., Zhang, Y., Song, Z., Deng, A., Zheng, C., et al. (2013). Impacts of cropping practices on yield-scaled greenhouse gas emissions from rice fields in China: A meta-analysis. *Agric. Ecosyst. Environ.* 164, 220–228. doi:10.1016/j.agee.2012.10.009.

Fennel, K., and Testa, J. M. (2019). Biogeochemical Controls on Coastal Hypoxia. *Ann. Rev. Mar. Sci.* 11, 105–130. doi:10.1146/annurev-marine-010318-095138.

Fernández-Martínez, M., Sardans, J., Chevallier, F., Ciais, P., Obersteiner, M., Vicca, S., et al. (2019). Global trends in carbon sinks and their relationships with CO2 and temperature. *Nat. Clim. Chang.* 9, 73–79. doi:10.1038/s41558-018-0367-7.

Ferrari, R., Jansen, M. F., Adkins, J. F., Burke, A., Stewart, A. L., and Thompson, A. F. (2014). Antarctic sea ice control on ocean circulation in present and glacial climates. *Proc. Natl. Acad. Sci.* 111, 8753–8758. doi:10.1073/pnas.1323922111.

Ferretti, D. F., Miller, J. B., White, J. W. C., Etheridge, D. M., Lassey, K. R., Lowe, D. C., et al. (2005). Unexpected changes to the global methane budget over the past 2000 years. *Science* 309, 1714–7. doi:10.1126/science.1115193.

Field, R. D., van der Werf, G. R., Fanin, T., Fetzer, E. J., Fuller, R., Jethva, H., et al. (2016). Indonesian fire activity and smoke pollution in 2015 show persistent nonlinear sensitivity to El Niño-induced drought. *Proc. Natl. Acad. Sci.* 113, 9204–9209. doi:10.1073/pnas.1524888113.

Finzi, A. C., Norby, R. J., Calfapietra, C., Gallet-Budynek, A., Gielen, B., Holmes, W. E., et al. (2007). Increases in nitrogen uptake rather than nitrogen-use efficiency support higher rates of temperate forest productivity under elevated CO2. *Proc. Natl. Acad. Sci.* 104, 14014–14019. doi:10.1073/pnas.0706518104.

Fischer, H., Meissner, K. J., Mix, A. C., Abram, N. J., Austermann, J., Brovkin, V., et al. (2018). Palaeoclimate constraints on the impact of 2°C anthropogenic warming and beyond. *Nat. Geosci.* 11, 474–485. doi:10.1038/s41561-018-0146-0.

Fleming, E. L., Jackman, C. H., Stolarski, R. S., and Douglass, A. R. (2011). A model study of the impact of source gas changes on the stratosphere for 1850–2100. *Atmos. Chem. Phys.* 11, 8515–8541. doi:10.5194/acp-11-8515-2011.

Forkel, M., Carvalhais, N., Rodenbeck, C., Keeling, R., Heimann, M., Thonicke, K., et al. (2016). Enhanced seasonal CO2 exchange caused by amplified plant productivity in northern ecosystems. *Science (80-.).* 351, 696–699. doi:10.1126/science.aac4971.

Fornara, D. A., Steinbeiss, S., McNamara, N. P., Gleixner, G., Oakley, S., Poulton, P. R., et al. (2011). Increases in soil organic carbon sequestration can reduce the global warming potential of long-term liming to permanent grassland. *Glob. Chang. Biol.* 17, 1925–1934. doi:10.1111/j.1365-2486.2010.02328.x.

Forster, P., Huppmann, D., Kriegler, E., Mundaca, L., Smith, C., Rogelj, J., et al. (2018). "Mitigation Pathways Compatible with 1.5°C in the Context of Sustainable Development Supplementary Material," in *Global Warming of 1.5°C. An IPCC Special Report on the impacts of global warming of 1.5°C above pre-industrial levels and related global greenhouse gas emission pathways, in the context of strengthening the global response to the threat of climate change,* eds. V. Masson-Delmotte, P. Zhai, H.-O. Pörtner, D. Roberts, J. Skea, P. R. Shukla, et al. Available at: https://www.ipcc.ch/sr15.

Foster, G. L., Royer, D. L., and Lunt, D. J. (2017). Future climate forcing potentially without precedent in the last 420 million years. *Nat. Commun.* 8, 14845. doi:10.1038/ncomms14845.

Fowell, S. E., Foster, G. L., Ries, J. B., Castillo, K. D., de la Vega, E., Tyrrell, T., et al. (2018). Historical Trends in pH and Carbonate Biogeochemistry on the Belize Mesoamerican Barrier Reef System. *Geophys. Res. Lett.* 45, 3228–3237. doi:10.1002/2017GL076496.

Frank, D. C., Poulter, B., Saurer, M., Esper, J., Huntingford, C., Helle, G., et al. (2015). Water-use efficiency and transpiration across European forests during the Anthropocene. *Nat. Clim. Chang.* 5, 579–583. doi:10.1038/nclimate2614.

Franks, P. J., Adams, M. A., Amthor, J. S., Barbour, M. M., Berry, J. A., Ellsworth, D. S., et al. (2013). Sensitivity of plants to changing atmospheric CO 2 concentration: from the geological past to the next century. *New Phytol.* 197, 1077–1094. doi:10.1111/nph.12104.

Freing, A., Wallace, D. W. R., and Bange, H. W. (2012). Global oceanic production of nitrous oxide. *Philos. Trans. R. Soc. B Biol. Sci.* 367, 1245–1255. doi:10.1098/rstb.2011.0360.

Friedlingstein, P., Andrew, R. M., Rogelj, J., Peters, G. P., Canadell, J. G., Knutti, R., et al. (2014a). Persistent growth of CO2 emissions and implications for reaching climate targets. *Nat. Geosci.* 7, 709–715. doi:10.1038/ngeo2248.

Friedlingstein, P., Bopp, L., Ciais, P., Dufresne, J., Fairhead, L., LeTreut, H., et al. (2001). Positive feedback between future climate change and the carbon cycle. *Geophys. Res. Lett.* 28, 1543–1546. doi:10.1029/2000GL012015.

Friedlingstein, P., Cox, P., Betts, R., Bopp, L., von Bloh, W., Brovkin, V., et al. (2006). Climate–Carbon Cycle Feedback Analysis: Results from the C 4 MIP Model Intercomparison. *J. Clim.* 19, 3337–3353. doi:10.1175/JCLI3800.1.

Friedlingstein, P., Dufresne, J.-L., Cox, P. M., and Rayner, P. (2003). How positive is the feedback between climate change and the carbon cycle? *Tellus B* 55, 692–700. doi:10.1034/j.1600-0889.2003.01461.x.

Friedlingstein, P., Meinshausen, M., Arora, V. K., Jones, C. D., Anav, A., Liddicoat, S. K., et al. (2014b). Uncertainties in CMIP5 Climate Projections due to Carbon Cycle Feedbacks. *J. Clim.* 27, 511–526. doi:10.1175/JCLI-D-12-00579.1.

Friend, A. D., Lucht, W., Rademacher, T. T., Keribin, R., Betts, R., Cadule, P., et al. (2014). Carbon residence time dominates uncertainty in terrestrial vegetation responses to future climate and atmospheric CO 2. *Proc. Natl. Acad. Sci.* 111, 3280–3285. doi:10.1073/pnas.1222477110.

Frölicher, T. L., and Joos, F. (2010). Reversible and irreversible impacts of greenhouse gas emissions in multi-century projections with the NCAR global coupled carbon cycle-climate model. *Clim. Dyn.* 35, 1439–1459. doi:10.1007/s00382-009-0727-0.

Frölicher, T. L., Sarmiento, J. L., Paynter, D. J., Dunne, J. P., Krasting, J. P., and Winton, M. (2015). Dominance of the Southern Ocean in Anthropogenic Carbon and Heat Uptake in CMIP5 Models. *J. Clim.* 28, 862–886. doi:10.1175/JCLI-D-14-00117.1.

Frölicher, T. L., Winton, M., and Sarmiento, J. L. (2014). Continued global warming after CO2 emissions stoppage. *Nat. Clim. Chang.* 4, 40–44. doi:10.1038/nclimate2060.

Frolking, S., and Roulet, N. T. (2007). Holocene radiative forcing impact of northern peatland carbon accumulation and methane emissions. *Glob. Chang. Biol.* 13, 1079–1088. doi:10.1111/j.1365-2486.2007.01339.x.

Fu, W., Randerson, J. T., and Moore, J. K. (2016). Climate change impacts on net primary production (NPP) and export production (EP) regulated by increasing stratification and phytoplankton community structure in the CMIP5 models. *Biogeosciences* 13, 5151–5170. doi:10.5194/bg-13-5151-2016.

Fuss, S., Lamb, W. F., Callaghan, M. W., Hilaire, J., Creutzig, F., Amann, T., et al. (2018). Negative emissions—Part 2: Costs, potentials and side effects. *Environ. Res. Lett.* 13, 063002. doi:10.1088/1748-9326/aabf9f.

Galbraith, E. D., and Eggleston, S. (2017). A lower limit to atmospheric CO2 concentrations over the past 800,000 years. *Nat. Geosci.* 10, 295–298. doi:10.1038/ngeo2914.

Galbraith, E. D., and Jaccard, S. L. (2015). Deglacial weakening of the oceanic soft tissue pump: global constraints from sedimentary nitrogen isotopes and oxygenation proxies. *Quat. Sci. Rev.* 109, 38–48. doi:10.1016/j.quascirev.2014.11.012.

Galbraith, E. D., and Kienast, M. (2013). The acceleration of oceanic denitrification during deglacial warming. *Nat. Geosci.* 6, 579–584. doi:10.1038/ngeo1832.

Gangstø, R., Joos, F., and Gehlen, M. (2011). Sensitivity of pelagic calcification to ocean acidification. *Biogeosciences* 8, 433–458. doi:10.5194/bg-8-433-2011.

Ganopolski, A., and Brovkin, V. (2017). Simulation of climate, ice sheets and CO2 evolution during the last four glacial cycles with an Earth system model of intermediate complexity. *Clim. Past* 13, 1695–1716. doi:10.5194/cp-13-1695-2017.

Gasser, T., Kechiar, M., Ciais, P., Burke, E. J., Kleinen, T., Zhu, D., et al. (2018). Path-dependent reductions in CO2 emission budgets caused by permafrost carbon release. *Nat. Geosci.* 11, 830–835. doi:10.1038/s41561-018-0227-0.

Gattuso, J.-P., Magnan, A., Billé, R., Cheung, W. W. L., Howes, E. L., Joos, F., et al. (2015). Contrasting futures for ocean and society from different anthropogenic CO 2 emissions scenarios. *Science (80-.).* 349, aac4722. doi:10.1126/science.aac4722.

Gedney, N. (2004). Climate feedback from wetland methane emissions. *Geophys. Res. Lett.* 31, L20503. doi:10.1029/2004GL020919.

Gerber, J. S., Carlson, K. M., Makowski, D., Mueller, N. D., Garcia de Cortazar-Atauri, I., Havlík, P., et al. (2016). Spatially explicit estimates of N2O emissions from croplands suggest climate mitigation opportunities from improved fertilizer management. *Glob. Chang. Biol.* 22, 3383–3394. doi:10.1111/gcb.13341.

Ghosh, A., Patra, P. K., Ishijima, K., Umezawa, T., Ito, A., Etheridge, D. M., et al. (2015). Variations in global methane sources and sinks during 1910–2010. *Atmos. Chem. Phys.* 15, 2595–2612. doi:10.5194/acp-15-2595-2015.

Gillett, N. P., Arora, V. K., Matthews, D., and Allen, M. R. (2013). Constraining the Ratio of Global Warming to Cumulative CO 2 Emissions Using CMIP5 Simulations*. *J. Clim.* 26, 6844–6858. doi:10.1175/JCLI-D-12-00476.1.

Gillett, N. P., Arora, V. K., Zickfeld, K., Marshall, S. J., and Merryfield, W. J. (2011). Ongoing climate change following a complete cessation of carbon dioxide emissions. *Nat. Geosci.* 4, 83–87. doi:10.1038/ngeo1047.

Gitz, V., and Ciais, P. (2003). Amplifying effects of land-use change on future atmospheric CO2 levels. *Global Biogeochem. Cycles* 17, 1–15. doi:10.1029/2002GB001963.

Glienke, S., Irvine, P. J., and Lawrence, M. G. (2015). The impact of geoengineering on vegetation in experiment G1 of the GeoMIP. *J. Geophys. Res. Atmos.* 120, 10,196-10,213. doi:10.1002/2015JD024202.

Goddard, M. A., Mikhailova, E. A., Christopher, J. P., and Schlautman, M. A. (2007). Atmospheric Mg 2+ wet deposition within the continental United States and implications for soil inorganic carbon sequestration. *Tellus B Chem. Phys. Meteorol.* 59, 50–56. doi:10.1111/j.1600-0889.2006.00228.x.

Goll, D. S., Brovkin, V., Parida, B. R., Reick, C. H., Kattge, J., Reich, P. B., et al. (2012). Nutrient limitation reduces land carbon uptake in simulations with a model of combined carbon, nitrogen and phosphorus cycling. *Biogeosciences* 9, 3547–3569. doi:10.5194/bg-9-3547-2012.

Goll, D. S., Winkler, A. J., Raddatz, T., Dong, N., Prentice, I. C., Ciais, P., et al. (2017). Carbon–nitrogen interactions in idealized simulations with JSBACH (version 3.10). *Geosci. Model Dev.* 10, 2009–2030. doi:10.5194/gmd-10-2009-2017.

González-Dávila, M., Santana-Casiano, J. M., Rueda, M. J., and Llinás, O. (2010). The water column distribution of carbonate system variables at the ESTOC site from 1995 to 2004. *Biogeosciences* 7, 3067–3081. doi:10.5194/bg-7-3067-2010.

González, M. F., and Ilyina, T. (2016). Impacts of artificial ocean alkalinization on the carbon cycle and climate in Earth system simulations. *Geophys. Res. Lett.* 43, 6493–6502. doi:10.1002/2016GL068576.

González, M. F., Ilyina, T., Sonntag, S., and Schmidt, H. (2018). Enhanced Rates of Regional Warming and Ocean Acidification After Termination of Large-Scale Ocean Alkalinization. *Geophys. Res. Lett.* 45, 7120–7129. doi:10.1029/2018GL077847.

González, M. F. T. (2016). Impacts of artificial ocean alkalinization on the carbon cycle and climate in Earth system simulations. *Geophys. Res. Lett.* 43, 6493.

Goodkin, N. F., Wang, B.-S., You, C.-F., Hughen, K. A., Grumet-Prouty, N., Bates, N. R., et al. (2015). Ocean circulation and biogeochemistry moderate interannual and decadal surface water pH changes in the Sargasso Sea. *Geophys. Res. Lett.* 42, 4931–4939. doi:10.1002/2015GL064431.

Goodwin, P., Katavouta, A., Roussenov, V. M., Foster, G. L., Rohling, E. J., and Williams, R. G. (2018). Pathways to 1.5 °C and 2 °C warming based on observational and geological constraints. *Nat. Geosci.* 11, 102–107. doi:10.1038/s41561-017-0054-8.

Goodwin, P., Williams, R. G., and Ridgwell, A. (2015). Sensitivity of climate to cumulative carbon emissions due to compensation of ocean heat and carbon uptake. *Nat. Geosci.* 8, 29–34. doi:10.1038/ngeo2304.

Gottschalk, J., Skinner, L. C., Lippold, J., Vogel, H., Frank, N., Jaccard, S. L., et al. (2016). Biological and physical controls in the Southern Ocean on past millennial-scale atmospheric CO2 changes. *Nat. Commun.* 7, 11539. doi:10.1038/ncomms11539.

Govindasamy, B., Thompson, S., Duffy, P. B., Caldeira, K., and Delire, C. (2002). Impact of geoengineering schemes on the terrestrial biosphere. *Geophys. Res. Lett.* 29, 18-1-18–4. doi:10.1029/2002GL015911.

Graham, L. A., Belisle, S. L., and Rieger, P. (2009). Nitrous oxide emissions from light duty vehicles. *Atmos. Environ.* 43, 2031–2044. doi:10.1016/j.atmosenv.2009.01.002.

Grandy, A. S., Salam, D. S., Wickings, K., McDaniel, M. D., Culman, S. W., and Snapp, S. S. (2013). Soil respiration and litter decomposition responses to nitrogen fertilization rate in no-till corn systems. *Agric. Ecosyst. Environ.* 179, 35–40. doi:10.1016/j.agee.2013.04.020.

Grassi, G., House, J., Kurz, W. A., Cescatti, A., Houghton, R. A., Peters, G. P., et al. (2018). Reconciling global-model estimates and country reporting of anthropogenic forest CO2 sinks. *Nat. Clim. Chang.* 8, 914–920. doi:10.1038/s41558-018-0283-x.

Graven, H. D., Keeling, R. F., Piper, S. C., Patra, P. K., Stephens, B. B., Wofsy, S. C., et al. (2013). Enhanced Seasonal Exchange of CO2 by Northern Ecosystems Since 1960. *Science (80-.).* 341, 1085–1089. doi:10.1126/science.1239207.

Gregor, L., Kok, S., Lebehot, A., and Scheel Monteiro, P. (2019). A comparative assessment of the uncertainties of global surface-ocean CO2 estimates using a machine learning ensemble – have we hit the wall? *Geosci. Model Dev. Discuss.*

Gregor, L., Kok, S., and Monteiro, P. M. S. (2018). Interannual drivers of the seasonal cycle of CO2 in the Southern Ocean. *Biogeosciences* 15, 2361–2378. doi:10.5194/bg-15-2361-2018.

Gregory, J. M., Jones, C. D., Cadule, P., and Friedlingstein, P. (2009). Quantifying Carbon Cycle Feedbacks. *J. Clim.* 22, 5232–5250. doi:10.1175/2009JCLI2949.1.

Grimm, R., Notz, D., Glud, R. N., Rysgaard, S., and Six, K. D. (2016). Assessment of the sea-ice carbon pump: Insights from a three-dimensional ocean-sea-ice-biogeochemical model (MPIOM/HAMOCC). *Elem. Sci. Anthr.* 4, 000136. doi:10.12952/journal.elementa.000136.

Griscom, B. W., Adams, J., Ellis, P. W., Houghton, R. A., Lomax, G., Miteva, D. A., et al. (2017). Natural climate solutions. *Proc. Natl. Acad. Sci.* 114, 11645–11650. doi:10.1073/pnas.1710465114.

Gruber, N. (2011). Warming up, turning sour, losing breath: ocean biogeochemistry under global change. *Philos. Trans. R. Soc. A Math. Phys. Eng. Sci.* 369, 1980–1996. doi:10.1098/rsta.2011.0003.

Gruber, N., Clement, D., Carter, B. R., Feely, R. A., van Heuven, S., Hoppema, M., et al. (2019). The oceanic sink for anthropogenic CO 2 from 1994 to 2007. *Science (80-.).* 363, 1193–1199. doi:10.1126/science.aau5153.

Gruber, N., Landschützer, P., and Lovenduski, N. S. (2019b). The Variable Southern Ocean Carbon Sink. *Ann. Rev. Mar. Sci.* 11, 159–186. doi:10.1146/annurev-marine-121916-063407.

Gu, J., Yuan, M., Liu, J., Hao, Y., Zhou, Y., Qu, D., et al. (2017). Trade-off between soil organic carbon sequestration and nitrous oxide emissions from winter wheat-summer maize rotations: Implications of a 25-year fertilization experiment in Northwestern China. *Sci. Total Environ.* 595, 371–379. doi:10.1016/j.scitotenv.2017.03.280.

Guanter, L., Zhang, Y., Jung, M., Joiner, J., Voigt, M., Berry, J. A., et al. (2014). Global and time-resolved monitoring of crop photosynthesis with chlorophyll fluorescence. *Proc. Natl. Acad. Sci.* 111, E1327–E1333. doi:10.1073/pnas.1320008111.

Guenet, B., Camino-Serrano, M., Ciais, P., Tifafi, M., Maignan, F., Soong, J. L., et al. (2018). Impact of priming on global soil carbon stocks. *Glob. Chang. Biol.* 24, 1873–1883. doi:10.1111/gcb.14069.

Guimberteau, M., Zhu, D., Maignan, F., Huang, Y., Yue, C., Dantec-Nédélec, S., et al. (2018). ORCHIDEE-MICT (v8.4.1), a land surface model for the high latitudes: model description and validation. *Geosci. Model Dev.* 11, 121–163. doi:10.5194/gmd-11-121-2018.

Gupta, G. V. M., Sudheesh, V., Sudharma, K. V, Saravanane, N., Dhanya, V., Dhanya, K. R., et al. (2016). Evolution to decay of upwelling and associated biogeochemistry over the southeastern Arabian Sea shelf. *J. Geophys. Res. Biogeosciences* 121, 159–175. doi:10.1002/2015JG003163.

Gutjahr, M., Ridgwell, A., Sexton, P. F., Anagnostou, E., Pearson, P. N., Pälike, H., et al. (2017). Very large release of mostly volcanic carbon during the Palaeocene–Eocene Thermal Maximum. *Nature* 548, 573–577. doi:10.1038/nature23646.

Hadi, A., Inubushi, K., Purnomo, E., Razie, F., Yamakawa, K., and Tsuruta, H. (2000). Effect of land-use changes on nitrous oxide (N2O) emission from tropical peatlands. *Chemosph. - Glob. Chang. Sci.* 2, 347–358. doi:10.1016/S1465-9972(00)00030-1.

Hahn, J., Brandt, P., Schmidtko, S., and Krahmann, G. (2017). Decadal oxygen change in the eastern tropical North Atlantic. *Ocean Sci.* 13, 551–576. doi:10.5194/os-13-551-2017.

Hain, M. P., Sigman, D. M., and Haug, G. H. (2010). Carbon dioxide effects of Antarctic stratification, North Atlantic Intermediate Water formation, and subantarctic nutrient drawdown during the last ice age: Diagnosis and synthesis in a geochemical box model. *Global Biogeochem. Cycles* 24, n/a-n/a. doi:10.1029/2010GB003790.

Hajima, T., I, T., Tachiiri, K., Kato, E., Watanabe, S., and Kawamiya, M. (2012). Climate Change, Allowable Emission, and Earth System Response to Representative Concentration Pathway Scenarios. *J. Meteorol. Soc. Japan. Ser. II* 90, 417–434. doi:10.2151/jmsj.2012-305.

Hall, A., and Qu, X. (2006). Using the current seasonal cycle to constrain snow albedo feedback in future climate change. *Geophys. Res. Lett.* 33, L03502. doi:10.1029/2005GL025127.

Hall, B. D., Dutton, G. S., and Elkins, J. W. (2007). The NOAA nitrous oxide standard scale for atmospheric observations. *J. Geophys. Res.* 112, D09305. doi:10.1029/2006JD007954.

Hansis, E., Davis, S. J., and Pongratz, J. (2015). Relevance of methodological choices for accounting of land use change carbon fluxes. *Global Biogeochem. Cycles* 29, 1230–1246. doi:10.1002/2014GB004997.

Harper, A. B., Powell, T., Cox, P. M., House, J., Huntingford, C., Lenton, T. M., et al. (2018). Land-use emissions play a critical role in land-based mitigation for Paris climate targets. *Nat. Commun.* 9, 2938. doi:10.1038/s41467-018-05340-z.

Harris, I., Jones, P. D., Osborn, T. J., and Lister, D. H. (2014). Updated high-resolution grids of monthly climatic observations - the CRU TS3.10 Dataset. *Int. J. Climatol.* 34, 623–642. doi:10.1002/joc.3711.

Harrison, S. P., Bartlein, P. J., Brovkin, V., Houweling, S., Kloster, S., and Prentice, I. C. (2018). The biomass burning contribution to climate–carbon-cycle feedback. *Earth Syst. Dyn.* 9, 663–677. doi:10.5194/esd-9-663-2018.

Hartmann, J., West, A. J., Renforth, P., Köhler, P., De La Rocha, C. L., Wolf-Gladrow, D. A., et al. (2013). Enhanced chemical weathering as a geoengineering strategy to reduce atmospheric carbon dioxide, supply nutrients, and mitigate ocean acidification. *Rev. Geophys.* 51, 113–149. doi:10.1002/rog.20004.

Hauck, J., Hoppema, M., Bellerby, R. G. J., Völker, C., and Wolf-Gladrow, D. (2010). Data-based estimation of anthropogenic carbon and acidification in the Weddell Sea on a decadal timescale. *J. Geophys. Res.* 115, C03004. doi:10.1029/2009JC005479.

Hauck, J., Köhler, P., Wolf-Gladrow, D., and Völker, C. (2016). Iron fertilisation and century-scale effects of open ocean dissolution of olivine in a simulated CO 2 removal experiment. *Environ. Res. Lett.* 11, 024007. doi:10.1088/1748-9326/11/2/024007.

Hauck, J., Lenton, A., Langlais, C., and Matear, R. (2018). The Fate of Carbon and Nutrients Exported Out of the Southern Ocean. *Global Biogeochem. Cycles* 32, 1556–1573. doi:10.1029/2018GB005977.

Hauck, J., and Völker, C. (2015). Rising atmospheric CO 2 leads to large impact of biology on Southern Ocean CO 2 uptake via changes of the Revelle factor. *Geophys. Res. Lett.* 42, 1459–1464. doi:10.1002/2015GL063070.

Hauck, J., Völker, C., Wolf-Gladrow, D. A., Laufkötter, C., Vogt, M., Aumont, O., et al. (2015). On the Southern Ocean CO2 uptake and the role of the biological carbon pump in the 21st century. *Global Biogeochem. Cycles* 29, 1451–1470. doi:10.1002/2015GB005140.

Hauri, C., Friedrich, T., and Timmermann, A. (2016). Abrupt onset and prolongation of aragonite undersaturation events in the Southern Ocean. *Nat. Clim. Chang.* 6, 172–176. doi:10.1038/nclimate2844.

Haustein, K., Allen, M. R., Forster, P. M., Otto, F. E. L., Mitchell, D. M., Matthews, H. D., et al. (2017). A real-time Global Warming Index. *Sci. Rep.* 7, 15417. doi:10.1038/s41598-017-14828-5.

Haywood, A. M., Dowsett, H. J., and Dolan, A. M. (2016). Integrating geological archives and climate models for the mid-Pliocene warm period. *Nat. Commun.* 7, 10646. doi:10.1038/ncomms10646.

Heck, V., Gerten, D., Lucht, W., and Boysen, L. R. (2016). Is extensive terrestrial carbon dioxide removal a 'green' form of geoengineering? A global modelling study. *Glob. Planet. Change* 137, 123–130. doi:10.1016/j.gloplacha.2015.12.008.

Heck, V., Gerten, D., Lucht, W., and Popp, A. (2018). Biomass-based negative emissions difficult to reconcile with planetary boundaries. *Nat. Clim. Chang.* 8, 151–155. doi:10.1038/s41558-017-0064-y.

Heinze, C. (2004). Simulating oceanic CaCO 3 export production in the greenhouse. *Geophys. Res. Lett.* 31, L16308. doi:10.1029/2004GL020613.

Heland, J., and Schäfer, K. (1998). Determination of major combustion products in aircraft exhausts by FTIR emission spectroscopy. *Atmos. Environ.* 32, 3067–3072. doi:10.1016/S1352-2310(97)00395-6.

Helm, K. P., Bindoff, N. L., and Church, J. A. (2011). Observed decreases in oxygen content of the global ocean. *Geophys. Res. Lett.* 38, L23602. doi:10.1029/2011GL049513.

Henderson, B. B., Gerber, P. J., Hilinski, T. E., Falcucci, A., Ojima, D. S., Salvatore, M., et al. (2015). Greenhouse gas mitigation potential of the world's grazing lands: Modeling soil carbon and nitrogen fluxes of mitigation practices. *Agric. Ecosyst. Environ.* 207, 91–100. doi:10.1016/j.agee.2015.03.029.

Henson, S. A., Beaulieu, C., and Lampitt, R. (2016). Observing climate change trends in ocean biogeochemistry: when and where. *Glob. Chang. Biol.* 22, 1561–1571. doi:10.1111/gcb.13152.

Herrero, M., Henderson, B., Havlík, P., Thornton, P. K., Conant, R. T., Smith, P., et al. (2016). Greenhouse gas mitigation potentials in the livestock sector. *Nat. Clim. Chang.* 6, 452–461. doi:10.1038/nclimate2925.

Herrington, T., and Zickfeld, K. (2014). Path independence of climate and carbon cycle response over a broad range of cumulative carbon emissions. *Earth Syst. Dyn.* 5, 409–422. doi:10.5194/esd-5-409-2014.

Higgins, S. I., and Scheiter, S. (2012). Atmospheric CO2 forces abrupt vegetation shifts locally, but not globally. *Nature* 488, 209–212. doi:10.1038/nature11238.

Hirota, M., Holmgren, M., Van Nes, E. H., and Scheffer, M. (2011). Global Resilience of Tropical Forest and Savanna to Critical Transitions. *Science (80-.).* 334, 232–235. doi:10.1126/science.1210657.

Hoffman, F. M., Randerson, J. T., Arora, V. K., Bao, Q., Cadule, P., Ji, D., et al. (2014). Causes and implications of persistent atmospheric carbon dioxide biases in Earth System Models. *J. Geophys. Res. Biogeosciences* 119, 141–162. doi:10.1002/2013JG002381.

Hoffmann, S. S., McManus, J. F., and Swank, E. (2018). Evidence for Stable Holocene Basin-Scale Overturning Circulation Despite Variable Currents Along the Deep Western Boundary of the North Atlantic Ocean. *Geophys. Res. Lett.* 45, 13,427-13,436. doi:10.1029/2018GL080187.

Hofmann, D. J., Butler, J. H., Dlugokencky, E. J., Elkins, J. W., Masarie, K., Montzka, S. A., et al. (2006). The role of carbon dioxide in climate forcing from 1979 to 2004: introduction of the Annual Greenhouse Gas Index. *Tellus B Chem. Phys. Meteorol.* 58, 614–619. doi:10.1111/j.1600-0889.2006.00201.x.

Hofmann, G. E., Smith, J. E., Johnson, K. S., Send, U., Levin, L. A., Micheli, F., et al. (2011). High-Frequency Dynamics of Ocean pH: A Multi-Ecosystem Comparison. *PLoS One* 6, e28983. doi:10.1371/journal.pone.0028983.

Hofmann, M., and Schellnhuber, H.-J. (2009). Oceanic acidification affects marine carbon pump and triggers extended marine oxygen holes. *Proc. Natl. Acad. Sci.* 106, 3017–3022. doi:10.1073/pnas.0813384106.

Hollesen, J., Matthiesen, H., Møller, A. B., and Elberling, B. (2015). Permafrost thawing in organic Arctic soils accelerated by ground heat production. *Nat. Clim. Chang.* 5, 574–578. doi:10.1038/nclimate2590.

Hönisch, B., and Hemming, N. G. (2005). Surface ocean pH response to variations in pCO2 through two full glacial cycles. *Earth Planet. Sci. Lett.* 236, 305–314. doi:10.1016/j.epsl.2005.04.027.

Honisch, B., Ridgwell, A., Schmidt, D. N., Thomas, E., Gibbs, S. J., Sluijs, A., et al. (2012). The Geological Record of Ocean Acidification. *Science (80-.).* 335, 1058–1063. doi:10.1126/science.1208277.

Hoogakker, B. A. A., Elderfield, H., Schmiedl, G., McCave, I. N., and Rickaby, R. E. M. (2015). Glacial–interglacial changes in bottom-water oxygen content on the Portuguese margin. *Nat. Geosci.* 8, 40–43. doi:10.1038/ngeo2317.

Hoogakker, B. A. A., Lu, Z., Umling, N., Jones, L., Zhou, X., Rickaby, R. E. M., et al. (2018). Glacial expansion of oxygen-depleted seawater in the eastern tropical Pacific. *Nature* 562, 410–413. doi:10.1038/s41586-018-0589-x.

Hoogakker, B. A. A., and others (2018). (to be communicated). *Science (80-.).* (in press).

Hoppe, C. J. M., Hassler, C. S., Payne, C. D., Tortell, P. D., Rost, B., and Trimborn, S. (2013). Iron Limitation Modulates Ocean Acidification Effects on Southern Ocean Phytoplankton Communities. *PLoS One* 8, e79890. doi:10.1371/journal.pone.0079890.

Houghton, R. A. (2013). Keeping management effects separate from environmental effects in terrestrial carbon accounting. *Glob. Chang. Biol.* 19, 2609–2612. doi:10.1111/gcb.12233.

Houghton, R. A., Byers, B., and Nassikas, A. A. (2015). A role for tropical forests in stabilizing atmospheric CO2. *Nat. Clim. Chang.* 5, 1022–1023. doi:10.1038/nclimate2869.

Houghton, R. A., and Nassikas, A. A. (2017). Global and regional fluxes of carbon from land use and land cover change 1850-2015. *Global Biogeochem. Cycles* 31, 456–472. doi:10.1002/2016GB005546.

Hristov, A. N., Oh, J., Firkins, J. L., Dijkstra, J., Kebreab, E., Waghorn, G., et al. (2013a). SPECIAL TOPICS — Mitigation of methane and nitrous oxide emissions from animal operations: I. A review of enteric methane mitigation options1. *J. Anim. Sci.* 91, 5045–5069. doi:10.2527/jas.2013-6583.

Hristov, A. N., Oh, J., Lee, C., Meinen, R., Montes, F., Ott, T., et al. (2013b). *Mitigation of greenhouse gas emissions in livestock production – A review of technical options for non-CO2 emissions.* , ed. H. P. S. Gerber, Pierre J.; Henderson, Benjamin; Makkar Food and Agriculture Organization of the United Nations Available at: https://books.google.co.za/books?id=iSXinQEACAAJ.

Hu, M., Chen, D., and Dahlgren, R. A. (2016). Modeling nitrous oxide emission from rivers: a global assessment. *Glob. Chang. Biol.* 22, 3566–3582. doi:10.1111/gcb.13351.

Hugelius, G., Strauss, J., Zubrzycki, S., Harden, J. W., Schuur, E. A. G., Ping, C.-L., et al. (2014). Estimated stocks of circumpolar permafrost carbon with quantified uncertainty ranges and identified data gaps. *Biogeosciences* 11, 6573–6593. doi:10.5194/bg-11-6573-2014.

Hülse, D., Arndt, S., Wilson, J. D., Munhoven, G., and Ridgwell, A. (2017). Understanding the causes and consequences of past marine carbon cycling variability through models. *Earth-Science Rev.* 171, 349–382. doi:10.1016/j.earscirev.2017.06.004.

Humpenöder, F., Popp, A., Dietrich, J. P., Klein, D., Lotze-Campen, H., Bonsch, M., et al. (2014). Investigating afforestation and bioenergy CCS as climate change mitigation strategies. *Environ. Res. Lett.* 9, 064029. doi:10.1088/1748-9326/9/6/064029.

Humphrey, V., Zscheischler, J., Ciais, P., Gudmundsson, L., Sitch, S., and Seneviratne, S. I. (2018). Sensitivity of atmospheric CO2 growth rate to observed changes in terrestrial water storage. *Nature* 560, 628–631. doi:10.1038/s41586-018-0424-4.

Huntingford, C., Atkin, O. K., Martinez-de la Torre, A., Mercado, L. M., Heskel, M. A., Harper, A. B., et al. (2017). Implications of improved representations of plant respiration in a changing climate. *Nat. Commun.* 8, 1602. doi:10.1038/s41467-017-01774-z.

Huntingford, C., Zelazowski, P., Galbraith, D., Mercado, L. M., Sitch, S., Fisher, R., et al. (2013). Simulated resilience of tropical rainforests to CO2-induced climate change. *Nat. Geosci.* 6, 268–273. doi:10.1038/ngeo1741.

Huntzinger, D. N., Michalak, A. M., Schwalm, C., Ciais, P., King, A. W., Fang, Y., et al. (2017). Uncertainty in the response of terrestrial carbon sink to environmental drivers undermines carbon-climate feedback predictions. *Sci. Rep.* 7, 4765. doi:10.1038/s41598-017-03818-2.

Huppmann, D., Rogelj, J., Kriegler, E., Krey, V., and Riahi, K. (2018). A new scenario resource for integrated 1.5 °C research. *Nat. Clim. Chang.* 8, 1027–1030. doi:10.1038/s41558-018-0317-4.

Hurd, C. L., Lenton, A., Tilbrook, B., and Boyd, P. W. (2018). Current understanding and challenges for oceans in a higher-CO2 world. *Nat. Clim. Chang.* 8, 686–694. doi:10.1038/s41558-018-0211-0.

IEA (2017). CO2 emissions from fuel combustion.

Iida, Y., Kojima, A., Takatani, Y., Nakano, T., Sugimoto, H., Midorikawa, T., et al. (2015). Trends in pCO2 and sea–air CO2 flux over the global open oceans for the last two decades. *J. Oceanogr.* 71, 637–661. doi:10.1007/s10872-015-0306-4.

IPCC (2013). "Summary for Policymakers," in *Climate Change 2013: The Physical Science Basis. Contribution of Working Group I to the Fifth Assessment Report of the Intergovernmental Panel on Climate Change*, eds. D. Q. G.-K. P. M. T. S. K. A. J. B. A. N. Y. X. V. B. Stocker T.F. and P. M. Midgley (Cambridge, United Kingdom and New York, NY, USA: Cambridge University Press), 1–29.

IPCC (2014). Climate Change 2014: Synthesis Report. Contribution of Working Groups I, II and III to the Fifth Assessment Report of the Intergovernmental Panel on Climate Change. , eds. Core Writing Team, R. K. Pachauri, and L. A. Meyer Cambridge, United Kingdom and New York, NY, USA: Cambridge University Press.

IPCC (2018a). Global Warming of 1.5°C. An IPCC Special Report on the impacts of global warming of 1.5°C above pre-industrial levels and related global greenhouse gas emission pathways, in the context of strengthening the global response to the threat of climate change,. , eds. V. Masson-Delmotte, P. Zhai, H.-O. Pörtner, D. Roberts, J. Skea, P. R. Shukla, et al. In Press.

IPCC (2018b). "Index," in *Global Warming of 1.5°C. An IPCC Special Report on the impacts of global warming of 1.5°C above pre-industrial levels and related global greenhouse gas emission pathways, in the context of strengthening the global response to the threat of climate change,* eds. V. Masson-Delmotte, P. Zhai, H.-O. Pörtner, D. Roberts, J. Skea, P. R. Shukla, et al. (In Press).

Ishii, M., Kosugi, N., Sasano, D., Saito, S., Midorikawa, T., and Inoue, H. Y. (2011). Ocean acidification off the south coast of Japan: A result from time series observations of CO 2 parameters from 1994 to 2008. *J. Geophys. Res.* 116, C06022. doi:10.1029/2010JC006831.

Ishijima, K., Nakazawa, T., and Aoki, S. (2009). Variations of atmospheric nitrous oxide concentration in the northern and western Pacific. *Tellus B Chem. Phys. Meteorol.* 61, 408–415. doi:10.1111/j.1600-0889.2008.00406.x.

Ishijima, K., Sugawara, S., Kawamura, K., Hashida, G., Morimoto, S., Murayama, S., et al. (2007). Temporal variations of the atmospheric nitrous oxide concentration and its δ15N and δ18O for the latter half of the 20th century reconstructed from firn air analyses. *J. Geophys. Res.* 112, D03305. doi:10.1029/2006JD007208.

Ito, A. (2017). Solar radiation management and ecosystem functional responses. *Clim. Change* 142, 53–66. doi:10.1007/s10584-017-1930-3.

Ito, T., Bracco, A., Deutsch, C., Frenzel, H., Long, M., and Takano, Y. (2015). Sustained growth of the Southern Ocean carbon storage in a warming climate. *Geophys. Res. Lett.* 42, 4516–4522. doi:10.1002/2015GL064320.

Ito, T., Minobe, S., Long, M. C., and Deutsch, C. (2017). Upper ocean O 2 trends: 1958-2015. *Geophys. Res. Lett.* 44, 4214–4223. doi:10.1002/2017GL073613.

Jaccard, S., Galbraith, E., Frölicher, T., and Gruber, N. (2014). Ocean (De)oxygenation Across the Last Deglaciation: Insights for the Future. *Oceanography* 27, 26–35. doi:10.5670/oceanog.2014.05.

Jaccard, S. L., and Galbraith, E. D. (2012). Large climate-driven changes of oceanic oxygen concentrations during the last deglaciation. *Nat. Geosci.* 5, 151–156. doi:10.1038/ngeo1352.

Jaccard, S. L., Galbraith, E. D., Martínez-García, A., and Anderson, R. F. (2016). Covariation of deep Southern Ocean oxygenation and atmospheric CO2 through the last ice age. *Nature* 530, 207–210. doi:10.1038/nature16514.

Jaccard, S. L., Galbraith, E. D., Sigman, D. M., Haug, G. H., Francois, R., Pedersen, T. F., et al. (2009). Subarctic Pacific evidence for a glacial deepening of the oceanic respired carbon pool. *Earth Planet. Sci. Lett.* 277, 156–165. doi:10.1016/j.epsl.2008.10.017.

Jackson, R. B., Canadell, J. G., Le Quéré, C., Andrew, R. M., Korsbakken, J. I., Peters, G. P., et al. (2016). Reaching peak emissions. *Nat. Clim. Chang.* 6, 7–10. doi:10.1038/nclimate2892.

Jackson, R. B., Lajtha, K., Crow, S. E., Hugelius, G., Kramer, M. G., and Piñeiro, G. (2017). The Ecology of Soil Carbon: Pools, Vulnerabilities, and Biotic and Abiotic Controls. *Annu. Rev. Ecol. Evol. Syst.* 48, 419–445. doi:10.1146/annurev-ecolsys-112414-054234.

Janssens-Maenhout, G., Crippa, M., Guizzardi, D., Muntean, M., Schaaf, E., Dentener, F., et al. (2017). EDGAR v4.3.2 Global Atlas of the three major Greenhouse Gas Emissions for the period 1970-2012. *Earth Syst. Sci. Data Discuss.* (submitted, 1–55. doi:10.5194/essd-2017-79.

Janssens-Maenhout, G., Crippa, M., Guizzardi, D., Muntean, M., Schaaf, E., Dentener, F., et al. (2019). EDGAR v4.3.2 Global Atlas of the three major Greenhouse Gas Emissions for the period 1970-2012. *Earth Syst. Sci. Data Discuss.* 2010, 1–52. doi:10.5194/essd-2018-164.

Jeltsch-Thömmes, A., Battaglia, G., Cartapanis, O., Jaccard, S. L., and Joos, F. (2018). A large increase in the carbon inventory of the land biosphere since the Last Glacial Maximum: constraints from multi-proxy data. *Clim. Past Discuss.* (submitted, 1–48. doi:10.5194/cp-2018-167.

Ji, Q., Babbin, A. R., Jayakumar, A., Oleynik, S., and Ward, B. B. (2015). Nitrous oxide production by nitrification and denitrification in the Eastern Tropical South Pacific oxygen minimum zone. *Geophys. Res. Lett.* 42, 10,755-10,764. doi:10.1002/2015GL066853.

Jiang, Y., van Groenigen, K. J., Huang, S., Hungate, B. A., van Kessel, C., Hu, S., et al. (2017). Higher yields and lower methane emissions with new rice cultivars. *Glob. Chang. Biol.* 23, 4728–4738. doi:10.1111/gcb.13737.

Jickells, T. D., Buitenhuis, E., Altieri, K., Baker, A. R., Capone, D., Duce, R. A., et al. (2017). A reevaluation of the magnitude and impacts of anthropogenic atmospheric nitrogen inputs on the ocean. *Global Biogeochem. Cycles* 31, 289–305. doi:10.1002/2016GB005586.

Joiner, J., Yoshida, Y., Zhang, Y., Duveiller, G., Jung, M., Lyapustin, A., et al. (2018). Estimation of Terrestrial Global Gross Primary Production (GPP) with Satellite Data-Driven Models and Eddy Covariance Flux Data. *Remote Sens.* 10, 1346. doi:10.3390/rs10091346.

Jones, A., Haywood, J. M., Alterskjaer, K., Boucher, O., Cole, J. N. S., Curry, C. L., et al. (2013a). The impact of abrupt suspension of solar radiation management (termination effect) in experiment G2 of the Geoengineering Model Intercomparison Project (GeoMIP). *J. Geophys. Res. Atmos.* 118, 9743–9752. doi:10.1002/jgrd.50762.

Jones, C. D., Arora, V., Friedlingstein, P., Bopp, L., Brovkin, V., Dunne, J., et al. (2016a). C4MIP - The Coupled Climate–Carbon Cycle Model Intercomparison Project: experimental protocol for CMIP6. *Geosci. Model Dev.* 9, 2853–2880. doi:10.5194/gmd-9-2853-2016.

Jones, C. D., Ciais, P., Davis, S. J., Friedlingstein, P., Gasser, T., Peters, G. P., et al. (2016b). Simulating the Earth system response to negative emissions. *Environ. Res. Lett.* 11, 095012. doi:10.1088/1748-9326/11/9/095012.

Jones, C., Robertson, E., Arora, V., Friedlingstein, P., Shevliakova, E., Bopp, L., et al. (2013b). Twenty-First-Century Compatible CO2 Emissions and Airborne Fraction Simulated by CMIP5 Earth System Models under Four Representative Concentration Pathways. *J. Clim.* 26, 4398–4413. doi:10.1175/JCLI-D-12-00554.1.

Joos, F., Prentice, I. C., Sitch, S., Meyer, R., Hooss, G., Plattner, G.-K., et al. (2001). Global warming feedbacks on terrestrial carbon uptake under the Intergovernmental Panel on Climate Change (IPCC) Emission Scenarios. *Global Biogeochem. Cycles* 15, 891–907. doi:10.1029/2000GB001375.

Joos, F., Roth, R., Fuglestvedt, J. S., Peters, G. P., Enting, I. G., von Bloh, W., et al. (2013). Carbon dioxide and climate impulse response functions for the computation of greenhouse gas metrics: a multi-model analysis. *Atmos. Chem. Phys.* 13, 2793–2825. doi:10.5194/acp-13-2793-2013.

Joos, F., and Spahni, R. (2008). Rates of change in natural and anthropogenic radiative forcing over the past 20,000 years. *Proc. Natl. Acad. Sci.* 105, 1425–1430. doi:10.1073/pnas.0707386105.

Jung, M., Reichstein, M., Schwalm, C. R., Huntingford, C., Sitch, S., Ahlström, A., et al. (2017). Compensatory water effects link yearly global land CO2 sink changes to temperature. *Nature* 541, 516–520. doi:10.1038/nature20780.

Junium, C. K., Dickson, A. J., and Uveges, B. T. (2018). Perturbation to the nitrogen cycle during rapid Early Eocene global warming. *Nat. Commun.* 9, 3186. doi:10.1038/s41467-018-05486-w.

Kalidindi, S., Bala, G., Modak, A., and Caldeira, K. (2015). Modeling of solar radiation management: a comparison of simulations using reduced solar constant and stratospheric sulphate aerosols. *Clim. Dyn.* 44, 2909–2925. doi:10.1007/s00382-014-2240-3.

KAMMANN, C., IPPOLITO, J., HAGEMANN, N., BORCHARD, N., CAYUELA, M. L., ESTAVILLO, J. M., et al. (2017). BIOCHAR AS A TOOL TO REDUCE THE AGRICULTURAL GREENHOUSE-GAS BURDEN – KNOWNS, UNKNOWNS AND FUTURE RESEARCH NEEDS. *J. Environ. Eng. Landsc. Manag.* 25, 114–139. doi:10.3846/16486897.2017.1319375.

Katavouta, A., Williams, R. G., Goodwin, P., and Roussenov, V. (2018). Reconciling Atmospheric and Oceanic Views of the Transient Climate Response to Emissions. *Geophys. Res. Lett.* 45, 6205–6214. doi:10.1029/2018GL077849.

Kato, E., and Yamagata, Y. (2014). BECCS capability of dedicated bioenergy crops under a future land-use scenario targeting net negative carbon emissions. *Earth's Futur.* 2, 421–439. doi:10.1002/2014EF000249.

Kaushal, S. S., Likens, G. E., Pace, M. L., Utz, R. M., Haq, S., Gorman, J., et al. (2018). Freshwater salinization syndrome on a continental scale. *Proc. Natl. Acad. Sci.* 115, E574–E583. doi:10.1073/pnas.1711234115.

Keeling, C. D., Whorf, T. P., Wahlen, M., and van der Plicht, J. (2001). Exchanges of atmospheric CO2, and 13CO2, with the terrestrial biosphere and oceans from 1978 to 2000.

Keenan, T. F., Prentice, I. C., Canadell, J. G., Williams, C. A., Wang, H., Raupach, M., et al. (2016). Recent pause in the growth rate of atmospheric CO2 due to enhanced terrestrial carbon uptake. *Nat. Commun.* 7, 13428. doi:10.1038/ncomms13428.

Keith, D. W., Wagner, G., and Zabel, C. L. (2017). Solar geoengineering reduces atmospheric carbon burden. *Nat. Clim. Chang.* 7, 617–619. doi:10.1038/nclimate3376.

Kell, D. B. (2011). Breeding crop plants with deep roots: their role in sustainable carbon, nutrient and water sequestration. *Ann. Bot.* 108, 407–418. doi:10.1093/aob/mcr175.

Keller, D. P., Feng, E. Y., and Oschlies, A. (2014). Potential climate engineering effectiveness and side effects during a high carbon dioxide-emission scenario. *Nat. Commun.* 5, 3304. doi:10.1038/ncomms4304.

Keller, D. P., Lenton, A., Littleton, E. W., Oschlies, A., Scott, V., and Vaughan, N. E. (2018a). The Effects of Carbon Dioxide Removal on the Carbon Cycle. *Curr. Clim. Chang. Reports* 4, 250–265. doi:10.1007/s40641-018-0104-3.

Keller, D. P., Lenton, A., Scott, V., Vaughan, N. E., Bauer, N., Ji, D., et al. (2017). The Carbon Dioxide Removal Model Intercomparison Project (CDR-MIP): Rationale and experimental design. *Geosci. Model Dev. Discuss.*, 1–72. doi:10.5194/gmd-2017-168.

Keller, D. P., Lenton, A., Scott, V., Vaughan, N. E., Bauer, N., Ji, D., et al. (2018b). The Carbon Dioxide Removal Model Intercomparison Project (CDRMIP): rationale and experimental protocol for CMIP6. *Geosci. Model Dev.* 11, 1133–1160. doi:10.5194/gmd-11-1133-2018.

Kelly, J. W. G., Duursma, R. A., Atwell, B. J., Tissue, D. T., and Medlyn, B. E. (2016). Drought × CO 2 interactions in trees: a test of the low-intercellular CO 2 concentration (C i) mechanism. *New Phytol.* 209, 1600–1612. doi:10.1111/nph.13715.

Kessler, A., and Tjiputra, J. (2016). The Southern Ocean as a constraint to reduce uncertainty in future ocean carbon sinks. *Earth Syst. Dyn.* 7, 295–312. doi:10.5194/esd-7-295-2016.

Khatiwala, S., Graven, H., Payne, S., and Heimbach, P. (2018). Changes to the Air-Sea Flux and Distribution of Radiocarbon in the Ocean Over the 21st Century. *Geophys. Res. Lett.* 45, 5617–5626. doi:10.1029/2018GL078172.

Kirschke, S., Bousquet, P., Ciais, P., Saunois, M., Canadell, J. G., Dlugokencky, E. J., et al. (2013). Three decades of global methane sources and sinks. *Nat. Geosci.* 6, 813–823. doi:10.1038/ngeo1955.

Kizyakov, A., Khomutov, A., Zimin, M., Khairullin, R., Babkina, E., Dvornikov, Y., et al. (2018). Microrelief Associated with Gas Emission Craters: Remote-Sensing and Field-Based Study. *Remote Sens.* 10, 677. doi:10.3390/rs10050677.

Kizyakov, A., Zimin, M., Sonyushkin, A., Dvornikov, Y., Khomutov, A., and Leibman, M. (2017). Comparison of Gas Emission Crater Geomorphodynamics on Yamal and Gydan Peninsulas (Russia), Based on Repeat Very-High-Resolution Stereopairs. *Remote Sens.* 9, 1023. doi:10.3390/rs9101023.

Kleinen, T., Brovkin, V., and Munhoven, G. (2016). Modelled interglacial carbon cycle dynamics during the Holocene, the Eemian and Marine Isotope Stage (MIS) 11. *Clim. Past* 12, 2145–2160. doi:10.5194/cp-12-2145-2016.

Kluber, L. A., Miller, J. O., Ducey, T. F., Hunt, P. G., Lang, M., and S. Ro, K. (2014). Multistate assessment of wetland restoration on CO2 and N2O emissions and soil bacterial communities. *Appl. Soil Ecol.* 76, 87–94. doi:10.1016/j.apsoil.2013.12.014.

Knutti, R., and Rogelj, J. (2015). The legacy of our CO2 emissions: a clash of scientific facts, politics and ethics. *Clim. Change* 133, 361–373. doi:10.1007/s10584-015-1340-3.

Kock, A., Arévalo-Martínez, D. L., Löscher, C. R., and Bange, H. W. (2016). Extreme N2O accumulation in the coastal oxygen minimum zone off Peru. *Biogeosciences* 13, 827–840. doi:10.5194/bg-13-827-2016.

Kock, A., Schafstall, J., Dengler, M., Brandt, P., and Bange, H. W. (2012). Sea-to-air and diapycnal nitrous oxide fluxes in the eastern tropical North Atlantic Ocean. *Biogeosciences* 9, 957–964. doi:10.5194/bg-9-957-2012.

Köhler, P., Abrams, J. F., Völker, C., Hauck, J., and Wolf-Gladrow, D. A. (2013). Geoengineering impact of open ocean dissolution of olivine on atmospheric CO2 , surface ocean pH and marine biology. *Environ. Res. Lett.* 8, 014009. doi:10.1088/1748-9326/8/1/014009.

Köhler, P., Knorr, G., and Bard, E. (2014). Permafrost thawing as a possible source of abrupt carbon release at the onset of the Bølling/Allerød. *Nat. Commun.* 5, 5520. doi:10.1038/ncomms6520.

Köhler, P., Nehrbass-Ahles, C., Schmitt, J., Stocker, T. F., and Fischer, H. (2017). A 156 kyr smoothed history of the atmospheric greenhouse gases CO2, CH4, and N2O and their radiative forcing. *Earth Syst. Sci. Data* 9, 363–387. doi:10.5194/essd-9-363-2017.

Kondo, M., Ichii, K., Patra, P. K., Poulter, B., Calle, L., Koven, C., et al. (2018). Plant Regrowth as a Driver of Recent Enhancement of Terrestrial CO2 Uptake. *Geophys. Res. Lett.* 45, 4820–4830. doi:10.1029/2018GL077633.

Korth, H., Tsyganenko, N. A., Johnson, C. L., Philpott, L. C., Anderson, B. J., Al Asad, M. M., et al. (2015). Modular model for Mercury's magnetospheric magnetic field confined within the average observed magnetopause. *J. Geophys. Res. Sp. Phys.* 120, 4503–4518. doi:10.1002/2015JA021022.

Kouketsu, S., and Murata, A. M. (2014). Detecting decadal scale increases in anthropogenic CO 2 in the ocean. *Geophys. Res. Lett.* 41, 4594–4600. doi:10.1002/2014GL060516.

Koven, C. D., Chambers, J. Q., Georgiou, K., Knox, R., Negron-Juarez, R., Riley, W. J., et al. (2015a). Controls on terrestrial carbon feedbacks by productivity versus turnover in the CMIP5 Earth System Models. *Biogeosciences* 12, 5211–5228. doi:10.5194/bg-12-5211-2015.

Koven, C. D., Hugelius, G., Lawrence, D. M., and Wieder, W. R. (2017). Higher climatological temperature sensitivity of soil carbon in cold than warm climates. *Nat. Clim. Chang.* 7, 817–822. doi:10.1038/nclimate3421.

Koven, C. D., Lawrence, D. M., and Riley, W. J. (2015b). Permafrost carbon−climate feedback is sensitive to deep soil carbon decomposability but not deep soil nitrogen dynamics. *Proc. Natl. Acad. Sci.* 112, 201415123. doi:10.1073/pnas.1415123112.

Koven, C. D., Ringeval, B., Friedlingstein, P., Ciais, P., Cadule, P., Khvorostyanov, D., et al. (2011). Permafrost carbon-climate feedbacks accelerate global warming. *Proc. Natl. Acad. Sci.* 108, 14769–14774. doi:10.1073/pnas.1103910108.

Koven, C. D., Schuur, E. A. G., Schädel, C., Bohn, T. J., Burke, E. J., Chen, G., et al. (2015c). A simplified, data-constrained approach to estimate the permafrost carbon–climate feedback. *Philos. Trans. R. Soc. A Math. Phys. Eng. Sci.* 373, 20140423. doi:10.1098/rsta.2014.0423.

Krasting, J. P., Dunne, J. P., Shevliakova, E., and Stouffer, R. J. (2014). Trajectory sensitivity of the transient climate response to cumulative carbon emissions. *Geophys. Res. Lett.* 41, 2520–2527. doi:10.1002/2013GL059141.

Krause, A., Pugh, T. A. M., Bayer, A. D., Doelman, J. C., Humpenöder, F., Anthoni, P., et al. (2017). Global consequences of afforestation and bioenergy cultivation on ecosystem service indicators. *Biogeosciences* 14, 4829–4850. doi:10.5194/bg-14-4829-2017.

Kravitz, B., Robock, A., Tilmes, S., Boucher, O., English, J. M., Irvine, P. J., et al. (2015). The Geoengineering Model Intercomparison Project Phase 6 (GeoMIP6): simulation design and preliminary results. *Geosci. Model Dev.* 8, 3379–3392. doi:10.5194/gmd-8-3379-2015.

Kraxner, F., Nordström, E.-M., Havlík, P., Gusti, M., Mosnier, A., Frank, S., et al. (2013). Global bioenergy scenarios – Future forest development, land-use implications, and trade-offs. *Biomass and Bioenergy* 57, 86–96. doi:10.1016/j.biombioe.2013.02.003.

Kretschmer, K., Biastoch, A., Rüpke, L., and Burwicz, E. (2015). Modeling the fate of methane hydrates under global warming. *Global Biogeochem. Cycles* 29, 610–625. doi:10.1002/2014GB005011.

Kroeker, K. J., Kordas, R. L., Crim, R., Hendriks, I. E., Ramajo, L., Singh, G. S., et al. (2013). Impacts of ocean acidification on marine organisms: quantifying sensitivities and interaction with warming. *Glob. Chang. Biol.* 19, 1884–1896. doi:10.1111/gcb.12179.

Kubota, K., Yokoyama, Y., Ishikawa, T., Suzuki, A., and Ishii, M. (2017). Rapid decline in pH of coral calcification fluid due to incorporation of anthropogenic CO2. *Sci. Rep.* 7, 7694. doi:10.1038/s41598-017-07680-0.

Kurz, W. A., Smyth, C., and LemprièreT.C (2016). Climate change mitigation through forest sector activities: principles, potential and priorities 1 - ProQuest. *Unasylva* 67, 61.

Kwiatkowski, L., Aumont, O., Bopp, L., and Ciais, P. (2018). The Impact of Variable Phytoplankton Stoichiometry on Projections of Primary Production, Food Quality, and Carbon Uptake in the Global Ocean. *Global Biogeochem. Cycles* 32, 516–528. doi:10.1002/2017GB005799.

Kwiatkowski, L., Bopp, L., Aumont, O., Ciais, P., Cox, P. M., Laufkötter, C., et al. (2017). Emergent constraints on projections of declining primary production in the tropical oceans. *Nat. Clim. Chang.* 7, 355–358. doi:10.1038/nclimate3265.

Kwiatkowski, L., and Orr, J. C. (2018). Diverging seasonal extremes for ocean acidification during the twenty-first century. *Nat. Clim. Chang.* 8, 141–145. doi:10.1038/s41558-017-0054-0.

Landolfi, A., Somes, C. J., Koeve, W., Zamora, L. M., and Oschlies, A. (2017). Oceanic nitrogen cycling and N 2 O flux perturbations in the Anthropocene. *Global Biogeochem. Cycles* 31, 1236–1255. doi:10.1002/2017GB005633.

Landschützer, P., Gruber, N., and Bakker, D. C. E. (2016). Decadal variations and trends of the global ocean carbon sink. *Global Biogeochem. Cycles* 30, 1396–1417. doi:10.1002/2015GB005359.

Landschützer, P., Gruber, N., Bakker, D. C. E., and Schuster, U. (2014). Recent variability of the global ocean carbon sink. *Global Biogeochem. Cycles* 28, 927–949. doi:10.1002/2014GB004853.

Landschützer, P., Gruber, N., Bakker, D. C. E., Stemmler, I., and Six, K. D. (2018). Strengthening seasonal marine CO2 variations due to increasing atmospheric CO2. *Nat. Clim. Chang.* 8, 146–150. doi:10.1038/s41558-017-0057-x.

Landschützer, P., Gruber, N., Haumann, F. A., Rödenbeck, C., Bakker, D. C. E., van Heuven, S., et al. (2015). The reinvigoration of the Southern Ocean carbon sink. *Science (80-.).* 349, 1221–1224. doi:10.1126/science.aab2620.

Laruelle, G. G., Lauerwald, R., Pfeil, B., and Regnier, P. (2014). Regionalized global budget of the CO 2 exchange at the air-water interface in continental shelf seas. *Global Biogeochem. Cycles* 28, 1199–1214. doi:10.1002/2014GB004832.

Lasslop, G., Brovkin, V., Reick, C. H., Bathiany, S., and Kloster, S. (2016). Multiple stable states of tree cover in a global land surface model due to a fire-vegetation feedback. *Geophys. Res. Lett.* 43, 6324–6331. doi:10.1002/2016GL069365.

Laufkötter, C., Vogt, M., Gruber, N., Aita-Noguchi, M., Aumont, O., Bopp, L., et al. (2015). Drivers and uncertainties of future global marine primary production in marine ecosystem models. *Biogeosciences* 12, 6955–6984. doi:10.5194/bg-12-6955-2015.

Laufkötter, C., Vogt, M., Gruber, N., Aumont, O., Bopp, L., Doney, S. C., et al. (2016). Projected decreases in future marine export production: the role of the carbon flux through the upper ocean ecosystem. *Biogeosciences* 13, 4023–4047. doi:10.5194/bg-13-4023-2016.

Laurent, A., Fennel, K., Cai, W.-J., Huang, W.-J., Barbero, L., and Wanninkhof, R. (2017). Eutrophication-induced acidification of coastal waters in the northern Gulf of Mexico: Insights into origin and processes from a coupled physical-biogeochemical model. *Geophys. Res. Lett.* 44, 946–956. doi:10.1002/2016GL071881.

Lauvset, S. K., Gruber, N., Landschützer, P., Olsen, A., and Tjiputra, J. (2015). Trends and drivers in global surface ocean pH over the past 3 decades. *Biogeosciences* 12, 1285–1298. doi:10.5194/bg-12-1285-2015.

Lauvset, S. K., Key, R. M., Olsen, A., van Heuven, S., Velo, A., Lin, X., et al. (2016). A new global interior ocean mapped climatology: the 1° × 1° GLODAP version 2. *Earth Syst. Sci. Data* 8, 325–340. doi:10.5194/essd-8-325-2016.

Law, Y., Ye, L., Pan, Y., and Yuan, Z. (2012). Nitrous oxide emissions from wastewater treatment processes. *Philos. Trans. R. Soc. B Biol. Sci.* 367, 1265–1277. doi:10.1098/rstb.2011.0317.

Le Page, Y., Morton, D., Hartin, C., Bond-Lamberty, B., Pereira, J. M. C., Hurtt, G., et al. (2017). Synergy between land use and climate change increases future fire risk in Amazon forests. *Earth Syst. Dyn.* 8, 1237–1246. doi:10.5194/esd-8-1237-2017.

Le Quéré, C., Andrew, R. M., Friedlingstein, P., Sitch, S., Hauck, J., Pongratz, J., et al. (2018a). Global Carbon Budget 2018. *Earth Syst. Sci. Data* 10, 2141–2194. doi:10.5194/essd-10-2141-2018.

Le Quéré, C., Andrew, R. M., Friedlingstein, P., Sitch, S., Pongratz, J., Manning, A. C., et al. (2018b). Global Carbon Budget 2017. *Earth Syst. Sci. Data* 10, 405–448. doi:10.5194/essd-10-405-2018.

Le Quéré, C., Takahashi, T., Buitenhuis, E. T., Rödenbeck, C., and Sutherland, S. C. (2010). Impact of climate change and variability on the global oceanic sink of CO 2. *Global Biogeochem. Cycles* 24, GB4007. doi:10.1029/2009GB003599.

Leduc, M., Matthews, H. D., and de Elía, R. (2015). Quantifying the Limits of a Linear Temperature Response to Cumulative CO 2 Emissions. *J. Clim.* 28, 9955–9968. doi:10.1175/JCLI-D-14-00500.1.

Leduc, M., Matthews, H. D., and de Elía, R. (2016). Regional estimates of the transient climate response to cumulative CO2 emissions. *Nat. Clim. Chang.* 6, 474–478. doi:10.1038/nclimate2913.

Lee, J.-E., Frankenberg, C., van der Tol, C., Berry, J. A., Guanter, L., Boyce, C. K., et al. (2013). Forest productivity and water stress in Amazonia: observations from GOSAT chlorophyll fluorescence. *Proc. R. Soc. B Biol. Sci.* 280, 20130171–20130171. doi:10.1098/rspb.2013.0171.

Lee, S.-J., Ryu, I.-S., Kim, B.-M., and Moon, S.-H. (2011). A review of the current application of N2O emission reduction in CDM projects. *Int. J. Greenh. Gas Control* 5, 167–176. doi:10.1016/j.ijggc.2010.07.001.

Lehmann, J., Abiven, S., Kleber, M., Pan, G., Singh, B. P., Sohi, S., et al. (2015). "Persistence of biochar in soil," in *Biochar for Environmental Management: Science, Technology and Implementation*, eds. J. Lehmann and S. Joseph (London, UK), 233--80. doi:https://doi.org/10.4324/9780203762264.

Leith, C. E. (1975). Climate Response and Fluctuation Dissipation. *J. Atmos. Sci.* 32, 2022–2026. doi:10.1175/1520-0469(1975)032<2022:CRAFD>2.0.CO;2.

Lenton, A., and Matear, R. J. (2007). Role of the Southern Annular Mode (SAM) in Southern Ocean CO 2 uptake. *Global Biogeochem. Cycles* 21, GB2016. doi:10.1029/2006GB002714.

Lenton, A., Tilbrook, B., Law, R. M., Bakker, D., Doney, S. C., Gruber, N., et al. (2013). Sea–air CO2 fluxes in the Southern Ocean for the period 1990-2009. *Biogeosciences* 10, 4037–4054. doi:10.5194/bg-10-4037-2013.

Lenton, T. M. (2011). Early warning of climate tipping points. *Nat. Clim. Chang.* 1, 201–209. doi:10.1038/nclimate1143.

Lenton, T. M. (2014). "CHAPTER 3. The Global Potential for Carbon Dioxide Removal," in *Issues in Environmental Science and Technology*, eds. R. Harrison and R. Hester (Cambridge: Royal Society of Chemistry), 52–79.

Lenton, T. M., Held, H., Kriegler, E., Hall, J. W., Lucht, W., Rahmstorf, S., et al. (2008). Tipping elements in the Earth's climate system. *Proc. Natl. Acad. Sci.* 105, 1786–1793. doi:10.1073/pnas.0705414105.

Levin, I., Naegler, T., Kromer, B., Diehl, M., Francey, R., Gomez-Pelaez, A., et al. (2010). Observations and modelling of the global distribution and long-term trend of atmospheric 14 CO 2. *Tellus B Chem. Phys. Meteorol.* 62, 26–46. doi:10.1111/j.1600-0889.2009.00446.x.

Levin, L. A. (2018). Manifestation, Drivers, and Emergence of Open Ocean Deoxygenation. *Ann. Rev. Mar. Sci.* 10, 229–260. doi:10.1146/annurev-marine-121916-063359.

Levine, N. M., Zhang, K., Longo, M., Baccini, A., Phillips, O. L., Lewis, S. L., et al. (2016). Ecosystem heterogeneity determines the ecological resilience of the Amazon to climate change. *Proc. Natl. Acad. Sci.* 113, 793–797. doi:10.1073/pnas.1511344112.

Li, H., and Ilyina, T. (2018a). Current and Future Decadal Trends in the Oceanic Carbon Uptake Are Dominated by Internal Variability. *Geophys. Res. Lett.* 45, 916–925. doi:10.1002/2017GL075370.

Li, H., and Ilyina, T. (2018b). Current and Future Decadal Trends in the Oceanic Carbon Uptake Are Dominated by Internal Variability. *Geophys. Res. Lett.* 45, 916–925. doi:10.1002/2017GL075370.

Li, M., Lee, Y. J., Testa, J. M., Li, Y., Ni, W., Kemp, W. M., et al. (2016a). What drives interannual variability of hypoxia in Chesapeake Bay: Climate forcing versus nutrient loading? *Geophys. Res. Lett.* 43, 2127–2134. doi:10.1002/2015GL067334.

Li, W., Ciais, P., Wang, Y., Peng, S., Broquet, G., Ballantyne, A. P., et al. (2016b). Reducing uncertainties in decadal variability of the global carbon budget with multiple datasets. *Proc. Natl. Acad. Sci.* 113, 13104–13108. doi:10.1073/pnas.1603956113.

Lippold, J., Gutjahr, M., Blaser, P., Christner, E., de Carvalho Ferreira, M. L., Mulitza, S., et al. (2016). Deep water provenance and dynamics of the (de)glacial Atlantic meridional overturning circulation. *Earth Planet. Sci. Lett.* 445, 68–78. doi:10.1016/j.epsl.2016.04.013.

Liu, Y., Peng, Z., Zhou, R., Song, S., Liu, W., You, C.-F., et al. (2015). Acceleration of modern acidification in the South China Sea driven by anthropogenic CO2. *Sci. Rep.* 4, 5148. doi:10.1038/srep05148.

Liu, Z., He, T., Cao, T., Yang, T., Meng, J., and Chen, W. (2017). Effects of biochar application on nitrogen leaching, ammonia volatilization and nitrogen use efficiency in two distinct soils. *J. soil Sci. plant Nutr.* 17, 515–528. doi:10.4067/S0718-95162017005000037.

Lloret, F., Escudero, A., Iriondo, J. M., Martínez-Vilalta, J., and Valladares, F. (2012). Extreme climatic events and vegetation: the role of stabilizing processes. *Glob. Chang. Biol.* 18, 797–805. doi:10.1111/j.1365-2486.2011.02624.x.

Lloyd, J., and Farquhar, G. D. (2008). Effects of rising temperatures and [CO2] on the physiology of tropical forest trees. *Philos. Trans. R. Soc. B Biol. Sci.* 363, 1811–1817. doi:10.1098/rstb.2007.0032.

Lombardozzi, D. L., Bonan, G. B., Smith, N. G., Dukes, J. S., and Fisher, R. A. (2015). Temperature acclimation of photosynthesis and respiration: A key uncertainty in the carbon cycle-climate feedback. *Geophys. Res. Lett.* 42, 8624–8631. doi:10.1002/2015GL065934.

Loulergue, L., Schilt, A., Spahni, R., Masson-Delmotte, V., Blunier, T., Lemieux, B., et al. (2008). Orbital and millennial-scale features of atmospheric CH4 over the past 800,000 years. *Nature* 453, 383–386. doi:10.1038/nature06950.

Lovenduski, N. S., Fay, A. R., and McKinley, G. A. (2015). Observing multidecadal trends in Southern Ocean CO 2 uptake: What can we learn from an ocean model? *Global Biogeochem. Cycles* 29, 416–426. doi:10.1002/2014GB004933.

Lowe, A. T., Bos, J., and Ruesink, J. (2019). Ecosystem metabolism drives pH variability and modulates long-term ocean acidification in the Northeast Pacific coastal ocean. *Sci. Rep.* 9, 963. doi:10.1038/s41598-018-37764-4.

Lowe, J. A., and Bernie, D. (2018). The impact of Earth system feedbacks on carbon budgets and climate response. *Philos. Trans. R. Soc. A Math. Phys. Eng. Sci.* 376, 20170263. doi:10.1098/rsta.2017.0263.

Lowe, J. A., Huntingford, C., Raper, S. C. B., Jones, C. D., Liddicoat, S. K., and Gohar, L. K. (2009). How difficult is it to recover from dangerous levels of global warming? *Environ. Res. Lett.* 4, 014012. doi:10.1088/1748-9326/4/1/014012.

Lucht, W., Schaphoff, S., Erbrecht, T., Heyder, U., and Cramer, W. (2006). Terrestrial vegetation redistribution and carbon balance under climate change. *Carbon Balance Manag.* 1, 6. doi:10.1186/1750-0680-1-6.

Łukawska-Matuszewska, K., Graca, B., Brocławik, O., and Zalewska, T. (2019). The impact of declining oxygen conditions on pyrite accumulation in shelf sediments (Baltic Sea). *Biogeochemistry* 142, 209–230. doi:10.1007/s10533-018-0530-2.

Luke, C. M., and Cox, P. M. (2011). Soil carbon and climate change: from the Jenkinson effect to the compost-bomb instability. *Eur. J. Soil Sci.* 62, 5–12. doi:10.1111/j.1365-2389.2010.01312.x.

Luo, Y., Ahlström, A., Allison, S. D., Batjes, N. H., Brovkin, V., Carvalhais, N., et al. (2016). Toward more realistic projections of soil carbon dynamics by Earth system models. *Global Biogeochem. Cycles* 30, 40–56. doi:10.1002/2015GB005239.

Lüthi, D., Le Floch, M., Bereiter, B., Blunier, T., Barnola, J.-M., Siegenthaler, U., et al. (2008). High-resolution carbon dioxide concentration record 650,000–800,000 years before present. *Nature* 453, 379–382. doi:10.1038/nature06949.

Luyssaert, S., Jammet, M., Stoy, P. C., Estel, S., Pongratz, J., Ceschia, E., et al. (2014). Land management and land-cover change have impacts of similar magnitude on surface temperature. *Nat. Clim. Chang.* 4, 389–393. doi:10.1038/nclimate2196.

Lyra, A., Imbach, P., Rodriguez, D., Chou, S. C., Georgiou, S., and Garofolo, L. (2017). Projections of climate change impacts on central America tropical rainforest. *Clim. Change* 141, 93–105. doi:10.1007/s10584-016-1790-2.

Maavara, T., Lauerwald, R., Laruelle, G. G., Akbarzadeh, Z., Bouskill, N. J., Van Cappellen, P., et al. (2019). Nitrous oxide emissions from inland waters: Are IPCC estimates too high? *Glob. Chang. Biol.* 25, 473–488. doi:10.1111/gcb.14504.

MacDougall, A. H. (2016). The Transient Response to Cumulative CO2 Emissions: a Review. *Curr. Clim. Chang. Reports* 2, 39–47. doi:10.1007/s40641-015-0030-6.

MacDougall, A. H. (2017). The oceanic origin of path-independent carbon budgets. *Sci. Rep.* 7, 10373. doi:10.1038/s41598-017-10557-x.

MacDougall, A. H., and Friedlingstein, P. (2015). The Origin and Limits of the Near Proportionality between Climate Warming and Cumulative CO 2 Emissions. *J. Clim.* 28, 4217–4230. doi:10.1175/JCLI-D-14-00036.1.

MacDougall, A. H., Swart, N. C., and Knutti, R. (2017). The Uncertainty in the Transient Climate Response to Cumulative CO 2 Emissions Arising from the Uncertainty in Physical Climate Parameters. *J. Clim.* 30, 813–827. doi:10.1175/JCLI-D-16-0205.1.

MacDougall, A. H., Zickfeld, K., Knutti, R., and Matthews, H. D. (2015). Sensitivity of carbon budgets to permafrost carbon feedbacks and non-CO2 forcings. *Environ. Res. Lett.* 10, 125003. doi:10.1088/1748-9326/10/12/125003.

MacFarling Meure, C., Etheridge, D., Trudinger, C., Steele, P., Langenfelds, R., van Ommen, T., et al. (2006). Law Dome CO2 , CH4 and N2O ice core records extended to 2000 years BP. *Geophys. Res. Lett.* 33, L14810. doi:10.1029/2006GL026152.

Madhupratap, M., Kumar, S. P., Bhattathiri, P. M. A., Kumar, M. D., Raghukumar, S., Nair, K. K. C., et al. (1996). Mechanism of the biological response to winter cooling in the northeastern Arabian Sea. *Nature* 384, 549–552. doi:10.1038/384549a0.

Mahowald, N. M., Scanza, R., Brahney, J., Goodale, C. L., Hess, P. G., Moore, J. K., et al. (2017). Aerosol Deposition Impacts on Land and Ocean Carbon Cycles. *Curr. Clim. Chang. Reports* 3, 16–31. doi:10.1007/s40641-017-0056-z.

Majorowicz, J., Grasby, S. E., Safanda, J., and Beauchamp, B. (2014). Gas hydrate contribution to Late Permian global warming. *Earth Planet. Sci. Lett.* 393, 243–253. doi:10.1016/j.epsl.2014.03.003.

Malhi, Y., Rowland, L., Aragão, L. E. O. C., and Fisher, R. A. (2018). New insights into the variability of the tropical land carbon cycle from the El Niño of 2015/2016. *Philos. Trans. R. Soc. B Biol. Sci.* 373, 20170298. doi:10.1098/rstb.2017.0298.

Manizza, M., Keeling, R. F., and Nevison, C. D. (2012). On the processes controlling the seasonal cycles of the air–sea fluxes of O2 and N2O: A modelling study. *Tellus B Chem. Phys. Meteorol.* 64, 18429. doi:10.3402/tellusb.v64i0.18429.

Mao, J., Ribes, A., Yan, B., Shi, X., Thornton, P. E., Séférian, R., et al. (2016). Human-induced greening of the northern extratropical land surface. *Nat. Clim. Chang.* 6, 959–963. doi:10.1038/nclimate3056.

Marañón, E., Lorenzo, M. P., Cermeño, P., and Mouriño-Carballido, B. (2018). Nutrient limitation suppresses the temperature dependence of phytoplankton metabolic rates. *ISME J.* 12, 1836–1845. doi:10.1038/s41396-018-0105-1.

Marcott, S. A., Bauska, T. K., Buizert, C., Steig, E. J., Rosen, J. L., Cuffey, K. M., et al. (2014). Centennial-scale changes in the global carbon cycle during the last deglaciation. *Nature* 514, 616–619. doi:10.1038/nature13799.

Marland, G., Boden, T. A., and Andres, R. J. Global, Regional, and National Fossil-Fuel CO2 Emissions. *Oak Ridge*. Available at: https://cdiac.ess-dive.lbl.gov/trends/emis/overview.html .

Martínez-Botí, M. A., Foster, G. L., Chalk, T. B., Rohling, E. J., Sexton, P. F., Lunt, D. J., et al. (2015a). Plio-Pleistocene climate sensitivity evaluated using high-resolution CO2 records. *Nature* 518, 49–54. doi:10.1038/nature14145.

Martínez-Botí, M. A., Marino, G., Foster, G. L., Ziveri, P., Henehan, M. J., Rae, J. W. B., et al. (2015b). Boron isotope evidence for oceanic carbon dioxide leakage during the last deglaciation. *Nature* 518, 219–222. doi:10.1038/nature14155.

Martínez-Botí, M. A., Marino, G., Foster, G. L., Ziveri, P., Henehan, M. J., Rae, J. W. B., et al. (2015c). Boron isotope evidence for oceanic carbon dioxide leakage during the last deglaciation. *Nature* 518, 219–222. doi:10.1038/nature14155.

Martinez-Garcia, A., Sigman, D. M., Ren, H., Anderson, R. F., Straub, M., Hodell, D. A., et al. (2014). Iron Fertilization of the Subantarctic Ocean During the Last Ice Age. *Science (80-.).* 343, 1347–1350. doi:10.1126/science.1246848.

Martinez-Rey, J., Bopp, L., Gehlen, M., Tagliabue, A., and Gruber, N. (2015). Projections of oceanic N₂O emissions in the 21st century using the IPSL Earth system model. *Biogeosciences* 12, 4133–4148. doi:10.5194/bg-12-4133-2015.

Matear, R. J., and Lenton, A. (2014). Quantifying the impact of ocean acidification on our future climate. *Biogeosciences* 11, 3965–3983. doi:10.5194/bg-11-3965-2014.

Matear, R. J., and Lenton, A. (2018). Carbon–climate feedbacks accelerate ocean acidification. *Biogeosciences* 15, 1721–1732. doi:10.5194/bg-15-1721-2018.

Mathesius, S., Hofmann, M., Caldeira, K., and Schellnhuber, H. J. (2015). Long-term response of oceans to CO2 removal from the atmosphere. *Nat. Clim. Chang.* 5, 1107–1113. doi:10.1038/nclimate2729.

Matsumoto, K. (2007). Biology-mediated temperature control on atmospheric p CO 2 and ocean biogeochemistry. *Geophys. Res. Lett.* 34, L20605. doi:10.1029/2007GL031301.

Matsumoto, K., Tokos, K., Chikamoto, M., and Ridgwell, A. (2010). Characterizing post-industrial changes in the ocean carbon cycle in an Earth system model. *Tellus B Chem. Phys. Meteorol.* 62, 296–313. doi:10.1111/j.1600-0889.2010.00461.x.

Matthews, H. D., and Caldeira, K. (2008). Stabilizing climate requires near-zero emissions. *Geophys. Res. Lett.* 35, L04705. doi:10.1029/2007GL032388.

Matthews, H. D., Gillett, N. P., Stott, P. A., and Zickfeld, K. (2009). The proportionality of global warming to cumulative carbon emissions. *Nature* 459, 829–832. doi:10.1038/nature08047.

Matthews, H. D., Landry, J.-S., Partanen, A.-I., Allen, M., Eby, M., Forster, P. M., et al. (2017). Estimating Carbon Budgets for Ambitious Climate Targets. *Curr. Clim. Chang. Reports* 3, 69–77. doi:10.1007/s40641-017-0055-0.

Matthews, H. D., and Solomon, S. (2013). Irreversible Does Not Mean Unavoidable. *Science (80-.).* 340, 438–439. doi:10.1126/science.1236372.

Matthews, H. D., Solomon, S., and Pierrehumbert, R. (2012). Cumulative carbon as a policy framework for achieving climate stabilization. *Philos. Trans. R. Soc. A Math. Phys. Eng. Sci.* 370, 4365–4379. doi:10.1098/rsta.2012.0064.

Matthews, H. D., and Zickfeld, K. (2012). Climate response to zeroed emissions of greenhouse gases and aerosols. *Nat. Clim. Chang.* 2, 338–341. doi:10.1038/nclimate1424.

McGuire, A. D., Christensen, T. R., Hayes, D., Heroult, A., Euskirchen, E., Kimball, J. S., et al. (2012). An assessment of the carbon balance of Arctic tundra: comparisons among observations, process models, and atmospheric inversions. *Biogeosciences* 9, 3185–3204. doi:10.5194/bg-9-3185-2012.

McGuire, A. D., Koven, C., Lawrence, D. M., Clein, J. S., Xia, J., Beer, C., et al. (2016). Variability in the sensitivity among model simulations of permafrost and carbon dynamics in the permafrost region between 1960 and 2009. *Global Biogeochem. Cycles* 30, 1015–1037. doi:10.1002/2016GB005405.

McGuire, A. D., Lawrence, D. M., Koven, C., Clein, J. S., Burke, E., Chen, G., et al. (2018). Dependence of the evolution of carbon dynamics in the northern permafrost region on the trajectory of climate change. *Proc. Natl. Acad. Sci.* 115, 3882–3887. doi:10.1073/pnas.1719903115.

McInerney, F. A., and Wing, S. L. (2011). The Paleocene-Eocene Thermal Maximum: A Perturbation of Carbon Cycle, Climate, and Biosphere with Implications for the Future. *Annu. Rev. Earth Planet. Sci.* 39, 489–516. doi:10.1146/annurev-earth-040610-133431.

McKinley, G. A., Fay, A. R., Lovenduski, N. S., and Pilcher, D. J. (2017). Natural Variability and Anthropogenic Trends in the Ocean Carbon Sink. *Ann. Rev. Mar. Sci.* 9, 125–150. doi:10.1146/annurev-marine-010816-060529.

Mcleod, E., Chmura, G. L., Bouillon, S., Salm, R., Björk, M., Duarte, C. M., et al. (2011). A blueprint for blue carbon: toward an improved understanding of the role of vegetated coastal habitats in sequestering CO 2. *Front. Ecol. Environ.* 9, 552–560. doi:10.1890/110004.

McManus, J. F., Francois, R., Gherardi, J.-M., Keigwin, L. D., and Brown-Leger, S. (2004). Collapse and rapid resumption of Atlantic meridional circulation linked to deglacial climate changes. *Nature* 428, 834–837. doi:10.1038/nature02494.

McNorton, J., Wilson, C., Gloor, M., Parker, R. J., Boesch, H., Feng, W., et al. (2018). Attribution of recent increases in atmospheric methane through 3-D inverse modelling. *Atmos. Chem. Phys.* 18, 18149–18168. doi:10.5194/acp-18-18149-2018.

Medlyn, B. E., De Kauwe, M. G., Zaehle, S., Walker, A. P., Duursma, R. A., Luus, K., et al. (2016). Using models to guide field experiments: a priori predictions for the CO 2 response of a nutrient- and water-limited native Eucalypt woodland. *Glob. Chang. Biol.* 22, 2834–2851. doi:10.1111/gcb.13268.

Medlyn, B. E., Zaehle, S., De Kauwe, M. G., Walker, A. P., Dietze, M. C., Hanson, P. J., et al. (2015). Using ecosystem experiments to improve vegetation models. *Nat. Clim. Chang.* 5, 528–534. doi:10.1038/nclimate2621.

Meier, I. C., Finzi, A. C., and Phillips, R. P. (2017). Root exudates increase N availability by stimulating microbial turnover of fast-cycling N pools. *Soil Biol. Biochem.* 106, 119–128. doi:10.1016/j.soilbio.2016.12.004.

Meinshausen, M., Meinshausen, N., Hare, W., Raper, S. C. B., Frieler, K., Knutti, R., et al. (2009). Greenhouse-gas emission targets for limiting global warming to 2°C. *Nature* 458, 1158–1162. doi:10.1038/nature08017.

Melillo, J. M., Butler, S., Johnson, J., Mohan, J., Steudler, P., Lux, H., et al. (2011). Soil warming, carbon-nitrogen interactions, and forest carbon budgets. *Proc. Natl. Acad. Sci.* 108, 9508–9512. doi:10.1073/pnas.1018189108.

Melillo, J. M., Frey, S. D., DeAngelis, K. M., Werner, W. J., Bernard, M. J., Bowles, F. P., et al. (2017). Long-term pattern and magnitude of soil carbon feedback to the climate system in a warming world. *Science (80-.).* 358, 101–105. doi:10.1126/science.aan2874.

Melton, J. R., Wania, R., Hodson, E. L., Poulter, B., Ringeval, B., Spahni, R., et al. (2013). Present state of global wetland extent and wetland methane modelling: conclusions from a model inter-comparison project (WETCHIMP). *Biogeosciences* 10, 753–788. doi:10.5194/bg-10-753-2013.

Mengis, N., Partanen, A.-I., Jalbert, J., and Matthews, H. D. (2018). 1.5 °C carbon budget dependent on carbon cycle uncertainty and future non-CO2 forcing. *Sci. Rep.* 8, 5831. doi:10.1038/s41598-018-24241-1.

Menviel, L., and Joos, F. (2012). Toward explaining the Holocene carbon dioxide and carbon isotope records: Results from transient ocean carbon cycle-climate simulations. *Paleoceanography* 27, PA1207. doi:10.1029/2011PA002224.

Mercado, L. M., Bellouin, N., Sitch, S., Boucher, O., Huntingford, C., Wild, M., et al. (2009). Impact of changes in diffuse radiation on the global land carbon sink. *Nature* 458, 1014–1017. doi:10.1038/nature07949.

Mercado, L. M., Medlyn, B. E., Huntingford, C., Oliver, R. J., Clark, D. B., Sitch, S., et al. (2018). Large sensitivity in land carbon storage due to geographical and temporal variation in the thermal response of photosynthetic capacity. *New Phytol.* 218, 1462–1477. doi:10.1111/nph.15100.

Merlivat, L., Boutin, J., Antoine, D., Beaumont, L., Golbol, M., and Vellucci, V. (2018). Increase of dissolved inorganic carbon and decrease in pH in near-surface waters in the Mediterranean Sea during the past two decades. *Biogeosciences* 15, 5653–5662. doi:10.5194/bg-15-5653-2018.

Midorikawa, T., Inoue, H. Y., Ishii, M., Sasano, D., Kosugi, N., Hashida, G., et al. (2012). Decreasing pH trend estimated from 35-year time series of carbonate parameters in the Pacific sector of the Southern Ocean in summer. *Deep Sea Res. Part I Oceanogr. Res. Pap.* 61, 131–139. doi:10.1016/j.dsr.2011.12.003.

Midorikawa, T., Ishii, M., Saito, S., Sasano, D., Kosugi, N., Motoi, T., et al. (2010). Decreasing pH trend estimated from 25-yr time series of carbonate parameters in the western North Pacific. *Tellus B Chem. Phys. Meteorol.* 62, 649–659. doi:10.1111/j.1600-0889.2010.00474.x.

Millar, R. J., and Friedlingstein, P. (2018). The utility of the historical record for assessing the transient climate response to cumulative emissions. *Philos. Trans. R. Soc. A Math. Phys. Eng. Sci.* 376, 20160449. doi:10.1098/rsta.2016.0449.

Millar, R. J., Fuglestvedt, J. S., Friedlingstein, P., Rogelj, J., Grubb, M. J., Matthews, H. D., et al. (2017). Emission budgets and pathways consistent with limiting warming to 1.5 °C. *Nat. Geosci.* 10, 741–747. doi:10.1038/ngeo3031.

Minschwaner, K., Salawitch, R. J., and McElroy, M. B. (1993). Absorption of solar radiation by O2 : Implications for O3 and lifetimes of N2O, CFCl3 , and CF2Cl2. *J. Geophys. Res.* 98, 10543. doi:10.1029/93JD00223.

Moffitt, S. E., Hill, T. M., Roopnarine, P. D., and Kennett, J. P. (2015). Response of seafloor ecosystems to abrupt global climate change. *Proc. Natl. Acad. Sci.* 112, 4684–4689. doi:10.1073/pnas.1417130112.

Molari, M., Guilini, K., Lott, C., Weber, M., de Beer, D., Meyer, S., et al. (2018). CO 2 leakage alters biogeochemical and ecological functions of submarine sands. *Sci. Adv.* 4, eaao2040. doi:10.1126/sciadv.aao2040.

Mongwe, N. P., Chang, N., and Monteiro, P. M. S. (2016). The seasonal cycle as a mode to diagnose biases in modelled CO2 fluxes in the Southern Ocean. *Ocean Model.* 106, 90–103. doi:10.1016/j.ocemod.2016.09.006.

Mongwe, N. P., Vichi, M., and Monteiro, P. M. S. (2018). The seasonal cycle of <i>p</i>CO₂ and CO₂ fluxes in the Southern Ocean: diagnosing anomalies in CMIP5 Earth system models. *Biogeosciences* 15, 2851–2872. doi:10.5194/bg-15-2851-2018.

Monnin, E. (2001). Atmospheric CO2 Concentrations over the Last Glacial Termination. *Science (80-.).* 291, 112–114. doi:10.1126/science.291.5501.112.

Mora, C., Wei, C.-L., Rollo, A., Amaro, T., Baco, A. R., Billett, D., et al. (2013). Biotic and Human Vulnerability to Projected Changes in Ocean Biogeochemistry over the 21st Century. *PLoS Biol.* 11, e1001682. doi:10.1371/journal.pbio.1001682.

Moreno, A. R., Hagstrom, G. I., Primeau, F. W., Levin, S. A., and Martiny, A. C. (2018). Marine phytoplankton stoichiometry mediates nonlinear interactions between nutrient supply, temperature, and atmospheric CO2. *Biogeosciences* 15, 2761–2779. doi:10.5194/bg-15-2761-2018.

Murata, A., and Saito, S. (2012). Decadal changes in the CaCO3 saturation state along 179°E in the Pacific Ocean. *Geophys. Res. Lett.* 39, n/a-n/a. doi:10.1029/2012GL052297.

Murray, R. H., Erler, D. V, and Eyre, B. D. (2015). Nitrous oxide fluxes in estuarine environments: response to global change. *Glob. Chang. Biol.* 21, 3219–3245. doi:10.1111/gcb.12923.

Nakano, H., Ishii, M., Rodgers, K. B., Tsujino, H., and Yamanaka, G. (2015). Anthropogenic CO 2 uptake, transport, storage, and dynamical controls in the ocean imposed by the meridional overturning circulation: A modeling study. *Global Biogeochem. Cycles* 29, 1706–1724. doi:10.1002/2015GB005128.

Naqvi, S. W. A., Bange, H. W., Farías, L., Monteiro, P. M. S., Scranton, M. I., and Zhang, J. (2010). Marine hypoxia/anoxia as a source of CH_4 and N_2O. *Biogeosciences* 7, 2159–2190. doi:10.5194/bg-7-2159-2010.

Natchimuthu, S., Wallin, M. B., Klemedtsson, L., and Bastviken, D. (2017). Spatio-temporal patterns of stream methane and carbon dioxide emissions in a hemiboreal catchment in Southwest Sweden. *Sci. Rep.* 7, 39729. doi:10.1038/srep39729.

National Academies of Sciences and Medicine, E. (2019). *Negative Emissions Technologies and Reliable Sequestration*. Washington, D.C.: National Academies Press doi:10.17226/25259.

Naudts, K., Chen, Y., McGrath, M. J., Ryder, J., Valade, A., Otto, J., et al. (2016). Europes forest management did not mitigate climate warming. *Science (80-.).* 351, 597–600. doi:10.1126/science.aad7270.

Naus, S., Montzka, S. A., Pandey, S., Basu, S., Dlugokencky, E. J., and Krol, M. (2019). Constraints and biases in a tropospheric two-box model of OH. *Atmos. Chem. Phys.* 19, 407–424. doi:10.5194/acp-19-407-2019.

Negrete-García, G., Lovenduski, N. S., Hauri, C., Krumhardt, K. M., and Lauvset, S. K. (2019). Sudden emergence of a shallow aragonite saturation horizon in the Southern Ocean. *Nat. Clim. Chang.* 9, 313–317. doi:10.1038/s41558-019-0418-8.

Nevison, C. D., Dlugokencky, E., Dutton, G., Elkins, J. W., Fraser, P., Hall, B., et al. (2011). Exploring causes of interannual variability in the seasonal cycles of tropospheric nitrous oxide. *Atmos. Chem. Phys.* 11, 3713–3730. doi:10.5194/acp-11-3713-2011.

Nevison, C. D., Lueker, T. J., and Weiss, R. F. (2004). Quantifying the nitrous oxide source from coastal upwelling. *Global Biogeochem. Cycles* 18, GB1018. doi:10.1029/2003GB002110.

Nevison, C. D., Mahowald, N. M., Weiss, R. F., and Prinn, R. G. (2007). Interannual and seasonal variability in atmospheric N2O. *Global Biogeochem. Cycles* 21, GB3017. doi:10.1029/2006GB002755.

Ni, X., and Groffman, P. M. (2018). Declines in methane uptake in forest soils. *Proc. Natl. Acad. Sci.* 115, 8587–8590. doi:10.1073/pnas.1807377115.

Nicely, J. M., Canty, T. P., Manyin, M., Oman, L. D., Salawitch, R. J., Steenrod, S. D., et al. (2018). Changes in Global Tropospheric OH Expected as a Result of Climate Change Over the Last Several Decades. *J. Geophys. Res. Atmos.* 123, 10,710-774,795. doi:doi:10.1029/2018JD028388.

Nickelsen, L., and Oschlies, A. (2015). Enhanced sensitivity of oceanic CO2 uptake to dust deposition by iron-light colimitation. *Geophys. Res. Lett.* 42, 492–499. doi:10.1002/2014GL062969.

Nisbet, E. G., Dlugokencky, E. J., Manning, M. R., Lowry, D., Fisher, R. E., France, J. L., et al. (2016). Rising atmospheric methane: 2007-2014 growth and isotopic shift. *Global Biogeochem. Cycles* 30, 1356–1370. doi:10.1002/2016GB005406.

Nisbet, E. G., Manning, M. R., Dlugokencky, E. J., Fisher, R. E., Lowry, D., Michel, S. E., et al. (2019). Very Strong Atmospheric Methane Growth in the 4 Years 2014–2017: Implications for the Paris Agreement. *Global Biogeochem. Cycles* 33, 2018GB006009. doi:10.1029/2018GB006009.

Norby, R. J., Warren, J. M., Iversen, C. M., Medlyn, B. E., and McMurtrie, R. E. (2010). CO2 enhancement of forest productivity constrained by limited nitrogen availability. *Proc. Natl. Acad. Sci.* 107, 19368–19373. doi:10.1073/pnas.1006463107.

O'Sullivan, M., Spracklen, D. V, Batterman, S., Arnold, S. R., Gloor, M., and Buermann, W. (2019). Have synergies between nitrogen deposition and atmospheric CO 2 driven the recent enhancement of the terrestrial carbon sink? *Global Biogeochem. Cycles* 33, 163–180. doi:10.1029/2018GB005922.

O'Neill, B. C., Tebaldi, C., van Vuuren, D. P., Eyring, V., Friedlingstein, P., Hurtt, G., et al. (2016). The Scenario Model Intercomparison Project (ScenarioMIP) for CMIP6. *Geosci. Model Dev.* 9, 3461–3482. doi:10.5194/gmd-9-3461-2016.

Oka, E., Qiu, B., Takatani, Y., Enyo, K., Sasano, D., Kosugi, N., et al. (2015). Decadal variability of Subtropical Mode Water subduction and its impact on biogeochemistry. *J. Oceanogr.* 71, 389–400. doi:10.1007/s10872-015-0300-x.

Oka, E., Yamada, K., Sasano, D., Enyo, K., Nakano, T., and Ishii, M. (2019). Remotely Forced Decadal Physical and Biogeochemical Variability of North Pacific Subtropical Mode Water Over the Last 40 Years. *Geophys. Res. Lett.* 46, 1555–1561. doi:10.1029/2018GL081330.

Olsen, A., Key, R. M., van Heuven, S., Lauvset, S. K., Velo, A., Lin, X., et al. (2016). The Global Ocean Data Analysis Project version 2 (GLODAPv2) – an internally consistent data product for the world ocean. *Earth Syst. Sci. Data* 8, 297–323. doi:10.5194/essd-8-297-2016.

Oo, A. Z., Sudo, S., Inubushi, K., Mano, M., Yamamoto, A., Ono, K., et al. (2018). Methane and nitrous oxide emissions from conventional and modified rice cultivation systems in South India. *Agric. Ecosyst. Environ.* 252, 148–158. doi:10.1016/j.agee.2017.10.014.

Oschlies, A. (2010). Climate engineering by artificial ocean upwelling: channelling the sorcerer's apprentice. *Geophys. Res. Lett.* 37.

Oschlies, A., Brandt, P., Stramma, L., and Schmidtko, S. (2018). Drivers and mechanisms of ocean deoxygenation. *Nat. Geosci.* 11, 467–473. doi:10.1038/s41561-018-0152-2.

Oschlies, A., Koeve, W., Rickels, W., and Rehdanz, K. (2010a). Side effects and accounting aspects of hypothetical large-scale Southern Ocean iron fertilization. *Biogeosciences* 7, 4017–4035. doi:10.5194/bg-7-4017-2010.

Oschlies, A., Pahlow, M., Yool, A., and Matear, R. J. (2010b). Climate engineering by artificial ocean upwelling: Channelling the sorcerer's apprentice. *Geophys. Res. Lett.* 37, L04701. doi:10.1029/2009GL041961.

P. Ciais, J. Tan, X. Wang, C. Roedenbeck, F. Chevallier, S. Piao, R. Moriarty, G. Broquet, C. Le Quéré, J. Canadell, S. Peng, B. Poulter, Z. Liu, P. T. (2019). Five decades of northern land carbon uptake revealed by the interhemispheric CO2 gradient. *Nature*. doi:10.1038/s41586-019-1078-6.

Pälike, C., Delaney, M. L., and Zachos, J. C. (2014). Deep-sea redox across the Paleocene-Eocene thermal maximum. *Geochemistry, Geophys. Geosystems* 15, 1038–1053. doi:10.1002/2013GC005074.

Panchuk, K., Ridgwell, A., and Kump, L. R. (2008). Sedimentary response to Paleocene-Eocene Thermal Maximum carbon release: A model-data comparison. *Geology* 36, 315. doi:10.1130/G24474A.1.

Pangala, S. R., Enrich-Prast, A., Basso, L. S., Peixoto, R. B., Bastviken, D., Hornibrook, E. R. C., et al. (2017). Large emissions from floodplain trees close the Amazon methane budget. *Nature* 552, 230–234. doi:10.1038/nature24639.

Park, S., Croteau, P., Boering, K. A., Etheridge, D. M., Ferretti, D., Fraser, P. J., et al. (2012). Trends and seasonal cycles in the isotopic composition of nitrous oxide since 1940. *Nat. Geosci.* 5, 261–265. doi:10.1038/ngeo1421.

Patra, P. K., Saeki, T., Dlugokencky, E. J., Ishijima, K., Umezawa, T., Ito, A., et al. (2016). Regional methane emission estimation based on observed atmospheric concentrations (2002-2012). *J. Meteorol. Soc. Japan* 94. doi:10.2151/jmsj.2016-006..

Pau, S., Detto, M., Kim, Y., and Still, C. J. (2018). Tropical forest temperature thresholds for gross primary productivity. *Ecosphere* 9, e02311. doi:10.1002/ecs2.2311.

Paulmier, A., and Ruiz-Pino, D. (2009). Oxygen minimum zones (OMZs) in the modern ocean. *Prog. Oceanogr.* 80, 113–128. doi:10.1016/j.pocean.2008.08.001.

Paulsen, H., Ilyina, T., Six, K. D., and Stemmler, I. (2017). Incorporating a prognostic representation of marine nitrogen fixers into the global ocean biogeochemical model HAMOCC. *J. Adv. Model. Earth Syst.* 9, 438–464. doi:10.1002/2016MS000737.

Paustian, K., Lehmann, J., Ogle, S., Reay, D., Robertson, G. P., and Smith, P. (2016). Climate-smart soils. *Nature* 532, 49–57. doi:10.1038/nature17174.

Pavlov, I. N. (2015). Biotic and abiotic factors as causes of coniferous forests dieback in Siberia and Far East. *Contemp. Probl. Ecol.* 8, 440–456. doi:10.1134/S1995425515040125.

Pelejero, C. (2005). Preindustrial to Modern Interdecadal Variability in Coral Reef pH. *Science (80-.).* 309, 2204–2207. doi:10.1126/science.1113692.

Peng, S., Piao, S., Bousquet, P., Ciais, P., Li, B., Lin, X., et al. (2016). Inventory of anthropogenic methane emissions in mainland China from 1980 to 2010. *Atmos. Chem. Phys.* 16, 14545–14562. doi:10.5194/acp-16-14545-2016.

Penman, D. E., Hönisch, B., Zeebe, R. E., Thomas, E., and Zachos, J. C. (2014). Rapid and sustained surface ocean acidification during the Paleocene-Eocene Thermal Maximum. *Paleoceanography* 29, 357–369. doi:10.1002/2014PA002621.

Pépin, L., Raynaud, D., Barnola, J.-M., and Loutre, M. F. (2001). Hemispheric roles of climate forcings during glacial-interglacial transitions as deduced from the Vostok record and LLN-2D model experiments. *J. Geophys. Res. Atmos.* 106, 31885–31892. doi:10.1029/2001JD900117.

Pérez-Ramírez, J., Kapteijn, F., Schöffel, K., and Moulijn, J. . (2003). Formation and control of N2O in nitric acid production. *Appl. Catal. B Environ.* 44, 117–151. doi:10.1016/S0926-3373(03)00026-2.

Perez, F. F., Fontela, M., García-Ibáñez, M. I., Mercier, H., Velo, A., Lherminier, P., et al. (2018). Meridional overturning circulation conveys fast acidification to the deep Atlantic Ocean. *Nature* 554, 515–518. doi:10.1038/nature25493.

Pérez, F. F., Mercier, H., Vázquez-Rodríguez, M., Lherminier, P., Velo, A., Pardo, P. C., et al. (2013). Atlantic Ocean CO2 uptake reduced by weakening of the meridional overturning circulation. *Nat. Geosci.* 6, 146–152. doi:10.1038/ngeo1680.

Peters, G. P., Marland, G., Le Quéré, C., Boden, T., Canadell, J. G., and Raupach, M. R. (2012). Rapid growth in CO2 emissions after the 2008–2009 global financial crisis. *Nat. Clim. Chang.* 2, 2–4. doi:10.1038/nclimate1332.

Peterson, C. D., Lisiecki, L. E., and Stern, J. V. (2014). Deglacial whole-ocean δ 13 C change estimated from 480 benthic foraminiferal records. *Paleoceanography* 29, 549–563. doi:10.1002/2013PA002552.

Petit, J. R., Jouzel, J., Raynaud, D., Barkov, N. I., Barnola, J.-M., Basile, I., et al. (1999). Climate and atmospheric history of the past 420,000 years from the Vostok ice core, Antarctica. *Nature* 399, 429–436. doi:10.1038/20859.

Petrenko, V. V, Smith, A. M., Schaefer, H., Riedel, K., Brook, E., Baggenstos, D., et al. (2017). Minimal geological methane emissions during the Younger Dryas–Preboreal abrupt warming event. *Nature* 548, 443–446. doi:10.1038/nature23316.

Peylin, P., Law, R. M., Gurney, K. R., Chevallier, F., Jacobson, A. R., Maki, T., et al. (2013). Global atmospheric carbon budget: results from an ensemble of atmospheric CO2 inversions. *Biogeosciences* 10, 6699–6720. doi:10.5194/bg-10-6699-2013.

Pfleiderer, P., Schleussner, C.-F., Mengel, M., and Rogelj, J. (2018). Global mean temperature indicators linked to warming levels avoiding climate risks. *Environ. Res. Lett.* 13, 064015. doi:10.1088/1748-9326/aac319.

Pham-Duc, B., Prigent, C., Aires, F., and Papa, F. (2017). Comparisons of Global Terrestrial Surface Water Datasets over 15 Years. *J. Hydrometeorol.* 18, 993–1007. doi:10.1175/JHM-D-16-0206.1.

Piao, S., Huang, M., Liu, Z., Wang, X., Ciais, P., Canadell, J. G., et al. (2018a). Lower land-use emissions responsible for increased net land carbon sink during the slow warming period. *Nat. Geosci.* 11, 739–743. doi:10.1038/s41561-018-0204-7.

Piao, S., Huang, M., Liu, Z., Wang, X., Ciais, P., Canadell, J. G., et al. (2018b). Lower land-use emissions responsible for increased net land carbon sink during the slow warming period. *Nat. Geosci.* 11, 739–743. doi:10.1038/s41561-018-0204-7.

Piao, S., Liu, Z., Wang, T., Peng, S., Ciais, P., Huang, M., et al. (2017). Weakening temperature control on the interannual variations of spring carbon uptake across northern lands. *Nat. Clim. Chang.* 7, 359–363. doi:10.1038/nclimate3277.

Piao, S., Liu, Z., Wang, Y., Ciais, P., Yao, Y., Peng, S., et al. (2018c). On the causes of trends in the seasonal amplitude of atmospheric CO2. *Glob. Chang. Biol.* 24, 608–616. doi:10.1111/gcb.13909.

Piao, S., Sitch, S., Ciais, P., Friedlingstein, P., Peylin, P., Wang, X., et al. (2013). Evaluation of terrestrial carbon cycle models for their response to climate variability and to CO 2 trends. *Glob. Chang. Biol.* 19, 2117–2132. doi:10.1111/gcb.12187.

Pison, I., Ringeval, B., Bousquet, P., Prigent, C., and Papa, F. (2013). Stable atmospheric methane in the 2000s: key-role of emissions from natural wetlands. *Atmos. Chem. Phys.* 13, 11609–11623. doi:10.5194/acp-13-11609-2013.

Poeplau, C., and Don, A. (2015). Carbon sequestration in agricultural soils via cultivation of cover crops – A meta-analysis. *Agric. Ecosyst. Environ.* 200, 33–41. doi:10.1016/j.agee.2014.10.024.

Pongratz, J., Dolman, H., Don, A., Erb, K.-H., Fuchs, R., Herold, M., et al. (2018a). Models meet data: Challenges and opportunities in implementing land management in Earth system models. *Glob. Chang. Biol.* 24, 1470–1487. doi:10.1111/gcb.13988.

Pongratz, J., Dolman, H., Don, A., Erb, K.-H., Fuchs, R., Herold, M., et al. (2018b). Models meet data: Challenges and opportunities in implementing land management in Earth system models. *Glob. Chang. Biol.* 24, 1470–1487. doi:10.1111/gcb.13988.

Pongratz, J., Reick, C. H., Houghton, R. A., and House, J. I. (2014). Terminology as a key uncertainty in net land use and land cover change carbon flux estimates. *Earth Syst. Dyn.* 5, 177–195. doi:10.5194/esd-5-177-2014.

Pongratz, J., Reick, C. H., Raddatz, T., and Claussen, M. (2010). Biogeophysical versus biogeochemical climate response to historical anthropogenic land cover change. *Geophys. Res. Lett.* 37, L08702. doi:10.1029/2010GL043010.

Poulter, B., Bousquet, P., Canadell, J. G., Ciais, P., Peregon, A., Saunois, M., et al. (2017). Global wetland contribution to 2000–2012 atmospheric methane growth rate dynamics. *Environ. Res. Lett.* 12, 094013. doi:10.1088/1748-9326/aa8391.

Poulter, B., Frank, D., Ciais, P., Myneni, R. B., Andela, N., Bi, J., et al. (2014). Contribution of semi-arid ecosystems to interannual variability of the global carbon cycle. *Nature* 509, 600–603. doi:10.1038/nature13376.

Praetorius, S. K., Mix, A. C., Walczak, M. H., Wolhowe, M. D., Addison, J. A., and Prahl, F. G. (2015). North Pacific deglacial hypoxic events linked to abrupt ocean warming. *Nature* 527, 362–366. doi:10.1038/nature15753.

Prather, M. J., Hsu, J., DeLuca, N. M., Jackman, C. H., Oman, L. D., Douglass, A. R., et al. (2015). Measuring and modeling the lifetime of nitrous oxide including its variability. *J. Geophys. Res. Atmos.* 120, 5693–5705. doi:10.1002/2015JD023267.

Prinn, R. G., Weiss, R. F., Fraser, P. J., Simmonds, P. G., Cunnold, D. M., Alyea, F. N., et al. (2000). A history of chemically and radiatively important gases in air deduced from ALE/GAGE/AGAGE. *J. Geophys. Res. Atmos.* 105, 17751–17792. doi:10.1029/2000JD900141.

Prinn, R. G., Weiss, R. F., Krummel, P. B., O'Doherty, S., Fraser, P. J., Muhle, J., et al. (2016). The ALE / GAGE AGAGE Network.

Proctor, J., Hsiang, S., Burney, J., Burke, M., and Schlenker, W. (2018). Estimating global agricultural effects of geoengineering using volcanic eruptions. *Nature* 560, 480–483. doi:10.1038/s41586-018-0417-3.

Prokopiou, M., Martinerie, P., Sapart, C. J., Witrant, E., Monteil, G., Ishijima, K., et al. (2017). Constraining N₂O emissions since 1940 using firn air isotope measurements in both hemispheres. *Atmos. Chem. Phys.* 17, 4539–4564. doi:10.5194/acp-17-4539-2017.

Pugh, T. A. M., Lindeskog, M., Smith, B., Poulter, B., Arneth, A., Haverd, V., et al. (2019). Role of forest regrowth in global carbon sink dynamics. *Proc. Natl. Acad. Sci.* 116, 4382–4387. doi:10.1073/pnas.1810512116.

Qi, D., Chen, L., Chen, B., Gao, Z., Zhong, W., Feely, R. A., et al. (2017). Increase in acidifying water in the western Arctic Ocean. *Nat. Clim. Chang.* 7, 195–199. doi:10.1038/nclimate3228.

Qian, W., Dai, M., Xu, M., Kao, S., Du, C., Liu, J., et al. (2017). Non-local drivers of the summer hypoxia in the East China Sea off the Changjiang Estuary. *Estuar. Coast. Shelf Sci.* 198, 393–399. doi:10.1016/j.ecss.2016.08.032.

Quéré, C. Le, Andrew, R. M., Friedlingstein, P., Sitch, S., Hauck, J., Pickers, P., et al. Submitted paper . Do not cite or quote . Global Carbon Budget 2018 Submitted paper . Do not cite or quote .

Quéré, C. Le, Andrew, R. M., Friedlingstein, P., Sitch, S., Hauck, J., Pongratz, J., et al. (2018). Global Carbon Budget 2018. *Earth Syst. Sci. Data* (submitted.

Rabalais, N., Cai, W.-J., Carstensen, J., Conley, D., Fry, B., Hu, X., et al. (2014). Eutrophication-Driven Deoxygenation in the Coastal Ocean. *Oceanography* 27, 172–183. doi:10.5670/oceanog.2014.21.

Rae, J. W. B., Burke, A., Robinson, L. F., Adkins, J. F., Chen, T., Cole, C., et al. (2018). CO2 storage and release in the deep Southern Ocean on millennial to centennial timescales. *Nature* 562, 569–573. doi:10.1038/s41586-018-0614-0.

Randerson, J. T., Lindsay, K., Munoz, E., Fu, W., Moore, J. K., Hoffman, F. M., et al. (2015). Multicentury changes in ocean and land contributions to the climate-carbon feedback. *Global Biogeochem. Cycles* 29, 744–759. doi:10.1002/2014GB005079.

Rau, G. H. (2014). "Enhancing the Ocean's Role in CO2 Mitigation," in *Global Environmental Change*, ed. B. Freedman (Dordrecht: Springer Netherlands), 817–824. doi:10.1007/978-94-007-5784-4_54.

Ravishankara, A. R., Daniel, J. S., and Portmann, R. W. (2009). Nitrous Oxide (N2O): The Dominant Ozone-Depleting Substance Emitted in the 21st Century. *Science (80-.).* 326, 123–125. doi:10.1126/science.1176985.

Raynaud, D., Barnola, J.-M., Souchez, R., Lorrain, R., Petit, J.-R., Duval, P., et al. (2005). The record for marine isotopic stage 11. *Nature* 436, 39–40. doi:10.1038/43639b.

Rayner, P. J., Stavert, A., Scholze, M., Ahlström, A., Allison, C. E., and Law, R. M. (2015). Recent changes in the global and regional carbon cycle: analysis of first-order diagnostics. *Biogeosciences* 12, 835–844. doi:10.5194/bg-12-835-2015.

Regnier, P., Friedlingstein, P., Ciais, P., Mackenzie, F. T., Gruber, N., Janssens, I. A., et al. (2013). Anthropogenic perturbation of the carbon fluxes from land to ocean. *Nat. Geosci.* 6, 597–607. doi:10.1038/ngeo1830.

Reich, P. B., and Hobbie, S. E. (2013). Decade-long soil nitrogen constraint on the CO2 fertilization of plant biomass. *Nat. Clim. Chang.* 3, 278–282. doi:10.1038/nclimate1694.

Renforth, P., and Henderson, G. (2017). Assessing ocean alkalinity for carbon sequestration. *Rev. Geophys.* 55, 636–674. doi:10.1002/2016RG000533.

Resplandy, L., Keeling, R. F., Rödenbeck, C., Stephens, B. B., Khatiwala, S., Rodgers, K. B., et al. (2018). Revision of global carbon fluxes based on a reassessment of oceanic and riverine carbon transport. *Nat. Geosci.* 11, 504–509. doi:10.1038/s41561-018-0151-3.

REVELLE, R., and SUESS, H. E. (1957). Carbon Dioxide Exchange Between Atmosphere and Ocean and the Question of an Increase of Atmospheric CO 2 during the Past Decades. *Tellus* 9, 18–27. doi:10.1111/j.2153-3490.1957.tb01849.x.

Rice, A. L., Butenhoff, C. L., Teama, D. G., Röger, F. H., Khalil, M. A. K., and Rasmussen, R. A. (2016). Atmospheric methane isotopic record favors fossil sources flat in 1980s and 1990s with recent increase. *Proc. Natl. Acad. Sci.* 113, 10791–10796. doi:10.1073/pnas.1522923113.

Richardson, M., Cowtan, K., and Millar, R. J. (2018). Global temperature definition affects achievement of long-term climate goals. *Environ. Res. Lett.* 13, 054004. doi:10.1088/1748-9326/aab305.

Ricke, K. L., and Caldeira, K. (2014). Maximum warming occurs about one decade after a carbon dioxide emission. *Environ. Res. Lett.* 9, 124002. doi:10.1088/1748-9326/9/12/124002.

Ridgwell, A., and Schmidt, D. N. (2010). Past constraints on the vulnerability of marine calcifiers to massive carbon dioxide release. *Nat. Geosci.* 3, 196–200. doi:10.1038/ngeo755.

Ridgwell, A., Zondervan, I., Hargreaves, J. C., Bijma, J., and Lenton, T. M. (2007). Assessing the potential long-term increase of oceanic fossil fuel CO2 uptake due to CO2-calcification feedback. *Biogeosciences* 4, 481–492. doi:10.5194/bg-4-481-2007.

Rigby, M., Montzka, S. A., Prinn, R. G., White, J. W. C., Young, D., O'Doherty, S., et al. (2017). Role of atmospheric oxidation in recent methane growth. *Proc. Natl. Acad. Sci. U. S. A.* 114, 5373–5377. doi:10.1073/pnas.1616426114.

Ringeval, B., Friedlingstein, P., Koven, C., Ciais, P., de Noblet-Ducoudré, N., Decharme, B., et al. (2011). Climate-CH4 feedback from wetlands and its interaction with the climate-CO2 feedback. *Biogeosciences* 8, 2137–2157. doi:10.5194/bg-8-2137-2011.

Ríos, A. F., Resplandy, L., García-Ibáñez, M. I., Fajar, N. M., Velo, A., Padin, X. A., et al. (2015a). Decadal acidification in the water masses of the Atlantic Ocean. *Proc. Natl. Acad. Sci.* 112, 9950–9955. doi:10.1073/pnas.1504613112.

Robinson, C. (2019). Microbial Respiration, the Engine of Ocean Deoxygenation. *Front. Mar. Sci.* 5, 533. doi:10.3389/fmars.2018.00533.

Robinson, J., Popova, E. E., Yool, A., Srokosz, M., Lampitt, R. S., and Blundell, J. R. (2014). How deep is deep enough? Ocean iron fertilization and carbon sequestration in the Southern Ocean. *Geophys. Res. Lett.* 41, 2489–2495. doi:10.1002/2013GL058799.

Robinson, S. A. (2011). Shallow-water carbonate record of the Paleocene-Eocene Thermal Maximum from a Pacific Ocean guyot. *Geology* 39, 51–54. doi:10.1130/G31422.1.

Rödenbeck, C., Bakker, D. C. E., Gruber, N., Iida, Y., Jacobson, A. R., Jones, S., et al. (2015). Data-based estimates of the ocean carbon sink variability – first results of the Surface Ocean pCO2 Mapping intercomparison (SOCOM). *Biogeosciences* 12, 7251–7278. doi:10.5194/bg-12-7251-2015.

Rödenbeck, C., Bakker, D. C. E., Metzl, N., Olsen, A., Sabine, C., Cassar, N., et al. (2014). Interannual sea–air CO2 flux variability from an observation-driven ocean mixed-layer scheme. *Biogeosciences* 11, 4599–4613. doi:10.5194/bg-11-4599-2014.

Rödenbeck, C., Keeling, R. F., Bakker, D. C. E., Metzl, N., Olsen, A., Sabine, C., et al. (2013). Global surface-ocean pCO2 and sea–air CO2 flux variability from an observation-driven ocean mixed-layer. *Ocean Sci.* 9, 193–216. doi:10.5194/os-9-193-2013.

Rödenbeck, C., Zaehle, S., Keeling, R., and Heimann, M. (2018). History of El Niño impacts on the global carbon cycle 1957–2017: a quantification from atmospheric CO 2 data. *Philos. Trans. R. Soc. B Biol. Sci.* 373, 20170303. doi:10.1098/rstb.2017.0303.

Rodgers, K. B., and others No Title.

Rogelj, J., Meinshausen, M., and Knutti, R. (2012). Global warming under old and new scenarios using IPCC climate sensitivity range estimates. *Nat. Clim. Chang.* 2, 248–253. doi:10.1038/nclimate1385.

Rogelj, J., Meinshausen, M., Schaeffer, M., Knutti, R., and Riahi, K. (2015a). Impact of short-lived non-CO2 mitigation on carbon budgets for stabilizing global warming. *Environ. Res. Lett.* 10, 075001. doi:10.1088/1748-9326/10/7/075001.

Rogelj, J., Reisinger, A., McCollum, D. L., Knutti, R., Riahi, K., and Meinshausen, M. (2015b). Mitigation choices impact carbon budget size compatible with low temperature goals. *Environ. Res. Lett.* 10, 075003. doi:10.1088/1748-9326/10/7/075003.

Rogelj, J., Schaeffer, M., Friedlingstein, P., Gillett, N. P., van Vuuren, D. P., Riahi, K., et al. (2016). Differences between carbon budget estimates unravelled. *Nat. Clim. Chang.* 6, 245–252. doi:10.1038/nclimate2868.

Rogelj, J., Shindell, D., Jiang, K., Fifita, S., Forster, P., Ginzburg, V., et al. (2018). "Mitigation Pathways Compatible with 1.5°C in the Context of Sustainable Development," in *Global Warming of 1.5°C. An IPCC Special Report on the impacts of global warming of 1.5°C above pre-industrial levels and related global greenhouse gas emission pathways, in the context of strengthening the global response to the threat of climate change,* eds. V. Masson-Delmotte, P. Zhai, H.-O. Pörtner, D. Roberts, J. Skea, P. R. Shukla, et al. (In Press).

Rogers, K., Kelleway, J. J., Saintilan, N., Megonigal, J. P., Adams, J. B., Holmquist, J. R., et al. (2019). Wetland carbon storage controlled by millennial-scale variation in relative sea-level rise. *Nature* 567, 91–95. doi:10.1038/s41586-019-0951-7.

Rohling, E. J., Marino, G., Foster, G. L., Goodwin, P. A., von der Heydt, A. S., and Köhler, P. (2018). Comparing Climate Sensitivity, Past and Present. *Ann. Rev. Mar. Sci.* 10, 261–288. doi:10.1146/annurev-marine-121916-063242.

Rohling, E. J., Sluijs, A., Dijkstra, H. A., Köhler, P., Van De Wal, R. S. W., Von Der Heydt, A. S., et al. (2012). Making sense of palaeoclimate sensitivity. *Nature* 491, 683–691. doi:10.1038/nature11574.

Roobaert, A., Laruelle, G. G., Landschützer, P., and Regnier, P. (2018). Uncertainty in the global oceanic CO2 uptake induced by wind forcing: quantification and spatial analysis. *Biogeosciences* 15, 1701–1720. doi:10.5194/bg-15-1701-2018.

Rosentreter, J. A., Maher, D. T., Erler, D. V., Murray, R. H., and Eyre, B. D. (2018). Methane emissions partially offset "blue carbon" burial in mangroves. *Sci. Adv.* 4, eaao4985. doi:10.1126/sciadv.aao4985.

Ruddiman, W. F., Fuller, D. Q., Kutzbach, J. E., Tzedakis, P. C., Kaplan, J. O., Ellis, E. C., et al. (2016). Late Holocene climate: Natural or anthropogenic? *Rev. Geophys.* 54, 93–118. doi:10.1002/2015RG000503.

Ruppel, C. D., and Kessler, J. D. (2017). The interaction of climate change and methane hydrates. *Rev. Geophys.* 55, 126–168. doi:10.1002/2016RG000534.

Rysgaard, S., Søgaard, D. H., Cooper, M., Pućko, M., Lennert, K., Papakyriakou, T. N., et al. (2013). Ikaite crystal distribution in winter sea ice and implications for CO2 system dynamics. *Cryosph.* 7, 707–718. doi:10.5194/tc-7-707-2013.

Saatchi, S. S., Harris, N. L., Brown, S., Lefsky, M., Mitchard, E. T. A., Salas, W., et al. (2011). Benchmark map of forest carbon stocks in tropical regions across three continents. *Proc. Natl. Acad. Sci.* 108, 9899–9904. doi:10.1073/pnas.1019576108.

Saeki, T., and Patra, P. K. (2017). Implications of overestimated anthropogenic CO2 emissions on East Asian and global land CO2 flux inversion. *Geosci. Lett.* 4, 9. doi:10.1186/s40562-017-0074-7.

Saikawa, E., Prinn, R. G., Dlugokencky, E., Ishijima, K., Dutton, G. S., Hall, B. D., et al. (2014). Global and regional emissions estimates for N2O. *Atmos. Chem. Phys.* 14, 4617–4641. doi:10.5194/acp-14-4617-2014.

Sakaguchi, K., Zeng, X., Leung, L., and Shao, P. (2016). Influence of dynamic vegetation on carbon-nitrogen cycle feedback in the Community Land Model (CLM4). *Environ. Res. Lett.* 11, 124029. doi:10.1088/1748-9326/aa51d9.

Sakschewski, B., von Bloh, W., Boit, A., Poorter, L., Peña-Claros, M., Heinke, J., et al. (2016). Resilience of Amazon forests emerges from plant trait diversity. *Nat. Clim. Chang.* 6, 1032–1036. doi:10.1038/nclimate3109.

Sallée, J.-B., Matear, R. J., Rintoul, S. R., and Lenton, A. (2012). Localized subduction of anthropogenic carbon dioxide in the Southern Hemisphere oceans. *Nat. Geosci.* 5, 579–584. doi:10.1038/ngeo1523.

Salter, I., Schiebel, R., Ziveri, P., Movellan, A., Lampitt, R., and Wolff, G. A. (2014). Carbonate counter pump stimulated by natural iron fertilization in the Polar Frontal Zone. *Nat. Geosci.* 7, 885–889. doi:10.1038/ngeo2285.

Sanderman, J., Hengl, T., and Fiske, G. J. (2018). Correction for Sanderman et al., Soil carbon debt of 12,000 years of human land use. *Proc. Natl. Acad. Sci.* 115, E1700–E1700. doi:10.1073/pnas.1800925115.

Sarmiento, J. L., Gloor, M., Gruber, N., Beaulieu, C., Jacobson, A. R., Mikaloff Fletcher, S. E., et al. (2010). Trends and regional distributions of land and ocean carbon sinks. *Biogeosciences* 7, 2351–2367. doi:10.5194/bg-7-2351-2010.

Sarmiento, J. L., and Gruber, N. (2006). *Ocean Biogeochemical Dynamics*. Princenton, NJ, USA: Princenton University Press.

Sarnthein, M., Schneider, B., and Grootes, P. M. (2013). Peak glacial 14C ventilation ages suggest major draw-down of carbon into the abyssal ocean. *Clim. Past* 9, 2595–2614. doi:10.5194/cp-9-2595-2013.

Sasano, D., Takatani, Y., Kosugi, N., Nakano, T., Midorikawa, T., and Ishii, M. (2015). Multidecadal trends of oxygen and their controlling factors in the western North Pacific. *Global Biogeochem. Cycles* 29, 935–956. doi:10.1002/2014GB005065.

Sasano, D., Takatani, Y., Kosugi, N., Nakano, T., Midorikawa, T., and Ishii, M. (2018). Decline and Bidecadal Oscillations of Dissolved Oxygen in the Oyashio Region and Their Propagation to the Western North Pacific. *Global Biogeochem. Cycles* 32, 909–931. doi:10.1029/2017GB005876.

Sasse, T. P., McNeil, B. I., Matear, R. J., and Lenton, A. (2015). Quantifying the influence of CO2 seasonality on future aragonite undersaturation onset. *Biogeosciences* 12, 6017–6031. doi:10.5194/bg-12-6017-2015.

Saunders, K. M., Roberts, S. J., Perren, B., Butz, C., Sime, L., Davies, S., et al. (2018). Holocene dynamics of the Southern Hemisphere westerly winds and possible links to CO2 outgassing. *Nat. Geosci.* 11, 650–655. doi:10.1038/s41561-018-0186-5.

Saunois, M., Bousquet, P., Poulter, B., Peregon, A., Ciais, P., Canadell, J. G., et al. (2016a). The global methane budget 2000–2012. *Earth Syst. Sci. Data* 8, 697–751. doi:10.5194/essd-8-697-2016.

Saunois, M., Bousquet, P., Poulter, B., Peregon, A., Ciais, P., Canadell, J. G., et al. (2017). Variability and quasi-decadal changes in the methane budget over the period 2000-2012. *Atmos. Chem. Phys.* 17. doi:10.5194/acp-17-11135-2017.

Saunois, M., Jackson, R. B., Bousquet, P., Poulter, B., and Canadell, J. G. (2016b). The growing role of methane in anthropogenic climate change. *Environ. Res. Lett.* 11. doi:10.1088/1748-9326/11/12/120207.

Schädel, C., Bader, M. K.-F., Schuur, E. A. G., Biasi, C., Bracho, R., Čapek, P., et al. (2016). Potential carbon emissions dominated by carbon dioxide from thawed permafrost soils. *Nat. Clim. Chang.* 6, 950–953. doi:10.1038/nclimate3054.

Schädel, C., Schuur, E. A. G., Bracho, R., Elberling, B., Knoblauch, C., Lee, H., et al. (2014). Circumpolar assessment of permafrost C quality and its vulnerability over time using long-term incubation data. *Glob. Chang. Biol.* 20, 641–652. doi:10.1111/gcb.12417.

Schaefer, H., Fletcher, S. E. M., Veidt, C., Lassey, K. R., Brailsford, G. W., Bromley, T. M., et al. (2016). A 21st-century shift from fossil-fuel to biogenic methane emissions indicated by 13CH4. *Science (80-.).* 352, 80–84. doi:10.1126/science.aad2705.

Schaefer, K., Zhang, T., Bruhwiler, L., and Barrett, A. P. (2011). Amount and timing of permafrost carbon release in response to climate warming. *Tellus B* 63, 165–180. doi:10.1111/j.1600-0889.2011.00527.x.

Scheffer, M., Bascompte, J., Brock, W. A., Brovkin, V., Carpenter, S. R., Dakos, V., et al. (2009). Early-warning signals for critical transitions. *Nature* 461, 53–59. doi:10.1038/nature08227.

Scheffer, M., Hirota, M., Holmgren, M., Van Nes, E. H., and Chapin, F. S. (2012). Thresholds for boreal biome transitions. *Proc. Natl. Acad. Sci.* 109, 21384–21389. doi:10.1073/pnas.1219844110.

Schilt, A., Baumgartner, M., Blunier, T., Schwander, J., Spahni, R., Fischer, H., et al. (2010a). Glacial–interglacial and millennial-scale variations in the atmospheric nitrous oxide concentration during the last 800,000 years. *Quat. Sci. Rev.* 29, 182–192. doi:10.1016/j.quascirev.2009.03.011.

Schilt, A., Baumgartner, M., Schwander, J., Buiron, D., Capron, E., Chappellaz, J., et al. (2010b). Atmospheric nitrous oxide during the last 140,000years. *Earth Planet. Sci. Lett.* 300, 33–43. doi:10.1016/j.epsl.2010.09.027.

Schilt, A., Brook, E. J., Bauska, T. K., Baggenstos, D., Fischer, H., Joos, F., et al. (2014). Isotopic constraints on marine and terrestrial N2O emissions during the last deglaciation. *Nature* 516, 234–237. doi:10.1038/nature13971.

Schimel, D., Stephens, B. B., and Fisher, J. B. (2015). Effect of increasing CO2 on the terrestrial carbon cycle. *Proc. Natl. Acad. Sci. U. S. A.* 112, 436–441. doi:10.1073/pnas.1407302112.

Schlesinger, W. H. (2013). An estimate of the global sink for nitrous oxide in soils. *Glob. Chang. Biol.* 19, 2929–2931. doi:10.1111/gcb.12239.

Schmidt, M. W. I., Torn, M. S., Abiven, S., Dittmar, T., Guggenberger, G., Janssens, I. A., et al. (2011). Persistence of soil organic matter as an ecosystem property. *Nature* 478, 49–56. doi:10.1038/nature10386.

Schmidtko, S., Stramma, L., and Visbeck, M. (2017). Decline in global oceanic oxygen content during the past five decades. *Nature* 542, 335–339. doi:10.1038/nature21399.

Schmitt, J., Schneider, R., Elsig, J., Leuenberger, D., Lourantou, A., Chappellaz, J., et al. (2012). Carbon Isotope Constraints on the Deglacial CO2 Rise from Ice Cores. *Science (80-.).* 336, 711–714. doi:10.1126/science.1217161.

Schmittner, A., Oschlies, A., Matthews, H. D., and Galbraith, E. D. (2008). Future changes in climate, ocean circulation, ecosystems, and biogeochemical cycling simulated for a business-as-usual CO 2 emission scenario until year 4000 AD. *Global Biogeochem. Cycles* 22, GB1013. doi:10.1029/2007GB002953.

Schneider von Deimling, T., Grosse, G., Strauss, J., Schirrmeister, L., Morgenstern, A., Schaphoff, S., et al. (2015). Observation-based modelling of permafrost carbon fluxes with accounting for deep carbon deposits and thermokarst activity. *Biogeosciences* 12, 3469–3488. doi:10.5194/bg-12-3469-2015.

Schneider von Deimling, T., Meinshausen, M., Levermann, A., Huber, V., Frieler, K., Lawrence, D. M., et al. (2012). Estimating the near-surface permafrost-carbon feedback on global warming. *Biogeosciences* 9, 649–665. doi:10.5194/bg-9-649-2012.

Schuur, E. A. G., McGuire, A. D., Schädel, C., Grosse, G., Harden, J. W., Hayes, D. J., et al. (2015). Climate change and the permafrost carbon feedback. *Nature* 520, 171–179. doi:10.1038/nature14338.

Schuur, E. A. G., Vogel, J. G., Crummer, K. G., Lee, H., Sickman, J. O., and Osterkamp, T. E. (2009). The effect of permafrost thaw on old carbon release and net carbon exchange from tundra. *Nature* 459, 556–559. doi:10.1038/nature08031.

Schwietzke, S., Sherwood, O. A., Bruhwiler, L. M. P., Miller, J. B., Etiope, G., Dlugokencky, E. J., et al. (2016). Upward revision of global fossil fuel methane emissions based on isotope database. *Nature* 538, 88–91. doi:10.1038/nature19797.

Schwinger, J., Goris, N., Tjiputra, J. F., Kriest, I., Bentsen, M., Bethke, I., et al. (2016). Evaluation of NorESM-OC (versions 1 and 1.2), the ocean carbon-cycle stand-alone configuration of the Norwegian Earth System Model (NorESM1). *Geosci. Model Dev.* 9, 2589–2622. doi:10.5194/gmd-9-2589-2016.

Scott, V., Haszeldine, R. S., Tett, S. F. B., and Oschlies, A. (2015). Fossil fuels in a trillion tonne world. *Nat. Clim. Chang.* 5, 419–423. doi:10.1038/nclimate2578.

Seitzinger, S. P., Kroeze, C., and Styles, R. V (2000). Global distribution of N2O emissions from aquatic systems: natural emissions and anthropogenic effects. *Chemosph. - Glob. Chang. Sci.* 2, 267–279. doi:10.1016/S1465-9972(00)00015-5.

Seki, O., Foster, G. L., Schmidt, D. N., Mackensen, A., Kawamura, K., and Pancost, R. D. (2010). Alkenone and boron-based Pliocene pCO2 records. *Earth Planet. Sci. Lett.* 292, 201–211. doi:10.1016/j.epsl.2010.01.037.

Seshadri, A. K. (2017). Origin of path independence between cumulative CO2 emissions and global warming. *Clim. Dyn.* 49, 3383–3401. doi:10.1007/s00382-016-3519-3.

Shakhova, N., Semiletov, I., Gustafsson, O., Sergienko, V., Lobkovsky, L., Dudarev, O., et al. (2017). Current rates and mechanisms of subsea permafrost degradation in the East Siberian Arctic Shelf. *Nat. Commun.* 8, 15872. doi:10.1038/ncomms15872.

Shakhova, N., Semiletov, I., Salyuk, A., Yusupov, V., Kosmach, D., and Gustafsson, O. (2010). Extensive Methane Venting to the Atmosphere from Sediments of the East Siberian Arctic Shelf. *Science (80-.).* 327, 1246–1250. doi:10.1126/science.1182221.

Shcherbak, I., Millar, N., and Robertson, G. P. (2014). Global metaanalysis of the nonlinear response of soil nitrous oxide (N2O) emissions to fertilizer nitrogen. *Proc. Natl. Acad. Sci.* 111, 9199–9204. doi:10.1073/pnas.1322434111.

Shen, Q., Hedley, M., Camps Arbestain, M., and Kirschbaum, M. U. . (2016). Can biochar increase the bioavailability of phosphorus? *J. soil Sci. plant Nutr.* 16. doi:10.4067/S0718-95162016005000022.

Shepherd, J. G. (2012). Geoengineering the climate: an overview and update. *Philos. Trans. R. Soc. A Math. Phys. Eng. Sci.* 370, 4166–4175. doi:10.1098/rsta.2012.0186.

Shinjo, R., Asami, R., Huang, K.-F., You, C.-F., and Iryu, Y. (2013). Ocean acidification trend in the tropical North Pacific since the mid-20th century reconstructed from a coral archive. *Mar. Geol.* 342, 58–64. doi:10.1016/j.margeo.2013.06.002.

Siegenthaler, U., Stocker, T. F., Monnin, E., Lüthi, D., Schwander, J., Stauffer, B., et al. (2005). EPICA Dome C carbon dioxide concentrations from 650 to 391 kyr BP. *PANGEA*. doi:10.1594/PANGAEA.728136.

Sigman, D. M., and Boyle, E. A. (2000). Glacial/interglacial variations in atmospheric carbon dioxide. *Nature* 407, 859–869. doi:10.1038/35038000.

Sigman, D. M., Jaccard, S. L., and Haug, G. H. (2004). Polar ocean stratification in a cold climate. *Nature* 428, 59–63. doi:10.1038/nature02357.

Simmons, C. T., and Matthews, H. D. (2016). Assessing the implications of human land-use change for the transient climate response to cumulative carbon emissions. *Environ. Res. Lett.* 11, 035001. doi:10.1088/1748-9326/11/3/035001.

Simpson, I. J., Sulbaek Andersen, M. P., Meinardi, S., Bruhwiler, L., Blake, N. J., Helmig, D., et al. (2012). Long-term decline of global atmospheric ethane concentrations and implications for methane. *Nature* 488, 490–494. doi:10.1038/nature11342.

Sitch, S., Friedlingstein, P., Gruber, N., Jones, S. D., Murray-Tortarolo, G., Ahlström, A., et al. (2015). Recent trends and drivers of regional sources and sinks of carbon dioxide. *Biogeosciences* 12, 653–679. doi:10.5194/bg-12-653-2015.

Skinner, L. C., Fallon, S., Waelbroeck, C., Michel, E., and Barker, S. (2010). Ventilation of the Deep Southern Ocean and Deglacial CO2 Rise. *Science (80-.).* 328, 1147–1151. doi:10.1126/science.1183627.

Skinner, L. C., Primeau, F., Freeman, E., de la Fuente, M., Goodwin, P. A., Gottschalk, J., et al. (2017). Radiocarbon constraints on the glacial ocean circulation and its impact on atmospheric CO2. *Nat. Commun.* 8, 16010. doi:10.1038/ncomms16010.

Skinner, L., McCave, I. N., Carter, L., Fallon, S., Scrivner, A. E., and Primeau, F. (2015). Reduced ventilation and enhanced magnitude of the deep Pacific carbon pool during the last glacial period. *Earth Planet. Sci. Lett.* 411, 45–52. doi:10.1016/j.epsl.2014.11.024.

Sluijs, A., Schouten, S., Pagani, M., Woltering, M., Brinkhuis, H., Damsté, J. S. S., et al. (2006). Subtropical Arctic Ocean temperatures during the Palaeocene/Eocene thermal maximum. *Nature* 441, 610–613. doi:10.1038/nature04668.

Smale, D. A., Wernberg, T., Oliver, E. C. J., Thomsen, M., Harvey, B. P., Straub, S. C., et al. (2019). Marine heatwaves threaten global biodiversity and the provision of ecosystem services. *Nat. Clim. Chang.* 9, 306–312. doi:10.1038/s41558-019-0412-1.

Smetacek, V., Klaas, C., Strass, V. H., Assmy, P., Montresor, M., Cisewski, B., et al. (2012). Deep carbon export from a Southern Ocean iron-fertilized diatom bloom. *Nature* 487, 313–319. doi:10.1038/nature11229.

Smith, C. J., Forster, P. M., Allen, M., Fuglestvedt, J., Millar, R. J., Rogelj, J., et al. (2019). Current fossil fuel infrastructure does not yet commit us to 1.5 °C warming. *Nat. Commun.* 10, 101. doi:10.1038/s41467-018-07999-w.

Smith, C. J., Forster, P. M., Allen, M., Leach, N., Millar, R. J., Passerello, G. A., et al. (2018a). FAIR v1.3: a simple emissions-based impulse response and carbon cycle model. *Geosci. Model Dev.* 11, 2273–2297. doi:10.5194/gmd-11-2273-2018.

Smith, D. R., Townsend, T. J., Choy, A. W. K., Hardy, I. C. W., and Sjögersten, S. (2012a). Short-term soil carbon sink potential of oil palm plantations. *GCB Bioenergy* 4, 588–596. doi:10.1111/j.1757-1707.2012.01168.x.

Smith, P. (2016). Soil carbon sequestration and biochar as negative emission technologies. *Glob. Chang. Biol.* 22, 1315–1324. doi:10.1111/gcb.13178.

Smith, P., Davis, S. J., Creutzig, F., Fuss, S., Minx, J., Gabrielle, B., et al. (2016). Biophysical and economic limits to negative CO2 emissions. *Nat. Clim. Chang.* 6, 42–50. doi:10.1038/nclimate2870.

Smith, P., Price, J., Molotoks, A., Warren, R., and Malhi, Y. (2018b). Impacts on terrestrial biodiversity of moving from a 2°C to a 1.5°C target. *Philos. Trans. R. Soc. A Math. Eng. Sci.* 376, 20160456. doi:10.1098/rsta.2016.0456.

Smith, S. J., and Mizrahi, A. (2013). Near-term climate mitigation by short-lived forcers. *Proc. Natl. Acad. Sci.* 110, 14202–14206. doi:10.1073/pnas.1308470110.

Smith, W. K., Zhao, M., and Running, S. W. (2012b). Global Bioenergy Capacity as Constrained by Observed Biospheric Productivity Rates. *Bioscience* 62, 911–922. doi:10.1525/bio.2012.62.10.11.

Smith, W., and Wagner, G. (2018). Stratospheric aerosol injection tactics and costs in the first 15 years of deployment. *Environ. Res. Lett.* 13, 124001. doi:10.1088/1748-9326/aae98d.

Sokolov, A. P., Kicklighter, D. W., Melillo, J. M., Felzer, B. S., Schlosser, C. A., and Cronin, T. W. (2008). Consequences of Considering Carbon–Nitrogen Interactions on the Feedbacks between Climate and the Terrestrial Carbon Cycle. *J. Clim.* 21, 3776–3796. doi:10.1175/2008JCLI2038.1.

Solomon, S., Daniel, J. S., Sanford, T. J., Murphy, D. M., Plattner, G.-K., Knutti, R., et al. (2010). Persistence of climate changes due to a range of greenhouse gases. *Proc. Natl. Acad. Sci.* 107, 18354–18359. doi:10.1073/pnas.1006282107.

Sonntag, S., Ferrer González, M., Ilyina, T., Kracher, D., Nabel, J. E. M. S., Niemeier, U., et al. (2018). Quantifying and Comparing Effects of Climate Engineering Methods on the Earth System. *Earth's Futur.* 6, 149–168. doi:10.1002/2017EF000620.

Sonntag, S., Pongratz, J., Reick, C., and Schmidt, H. (2015). Carbon sequestration potential and climatic effects of reforestation in an Earth system model. in, 13707.

Søren, R., Bendtsen, J., Delille, B., Dieckmann, G. S., Glud, R. N., Kennedy, H., et al. (2011). Sea ice contribution to the air–sea CO2 exchange in the Arctic and Southern Oceans. *Tellus B Chem. Phys. Meteorol.* 63, 823–830. doi:10.1111/j.1600-0889.2011.00571.x.

Statistics division. Food and Agriculture Organization of the United Nations (2018). Available at: http://www.fao.org/faostat/en/.

Staver, A. C., Archibald, S., and Levin, S. A. (2011). The Global Extent and Determinants of Savanna and Forest as Alternative Biome States. *Science (80-.).* 334, 230–232. doi:10.1126/science.1210465.

Steele, L. P., Dlugokencky, E. J., Lang, P. M., Tans, P. P., Martin, R. C., and Masarie, K. A. (1992). Slowing down of the global accumulation of atmospheric methane during the 1980s. *Nature* 358, 313–316. doi:10.1038/358313a0.

Steinacher, M., and Joos, F. (2016). Transient Earth system responses to cumulative carbon dioxide emissions: linearities, uncertainties, and probabilities in an observation-constrained model ensemble. *Biogeosciences* 13, 1071–1103. doi:10.5194/bg-13-1071-2016.

Stern, D. I., and Kaufmann, R. K. (1996). Estimates of global anthropogenic methane emissions 1860–1993. *Chemosphere* 33, 159–176. doi:10.1016/0045-6535(96)00157-9.

Stevenson, D. S., Dentener, F. J., Schultz, M. G., Ellingsen, K., van Noije, T. P. C., Wild, O., et al. (2006). Multimodel ensemble simulations of present-day and near-future tropospheric ozone. *J. Geophys. Res.* 111, D08301. doi:10.1029/2005JD006338.

Stocker, B. D., and Joos, F. (2015). Quantifying differences in land use emission estimates implied by definition discrepancies. *Earth Syst. Dyn.* 6, 731–744. doi:10.5194/esd-6-731-2015.

Stocker, B. D., Roth, R., Joos, F., Spahni, R., Steinacher, M., Zaehle, S., et al. (2013a). Multiple greenhouse-gas feedbacks from the land biosphere under future climate change scenarios. *Nat. Clim. Chang.* 3, 666–672. doi:10.1038/nclimate1864.

Stocker, B. D., Yu, Z., Massa, C., and Joos, F. (2017). Holocene peatland and ice-core data constraints on the timing and magnitude of CO2 emissions from past land use. *Proc. Natl. Acad. Sci.* 114, 1492–1497. doi:10.1073/pnas.1613889114.

Stocker, T. F., Qin, D., Plattner, G.-K., Alexander, L. V, Allen, S. K., Bindoff, N. L., et al. (2013b). "Technical Summary," in *Climate Change 2013: The Physical Science Basis. Contribution of Working Group I to the Fifth Assessment Report of the Intergovernmental Panel on Climate Change*, eds. D. Q. G.-K. P. M. T. S. K. A. J. B. A. N. Y. X. V. B. Stocker T.F. and P. M. Midgley (Cambridge, United Kingdom and New York, NY, USA: Cambridge University Press), 33–115.

Stramma, L., Johnson, G. C., Sprintall, J., and Mohrholz, V. (2008). Expanding Oxygen-Minimum Zones in the Tropical Oceans. *Science (80-.).* 320, 655–658. doi:10.1126/science.1153847.

Strauss, J., Schirrmeister, L., Grosse, G., Fortier, D., Hugelius, G., Knoblauch, C., et al. (2017). Deep Yedoma permafrost: A synthesis of depositional characteristics and carbon vulnerability. *Earth-Science Rev.* 172, 75–86. doi:10.1016/j.earscirev.2017.07.007.

Studer, A. S., Sigman, D. M., Martínez-García, A., Thöle, L. M., Michel, E., Jaccard, S. L., et al. (2018). Increased nutrient supply to the Southern Ocean during the Holocene and its implications for the pre-industrial atmospheric CO2 rise. *Nat. Geosci.* 11, 756–760. doi:10.1038/s41561-018-0191-8.

Suess, H. E. (1955). Radiocarbon Concentration in Modern Wood. *Science (80-.).* 122, 415–417. doi:10.1126/science.122.3166.415-a.

Sulman, B. N., Phillips, R. P., Oishi, A. C., Shevliakova, E., and Pacala, S. W. (2014). Microbe-driven turnover offsets mineral-mediated storage of soil carbon under elevated CO2. *Nat. Clim. Chang.* 4, 1099–1102. doi:10.1038/nclimate2436.

Suntharalingam, P., Buitenhuis, E., Le Quéré, C., Dentener, F., Nevison, C., Butler, J. H., et al. (2012). Quantifying the impact of anthropogenic nitrogen deposition on oceanic nitrous oxide. *Geophys. Res. Lett.* 39, L07605. doi:10.1029/2011GL050778.

Suthhof, A., Ittekkot, V., and Gaye-Haake, B. (2001). Millennial-scale oscillation of denitrification intensity in the Arabian Sea during the Late Quaternary and its potential influence on atmospheric N 2 O and global climate. *Global Biogeochem. Cycles* 15, 637–649. doi:10.1029/2000GB001337.

Sutton, A. J., Sabine, C. L., Feely, R. A., Cai, W.-J., Cronin, M. F., McPhaden, M. J., et al. (2016). Using present-day observations to detect when anthropogenic change forces surface ocean carbonate chemistry outside preindustrial bounds. *Biogeosciences* 13, 5065–5083. doi:10.5194/bg-13-5065-2016.

Swann, A. L. S., Hoffman, F. M., Koven, C. D., and Randerson, J. T. (2016). Plant responses to increasing CO2 reduce estimates of climate impacts on drought severity. *Proc. Natl. Acad. Sci.* 113, 10019–10024. doi:10.1073/pnas.1604581113.

Swart, N. C., Fyfe, J. C., Saenko, O. A., and Eby, M. (2014). Wind-driven changes in the ocean carbon sink. *Biogeosciences* 11, 6107–6117. doi:10.5194/bg-11-6107-2014.

Tachiiri, K., Hajima, T., and Kawamiya, M. (2015). Increase of uncertainty in transient climate response to cumulative carbon emissions after stabilization of atmospheric CO 2 concentration. *Environ. Res. Lett.* 10, 125018. doi:10.1088/1748-9326/10/12/125018.

Tagliabue, A., Aumont, O., and Bopp, L. (2014). The impact of different external sources of iron on the global carbon cycle. *Geophys. Res. Lett.* 41, 920–926. doi:10.1002/2013GL059059.

Takahashi, T., Sutherland, S. C., Chipman, D. W., Goddard, J. G., Ho, C., Newberger, T., et al. (2014). Climatological distributions of pH, pCO2, total CO2, alkalinity, and CaCO3 saturation in the global surface ocean, and temporal changes at selected locations. *Mar. Chem.* 164, 95–125. doi:10.1016/j.marchem.2014.06.004.

Takata, K., Patra, P. K., Kotani, A., Mori, J., Belikov, D., Ichii, K., et al. (2017). Reconciliation of top-down and bottom-up CO<inf>2</inf>fluxes in Siberian larch forest. *Environ. Res. Lett.* 12. doi:10.1088/1748-9326/aa926d.

Takatani, Y., Sasano, D., Nakano, T., Midorikawa, T., and Ishii, M. (2012). Decrease of dissolved oxygen after the mid-1980s in the western North Pacific subtropical gyre along the 137°E repeat section. *Global Biogeochem. Cycles* 26, n/a-n/a. doi:10.1029/2011GB004227.

Takeshita, Y., Frieder, C. A., Martz, T. R., Ballard, J. R., Feely, R. A., Kram, S., et al. (2015). Including high-frequency variability in coastal ocean acidification projections. *Biogeosciences* 12, 5853–5870. doi:10.5194/bg-12-5853-2015.

Tan, Z.-H., Zeng, J., Zhang, Y.-J., Slot, M., Gamo, M., Hirano, T., et al. (2017). Optimum air temperature for tropical forest photosynthesis: mechanisms involved and implications for climate warming. *Environ. Res. Lett.* 12, 054022. doi:10.1088/1748-9326/aa6f97.

Tanhua, T., Hoppema, M., Jones, E. M., Stöven, T., Hauck, J., Dávila, M. G., et al. (2017). Temporal changes in ventilation and the carbonate system in the Atlantic sector of the Southern Ocean. *Deep Sea Res. Part II Top. Stud. Oceanogr.* 138, 26–38. doi:10.1016/j.dsr2.2016.10.004.

Taucher, J., and Oschlies, A. (2011). Can we predict the direction of marine primary production change under global warming? *Geophys. Res. Lett.* 38, L02603. doi:10.1029/2010GL045934.

Taylor, L. L., Quirk, J., Thorley, R. M. S., Kharecha, P. A., Hansen, J., Ridgwell, A., et al. (2015). Enhanced weathering strategies for stabilizing climate and averting ocean acidification. *Nat. Clim. Chang.* 6, 402.

Terrer, C., Vicca, S., Hungate, B. A., Phillips, R. P., and Prentice, I. C. (2016). Mycorrhizal association as a primary control of the CO 2 fertilization effect. *Science (80-.).* 353, 72–74. doi:10.1126/science.aaf4610.

Terrer, C., Vicca, S., Hungate, B. A., Phillips, R. P., Reich, P. B., Franklin, O., et al. (2017). Response to Comment on "Mycorrhizal association as a primary control of the CO2 fertilization effect." *Science (80-.).* 355, 358.3-358. doi:10.1126/science.aai8242.

Terrer, C., Vicca, S., Stocker, B. D., Hungate, B. A., Phillips, R. P., Reich, P. B., et al. (2018). Ecosystem responses to elevated CO2 governed by plant-soil interactions and the cost of nitrogen acquisition. *New Phytol.* 217, 507–522. doi:10.1111/nph.14872.

Thomas, E. (2007). "Cenozoic mass extinctions in the deep sea: What perturbs the largest habitat on Earth?," in *Special Paper 424: Large Ecosystem Perturbations: Causes and Consequences*, eds. S. Monechi, R. Coccioni, and M. R. Rampino (Geological Society of America), 1–23. doi:10.1130/2007.2424(01).

Thomas, R. Q., Brookshire, E. N. J., and Gerber, S. (2015). Nitrogen limitation on land: how can it occur in Earth system models? *Glob. Chang. Biol.* 21, 1777–1793. doi:10.1111/gcb.12813.

Thompson, R. L., Dlugokencky, E., Chevallier, F., Ciais, P., Dutton, G., Elkins, J. W., et al. (2013). Interannual variability in tropospheric nitrous oxide. *Geophys. Res. Lett.* 40, 4426–4431. doi:10.1002/grl.50721.

Thompson, R. L., Lassaletta, L., Patra, P. K., Wilson, C., Wells, K., Gressent, A., et al. Acceleration of global N2O emissions seen from two decades of atmospheric inversion. *J. Geophys. Res.*

Thompson, R. L., Nisbet, E. G., Pisso, I., Stohl, A., Blake, D., Dlugokencky, E. J., et al. (2018). Variability in Atmospheric Methane From Fossil Fuel and Microbial Sources Over the Last Three Decades. *Geophys. Res. Lett.* 45, 11,411-499,508. doi:doi:10.1029/2018GL078127.

Thompson, R. L., Patra, P. K., Ishijima, K., Saikawa, E., Corazza, M., Karstens, U., et al. (2014). TransCom N₂O model inter-comparison – Part 1: Assessing the influence of transport and surface fluxes on tropospheric N₂O variability. *Atmos. Chem. Phys.* 14, 4349–4368. doi:10.5194/acp-14-4349-2014.

Thornton, B. F., Wik, M., and Crill, P. M. (2016). Double-counting challenges the accuracy of high-latitude methane inventories. *Geophys. Res. Lett.* 43, 12,569-12,577. doi:10.1002/2016GL071772.

Thornton, P. E., Doney, S. C., Lindsay, K., Moore, J. K., Mahowald, N., Randerson, J. T., et al. (2009). Carbon-nitrogen interactions regulate climate-carbon cycle feedbacks: results from an atmosphere-ocean general circulation model. *Biogeosciences* 6, 2099–2120. doi:10.5194/bg-6-2099-2009.

Thurner, M., Beer, C., Santoro, M., Carvalhais, N., Wutzler, T., Schepaschenko, D., et al. (2014). Carbon stock and density of northern boreal and temperate forests. *Glob. Ecol. Biogeogr.* 23, 297–310. doi:10.1111/geb.12125.

Tian, H., Lu, C., Ciais, P., Michalak, A. M., Canadell, J. G., Saikawa, E., et al. (2016). The terrestrial biosphere as a net source of greenhouse gases to the atmosphere. *Nature* 531, 225–228. doi:10.0.4.14/nature16946.

Tian, H., Yang, J., Xu, R., Lu, C., Canadell, J. G., Davidson, E. A., et al. (2019). Global soil nitrous oxide emissions since the preindustrial era estimated by an ensemble of terrestrial biosphere models: Magnitude, attribution, and uncertainty. *Glob. Chang. Biol.* 25, 640–659. doi:10.1111/gcb.14514.

Tjiputra, J. F., Grini, A., and Lee, H. (2016). Impact of idealized future stratospheric aerosol injection on the large-scale ocean and land carbon cycles. *J. Geophys. Res. Biogeosciences* 121, 2–27. doi:10.1002/2015JG003045.

Todd-Brown, K. E. O., Randerson, J. T., Post, W. M., Hoffman, F. M., Tarnocai, C., Schuur, E. A. G., et al. (2013). Causes of variation in soil carbon simulations from CMIP5 Earth system models and comparison with observations. *Biogeosciences* 10, 1717–1736. doi:10.5194/bg-10-1717-2013.

Tokarska, K. B., Gillett, N. P., Arora, V. K., Lee, W. G., and Zickfeld, K. (2018). The influence of non-CO2 forcings on cumulative carbon emissions budgets. *Environ. Res. Lett.* 13, 034039. doi:10.1088/1748-9326/aaafdd.

Tokarska, K. B., Gillett, N. P., Weaver, A. J., Arora, V. K., and Eby, M. (2016). The climate response to five trillion tonnes of carbon. *Nat. Clim. Chang.* 6, 851–855. doi:10.1038/nclimate3036.

Tokarska, K. B., and Zickfeld, K. (2015). The effectiveness of net negative carbon dioxide emissions in reversing anthropogenic climate change. *Environ. Res. Lett.* 10, 094013. doi:10.1088/1748-9326/10/9/094013.

Tonitto, C., David, M. B., and Drinkwater, L. E. (2006). Replacing bare fallows with cover crops in fertilizer-intensive cropping systems: A meta-analysis of crop yield and N dynamics. *Agric. Ecosyst. Environ.* 112, 58–72. doi:10.1016/j.agee.2005.07.003.

Toyama, K., Rodgers, K. B., Blanke, B., Iudicone, D., Ishii, M., Aumont, O., et al. (2017). Large Reemergence of Anthropogenic Carbon into the Ocean's Surface Mixed Layer Sustained by the Ocean's Overturning Circulation. *J. Clim.* 30, 8615–8631. doi:10.1175/JCLI-D-16-0725.1.

Trisos, C. H., Amatulli, G., Gurevitch, J., Robock, A., Xia, L., and Zambri, B. (2018). Potentially dangerous consequences for biodiversity of solar geoengineering implementation and termination. *Nat. Ecol. Evol.* 2, 475–482. doi:10.1038/s41559-017-0431-0.

Turetsky, M., and others No Title.

Turetsky, M. R., Abbot, B., Jones, M., Walter Anthony, K., Olefeldt, D., Schuur, E. A. G., et al. Abrupt thaw amplifies the permafrost carbon feedback through upland erosion and. *Proc. Natl. Acad. Sci.*

Turi, G., Lachkar, Z., Gruber, N., and Münnich, M. (2016). Climatic modulation of recent trends in ocean acidification in the California Current System. *Environ. Res. Lett.* 11, 014007. doi:10.1088/1748-9326/11/1/014007.

Turnbull, J. C., Mikaloff Fletcher, S. E., Ansell, I., Brailsford, G. W., Moss, R. C., Norris, M. W., et al. (2017). Sixty years of radiocarbon dioxide measurements at Wellington, New Zealand: 1954–2014. *Atmos. Chem. Phys.* 17, 14771–14784. doi:10.5194/acp-17-14771-2017.

Turner, A. J., Frankenberg, C., Wennberg, P. O., and Jacob, D. J. (2017). Ambiguity in the causes for decadal trends in atmospheric methane and hydroxyl. *Proc. Natl. Acad. Sci.* 114, 5367–5372.

Turner, S. K. (2018). Constraints on the onset duration of the Paleocene–Eocene Thermal Maximum. *Philos. Trans. R. Soc. A Math. Phys. Eng. Sci.* 376, 20170082. doi:10.1098/rsta.2017.0082.

Tyrrell, T., and Lucas, M. I. (2002). Geochemical evidence of denitrification in the Benguela upwelling system. *Cont. Shelf Res.* 22, 2497–2511. doi:10.1016/S0278-4343(02)00077-8.

van der Sleen, P., Groenendijk, P., Vlam, M., Anten, N. P. R., Boom, A., Bongers, F., et al. (2015). No growth stimulation of tropical trees by 150 years of CO2 fertilization but water-use efficiency increased. *Nat. Geosci.* 8, 24–28. doi:10.1038/ngeo2313.

van der Werf, G. R., Randerson, J. T., Giglio, L., van Leeuwen, T. T., Chen, Y., Rogers, B. M., et al. (2017). Global fire emissions estimates during 1997–2016. *Earth Syst. Sci. Data* 9, 697–720. doi:10.5194/essd-9-697-2017.

van Gestel, N., Shi, Z., van Groenigen, K. J., Osenberg, C. W., Andresen, L. C., Dukes, J. S., et al. (2018). Predicting soil carbon loss with warming. *Nature* 554, E4–E5. doi:10.1038/nature25745.

van Groenigen, K. J., Osenberg, C. W., and Hungate, B. A. (2011). Increased soil emissions of potent greenhouse gases under increased atmospheric CO2. *Nature* 475, 214–216. doi:10.1038/nature10176.

van Groenigen, K. J., Osenberg, C. W., Terrer, C., Carrillo, Y., Dijkstra, F. A., Heath, J., et al. (2017). Faster turnover of new soil carbon inputs under increased atmospheric CO2. *Glob. Chang. Biol.* 23, 4420–4429. doi:10.1111/gcb.13752.

Vaughan, N. E., and Gough, C. (2016). Expert assessment concludes negative emissions scenarios may not deliver. *Environ. Res. Lett.* 11, 095003. doi:10.1088/1748-9326/11/9/095003.

Vaughan, N. E., Gough, C., Mander, S., Littleton, E. W., Welfle, A., Gernaat, D. E. H. J., et al. (2018). Evaluating the use of biomass energy with carbon capture and storage in low emission scenarios. *Environ. Res. Lett.* 13, 044014. doi:10.1088/1748-9326/aaaa02.

Vichi, M., Navarra, A., and Fogli, P. G. (2013). Adjustment of the natural ocean carbon cycle to negative emission rates. *Clim. Change* 118, 105–118. doi:10.1007/s10584-012-0677-0.

Vitousek, P. M., Porder, S., Houlton, B. Z., and Chadwick, O. a (2010). Terrestrial phosphorus limitation: mechanisms, implications, and nitrogen–phosphorus interactions. *Ecol. Appl.* 20, 5–15. doi:10.1890/08-0127.1.

Volodin, E. M. (2008). Methane cycle in the INM RAS climate model. *Izv. Atmos. Ocean. Phys.* 44, 153–159. doi:10.1134/S0001433808020023.

Volodin, E. M. (2015). Influence of methane sources in Northern Hemisphere high latitudes on the interhemispheric asymmetry of its atmospheric concentration and climate. *Izv. Atmos. Ocean. Phys.* 51, 251–258. doi:10.1134/S0001433815030123.

Voulgarakis, A., Naik, V., Lamarque, J.-F., Shindell, D. T., Young, P. J., Prather, M. J., et al. (2013). Analysis of present day and future OH and methane lifetime in the ACCMIP simulations. *Atmos. Chem. Phys.* 13, 2563–2587. doi:10.5194/acp-13-2563-2013.

Wagner-Riddle, C., Congreves, K. A., Abalos, D., Berg, A. A., Brown, S. E., Ambadan, J. T., et al. (2017). Globally important nitrous oxide emissions from croplands induced by freeze–thaw cycles. *Nat. Geosci.* 10, 279–283. doi:10.1038/ngeo2907.

Wakita, M., Nagano, A., Fujiki, T., and Watanabe, S. (2017). Slow acidification of the winter mixed layer in the subarctic western North Pacific. *J. Geophys. Res. Ocean.* 122, 6923–6935. doi:10.1002/2017JC013002.

Walker, A. P., De Kauwe, M. G., Medlyn, B. E., Zaehle, S., Iversen, C. M., Asao, S., et al. (2019). Decadal biomass increment in early secondary succession woody ecosystems is increased by CO2 enrichment. *Nat. Commun.* 10, 454. doi:10.1038/s41467-019-08348-1.

Walker, A. P., Zaehle, S., Medlyn, B. E., De Kauwe, M. G., Asao, S., Hickler, T., et al. (2015). Predicting long-term carbon sequestration in response to CO2 enrichment: How and why do current ecosystem models differ? *Global Biogeochem. Cycles* 29, 476–495. doi:10.1002/2014GB004995.

Wallace, R. B., Baumann, H., Grear, J. S., Aller, R. C., and Gobler, C. J. (2014). Coastal ocean acidification: The other eutrophication problem. *Estuar. Coast. Shelf Sci.* 148, 1–13. doi:10.1016/j.ecss.2014.05.027.

Wang, W., Ciais, P., Nemani, R. R., Canadell, J. G., Piao, S., Sitch, S., et al. (2013). Variations in atmospheric CO2 growth rates coupled with tropical temperature. *Proc. Natl. Acad. Sci.* 110, 13061–13066. doi:10.1073/pnas.1219683110.

Wang, X., Piao, S., Ciais, P., Friedlingstein, P., Myneni, R. B., Cox, P., et al. (2014). A two-fold increase of carbon cycle sensitivity to tropical temperature variations. *Nature* 506, 212–215. doi:10.1038/nature12915.

Wang, Y., Hendy, I., and Napier, T. J. (2017). Climate and Anthropogenic Controls of Coastal Deoxygenation on Interannual to Centennial Timescales. *Geophys. Res. Lett.* 44, 11,528-11,536. doi:10.1002/2017GL075443.

Wang, Y. P., Jiang, J., Chen-Charpentier, B., Agusto, F. B., Hastings, A., Hoffman, F., et al. (2016). Responses of two nonlinear microbial models to warming and increased carbon input. *Biogeosciences* 13, 887–902. doi:10.5194/bg-13-887-2016.

Wania, R., Meissner, K. J., Eby, M., Arora, V. K., Ross, I., and Weaver, A. J. (2012). Carbon-nitrogen feedbacks in the UVic ESCM. *Geosci. Model Dev.* 5, 1137–1160. doi:10.5194/gmd-5-1137-2012.

Wanninkhof, R., Doney, S. C., Bullister, J. L., Levine, N. M., Warner, M., and Gruber, N. (2010). Detecting anthropogenic CO 2 changes in the interior Atlantic Ocean between 1989 and 2005. *J. Geophys. Res.* 115, C11028. doi:10.1029/2010JC006251.

Wårlind, D., Smith, B., Hickler, T., and Arneth, A. (2014). Nitrogen feedbacks increase future terrestrial ecosystem carbon uptake in an individual-based dynamic vegetation model. *Biogeosciences* 11, 6131–6146. doi:10.5194/bg-11-6131-2014.

Wei, G., McCulloch, M. T., Mortimer, G., Deng, W., and Xie, L. (2009). Evidence for ocean acidification in the Great Barrier Reef of Australia. *Geochim. Cosmochim. Acta* 73, 2332–2346. doi:10.1016/j.gca.2009.02.009.

Wei, G., Wang, Z., Ke, T., Liu, Y., Deng, W., Chen, X., et al. (2015). Decadal variability in seawater pH in the West Pacific: Evidence from coral δ 11 B records. *J. Geophys. Res. Ocean.* 120, 7166–7181. doi:10.1002/2015JC011066.

Wenzel, S., Cox, P. M., Eyring, V., and Friedlingstein, P. (2014). Emergent constraints on climate-carbon cycle feedbacks in the CMIP5 Earth system models. *J. Geophys. Res. Biogeosciences* 119, 794–807. doi:10.1002/2013JG002591.

Wenzel, S., Cox, P. M., Eyring, V., and Friedlingstein, P. (2016). Projected land photosynthesis constrained by changes in the seasonal cycle of atmospheric CO2. *Nature* 538, 499–501. doi:10.1038/nature19772.

Werner, C., Butterbach-Bahl, K., Haas, E., Hickler, T., and Kiese, R. (2007). A global inventory of N2O emissions from tropical rainforest soils using a detailed biogeochemical model. *Global Biogeochem. Cycles* 21, GB3010. doi:10.1029/2006GB002909.

Wieder, W. R., Bonan, G. B., and Allison, S. D. (2013). Global soil carbon projections are improved by modelling microbial processes. *Nat. Clim. Chang.* 3, 909–912. doi:10.1038/nclimate1951.

Wieder, W. R., Cleveland, C. C., Smith, W. K., and Todd-Brown, K. (2015). Future productivity and carbon storage limited by terrestrial nutrient availability. *Nat. Geosci.* 8, 441–444. doi:10.1038/ngeo2413.

Wieder, W. R., Hartman, M. D., Sulman, B. N., Wang, Y.-P., Koven, C. D., and Bonan, G. B. (2018). Carbon cycle confidence and uncertainty: Exploring variation among soil biogeochemical models. *Glob. Chang. Biol.* 24, 1563–1579. doi:10.1111/gcb.13979.

Wiesen, P., Kleffmann, J., Kurtenbach, R., and Becker, K. H. (1994). Nitrous oxide and methane emissions from aero engines. *Geophys. Res. Lett.* 21, 2027–2030. doi:10.1029/94GL01709.

Wiesen, P., Kleffmann, J., Kurtenbach, R., and Becker, K. H. (1996). Emission of nitrous oxide and methane from aero engines: monitoring by tunable diode laser spectroscopy. *Infrared Phys. Technol.* 37, 75–81. doi:10.1016/S1350-4495(97)80763-3.

Wik, M., Thornton, B. F., Bastviken, D., Uhlbäck, J., and Crill, P. M. (2016a). Biased sampling of methane release from northern lakes: A problem for extrapolation. *Geophys. Res. Lett.* 43, 1256–1262. doi:10.1002/2015GL066501.

Wik, M., Varner, R. K., Anthony, K. W., MacIntyre, S., and Bastviken, D. (2016b). Climate-sensitive northern lakes and ponds are critical components of methane release. *Nat. Geosci.* 9, 99–105. doi:10.1038/ngeo2578.

Wilhelm, W. W., Johnson, J. M. F., Hatfield, J. L., Voorhees, W. B., and Linden, D. R. (2004). Crop and Soil Productivity Response to Corn Residue Removal. *Agron. J.* 96, 1–17. doi:10.2134/agronj2004.1000.

Williams, J., and Crutzen, P. J. (2010). Nitrous oxide from aquaculture. *Nat. Geosci.* 3, 143–143. doi:10.1038/ngeo804.

Williams, N. L., Feely, R. A., Sabine, C. L., Dickson, A. G., Swift, J. H., Talley, L. D., et al. (2015). Quantifying anthropogenic carbon inventory changes in the Pacific sector of the Southern Ocean. *Mar. Chem.* 174, 147–160. doi:10.1016/j.marchem.2015.06.015.

Williams, R. G., Goodwin, P., Roussenov, V. M., and Bopp, L. (2016). A framework to understand the transient climate response to emissions. *Environ. Res. Lett.* 11, 015003. doi:10.1088/1748-9326/11/1/015003.

Williamson, P., & Bodle, R. (2016). Update on Climate Geoengineering in Relation to the Convention on Biological Diversity: Potential Impacts and Regulatory Framework. Montreal.

Winguth, A. M. E., Thomas, E., and Winguth, C. (2012). Global decline in ocean ventilation, oxygenation, and productivity during the Paleocene-Eocene Thermal Maximum: Implications for the benthic extinction. *Geology* 40, 263–266. doi:10.1130/G32529.1.

Winiwarter, W., Höglund-Isaksson, L., Schöpp, W., Tohka, A., Wagner, F., and Amann, M. (2010). Emission mitigation potentials and costs for non-CO 2 greenhouse gases in Annex-I countries according to the GAINS model. *J. Integr. Environ. Sci.* 7, 235–243. doi:10.1080/19438151003774430.

Wolf, J., Asrar, G. R., and West, T. O. (2017). Revised methane emissions factors and spatially distributed annual carbon fluxes for global livestock. *Carbon Balance Manag.* 12, 16. doi:10.1186/s13021-017-0084-y.

Wolter, K., and Timlin, M. S. (1998). Measuring the strength of ENSO events: How does 1997/98 rank? *Weather* 53, 315–324. doi:10.1002/j.1477-8696.1998.tb06408.x.

Woolf, D., Amonette, J. E., Street-Perrott, F. A., Lehmann, J., and Joseph, S. (2010). Sustainable biochar to mitigate global climate change. *Nat. Commun.* 1, 1–9. doi:10.1038/ncomms1053.

Woosley, R. J., Millero, F. J., and Wanninkhof, R. (2016). Rapid anthropogenic changes in CO2 and pH in the Atlantic Ocean: 2003-2014. *Global Biogeochem. Cycles* 30, 70–90. doi:10.1002/2015GB005248.

Worden, J. R., Bloom, A. A., Pandey, S., Jiang, Z., Worden, H. M., Walker, T. W., et al. (2017). Reduced biomass burning emissions reconcile conflicting estimates of the post-2006 atmospheric methane budget. *Nat. Commun.* 8, 2227. doi:10.1038/s41467-017-02246-0.

Wu, H. C., Dissard, D., Douville, E., Blamart, D., Bordier, L., Tribollet, A., et al. (2018). Surface ocean pH variations since 1689 CE and recent ocean acidification in the tropical South Pacific. *Nat. Commun.* 9, 2543. doi:10.1038/s41467-018-04922-1.

Xu-Ri, Prentice, I. C., Spahni, R., and Niu, H. S. (2012). Modelling terrestrial nitrous oxide emissions and implications for climate feedback. *New Phytol.* 196, 472–488. doi:10.1111/j.1469-8137.2012.04269.x.

Yamamoto-Kawai, M., McLaughlin, F. A., Carmack, E. C., Nishino, S., and Shimada, K. (2009). Aragonite Undersaturation in the Arctic Ocean: Effects of Ocean Acidification and Sea Ice Melt. *Science (80-.).* 326, 1098–1100. doi:10.1126/science.1174190.

Yamamoto, A., Abe-Ouchi, A., and Yamanaka, Y. (2018). Long-term response of oceanic carbon uptake to global warming via physical and biological pumps. *Biogeosciences* 15, 4163–4180. doi:10.5194/bg-15-4163-2018.

Yang, G., Peng, Y., Marushchak, M. E., Chen, Y., Wang, G., Li, F., et al. (2018). Magnitude and Pathways of Increased Nitrous Oxide Emissions from Uplands Following Permafrost Thaw. *Environ. Sci. Technol.* 52, 9162–9169. doi:10.1021/acs.est.8b02271.

Yao, W., Paytan, A., and Wortmann, U. G. (2018). Large-scale ocean deoxygenation during the Paleocene-Eocene Thermal Maximum. *Science (80-.).* 361, 804–806. doi:10.1126/science.aar8658.

Yousefpour, R., Nabel, J. E. M. S., and Pongratz, J. (2018). Simulating sustained yield harvesting adaptive to future climate change. *Biogeosciences Discuss.*, 1–34. doi:10.5194/bg-2017-531.

Yu, J., Broecker, W. S., Elderfield, H., Jin, Z., McManus, J., and Zhang, F. (2010a). Loss of Carbon from the Deep Sea Since the Last Glacial Maximum. *Science (80-.).* 330, 1084–1087. doi:10.1126/science.1193221.

Yu, Z., Loisel, J., Brosseau, D. P., Beilman, D. W., and Hunt, S. J. (2010b). Global peatland dynamics since the Last Glacial Maximum. *Geophys. Res. Lett.* 37, LI3402. doi:10.1029/2010GL043584.

Zachos, J. C. (2005). Rapid Acidification of the Ocean During the Paleocene-Eocene Thermal Maximum. *Science (80-.).* 308, 1611–1615. doi:10.1126/science.1109004.

Zaehle, S. (2013). Terrestrial nitrogen-carbon cycle interactions at the global scale. *Philos. Trans. R. Soc. B Biol. Sci.* 368, 20130125–20130125. doi:10.1098/rstb.2013.0125.

Zaehle, S., Ciais, P., Friend, A. D., and Prieur, V. (2011). Carbon benefits of anthropogenic reactive nitrogen offset by nitrous oxide emissions. *Nat. Geosci.* 4, 601–605. doi:10.1038/ngeo1207.

Zaehle, S., Friedlingstein, P., and Friend, A. D. (2010). Terrestrial nitrogen feedbacks may accelerate future climate change. *Geophys. Res. Lett.* 37, L01401. doi:10.1029/2009GL041345.

Zaehle, S., Jones, C. D., Houlton, B., Lamarque, J.-F., and Robertson, E. (2015). Nitrogen Availability Reduces CMIP5 Projections of Twenty-First-Century Land Carbon Uptake*. *J. Clim.* 28, 2494–2511. doi:10.1175/JCLI-D-13-00776.1.

Zaehle, S., Medlyn, B. E., De Kauwe, M. G., Walker, A. P., Dietze, M. C., Hickler, T., et al. (2014). Evaluation of 11 terrestrial carbon-nitrogen cycle models against observations from two temperate Free-Air CO 2 Enrichment studies. *New Phytol.* 202, 803–822. doi:10.1111/nph.12697.

Zahariev, K., Christian, J. R., and Denman, K. L. (2008). Preindustrial, historical, and fertilization simulations using a global ocean carbon model with new parameterizations of iron limitation, calcification, and N-2 fixation. *Prog. Ocean.* 77, 56–82.

Zamora, L. M., Oschlies, A., Bange, H. W., Huebert, K. B., Craig, J. D., Kock, A., et al. (2012). Nitrous oxide dynamics in low oxygen regions of the Pacific: insights from the MEMENTO database. *Biogeosciences* 9, 5007–5022. doi:10.5194/bg-9-5007-2012.

Zeebe, R. E. (2013). What caused the long duration of the Paleocene-Eocene Thermal Maximum? *Paleoceanography* 28, 440–452. doi:10.1002/palo.20039.

Zeebe, R. E., Ridgwell, A., and Zachos, J. C. (2016). Anthropogenic carbon release rate unprecedented during the past 66 million years. *Nat. Geosci.* 9, 325–329. doi:10.1038/ngeo2681.

Zeebe, R. E., and Zachos, J. C. (2013). Long-term legacy of massive carbon input to the Earth system: Anthropocene versus Eocene. *Philos. Trans. R. Soc. A Math. Phys. Eng. Sci.* 371, 20120006–20120006. doi:10.1098/rsta.2012.0006.

Zeebe, R. E., Zachos, J. C., and Dickens, G. R. (2009). Carbon dioxide forcing alone insufficient to explain Palaeocene–Eocene Thermal Maximum warming. *Nat. Geosci.* 2, 576–580. doi:10.1038/ngeo578.

Zemp, D. C., Schleussner, C.-F., Barbosa, H. M. J., Hirota, M., Montade, V., Sampaio, G., et al. (2017). Self-amplified Amazon forest loss due to vegetation-atmosphere feedbacks. *Nat. Commun.* 8, 14681. doi:10.1038/ncomms14681.

Zeng, J., Nojiri, Y., Nakaoka, S., Nakajima, H., and Shirai, T. (2015). Surface ocean CO2 in 1990-2011 modelled using a feed-forward neural network. *Geosci. Data J.* 2, 47–51. doi:10.1002/gdj3.26.

Zhang, H., and Cao, L. (2016). Simulated effect of calcification feedback on atmospheric CO2 and ocean acidification. *Sci. Rep.* 6, 20284. doi:10.1038/srep20284.

Zhang, Q., Pitman, A. J., Wang, Y. P., Dai, Y. J., and Lawrence, P. J. (2013a). The impact of nitrogen and phosphorous limitation on the estimated terrestrial carbon balance and warming of land use change over the last 156 yr. *Earth Syst. Dyn.* 4, 333–345. doi:10.5194/esd-4-333-2013.

Zhang, Q., Wang, Y. P., Matear, R. J., Pitman, A. J., and Dai, Y. J. (2014). Nitrogen and phosphorous limitations significantly reduce future allowable CO 2 emissions. *Geophys. Res. Lett.* 41, 632–637. doi:10.1002/2013GL058352.

Zhang, X., Wang, Y.-P., Peng, S., Rayner, P. J., Ciais, P., Silver, J. D., et al. (2018a). Dominant regions and drivers of the variability of the global land carbon sink across timescales. *Glob. Chang. Biol.* 24, 3954–3968. doi:10.1111/gcb.14275.

Zhang, Y. G., Pagani, M., Liu, Z., Bohaty, S. M., and DeConto, R. (2013b). A 40-million-year history of atmospheric CO2. *Philos. Trans. R. Soc. A Math. Phys. Eng. Sci.* 371, 20130096–20130096. doi:10.1098/rsta.2013.0096.

Zhang, Z., Zimmermann, N. E., Calle, L., Hurtt, G., Chatterjee, A., and Poulter, B. (2018b). Enhanced response of global wetland methane emissions to the 2015–2016 El Niño-Southern Oscillation event. *Environ. Res. Lett.* 13, 074009. doi:10.1088/1748-9326/aac939.

Zhang, Z., Zimmermann, N. E., Stenke, A., Li, X., Hodson, E. L., Zhu, G., et al. (2017). Emerging role of wetland methane emissions in driving 21st century climate change. *Proc. Natl. Acad. Sci.* 114, 9647–9652. doi:10.1073/pnas.1618765114.

Zhou, F., Shang, Z., Zeng, Z., Piao, S., Ciais, P., Raymond, P. A., et al. (2015). New model for capturing the variations of fertilizer-induced emission factors of N 2 O. *Global Biogeochem. Cycles* 29, 885–897. doi:10.1002/2014GB005046.

Zhou, X., Thomas, E., Rickaby, R. E. M., Winguth, A. M. E., and Lu, Z. (2014). I/Ca evidence for upper ocean deoxygenation during the PETM. *Paleoceanography* 29, 964–975. doi:10.1002/2014PA002702.

Zhu, Z., Piao, S., Myneni, R. B., Huang, M., Zeng, Z., Canadell, J. G., et al. (2016). Greening of the Earth and its drivers. *Nat. Clim. Chang.* 6, 791–795. doi:10.1038/nclimate3004.

Zickfeld, K., Azevedo, D., and Matthews, H. D. (2019). Asymmetry in the climate-carbon cycle response to positive and negative CO2 emissions. (in prep.).

Zickfeld, K., Eby, M., Matthews, H. D., and Weaver, A. J. (2009). Setting cumulative emissions targets to reduce the risk of dangerous climate change. *Proc. Natl. Acad. Sci.* 106, 16129–16134. doi:10.1073/pnas.0805800106.

Zickfeld, K., Eby, M., Weaver, A. J., Alexander, K., Crespin, E., Edwards, N. R., et al. (2013). Long-Term Climate Change Commitment and Reversibility: An EMIC Intercomparison. *J. Clim.* 26, 5782–5809. doi:10.1175/JCLI-D-12-00584.1.

Zickfeld, K., and Herrington, T. (2015). The time lag between a carbon dioxide emission and maximum warming increases with the size of the emission. *Environ. Res. Lett.* 10, 031001. doi:10.1088/1748-9326/10/3/031001.

Zickfeld, K., MacDougall, A. H., and Matthews, H. D. (2016). On the proportionality between global temperature change and cumulative CO 2 emissions during periods of net negative CO 2 emissions. *Environ. Res. Lett.* 11, 055006. doi:10.1088/1748-9326/11/5/055006.

Ziegler, M., Diz, P., Hall, I. R., and Zahn, R. (2013). Millennial-scale changes in atmospheric CO2 levels linked to the Southern Ocean carbon isotope gradient and dust flux. *Nat. Geosci.* 6, 457–461. doi:10.1038/ngeo1782.

Figures

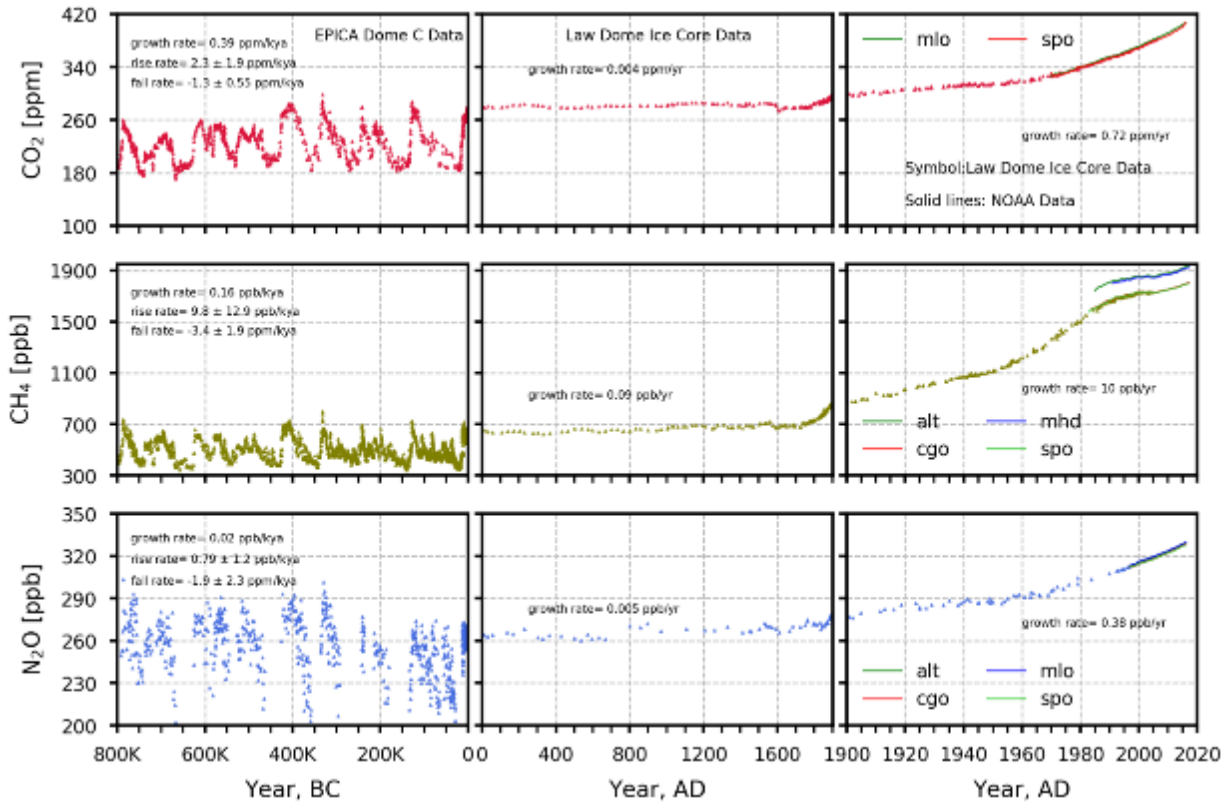

Figure 5.1: Atmospheric concentrations of CO2, CH4 and N2O in air bubble trapped in ice cores, dated period from 800,000 BCE to 1990 CE (note the variable x-axis range and tick mark intervals for the 3 columns). Ice core data is over-plotted by atmospheric observations from 1958 to present for CO2, from 1984 for CH4 and from 1994 for N2O. The linear growth rates for different time periods (800K–0 BCE, 0–1900 CE and 1900–2017 CE) are given in each panel. For the BCE period, mean rise and fall rates are calculated for the individual slopes between the peaks and troughs, which are given in the panels in left column. The data for BCE period are used from the Vostok, EPICA and Dome C ice cores (Loulergue et al., 2008; Lüthi et al., 2008; Monnin, 2001; Pépin et al., 2001; Petit et al., 1999; Raynaud et al., 2005; Schilt et al., 2010; Siegenthaler et al., 2005). The data until 0–yr CE are taken mainly from Law Dome ice core analysis (MacFarling Meure et al., 2006). The surface observations for all species are taken from NOAA cooperative research network (Dlugokencky and Tans, 2019), where ALT, MLO and SPO stand for Alert (Canada), Mauna Loa Observatory, and South Pole Observatory, respectively.

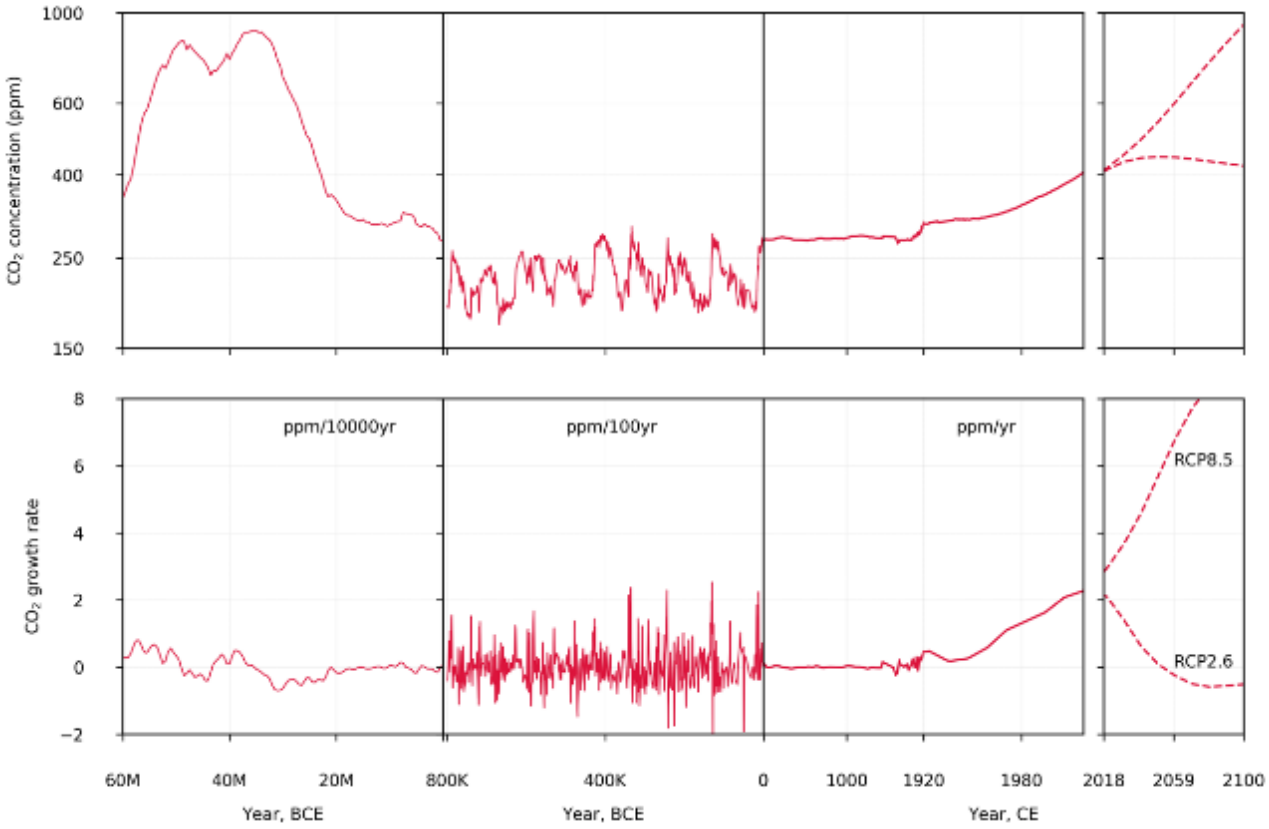

Figure 5.2: CO_2 concentrations and growth rates for the past 60 million years to 2100 using RCP2.6 and RCP8.5. Concentrations data as in Figure 5.1 and data prior to 800K years from (Foster et al., 2017). BCE = Before Current Era, CE = Current Era.

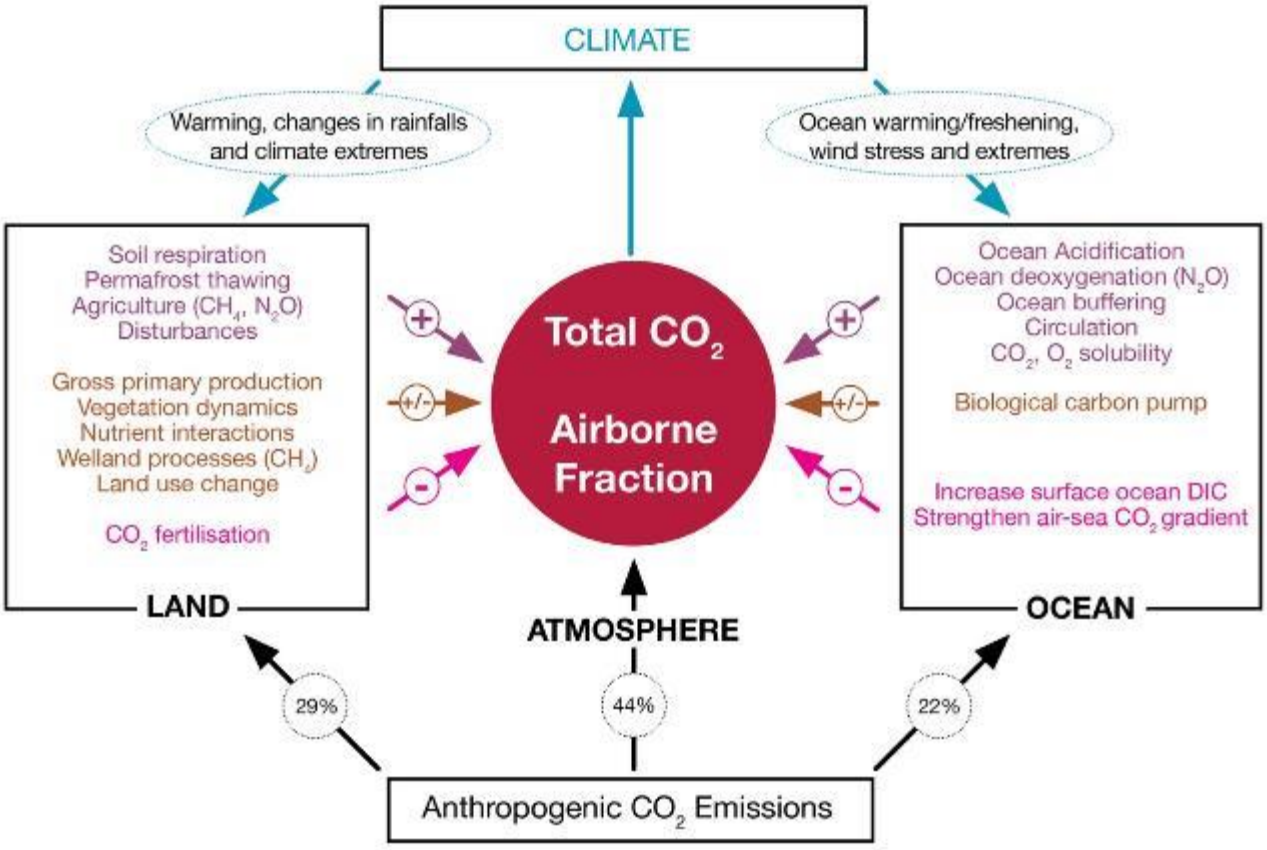

Figure 5.3: Schematic summarizing the key compartments, processes and pathways that govern historical and future carbon concentration and carbon – climate feedbacks through both terrestrial and ocean systems. Central to this is the influence of both carbon and climate feedbacks on the evolution of the GHG burden in the atmosphere and the airborne fraction of anthropogenic CO_2 (Red circle), which drives the Earth's energy imbalance that is partitioned between the ocean (93%) and the terrestrial residual (7%). The ocean dominates the heat feedback. The airborne fraction that drives this historical climate forcing (~ 44%) is largely regulated by the negative feedback of ocean (22%) and terrestrial (29%) sinks that partition anthropogenic CO_2 (black arrows) in ocean and terrestrial domains (magenta) and result in negative feedbacks (magenta) (partition excludes the estimated imbalance of 0.5PgC: see Table 5.1). Positive feedback processes (Purple arrows) although mostly weak in the historical period, are *likely* to strengthen in the coming decades and are influenced by both carbon and climate forcing simultaneously (Purple). Additional biosphere processes have been included that have an, as yet uncertain feedback bias (Brown arrows). Although this schematic is built around CO_2, the dominant GHG, some of the same processes also influence the fluxes of CH_4 and N_2O from the terrestrial and ocean systems. Those are noted as they contribute to the total radiative forcing.

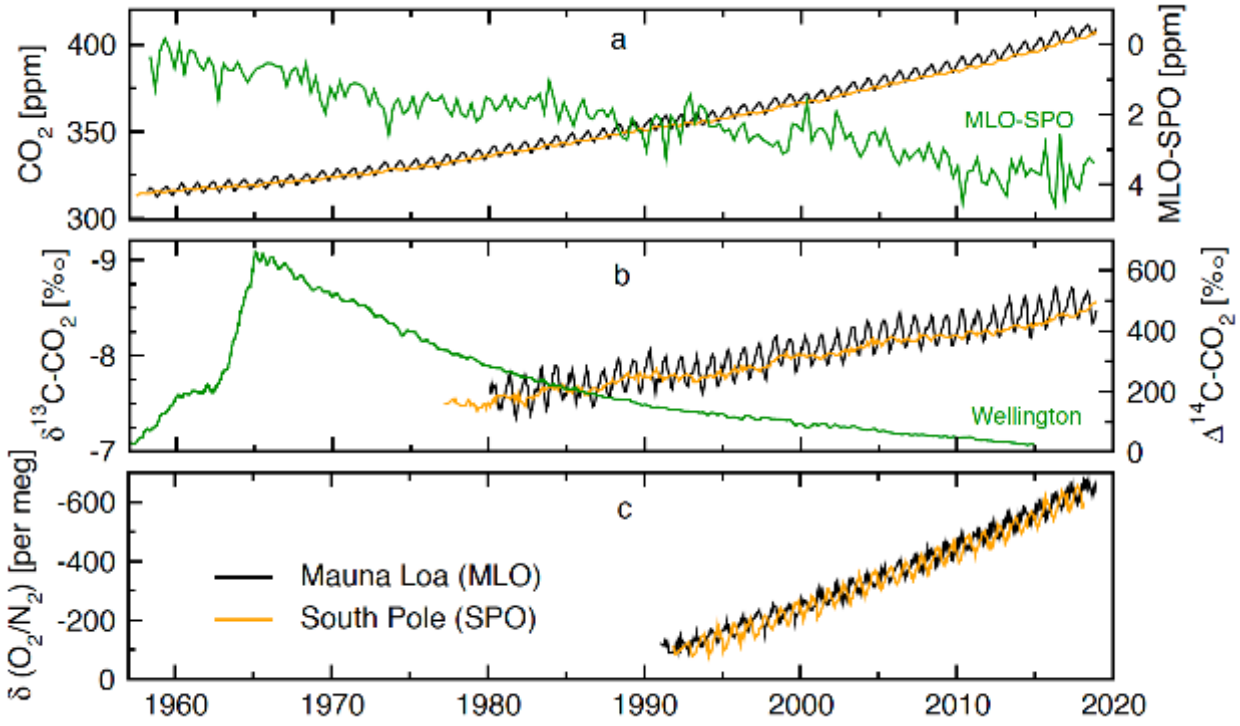

Figure 5.4: Time series of CO2 concentrations and related measurements in ambient air. All the data are taken from Mauna Loa Observatory (MLO) and South Pole Observatory (SPO) operated by the Scripps Institution of Oceanography (SIO)/University of California, San Diego (Keeling et al., 2001) except for the δ 14C-CO2 (panel b, right y-axis). The δ(O2/N2) are expressed in per meg units (= (FF/M)×106, where FF = moles of O2 consumed by fossil-fuel burning, M = 3.706×1019, total number of O2 molecules in the atmosphere) (Goddard et al., 2007). The 14CO2 time series at Wellington, New Zealand (BHD) is provided by GNS Science and NIWA (Turnbull et al., 2017).

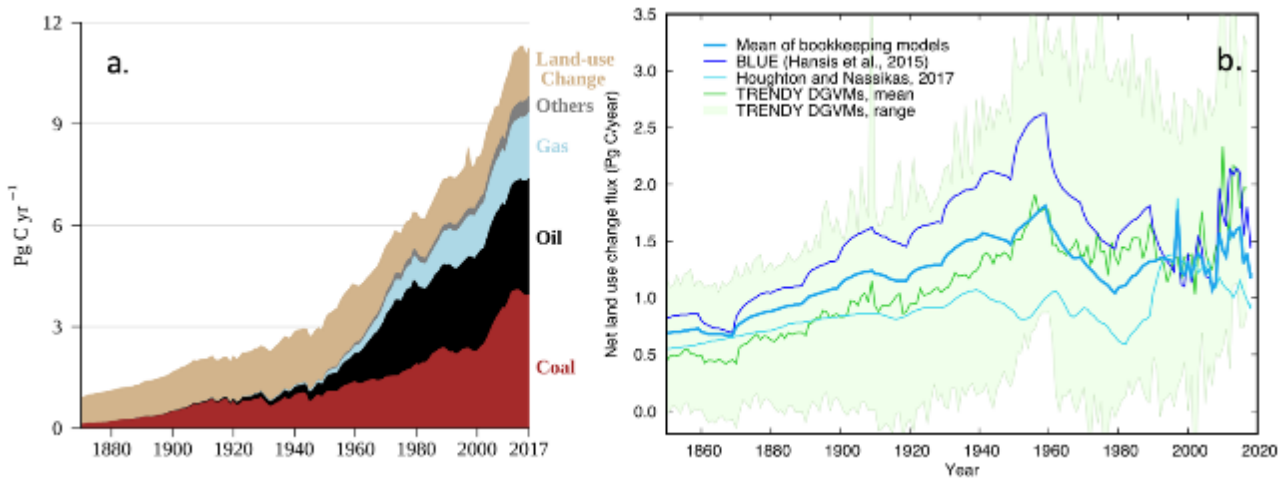

Figure 5.5: Global anthropogenic CO_2 emissions: A) Historical trends of anthropogenic CO_2 emission for the period 1870 to 2016. Data sources: (Andrew, 2018; BP, 2018; IEA, 2017; Marland et al.; Quéré et al., 2018). B) The net land use change CO_2 flux (Pg yr^{-1}) from two bookkeeping and 16 dynamic global vegetation models (Le Quéré et al., 2018a). Bookkeeping models are BLUE (Hansis et al., 2015; Houghton and Nassikas, 2017) both updated as described in (Le Quéré et al., 2018a). All estimates are unsmoothed annual data. Note that the estimates differ in process comprehensiveness of the models and in definition of flux components included in the net land use change flux.

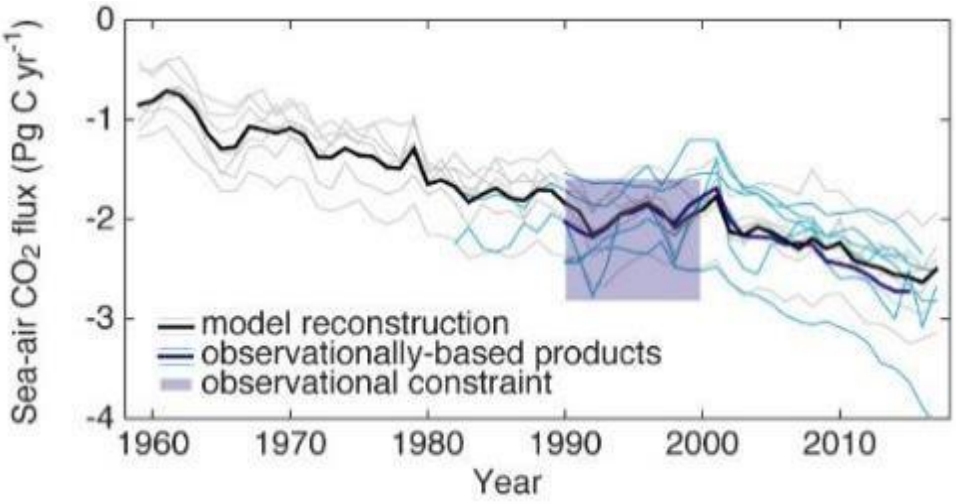

Figure 5.6: Temporal evolution of the globally-integrated sea-air CO_2 flux as reconstructed by (grey/black) ocean physical and biogeochemical models forced with observed atmospheric history (Aumont and Bopp, 2006; Berthet et al.; Doney et al., 2009; Hauck et al., 2018; Le Quéré et al., 2010; Paulsen et al., 2017; Schwinger et al., 2016), and (blue) observationally-based products that represent spatial and temporal variability in the flux from sparse observations of surface ocean pCO_2 (Denvil-Sommer et al., 2018; Gregor et al., 2019; Iida et al., 2015; Landschützer et al., 2016; Rödenbeck et al., 2013; Zeng et al., 2015). Thick lines represent the multi-model mean. Observationally-based products have been corrected for a 0.45 PgC yr^{-1} pre-industrial riverine source of carbon, as in (Le Quéré et al., 2018b). Dark blue box represents the observed range in the 1990s (using a 90% confidence interval, as in Le Quéré et al., 2018b). [[Placeholder: include ensemble from inversion models]]

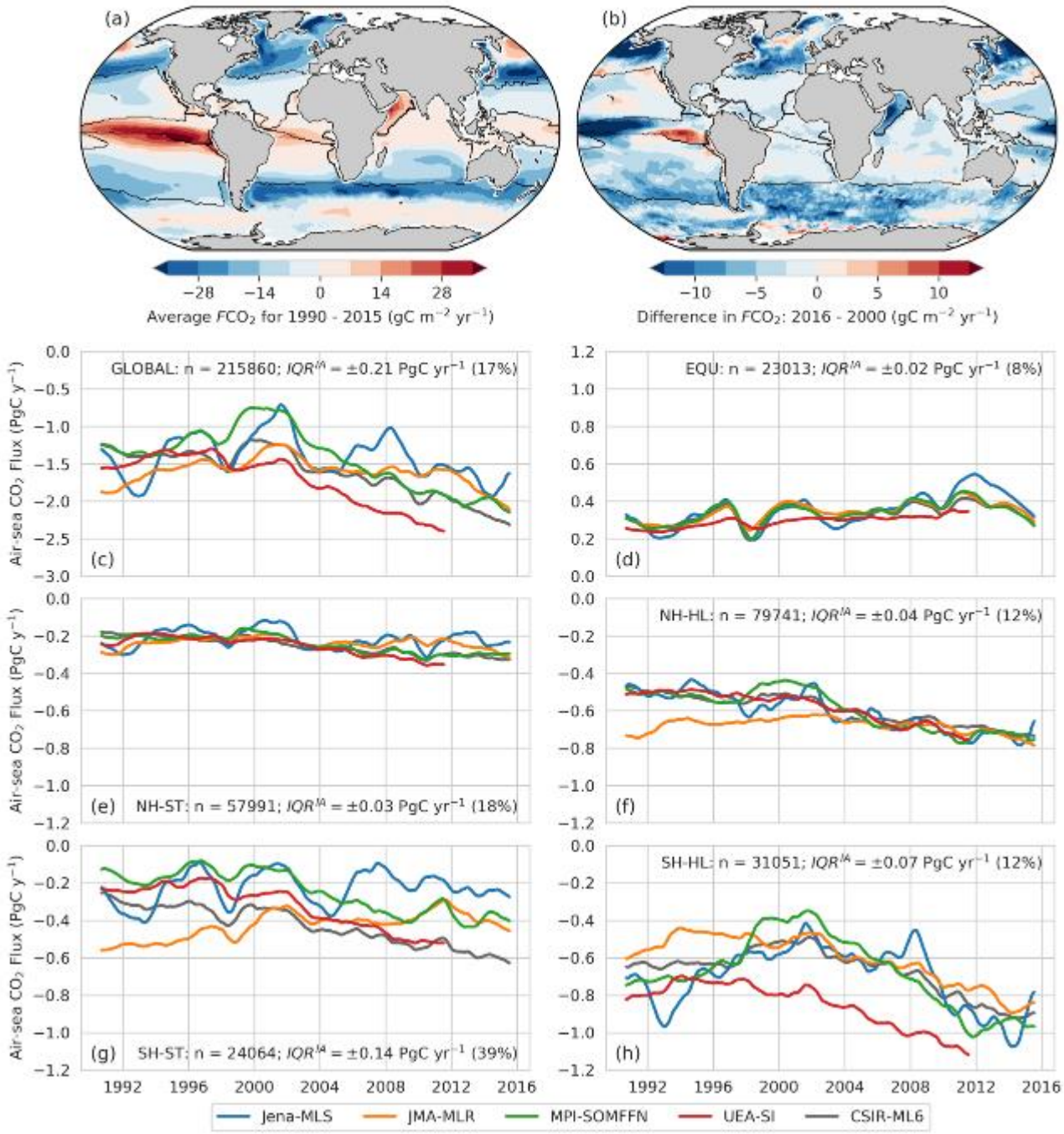

Figure 5.7: Regional characteristics of the mean multi-decadal fluxes showing: (a) ocean CO_2 uptake is dominated by the mid-latitude oceans and (b) mid- to high latitudes contributed the most to the decadal invigoration in ocean CO_2 uptake (2000–2016). The trends plotted in the lower panels show that (1) the Southern Ocean is critical to global variability, (2) the tropics are characterised by a strengthening outgassing and 3) most of the inter-model uncertainty arises from the Southern Hemisphere where observations are sparse (Gregor et al., 2019). [[Placeholder: This figure may be changed to means of model types – empirical, inversion, ESM]]

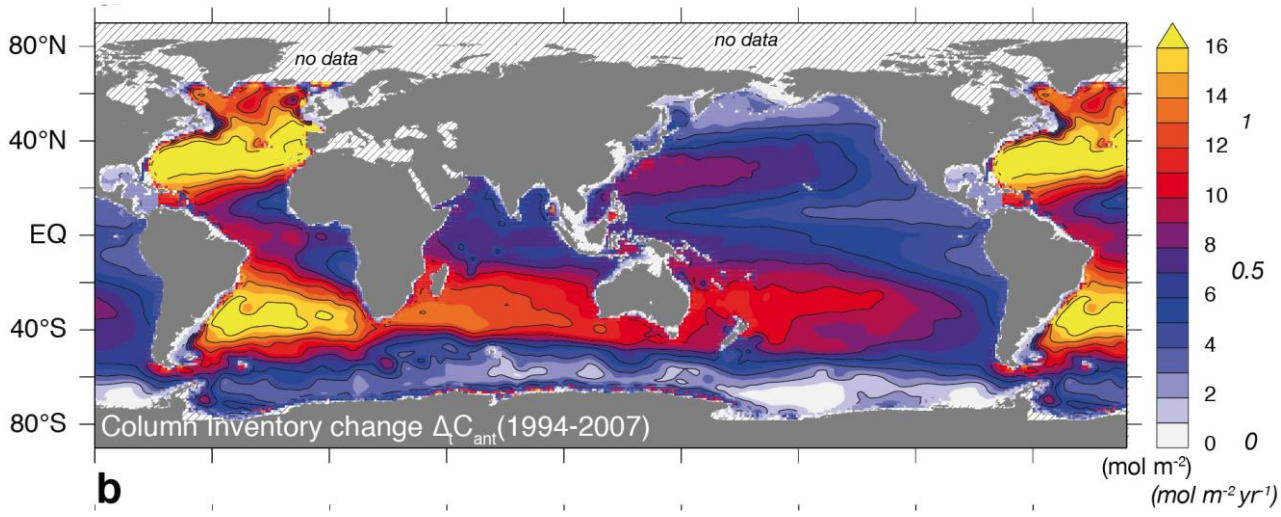

Figure 5.8: Map of column inventory change of anthropogenic CO_2 between 1994 and 2007 (Gruber et al., 2019). It shows that regional ocean inventories are dominated by the Mode and Intermediate waters of the Atlantic Ocean and to a letter extent the Indian and Pacific Ocean. Most of the net increase in storage relative to the previous decade is in the Southern Hemisphere reservoirs.

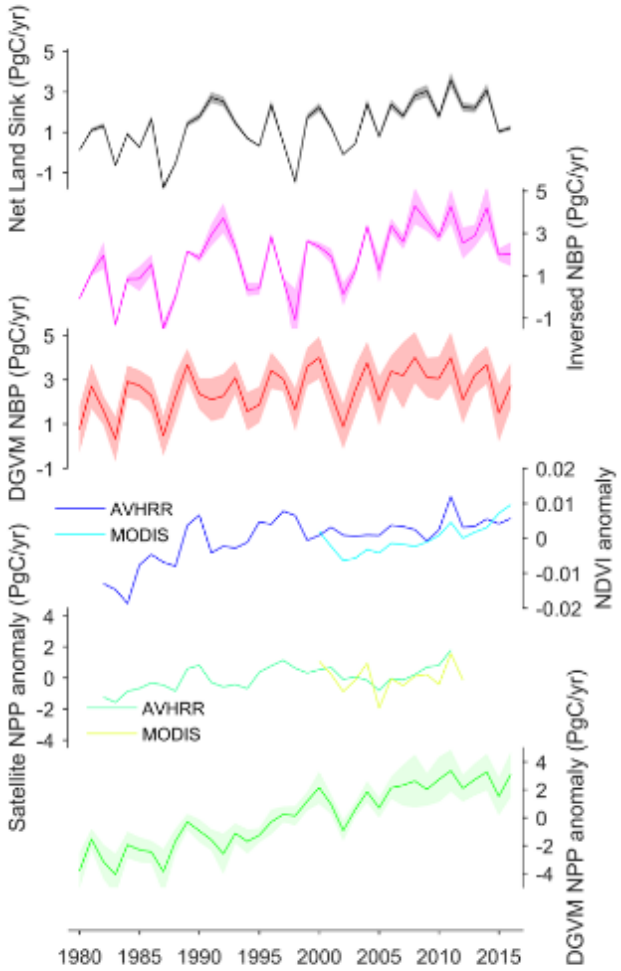

Figure 5.9: Change of net land CO_2 sink, Normalised Difference Vegetation Index (NDVI) and net primary productivity during 1980–2016. Net land CO_2 sink is estimated from the global CO_2 mass balance (Le Quéré et al., 2018b). Inversion Net Biome Productivity (NBP) is the net land CO_2 flux estimated by an ensemble of atmospheric inversion models. Positive net land CO_2 sink and NBP values indicate net CO_2 uptake from the atmosphere. DGVM NBP is the ensemble net land CO_2 flux estimated by 16 Dynamic Global Vegetation Models driven by climate change, rising atmospheric CO_2, land use change and nitrogen deposition change (for carbon-nitrogen models). NDVI anomaly is the anomaly of global area-weighted NDVI observed by AVHRR and MODIS satellite sensors. AVHRR data are available during 1982–2016 and MODIS data are available during 2000–2016. Net Primary Productivity based on the two satellites data have the temporal coverage of 1982–2011 for AVHRR NPP and 2000-2012 for MODIS NPP. DGVM NPP is the ensemble global NPP estimated by the same 16 DGVMs as the DGVM NBP estimates. Shaded area for net land CO_2 sink is the uncertainty range (Le Quéré et al., 2018b). Shaded area for other panels indicates standard deviation of different atmospheric inversions or DGVMs.

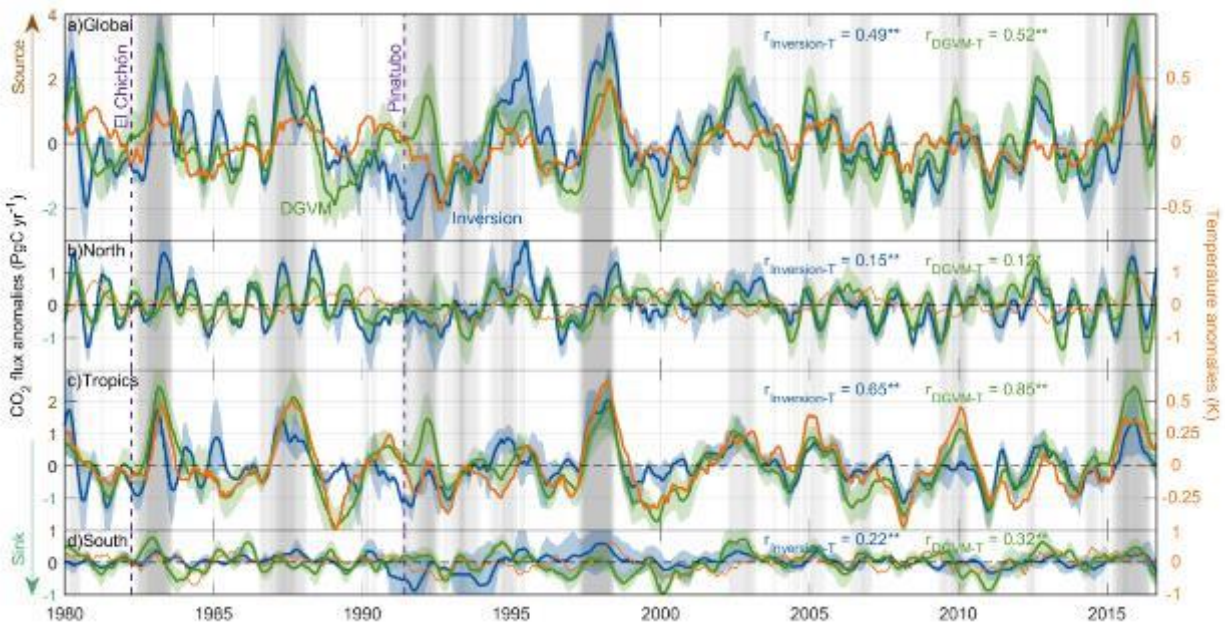

Figure 5.10: Interannual variation in detrended anomalies of net land CO_2 sink (NLS) and temperature (T) and correlations of NLS anomalies and temperature anomalies at the globe or at the latitudinal bands during 1980–2016. NLS is estimated by atmospheric inversions and Dynamic Global Vegetation Models (DGVMs). Solid lines show model mean detrended anomalies of NLS. The ensemble mean of inversion models or TRENDY models is bounded by the 1–σ inter-model spread in each large latitude band (North 20°N–90°N, Tropics 20°S–20°N, South 90°S–20°S) and the globe. For each latitudinal band, the CO_2 flux anomalies and temperature anomalies were obtained by removing the long-term trend signal and seasonal cycle. Six-month running mean was taken to reduce high-frequency noise. Years on the horizontal axis indicate January of this year as the third month in the moving 6-month window. Correlation coefficients of NLS anomalies and temperature anomalies are shown for each region and two asterisks indicate the 99% significance and one indicates the 95% significance. Grey shaded area shows the intensity of El Niño-Southern Oscillation (ENSO) as defined by the multivariate ENSO index. Two volcanic eruptions (El Chichón eruption and Pinatubo eruption) are indicated with purple dashed lines. A positive flux anomaly means a larger than normal source of CO_2 to the atmosphere (or a smaller CO_2 sink). Net land CO_2 sink are estimated by four atmospheric inversions and thirteen DGVMs respectively (Le Quéré et al., 2018a). Temperature data are from Harris et al., (2014).

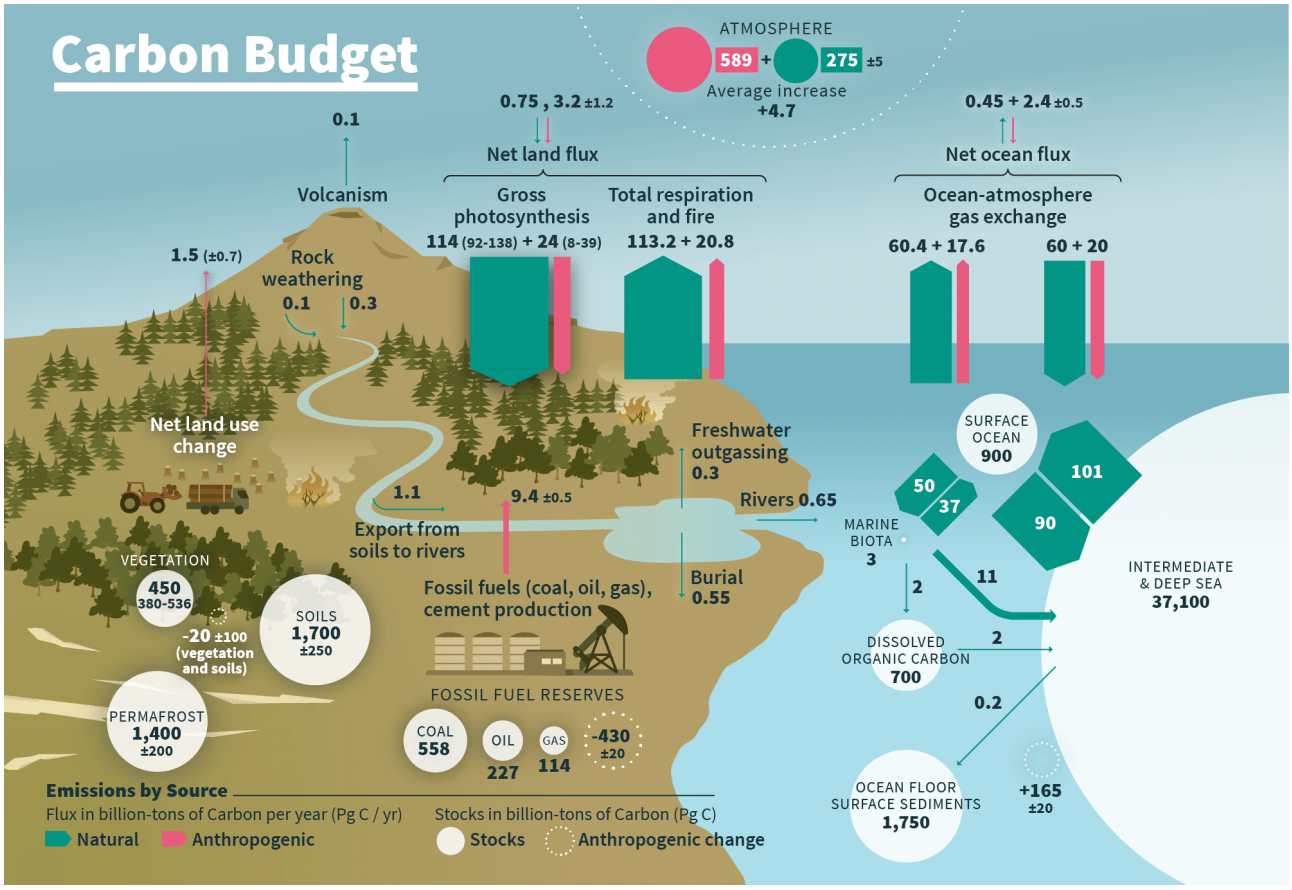

Figure 5.11: The global carbon cycle. Blue arrows represent annual carbon exchange fluxes (in PgC yr^{-1}) associated with the natural carbon cycle estimated for the time prior to the Industrial Era, around 1750. Pink arrows represent anthropogenic fluxes averaged over the period 2008–2017. The rate of carbon accumulation in the atmosphere is equal to net land-use change emissions plus fossil fuel emissions, minus land and ocean sinks (plus a small budget imbalance, Table 1). Numbers in white circles represent pre-industrial carbon stocks in PgC. Numbers in dashed circles represent anthropogenic changes to these stocks (cumulative anthropogenic fluxes) since 1750. Anthropogenic net fluxes are reproduced from le Le Quéré et al., (2018c). The relative change of *Gross photosynthesis* since pre-industrial times is estimated as the range of observation-based of 31±3 % (Campbell et al., 2017) and land-model of 19±12% (Sitch et al., 2015) estimates. This is used to estimate the pre-industrial *Gross photosynthesis*, assuming a present-day range of 116–175 $PgCy^{-1}$ (Joiner et al., 2018). The corresponding emissions by *Total respiration and fire* are those required to match the *Net land flux*. The cumulative change of anthropogenic carbon in the terrestrial reservoir is the sum of carbon cumulatively lost by net land use change emissions, and net carbon accumulated since 1750 in response to environmental drivers (warming, rising CO_2, nitrogen deposition) (Le Quéré et al., 2018a).The change in *Ocean-atmosphere gas exchange* (red arrows of ocean atmosphere gas exchange) is estimated from the difference in atmospheric partial pressure of CO_2 since 1750 (Sarmiento and Gruber, 2006). Individual gross fluxes and their changes since the beginning of the Industrial Era have typical uncertainties of more than 20%, while their differences (*Net ocean flux*) are determined from independent measurements with a much higher accuracy. Therefore, to achieve an overall balance, the values of the more uncertain gross fluxes have been adjusted so that their difference matches the and *Net ocean flux* estimate. The sediment storage is a sum of 150 PgC of the organic carbon in the mixed layer (Emerson and Hedges, 1988) and 1600 PgC of the deep-sea $CaCO_3$ sediments available to neutralize fossil fuel CO_2 (Archer et al., 1998). Note that the mass balance of the two ocean carbon stocks *Surface ocean* and *Intermediate and deep ocean* includes a yearly accumulation of anthropogenic carbon (not shown). Fossil fuel reserves are from (BGR, 2017). Permafrost region stores are from (Hugelius et al., 2014; Strauss et al., 2017) and soil carbon stocks outside of permafrost region from (Batjes, 2016; Jackson et al., 2017). Biomass stocks (range of seven estimates) are from (Erb et al., 2018). Fluxes from volcanic eruptions, rock weathering (removal of atmospheric CO_2 in weathering reactions and chemical weathering of C contained in rocks) export of carbon from soils to rivers, burial of carbon in freshwater lakes and reservoirs and transport of carbon by rivers to the ocean are all assumed to be pre-industrial fluxes and are sourced from (Regnier et al., 2013).

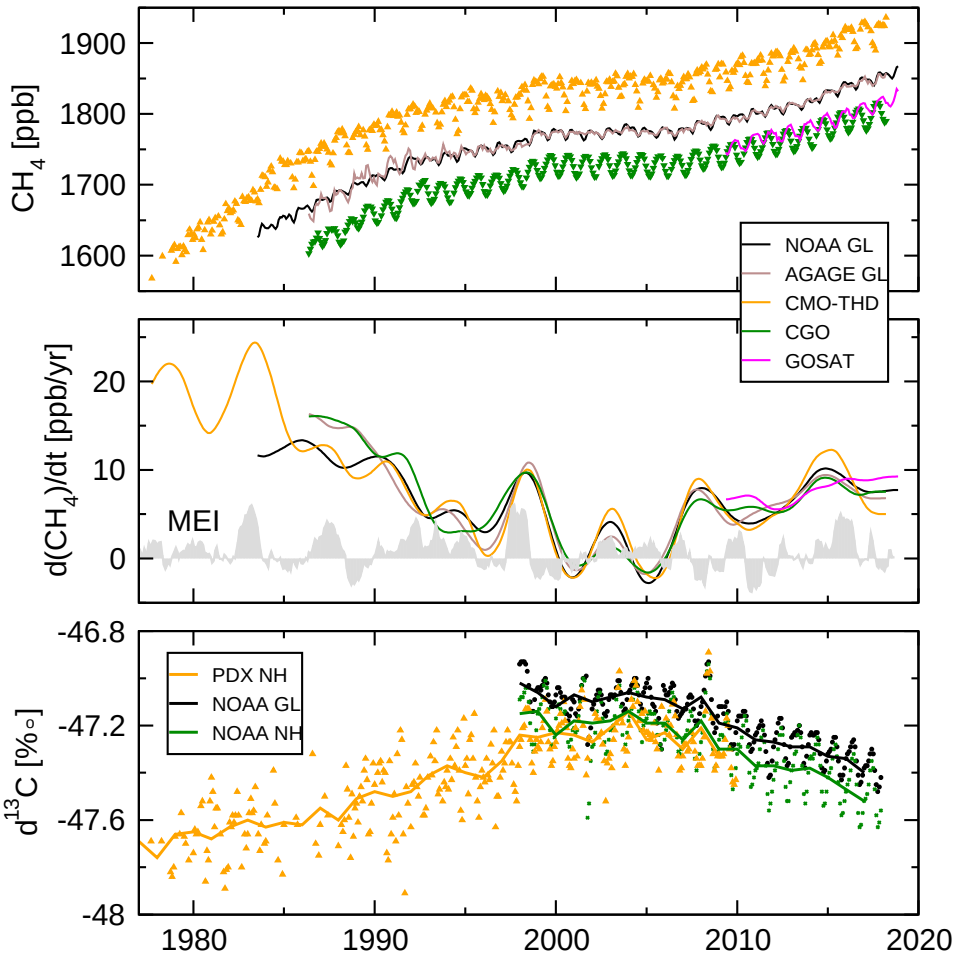

Figure 5.12: Time series of CH_4 mole fraction (in ppb), growth rate (ppb yr^{-1}) and $\delta^{13}C$ from selected sites from NOAA, AGAGE and PDX surface networks (data sources: Portland State University - PDX; www.esrl.noaa.gov/gmd/ccgg/trends_ch4/; https://agage.mit.edu/data/agage-data). To maintain clarity, data from many other measurement networks are not included here. Global mean values of XCH_4 (total-column) from Greenhouse gases Observation SATellite (GOSAT; www.gosat.nies.go.jp/en/recent-global-ch4.html) are shown. Cape Grim Observatory (CGO) and Trinidad Head (THD) data are taken from the AGAGE network, NOAA global (GL) and northern hemispheric (NH) means for $\delta^{13}C$ are calculated from 10 and 6 sites, respectively. The PDX data adjusted to NH (period: 1977–1996) are merged with THD (period: 1997–2018) for CH_4 concentration and growth rate analysis, and PDX and NOAA NH means of $\delta^{13}C$ data are used for joint interpretation of long-term trends analysis.

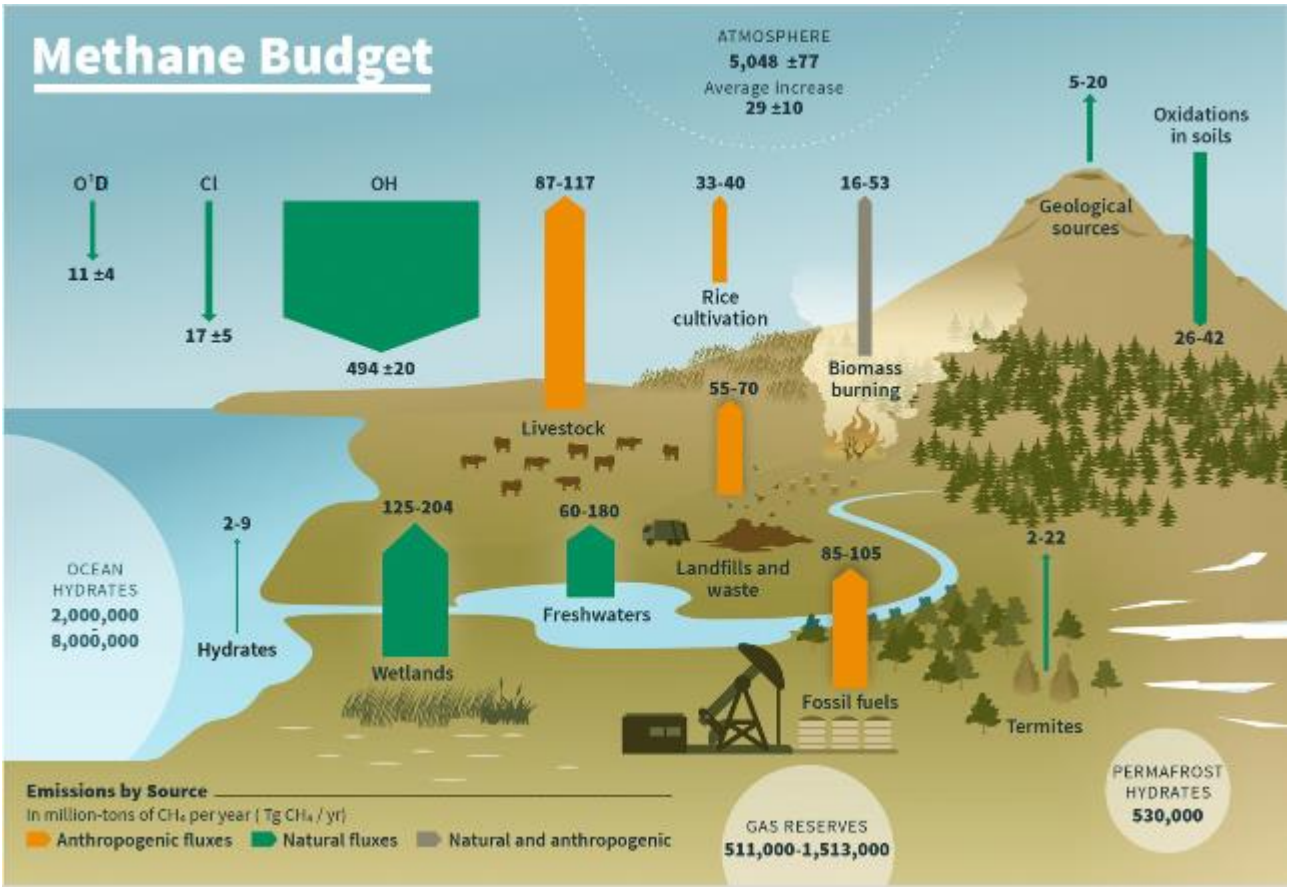

Figure 5.13: Schematic diagram of major sources and sinks of CH_4 for the decade 2010–2017. Values and data sources as in Table 5.2.

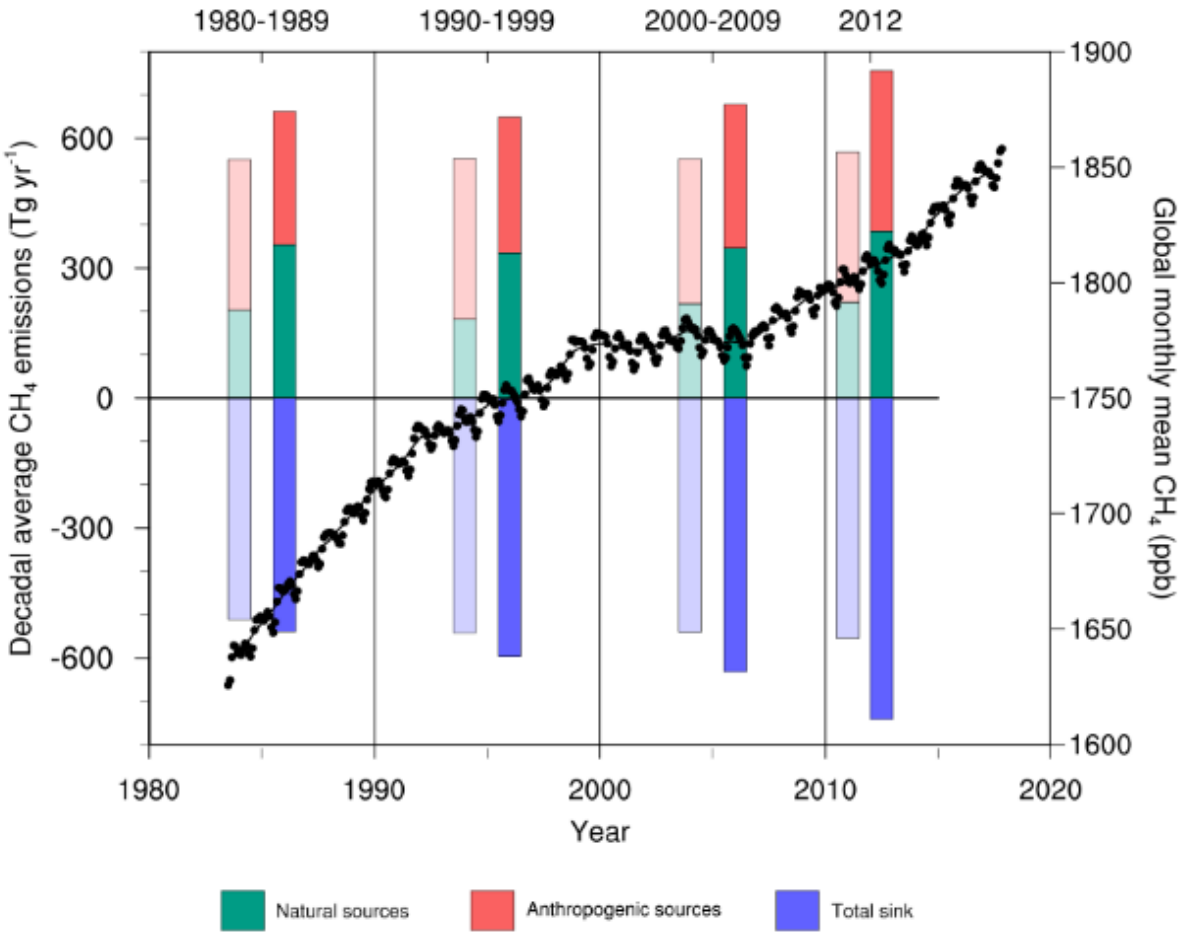

Cross-Chapter Box 5.1, Figure 1: Methane budget estimates for four decades from top-down (light colour, left) and bottom-up (dark colour, right) analyses (plotted on the left y axis). Sources are positive and sinks are negative. The black dots represent observed global monthly mean atmospheric CH_4 dry-air mole fractions for 1983–2017 (Dlugokencky et al.) (www.esrl.noaa.gov/gmd/ccgg/trends_ch4) and the solid black line represents the smoothed global monthly means (plotted on the right y axis). The bottom-up total sinks are inferred from the global mass balance (i.e., source minus growth) and not directly computed. [[Placeholder: To be updated]].

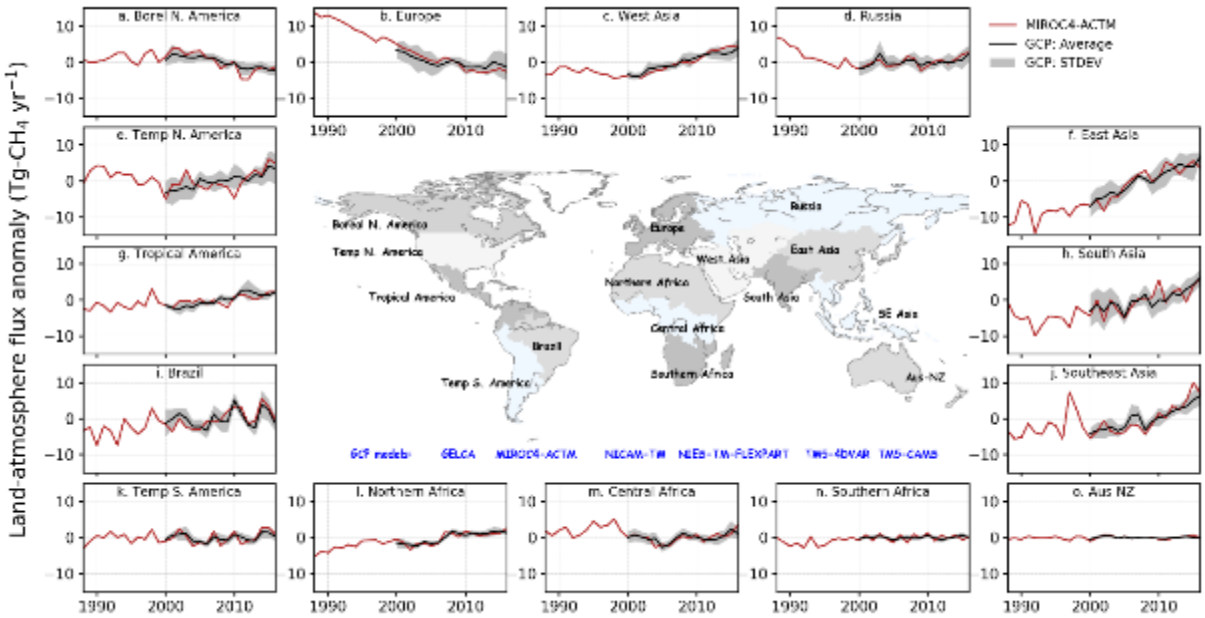

Cross-Chapter Box 5.1, Figure 2: Anomalies in regional CH_4 emissions during 1988-2016. Results for 2000-2016 are shown for 8 inversion models that participated in GCP-CH_4 budget assessment (update from Saunois et al., 2017), and results for 1988-1999 are available from only one inversion (Chandra, in prep). A long-term mean is subtracted from the annual-mean time series for the calculation of anomalies for each region.

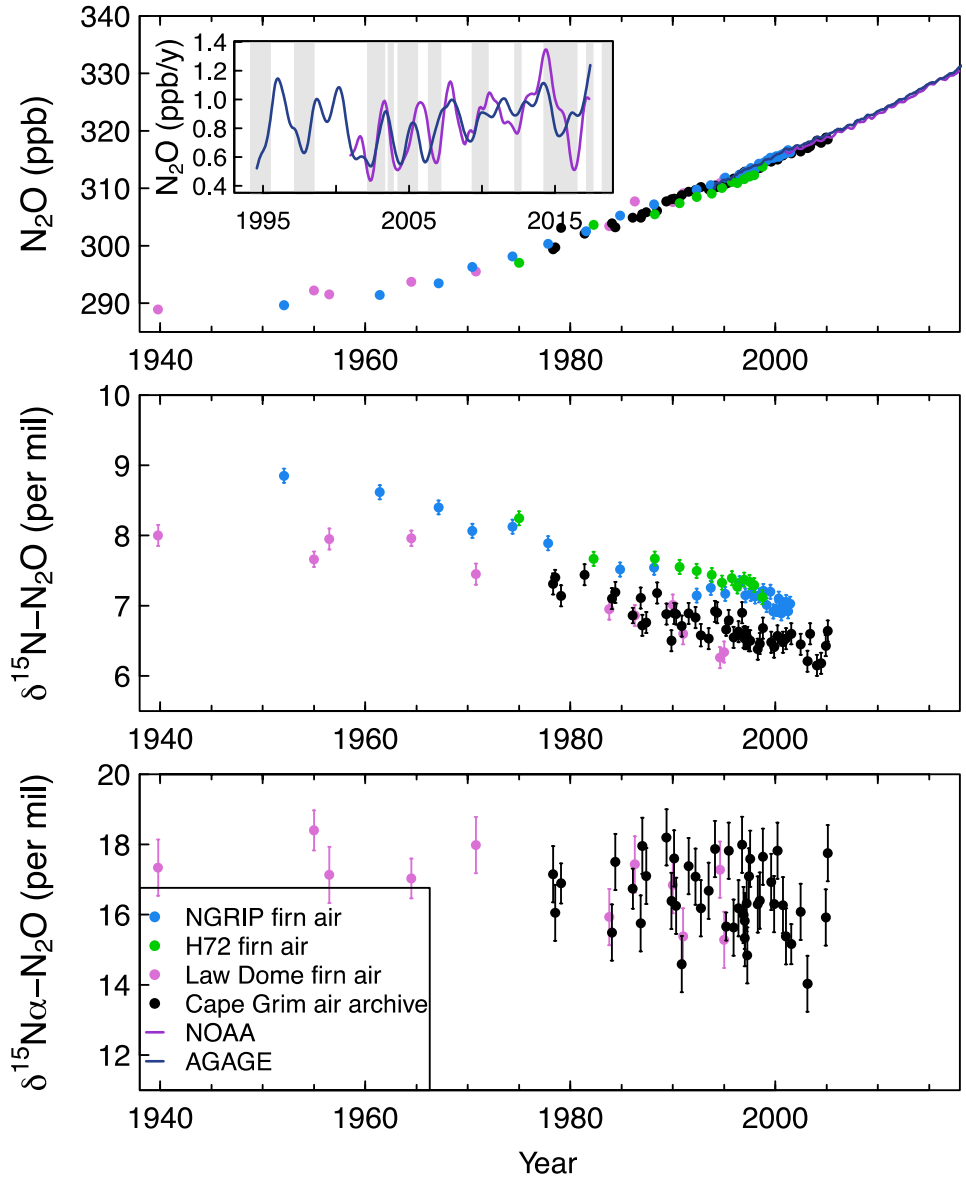

Figure 5.14: (a) Atmospheric N_2O abundance (parts per billion, ppb) and growth rate (ppb yr^{-1}), (b) δ15N of atmospheric N_2O, and (c) alpha-site 15N–N_2O, based on direct atmospheric measurements in the AGAGE and NOAA (Elkins et al., 2018; Hall et al., 2007; Prinn et al., 2000, 2016) networks, archived air samples from Cape Grim, Australia (Park et al., 2012), and firn air from NGRIP Greenland and H72 Antarctica (Ishijima et al., 2007), and Law Dome Antarctica (Park et al., 2012). Grey shading in (a) are times of positive values of the multivariate ENSO index, indicating El Nino conditions (Wolter and Timlin, 1998).

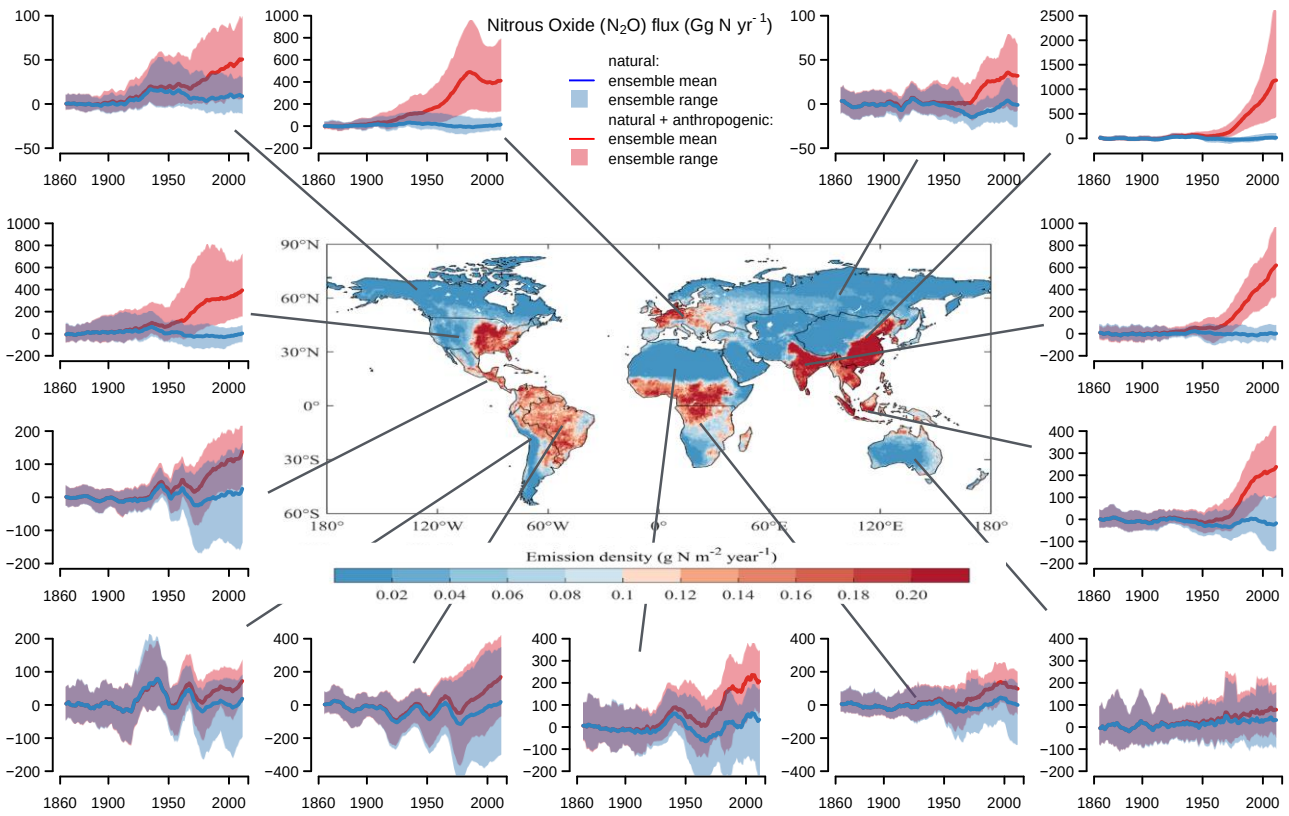

Figure 5.15: Trends in the N_2O emissions from terrestrial soils (natural and agriculture) simulated from the NMIP ensemble of terrestrial biosphere models (Tian et al., 2019). The effect of anthropogenic nitrogen additions (atmospheric deposition, manure addition, fertiliser use) is evaluated against the background flux driven by changes in atmospheric CO_2 concentration, climate change, and land cover change. The map in the centre shows the ensemble average of the decadal mean N_2O emissions for 2007–2016 including all forcings.

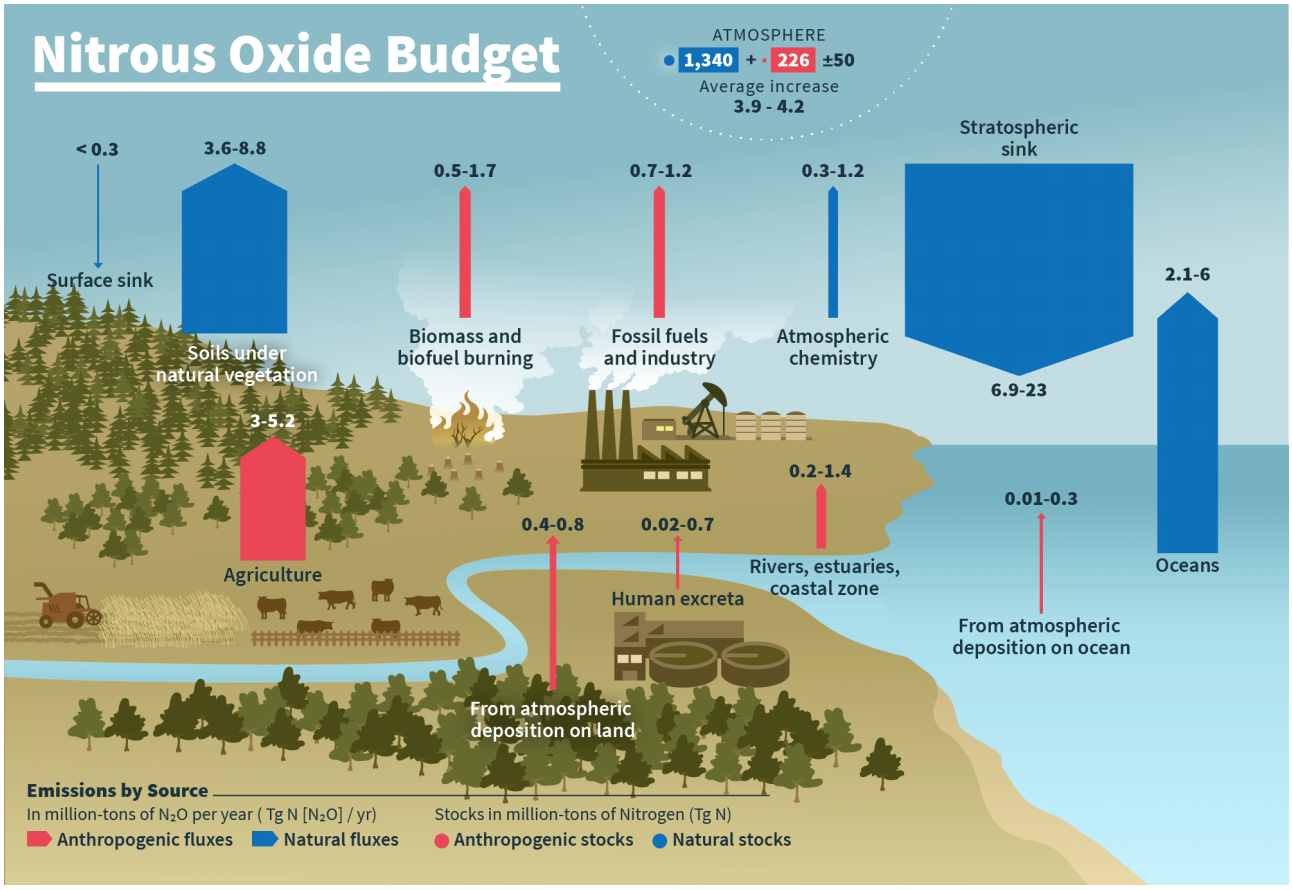

Figure 5.16: Global nitrous oxide (N_2O) budget for the period 2007–2016. Annual nitrous oxide fluxes ($TgN_2O–N\ yr^{-1}$) and nitrous oxide pools ($TgN_2O–N$), as described in Table 5.3.

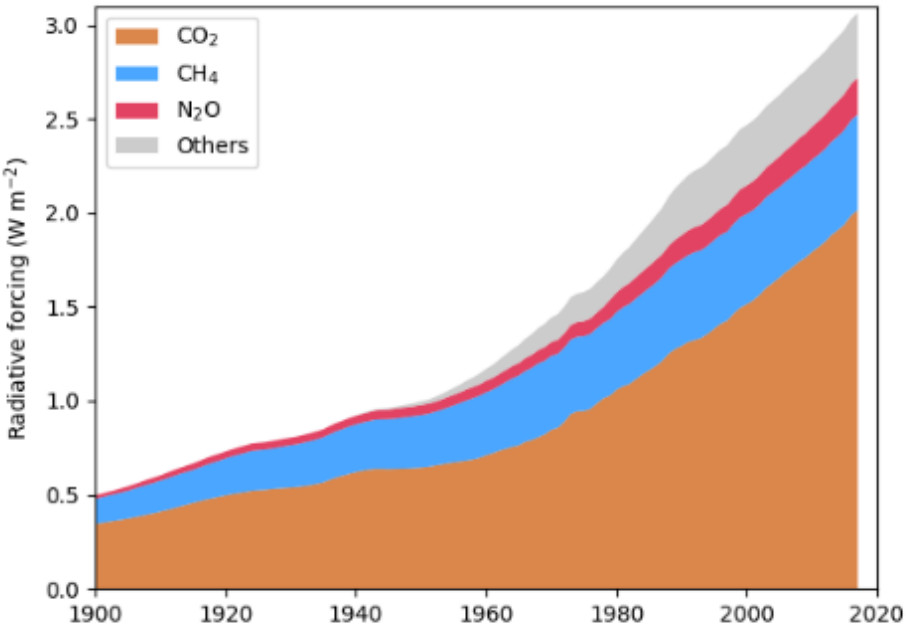

Figure 5.17: Change in radiative forcing by long-lived GHGs since 1900 (values relative to 1750, as a reference of the preindustrial era). The concentration time series of CO_2, CH_4 and N_2O are taken from Figure 5.1 for the calculation of radiative forcings using the simplified expressions given in (Etminan et al., 2016); the calculation includes shortwave forcing and the overlap between CO_2 and N_2O. The radiative forcing of synthetic gases (others) for the period 1979–2017 is taken from (Hofmann et al., 2006), with an extrapolation to 0 at 1940 when the CFCs were first introduced for industrial use.

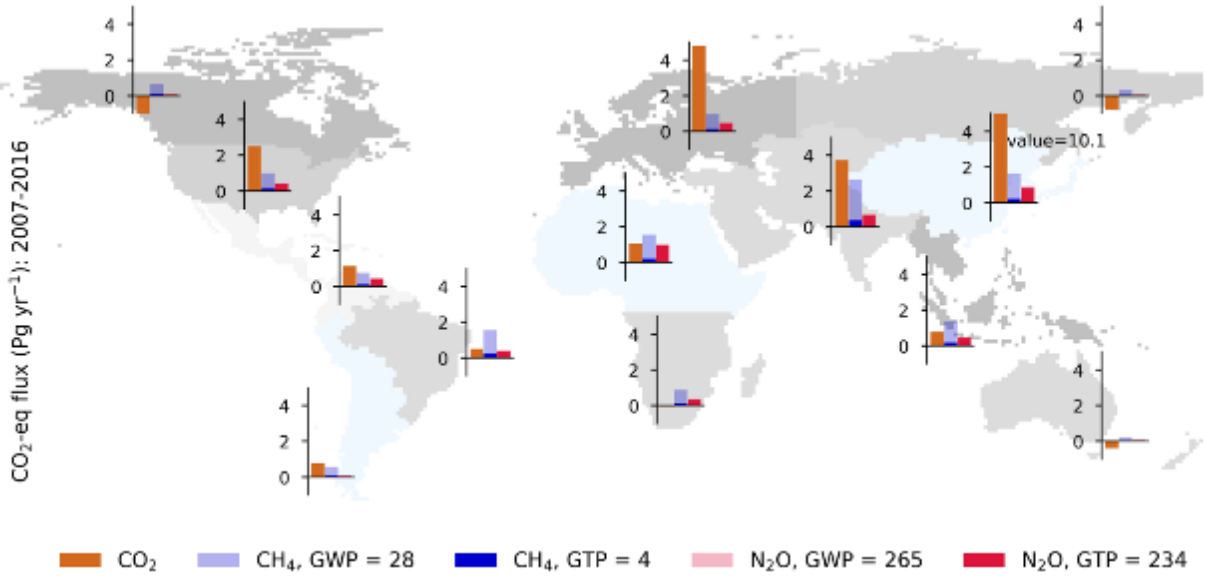

Figure 5.18: Regional attribution of global fluxes of CO_2, CH_4 and N_2O derived from concentrations as in Figure 5.1. The fluxes include anthropogenic sources and sinks, and natural fluxes that result from responses to anthropogenic GHGs and climate forcing (feedbacks) as in the three budgets shown in Sections 5.2.1.5, 5.2.2.5, and 5.2.3.5. The CH_4 and N_2O emissions are weighted by their global warming potential (GWP) and global temperature-change potential (GTP) over 100-year time horizon (GTP and GWP values from Chapter 7). Fluxes are from MIROC4-ACTM inverse modelling (updated from (Patra et al., 2016; Saeki and Patra, 2017; Thompson et al.)) and will be replaced by multi-model results from GCP budgets-2019 and AR6.

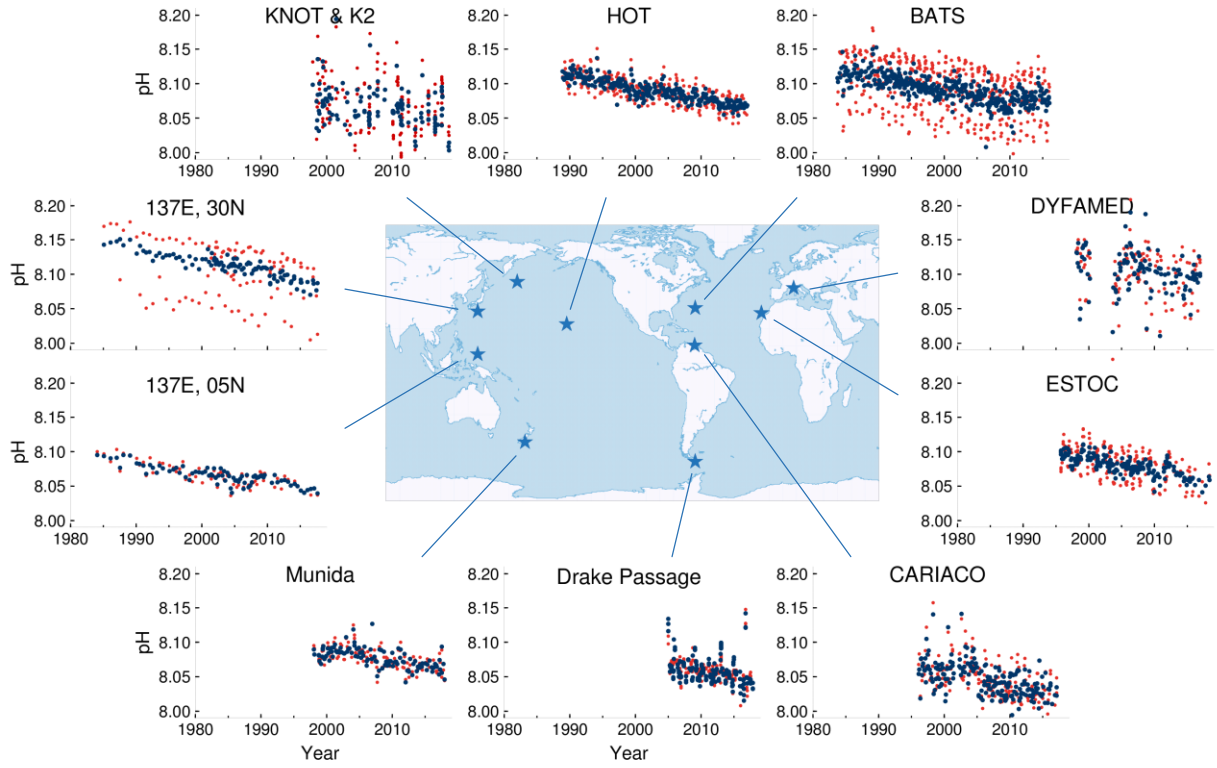

Figure 5.19: Time-series of pH (red) and seasonally-detrended pH (blue) in surface layer at various sites of the oceans. [[Placeholder: to be updated]]

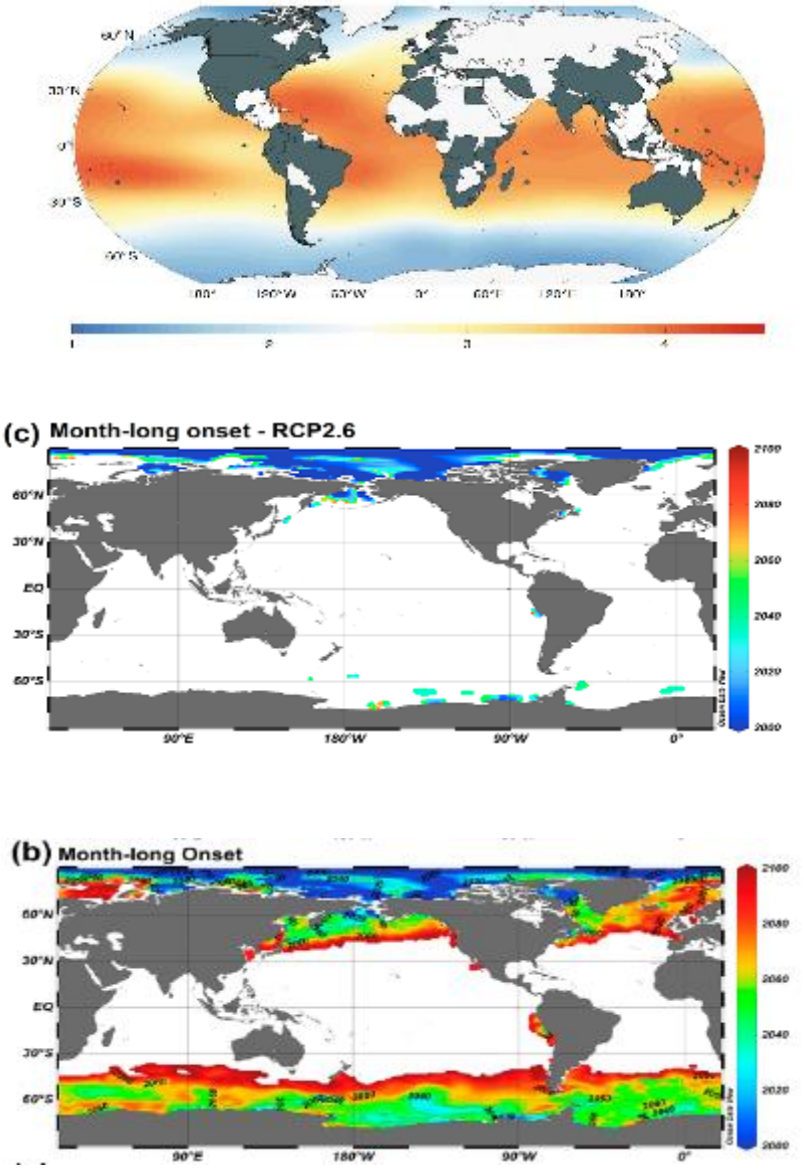

Figure 5.20: Upper the observed aragonite saturation state in the present day (Hurd et al., 2018), and lower year that surface waters will become undersaturated with respect to aragonite at the monthly scale for high and low emissions pathways (RCP2.6 and RCP8.5) from Sasse et al., (2015).

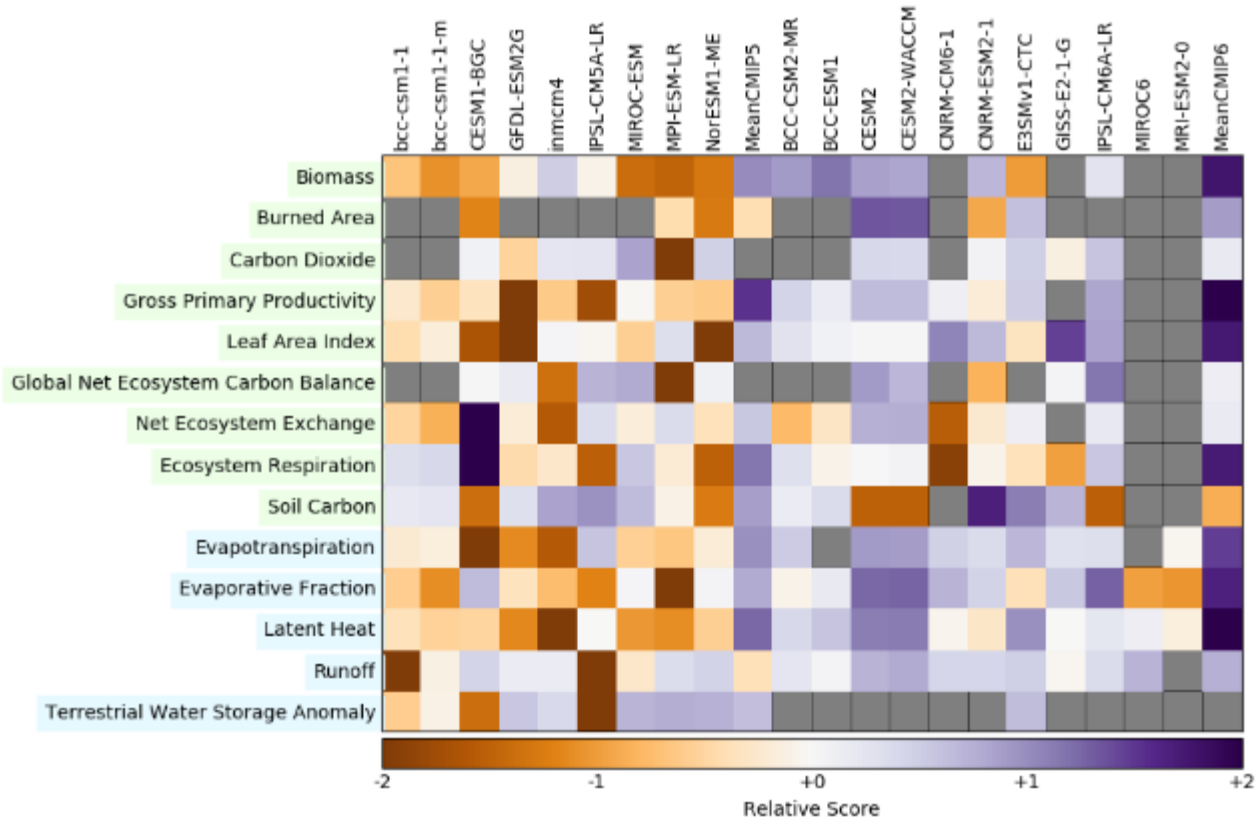

Figure 5.21: Overview scores of CMIP5 (left hand side of table) and CMIP6 (right hand side of table) models, for multiple land-surface benchmarks against different datasets. Scores are relative to other models within each benchmark row, with positive scores indicating a better agreement with observations. [[Placeholder: Figure to be updated in SOD to include all and only the models used for carbon cycle feedback parameter assessments in AR5 and AR6, as well as to sort out some artefacts in current figure associated with unit conversions that are resulting in missing values (grey squares), etc.]]

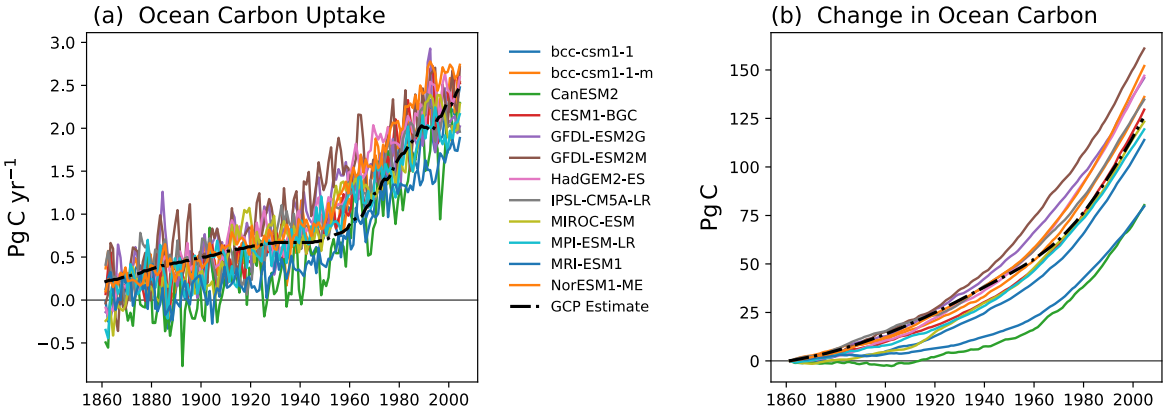

Figure 5.22: Modelled ocean carbon sink for 1850 to 2005 in historical ESM simulations, compared to observation-based estimates (from GCP); panel (a): uptake rate (PgC yr^{-1}), panel (b): change in carbon store (PgC).

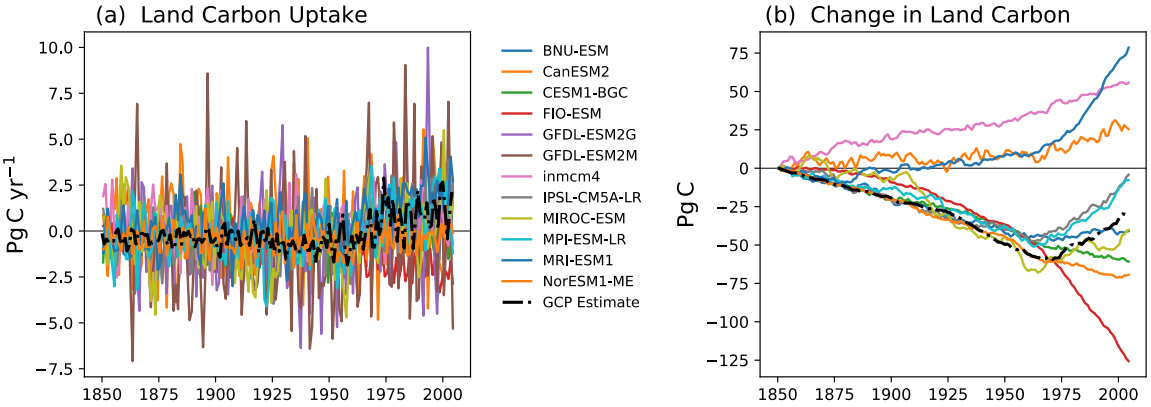

Figure 5.23: Modelled net land carbon sink for 1850 to 2005 in historical ESM simulations, compared to observation-based estimates (from GCP); panel (a): net uptake rate (PgC yr^{-1}), panel (b): change in carbon store (PgC).

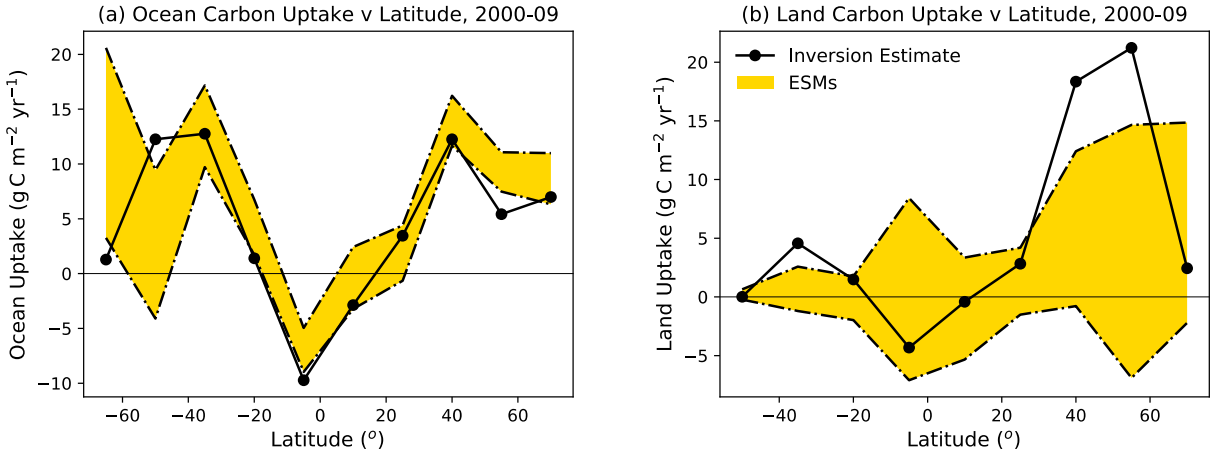

Figure 5.24: Evaluation of the modelled zonal distribution of carbon sinks against atmospheric inversion estimates for 2000–2009, (a) ocean carbon uptake; (b) net land uptake. The model results are shown as the mean plus and minus one standard deviation of the annual values across the model ensemble.

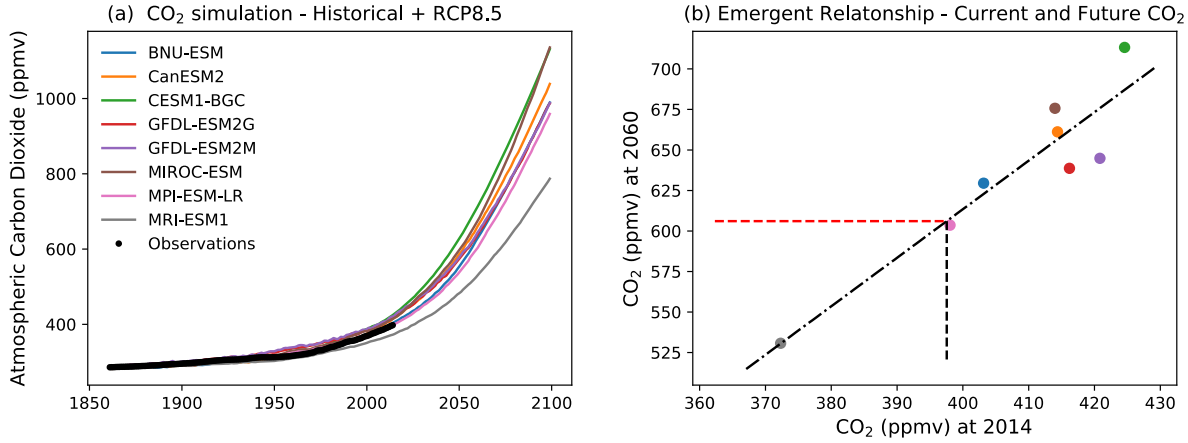

Figure 5.25: Modelled global mean, annual mean, carbon dioxide concentration compared to observations. (a) CO_2 concentration for 1860 to 2100 from emissions-driven RCP8.5 runs, compared to observed global mean CO_2 concentration (as used in prescribed concentration runs) for 1860–2018; (b) Relationship between CO_2 concentration simulated for 2014 and CO_2 concentration projected for 2060 under RCP8.5 emissions (after Hoffman et al., 2014).

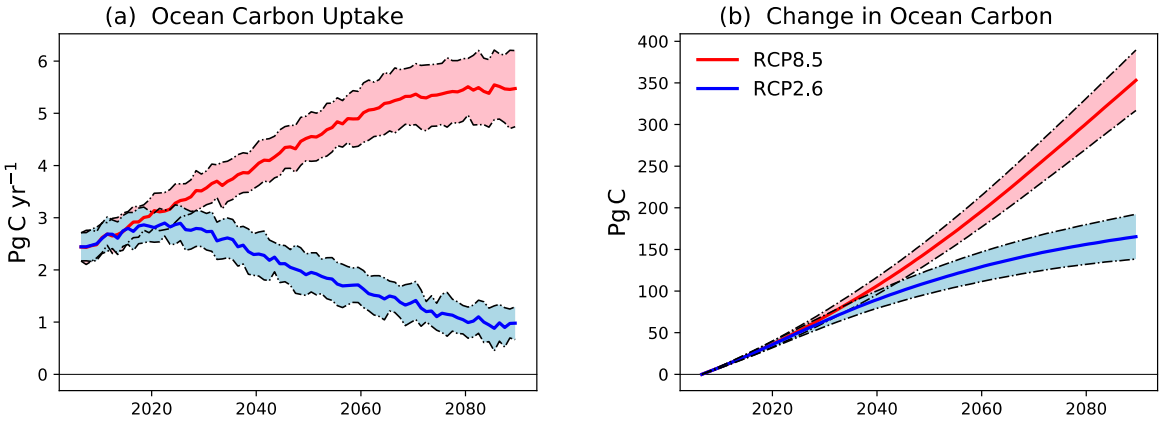

Figure 5.26: Projected evolution of the ocean carbon sink for 2005 to 2090 in concentration-driven RCP2.6 (blue) and RCP8.5 (red) scenarios. Panel (a): net uptake rate (PgC yr^{-1}); panel (b): change in carbon store (PgC). Thick lines represent the ensemble mean of the available ESM runs, and the shaded area represents ± one standard deviation about that mean.

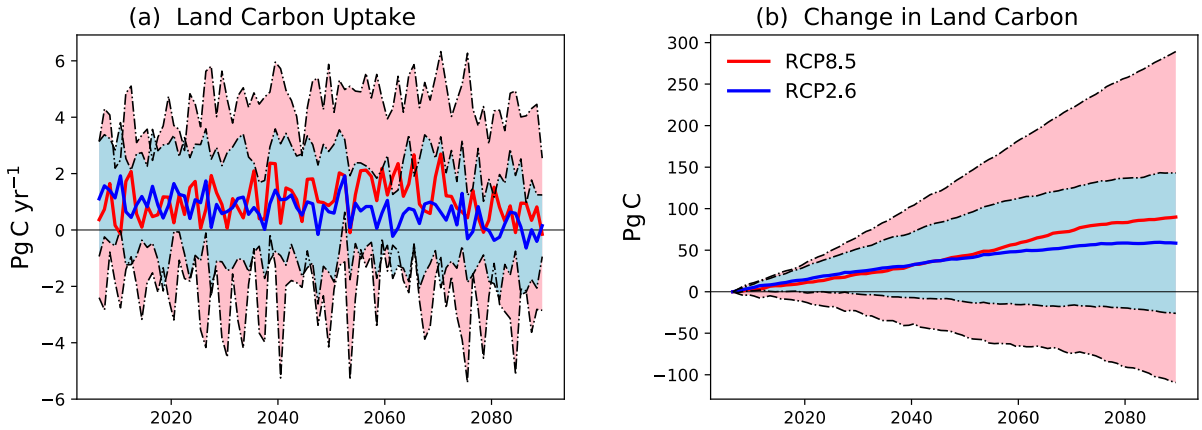

Figure 5.27: Projected evolution of the net land carbon sink for 2005 to 2090 in concentration-driven RCP2.6 (blue) and RCP8.5 (red) scenarios. Panel (a): net uptake rate (PgC yr^{-1}); panel (b): change in carbon store (PgC). Thick lines represent the ensemble mean of the available ESM runs, and the shaded area represents ± one standard deviation about that mean.

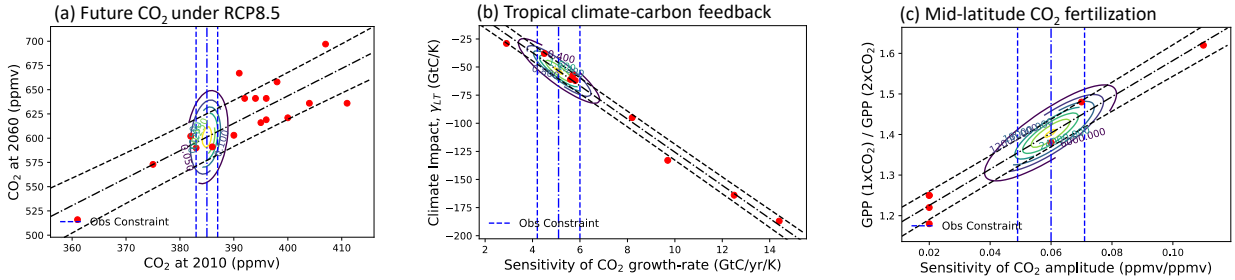

Figure 5.28: Examples of emergent constraints on the carbon cycle in ESMs. (a) projected global mean atmospheric CO_2 concentration by 2100 under the RCP8.5 emissions scenario against the error in simulation of global mean atmospheric CO_2 by 2010 in historical simulations (Friedlingstein et al., 2014; Hoffman et al., 2014); (b) γ-factor for tropical land (γ_{LT}) against the sensitivity of the atmospheric CO_2 growth-rate to tropical temperature variability (Cox et al., 2013; Wenzel et al., 2014); (c) β-factor for mid and high-latitude land (β_{LM}) against the sensitivity of the amplitude of the CO_2 seasonal cycle at Kumukahi, Hawaii to atmospheric CO_2 concentration (Wenzel et al., 2016).

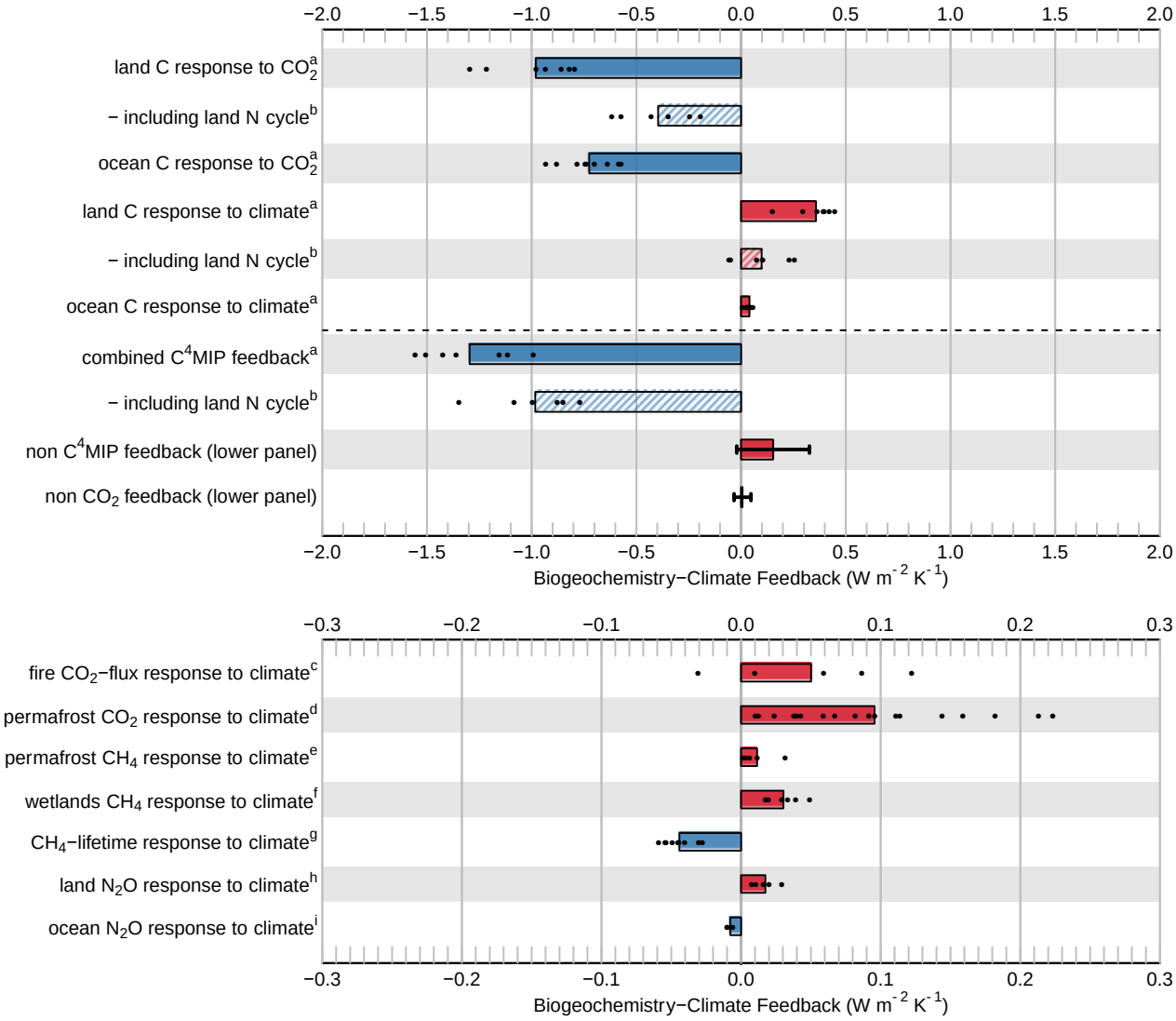

Figure 5.29: A synthesis of the magnitude of biogeochemical feedbacks on climate expressing non-climate feedbacks in common units (W m-2 K-1) with physical feedbacks, following (Arneth et al., 2010; Gregory et al., 2009) and revised radiative forcing calculations (Etminan et al., 2016). Black dots represent single estimates, and coloured bars denote the simple mean of the dots with no weighting or assessment being made to likelihood of any single estimate. These feedback metrics have, where possible, been assessed for the RCP8.5 scenario in year 2100. They may be state or scenario dependent and therefore cannot always be compared like-for-like. Note the different x-axis scale for the lower portion of the Figure. There is low confidence in the magnitude of the feedbacks in the lower panel of the figure. The role of nitrogen limitation on terrestrial carbon sinks is also shown this is not a separate feedback, but rather a modulation to the climate-carbon and concentration-carbon feedbacks. Results have been compiled from (a) C-cycle ESMs of C4MIP (Arora et al., 2013); (b) CN-cycle ESMs of C4MIP (Arora et al., 2013) and (Sokolov et al., 2008; Thornton et al., 2009; Zaehle et al., 2010; Zhang et al., 2013a); (c) (Arneth et al., 2010; Eliseev et al., 2014; Harrison et al., 2018); (d) (Burke et al., 2013; Gasser et al., 2018; Koven et al., 2015b; Schneider von Deimling et al., 2012), (e) (Schneider von Deimling et al., 2012, 2015; Turetsky et al.No title); (f) (Denisov et al., 2013; Stocker et al., 2013; Zhang et al., 2017); (g) (Voulgarakis et al., 2013); (h) (Stocker et al., 2013a; Tian et al., 2019; Xu-Ri et al., 2012; Zaehle, 2013); (i) (Battaglia and Joos, 2018; Landolfi et al., 2017; Martinez-Rey et al., 2015).

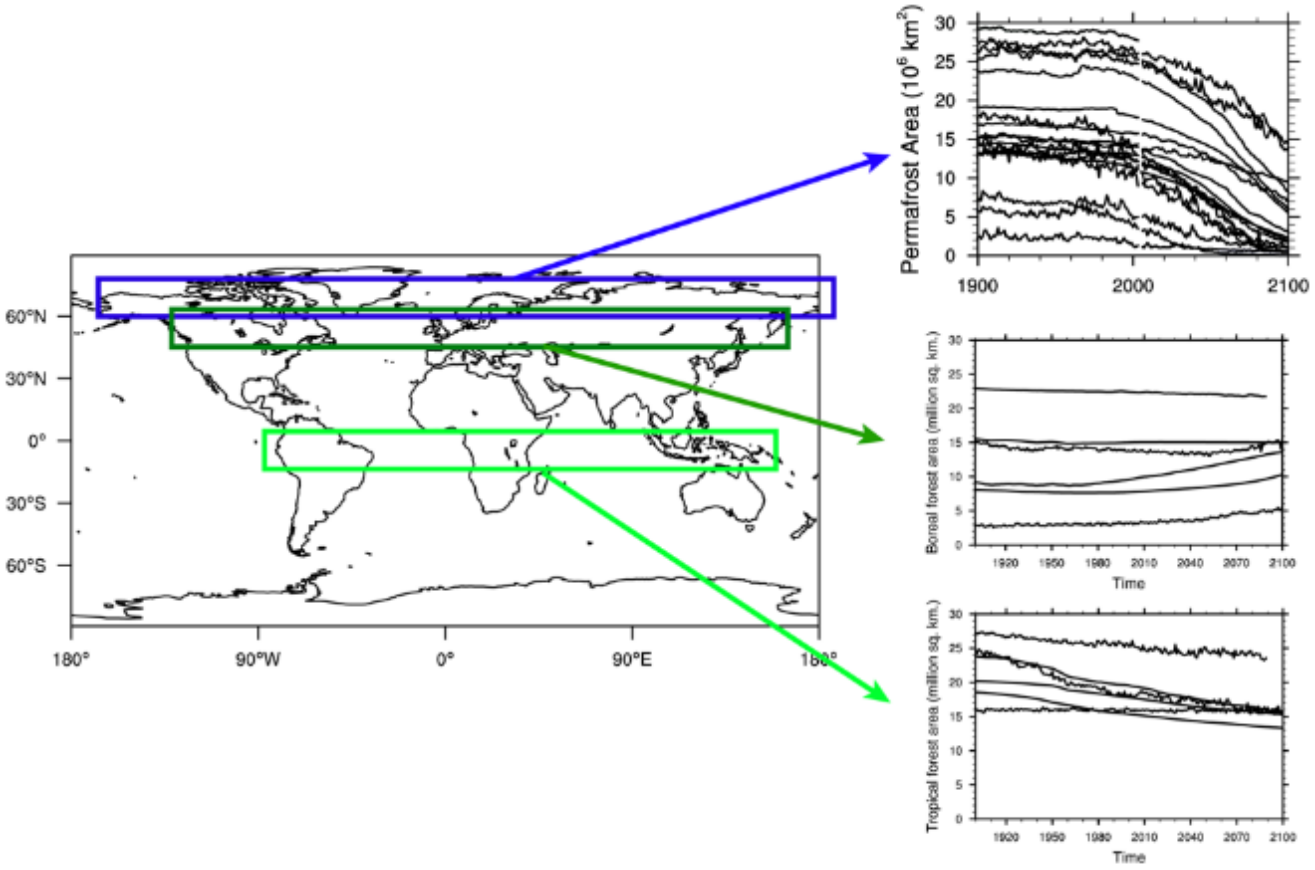

Figure 5.30: Projections of some tipping points in the Earth system: physical permafrost extent, boreal forest area, and tropical forest area. Each curve is from a different CMIP5 model, for the historical and RCP8.5 scenarios. For forest area projections, only models with active dynamic vegetation models were used. [[Placeholder: To be updated and expanded for CMIP6 models when available]].

1

Fig. 1 Schematic representation of the main carbon flows among atmospheric, land, ocean, and geological reservoirs for (a) the Earth before significant anthropogenic impacts; and how carbon flows have or may have changed due to anthropogenic activities such as (b) industrial era fossil fuel combustion, (c) when carbon dioxide removal (CDR) begins, but net CO_2 emissions are positive, and (d) when CO_2 is removed from the atmosphere, i.e., "net negative emissions." Note that when net emissions are negative as in (d), it is still possible to have some emissions, but these are not depicted here. Carbon exchanges depicted in (a; black and dashed lines) also occur in b, c, and d. The question mark in the land to ocean carbon flux perturbation in c and d indicates that it is unknown how or if this carbon cycle perturbation will be affected by CDR. Adapted from [1••, 71]

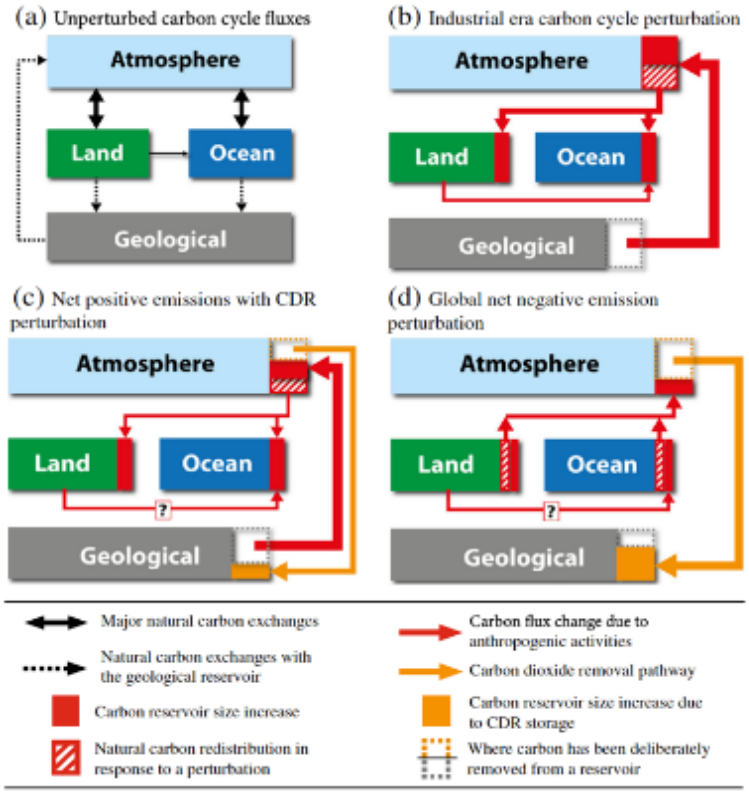

2
3

4 **Box 5.1, Figure 1:** Schematic representation of carbon fluxes between atmosphere, land, ocean and geologic reservoirs
5 for (a) an unperturbed Earth System, (b) an Earth system perturbed by fossil fuel CO_2 emissions, (c)
6 an Earth system with fossil fuel CO_2 emissions are partially offset by CDR, (d) an Earth system in
7 which CDR exceeds CO_2 emissions from fossil fuels ("net negative emissions"). Carbon fluxes
8 depicted in (a) (solid and dashed black lines) also occur in (b)-(d). From (Keller et al., 2018).

9

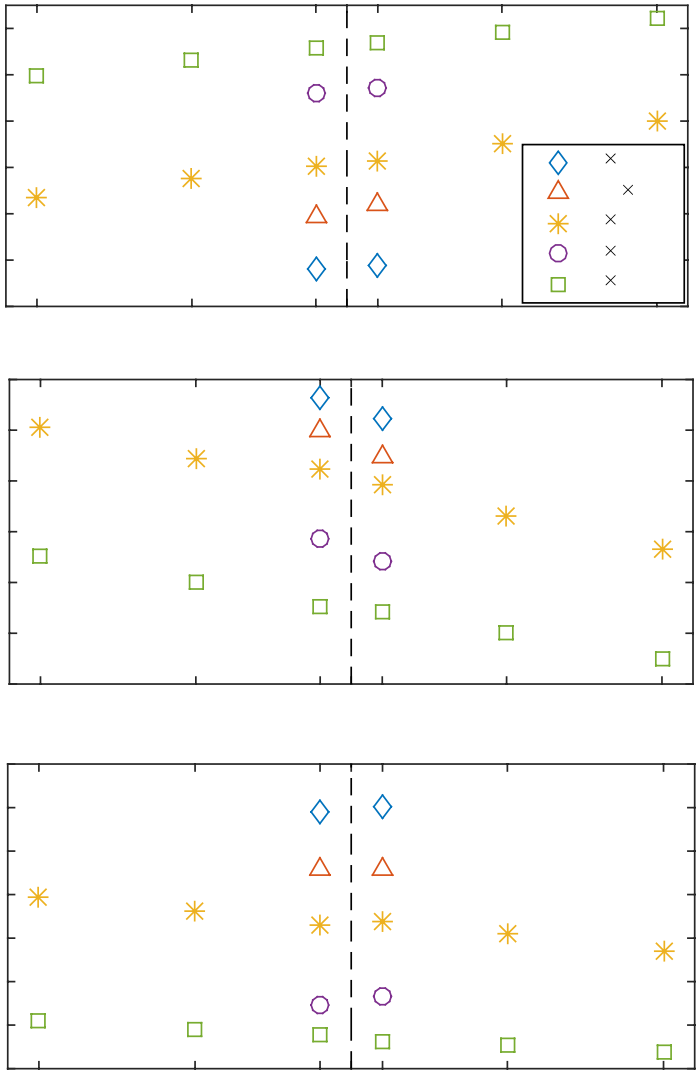

Figure 5.31: Changes in carbon stores (atmosphere, ocean, land) as a fraction of cumulative CO_2 emissions (equivalent to CO_2 pulse size) 1000 years after the pulse emission/removal (±100 PgC, ±500 PgC, ±1000 PgC) for simulations initialised from different equilibrium states (1 times to 4 times the pre-industrial atmospheric CO_2 concentration). Changes in carbon stores are positive (i.e. uptake) for positive CO_2 pulses and negative (i.e. outgassing) for negative CO_2 pulses. (Top) Atmospheric carbon burden change fraction, (Middle) ocean carbon store change fraction, (Bottom) land carbon store change fraction. In each panel the parts of the graph on the left and right hand-side of the zero line (black dashed line) are not mirror images of each other, indicating that the response is asymmetric, particularly for higher pulse emissions/removals. From (Zickfeld et al., 2019). [[Placeholder: Will be updated based on results from CDR-MIP simulations.]]

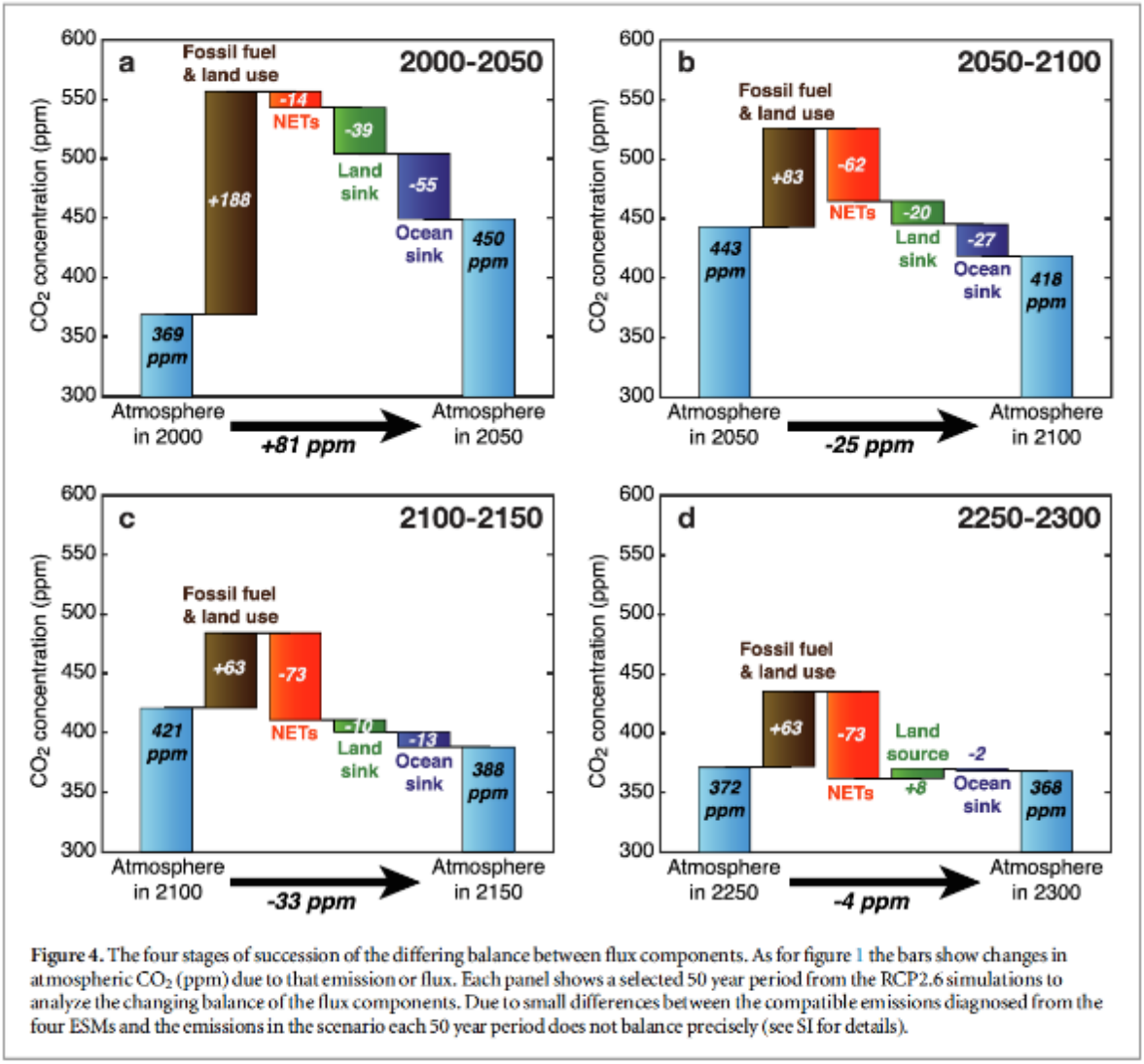

Figure 4. The four stages of succession of the differing balance between flux components. As for figure 1 the bars show changes in atmospheric CO_2 (ppm) due to that emission or flux. Each panel shows a selected 50 year period from the RCP2.6 simulations to analyze the changing balance of the flux components. Due to small differences between the compatible emissions diagnosed from the four ESMs and the emissions in the scenario each 50 year period does not balance precisely (see SI for details).

Figure 5.32: Carbon flux components during different stages of ESM simulations driven by RCP2.6. (a) Large positive CO_2 emissions, (b) Small net positive CO_2 emissions, (c) Net negative CO_2 emissions (short-term response), (d) Net negative CO_2 emissions (long-term response). From (Jones et al., 2016a). [[Placeholder. Will be replotted based on CMIP6 simulations (scenarios SSP1-2.6 and SSP5-3.4OS)]].

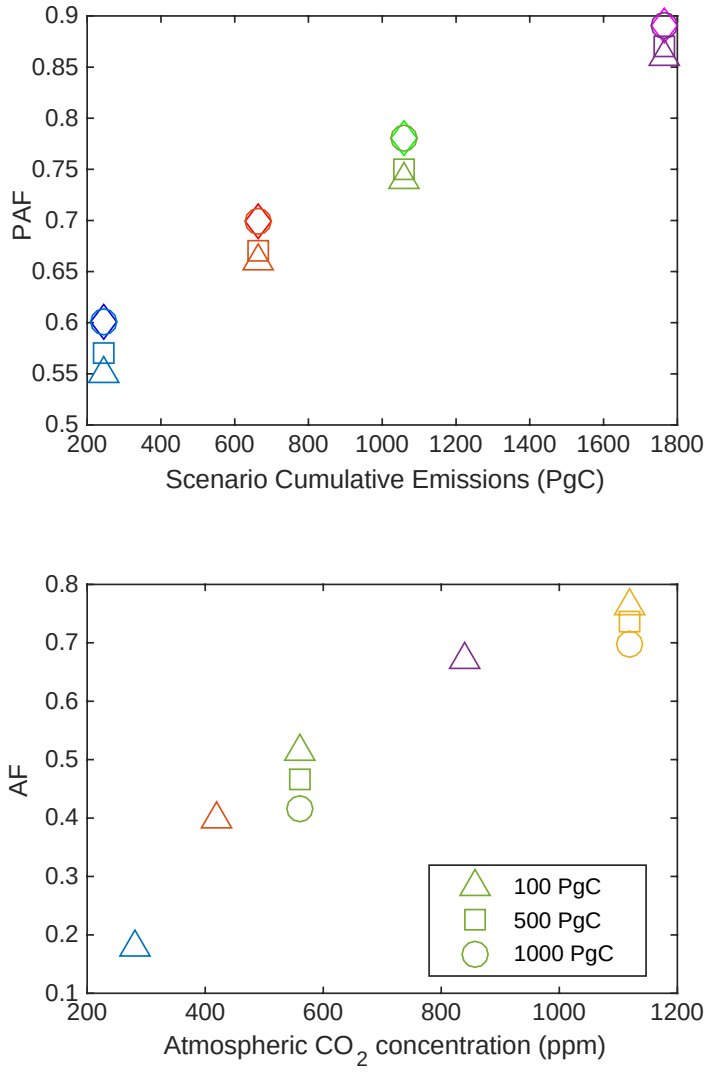

Figure 5.33: Effectiveness of CDR. (Top) Perturbation airborne fraction (PAF) for model simulations where CDR is applied from four different RCPs (shown on the horizontal axis in terms of their cumulative CO_2 emissions over the 2020–2099 period). Symbols indicate results for four CDR scenarios, which differ in terms of the magnitude and rate of CDR (see Jones et al., (2016b) for details). Results are based on simulations with the Hadley Centre Simple Climate-Carbon Model. From Jones et al., (2016b). (Bottom) Airborne fraction of cumulative emissions (AF) for idealised model simulations with CDR applied instantly (pulse removals) from climate states in equilibrium with different atmospheric CO_2 concentration levels (shown on the horizontal axis). Symbols indicate results for different magnitudes of CDR. Based on simulations with the UVic ESCM model of intermediate complexity. From (Zickfeld et al., 2019). [[Placeholder: Will be supplemented with results from new studies and CDR-MIP simulations]].

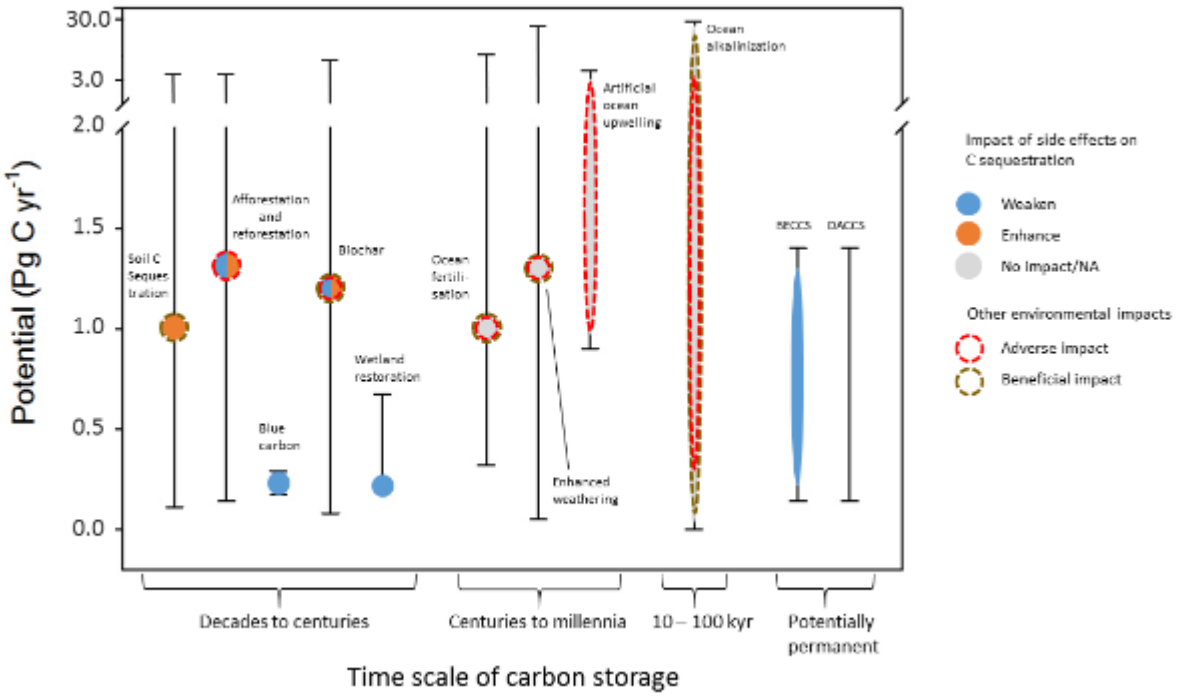

Figure 5.34: Relative sequestration potentials of CDR methods plotted against the time scale of C storage. Colour of the full circle indicate whether side effects act to weaken or enhance the carbon sequestration potential, surrounding dashed lines denote the sign of other environmental impacts. Vertical bars indicate the uncertainty ranges in potentials, horizontal bars the uncertainty ranges in the time scale of C storage. [[Placeholder: To be completed and underlying numbers to be checked and updated]].

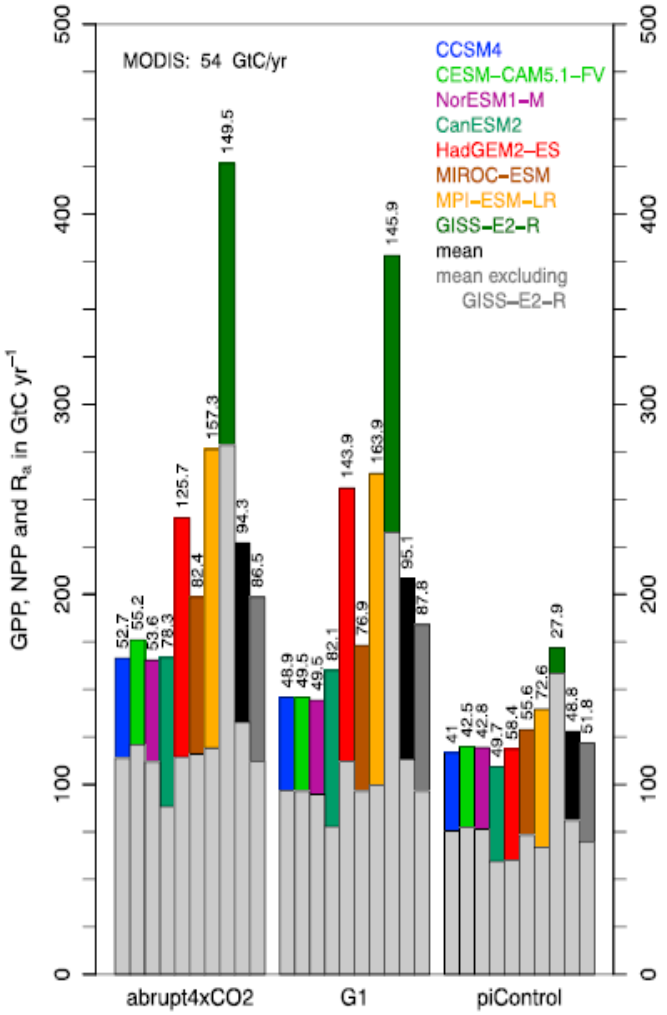

Figure 1. Global mean values for NPP averaged over land (colored with numbers above), R_a (grey) and GPP (total) for all models of the three experiments abrupt4 × CO2, G1, and piControl. The number in the top left corner is the global average of NPP determined from MODIS data.

Figure 5.35: [[Placeholder: From (Glienke et al., 2015). abrupt4×CO_2 is an experiment with an abrupt quadrupling of atmospheric CO_2 and G1 is a GEOMIP experiment in which a decrease in the solar constant offsets the global radiative forcing of 4×CO_2.]]

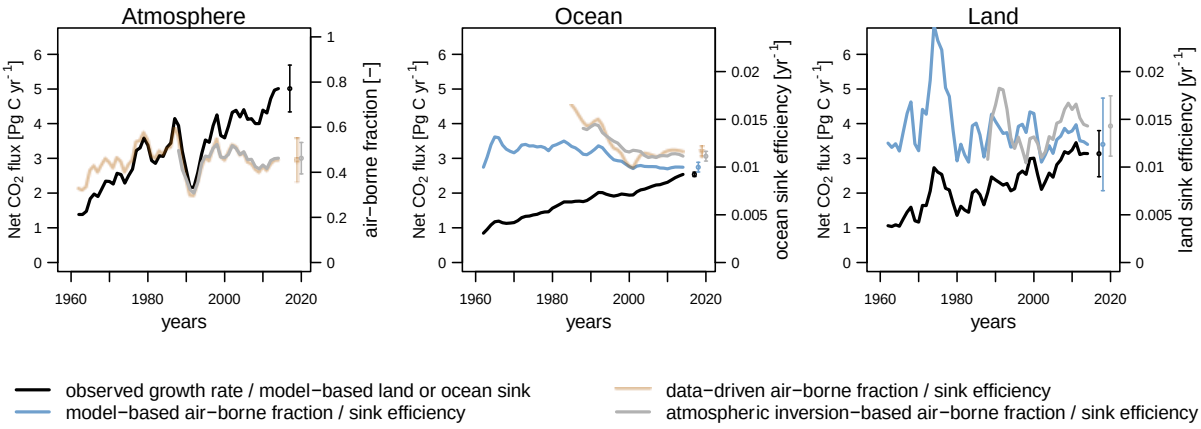

FAQ 5.1, Figure 1: Growth rate of the CO_2 inventory in the atmosphere, ocean and land, as well as the air-borne fraction of anthropogenic CO_2 emissions, and the efficiency of the ocean and land carbon sinks (defined as the size of the sink divided by the excess of anthropogenic CO_2 in the atmosphere). Estimates are derived from atmospheric observations, process-based models, data-driven ocean flux products, and atmospheric inversions (Le Quéré et al., 2018a). Dots and arrow bars denote the year-to-year variability as ±1 standard deviation. Uncertainties in the estimates will be added for the SOD.